

AWARD NUMBER: W81XWH-17-1-0178

TITLE: Interrogating SOS1/2 (Son of Sevenless 1 and 2) as Therapeutic Targets in Treatment-Resistant EGFR and K-ras-Driven Lung Cancer

PRINCIPAL INVESTIGATOR: Dr. Robert L. Kortum

RECIPIENT: The Henry M. Jackson Foundation for the Advancement of Military Medicine, Inc.

REPORT DATE: SEPTEMBER 2020

TYPE OF REPORT: Final

**PREPARED FOR: U.S. Army Medical Research and Materiel Command
Fort Detrick, Maryland 21702-5012**

**DISTRIBUTION STATEMENT: Approved for Public Release;
Distribution Unlimited**

The views, opinions and/or findings contained in this report are those of the author(s) and should not be construed as an official Department of the Army position, policy or decision unless so designated by other documentation.

REPORT DOCUMENTATION PAGE

Form Approved
OMB No. 0704-0188

Public reporting burden for this collection of information is estimated to average 1 hour per response, including the time for reviewing instructions, searching existing data sources, gathering and maintaining the data needed, and completing and reviewing this collection of information. Send comments regarding this burden estimate or any other aspect of this collection of information, including suggestions for reducing this burden to Department of Defense, Washington Headquarters Services, Directorate for Information Operations and Reports (0704-0188), 1215 Jefferson Davis Highway, Suite 1204, Arlington, VA 22202-4302. Respondents should be aware that notwithstanding any other provision of law, no person shall be subject to any penalty for failing to comply with a collection of information if it does not display a currently valid OMB control number. **PLEASE DO NOT RETURN YOUR FORM TO THE ABOVE ADDRESS.**

1. REPORT DATE SEPTEMBER 2020			2. REPORT TYPE Final		3. DATES COVERED 6/1/2017 - 5/31/2020	
4. TITLE AND SUBTITLE Interrogating SOS1/2 (Son of Sevenless 1 and 2) as Therapeutic Targets in Treatment-Resistant EGFR and K-ras-Driven Lung Cancer					5a. CONTRACT NUMBER	
					5b. GRANT NUMBER W81XWH-17-1-0178	
					5c. PROGRAM ELEMENT NUMBER	
6. AUTHOR(S) Dr. Robert Kortum E-Mail: robert.kortum@usuhs.edu					5d. PROJECT NUMBER	
					5e. TASK NUMBER	
					5f. WORK UNIT NUMBER	
7. PERFORMING ORGANIZATION NAME(S) AND ADDRESS(ES) The Henry M. Jackson Foundation for the Advancement of Military Medicine, Inc. 6720A Rockledge Drive, Suite 100 Bethesda, Maryland 20817					8. PERFORMING ORGANIZATION REPORT NUMBER	
9. SPONSORING / MONITORING AGENCY NAME(S) AND ADDRESS(ES) U.S. Army Medical Research and Development Command Fort Detrick, Maryland 21702-5012					10. SPONSOR/MONITOR'S ACRONYM(S)	
					11. SPONSOR/MONITOR'S REPORT NUMBER(S)	
12. DISTRIBUTION / AVAILABILITY STATEMENT Approved for Public Release; Distribution Unlimited						
13. SUPPLEMENTARY NOTES						
14. ABSTRACT Lung adenocarcinoma is the leading cause of cancer death. Traditional chemotherapeutic treatment of lung cancer has involved using nonspecific cytotoxic drugs that harm the rapidly growing tumor cells to a greater extent than their normal surroundings. However, new treatments now focus on identifying and then targeting those intracellular signals that specifically drive tumor growth and survival. The objective of this project is to identify novel therapeutic targets to treat lung adenocarcinoma. For 75% of lung adenocarcinomas, these intracellular driver signals involve components of one signaling pathway that originates at a cell-surface receptor known as epidermal growth factor receptor (EGFR) and signal to its downstream components, including the oncogene K-Ras. Therapeutics directly targeting the EGFR enhance survival in a subset of patients. However, resistance almost invariably occurs, leading to recurrence of the tumor. Therefore, identifying other therapeutic targets within this signaling pathway holds enormous therapeutic promise. This proposal tests one such family of targets, the proteins Sos1 and Sos2, which are central to signaling from EGFR to the oncogene K-Ras. We hypothesize that Sos1 and Sos2 are viable therapeutic targets both in primary tumors and in tumors resistant to current targeted therapies.						
15. SUBJECT TERMS Lung cancer, KRAS, EGFR, MEK, osimertinib, trametinib, Son of Sevenless, SOS2, SOS1						
16. SECURITY CLASSIFICATION OF:			17. LIMITATION OF ABSTRACT	18. NUMBER OF PAGES	19a. NAME OF RESPONSIBLE PERSON	
a. REPORT	b. ABSTRACT	c. THIS PAGE	Unclassified	34	USAMRMC	
Unclassified	Unclassified	Unclassified			19b. TELEPHONE NUMBER (include area code)	

Standard Form 298 (Rev. 8-98)
Prescribed by ANSI Std. Z39.18

TABLE OF CONTENTS

	<u>Page</u>
1. Introduction	4
2. Keywords	4
3. Accomplishments	4
4. Impact	24
5. Changes/Problems	26
6. Products	28
7. Participants & Other Collaborating Organizations	31
8. Special Reporting Requirements	34
9. Appendices	34

- 1. INTRODUCTION:** Narrative that briefly (one paragraph) describes the subject, purpose and scope of the research.

This is the final report for the research project “Interrogating SOS1/2 (Son of Sevenless 1 and 2) as therapeutic targets in treatment-resistant EGFR– and K-Ras–driven lung cancer”; the subject of this is to examine SOS1 and SOS2 as novel therapeutic targets in NSCLC harboring EGFR or KRAS mutations. The purpose of this research is to test the hypothesis that Sos1 and Sos2 are unexploited, critical therapeutic targets to treat lung cancers driven by mutated *EGFR* and *KRAS*. This project is a career development award; the scope of the project was to obtain preliminary data to allow the investigator to write a full lung cancer proposal (CDMRP or R01) at the end of the cycle investigating novel therapeutic targets in lung cancer. The investigator has received a second CDMRP award, LC180213 and is currently writing an R01 focused exclusively on lung adenocarcinoma that is due October 5, 2020.

- 2. KEYWORDS:** Provide a brief list of keywords (limit to 20 words).

Lung cancer, KRAS, EGFR, Son of Sevenless, SOS1, SOS2

- 3. ACCOMPLISHMENTS:** The PI is reminded that the recipient organization is required to obtain prior written approval from the awarding agency grants official whenever there are significant changes in the project or its direction.

What were the major goals of the project?

List the major goals of the project as stated in the approved SOW. If the application listed milestones/target dates for important activities or phases of the project, identify these dates and show actual completion dates or the percentage of completion.

Aim 1, Major Task 1: Determine if EGFR-TKI-sensitive and –resistant lung cancer cell lines require Sos1 or Sos2 to maintain their transformed phenotype.

1. Successful shRNA-mediated knockdown (or CRISRP-mediated knockout) of *SOS1* and *SOS2* in human lung cancer cells. Target Date (month 8). Completed 03/2018.
2. Assessment of proliferation and apoptosis in above cells (month 15). Completed 12/2019.
3. Successful cloning of shRNA-resistant Sos1 and Sos2 constructs (month 9). Completed 12/2017.
4. Successful introduction of shRNA-resistant Sos1 and Sos2 mutants into lung cancer cell lines (month 15). 100% complete as of 12/2020.
5. Assessment of proliferation and apoptosis in above cells (month 18). Completed 12/2020.
6. Assessment of proliferation, apoptosis, and transformation in above cells after combined EGFR-TKI treatment+ RTK stimulation (month 24). Completed 06/2020.

Aim 1, Major Task 2: Determine if Sos1 or Sos2 knockdown can synergize with EGFR-TKIs and limit the emergence of EGFR-TKI resistance.

1. Test EGFR-TKI treatment in lung cancer cell lines (month 16). Completed 05/2019.

2. Assess combined EGFR-TKI treatment and *sos1* or *sos2* knockdown in above (month 24). Completed 12/2019.
3. Assessment of EGFR-TKI resistance following *Sos1* or *Sos2* re-introduction (month 24). Completed 05/2020.
4. Assessment of EGFR-TKI resistance in WT and SOS KO MEFs using 96 well plate assay. (month 24). Completed 05/2020.

Aim 1, Major Task 3: Determine whether *Sos1* or *Sos2* are required for mutant EGFR-driven tumorigenesis *in vivo*

1. No animal use will be initiated until ACURO approval has been obtained (month 4). 5 Completed 12/2017.
2. Crossing of *Sos1^{fl/fl}* and *Sos1^{fl/fl}Sos2^{-/-}* mice separately onto each of three transgenic backgrounds (tetO-EGFR, CC10^{rtTA}, and Nkx2.1-CRE^{ERT2}) (month 8). Completed 05/2020.
3. Getting the first “informative mice” out of the above crosses (month 15). Not started as of 03/2020.
4. Preliminary assessment of tumor development in above mice (month 24). Not started as of 03/2020.

Aim 2, Major Task 1: Determine if inhibiting K-Ras–Sos–Ras positive feedback signaling can synergize with targeted therapeutics to kill KRAS–mutated lung cancer cells

1. Successful knockdown (or knockout) of *Sos1* and *Sos2* in *KRAS* NSCLC cells (month 6). Completed 11/2017.
2. Assessment of proliferation and apoptosis, in above cells (month 14). Completed 12/2019.
3. Successful re-introduction of *Sos1* or *Sos2* mutants (month 9). Completed 12/2019.
4. Assessment of proliferation and apoptosis, in above cells (month 18). Completed 12/2019.
5. Test *KRAS* “synthetic lethal” inhibitors treatment in NSCLC cells (month 9). Completed 04/2018.
6. Assessment of synergy between *sos1* or *sos2* deletion and inhibitor treatments in above cells (month 18). Completed 04/2020.

Aim 2, Major Task 2: Determine the potential for targeting Sos–dependent feedback signaling to treat KRAS–driven lung adenocarcinoma *in vivo*

1. No animal use will be initiated until ACURO approval has been obtained (month 4). Complete as of 08/2017.
2. Successful cloning of shRNAs into a doxycycline-inducible lentiviral vector (month 8). Complete as of 04/2018.
3. Successful introduction of doxycycline inducible shRNA constructs into *KRAS* mutant NSCLC cell lines. Completed 06/2019.
4. Successful knockdown of *Sos1* and *Sos2* in a doxycycline-inducible manner in the above cells. Completed 02/2020.

5. Assessment of tumor xenograft growth in NSCLC cells where *sos1* or *sos2* have been knocked either prior to tumor cell injection, at the time of tumor injection, or after tumor formation occurs (month 24). Not started as of 03/2020.

What was accomplished under these goals?

For this reporting period describe: 1) major activities; 2) specific objectives; 3) significant results or key outcomes, including major findings, developments, or conclusions (both positive and negative); and/or 4) other achievements. Include a discussion of stated goals not met. Description shall include pertinent data and graphs in sufficient detail to explain any significant results achieved. A succinct description of the methodology used shall be provided. As the project progresses to completion, the emphasis in reporting in this section should shift from reporting activities to reporting accomplishments.

Aim 1, Major Task 1: Determine if EGFR-TKI-sensitive and –resistant lung cancer cell lines require *Sos1* or *Sos2* to maintain their transformed phenotype.

1. *Successful shRNA-mediated knockdown (or CRISPR-mediated knockout) of *sos1* and *sos2* in human lung cancer cells.*

We have decided to use CRISPR/Cas9 to delete *SOS1* and *SOS2* in lung cancer lines, as we have found that this completely removes the gene in a majority of cells rather than reducing expression in all cells. We have designed and tested several sgRNAs that target *SOS1* or *SOS2*, and have found at least 3 sgRNAs that delete *SOS1* or *SOS2* in >80% of cells, and have successfully deleted *SOS1* and *SOS2* in all NSCLC cell lines.

These results are shown in Fig. 1.

2. Assessment of proliferation and apoptosis in above cells (month 15). 60% complete as of 06/2018.

We have assessed proliferation and transformation in NCI-H1650, NCI-H1975, HCC-827, PC9, PC9-TM, NCI-H3255, and NCI-H3255-TM cells after *SOS1* or *SOS2* deletion. We found that anchorage-dependent (2D) proliferation is unaffected by either *SOS1* or *SOS2* deletion. In contrast, anchorage-independent (3D) transformation is ablated after *SOS1* deletion. These data, along with confirmation of *SOS1* and *SOS2* deletion using CRISPR/Cas9, are shown in Fig. 1. These data were published in our 2020 eLife manuscript (Theard et al., *eLife*, 2020).

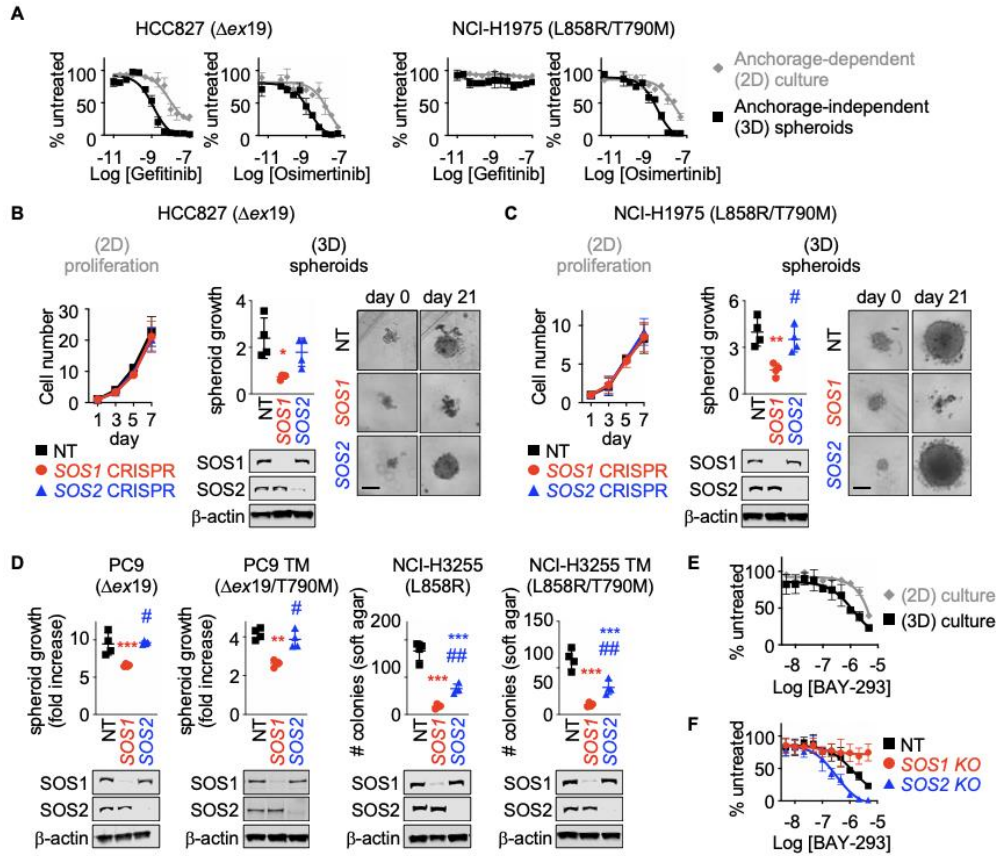


Fig. 1 (LC160222). SOS1 deletion inhibits anchorage-dependent (3D) transformation in EGFR-mutated NSCLC cell lines.
(A) Dose-response curves of EGFR-mutated HCC827 (Dex19) (left) or NCI-H1975 (L858R/T790M) (right) cells treated with gefitinib or osimertinib under 2D anchorage-dependent (gray diamonds) or 3D spheroid (black squares) culture conditions.
(B-C) 2D proliferation (left) or 3D spheroid growth (right) in pooled populations of **(B)** HCC827 or **(C)** NCI-H1975 cells where SOS1 or SOS2 has been deleted using CRISPR/Cas9 vs NT controls. 10x images of representative spheroids at day 0 and 21 are shown, scale bar=250 mm.
(D) 3D transformation in pooled populations of the indicated EGFR-mutated NSCLC cell lines where SOS1 or SOS2 has been deleted using CRISPR/Cas9 vs NT controls.
(E) Dose-response curve cells of NCI-H1975 cells treated with the SOS1 inhibitor BAY-293 under 2D anchorage-dependent (gray diamonds) or 3D spheroid (black squares) culture conditions. Data are represented as cell # versus untreated for each individual cell line.
(F) Dose-response curves of NCI-H1975 cells where SOS1 (red circles) or SOS2 (blue triangles) has been deleted using CRISPR/Cas9 vs NT controls (black squares) treated with BAY-293 under 3D spheroid culture conditions. For each condition, the untreated sample was set to 100%, and drug-treated samples were compared to untreated for each cell line. Dose-response curves and 2D proliferation are presented as mean +/- s.d. from a least three independent experiments. For transformation studies, data are from four independent experiments. Each individual experiment was performed using populations (not clones) of independently CRISPR'd cells. For each experiment, three technical replicates were assessed. Statistical significance was determined by ANOVA using Tukey's method for multiple comparisons. * p<0.05, **p<0.01, ***p<0.001 vs. NT cells. # p<0.05, ##p<0.01 vs. SOS1 KO cells.

3. Successful cloning of shRNA-resistant Sos1 and Sos2 constructs.

We have made point mutations in the 'NGG' protospacer adjacent motif (PAM) required for efficient Cas9 binding in SOS1 or SOS2 for each of three different sgRNAs.

4. Successful introduction of shRNA-resistant Sos1 and Sos2 mutants into lung cancer cell lines.

We have tested the above constructs for rescue of *SOS1* or *SOS2* expression. We found that we could efficiently rescue *SOS1* or *SOS2* expression in cells where we have deleted *SOS1* or *SOS2*. These data were shown in the 2018 report.

5. Assessment of proliferation, transformation, and apoptosis in above cells.

We have assessed transformation following *SOS1* or *SOS2* re-expression using the constructs in Subtask 1.3 and 1.4 in both proliferation and transformation. We found that re-expression of *SOS1* rescued transformation following *SOS1* deletion. Example data from NCI-H1975 cells are shown in Fig. 2.

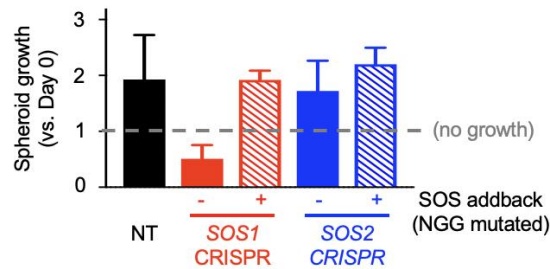


Fig. 2 (LC160222). Restoration of *SOS1* expression using a CRISPR-resistant (NGG mutated) construct restores transformation in *EGFR* (L858R/T790M) mutated NSCLC cells after *SOS1* deletion.

6. Assessment of proliferation, apoptosis, and transformation in above cells after combined *EGFR*-TKI treatment+ RTK stimulation.

We have assessed HGF-induced 2D proliferation, 3D transformation, apoptosis, and osimertinib resistance in *SOS1* and *SOS2* deleted *EGFR*-mutated cells versus NT controls. We found that either *SOS1* or *SOS2* deletion both reduces HGF-induced transformation (3D culture) and partially blocks osimertinib resistance (oncogenic shift) only in 3D culture. Example data are shown in Fig. 3.

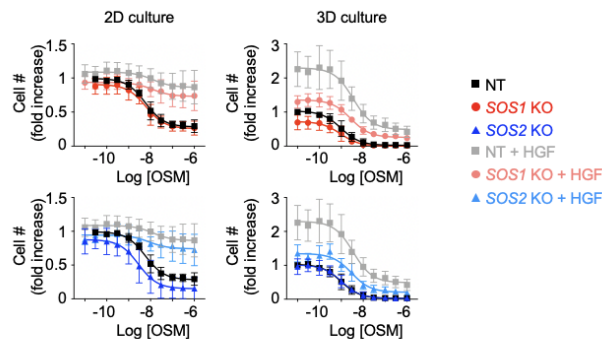


Fig. 3 (LC160222). *SOS1* or *SOS2* deletion inhibit HGF-dependent osimertinib resistance in 3D cultured H1975 cells. NT controls, *SOS1* KO or *SOS2* KO cells were cultured under either 2D or 3D conditions and treated with increasing doses osimertinib alone or in the presence of 30 ng/mL HGF to induce osimertinib resistance. Western blots confirming deletion are in Fig. 1. We found that while *SOS1* KO or *SOS2* KO alone did not alter the osimertinib dose-response curve in 10% serum, either *SOS1* KO or *SOS2* KO blocked HGF-induced osimertinib resistance under 3D culture conditions.

Aim 1, Major Task 2: Determine if Sos1 or Sos2 knockdown can synergize with EGFR-TKIs and limit the emergence of EGFR-TKI resistance.

1. Test EGFR-TKI treatment in lung cancer cell lines.

We have tested baseline efficacy of each EGFR-TKI (Gefitinib and Osimertinib) in NCI-H1650, NCI-H1975, PC9, HCC-3255, and HCC-3255 L/T cells cultured under both 2D and 3D growth conditions. 3D data are shown in Fig. 4.

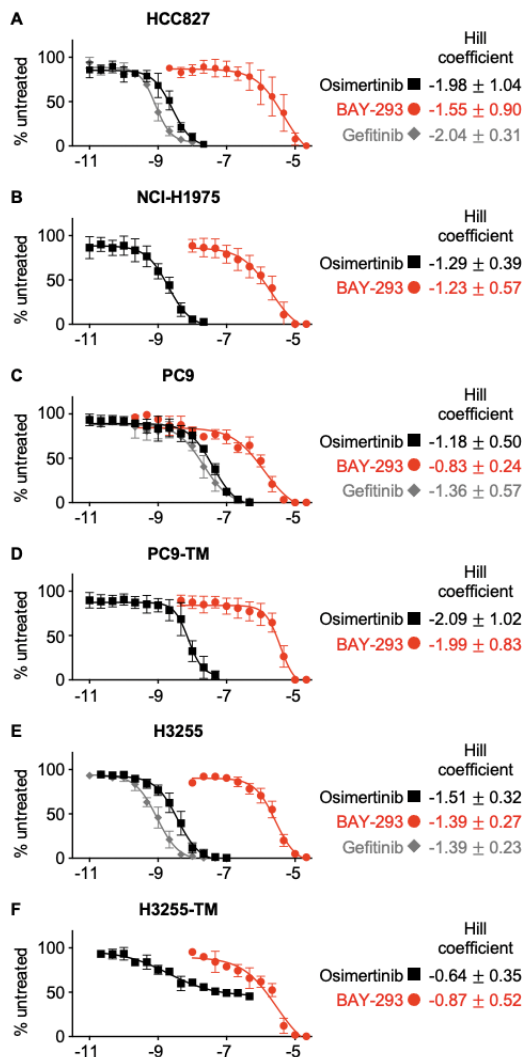


Fig. 4 (LC160222). Osimertinib, Gefitinib, and BAY-393 dependent growth inhibition in 3D spheroid cultures of EGFR-mutated LUAD cell lines.

2. Assess combined EGFR-TKI treatment and *sos1* or *sos2* knockdown in above.

For SOS1, in the course of our experiments a potent SOS1 inhibitor suitable for *in situ* studies, BAY-293, was published (Hillig et al., *PNAS*, 2019). Using this inhibitor, we found strong synergy between SOS1 inhibition and EGFR-TKIs in all cell lines studied, but only under 3D transforming conditions. These data were published in 2020 (Theard et al., *eLife*, 2020) and are shown in Figures 5, 6, and 7.

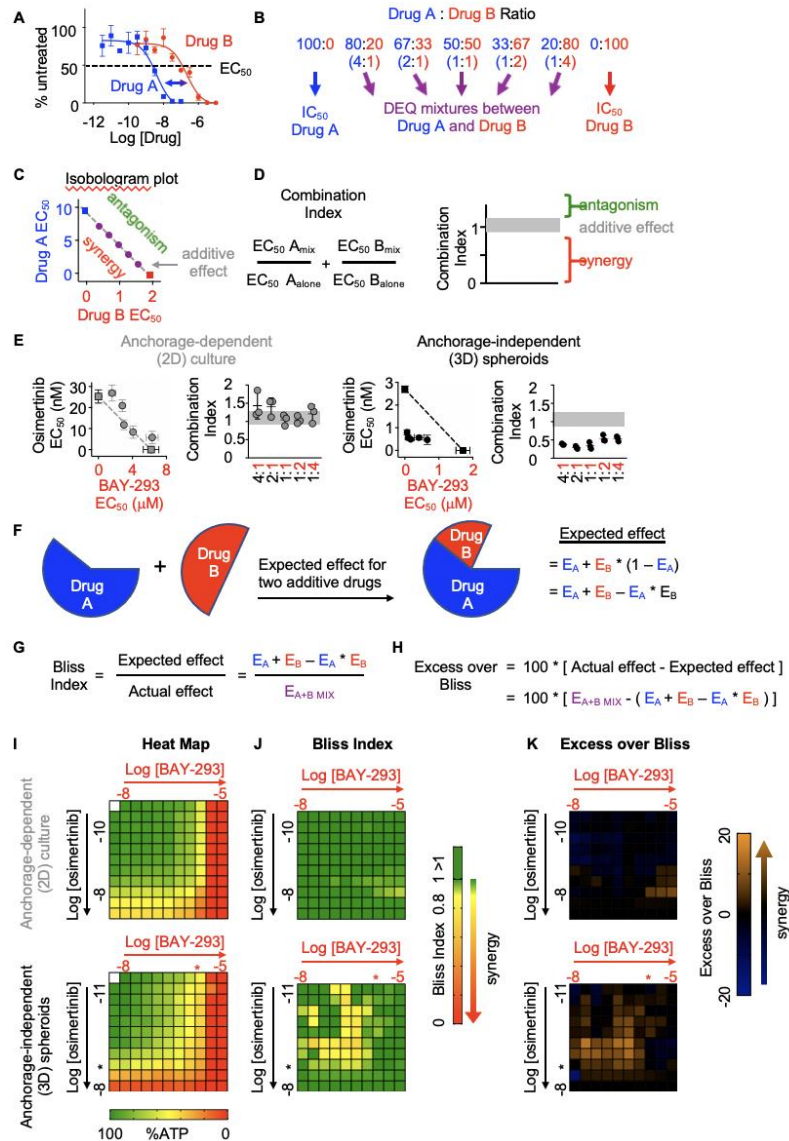


Figure 5 (LC160222). SOS1 inhibition synergizes with the EGFR-TKI inhibitor osimertinib to inhibit cell survival under anchorage-independent (3D) culture conditions. (A-D) Isobologram analysis examines drug-drug synergy by comparing dose equivalent (DEQ) mixtures of two drugs based on their EC_{50} values to treatment with either drug alone (A and B). From the dose-response curves of the DEQ mixtures, plotting the fractional EC_{50} for each drug in the combination (purple) relative to the individual drug EC_{50} values (blue, red) on an isobologram plot (C) and calculation of the combination index (CI, D and E) allows assessment of drug-drug synergy. Additive effects occur on the dashed lines of the isobologram plot and have a CI 0.8-1.2 (gray box), whereas synergistic interactions fall below the dashed lines and have a CI < 0.8. (E) Isobologram plots and CI from dose-equivalent treatments of H1975 EGFR-mutated NSCLC cells treated with DEQ combinations of osimertinib and BAY-293. Isobologram and CI data are presented as mean +/- s.d. from three independent experiments. (F) Bliss additivity evaluates whether the overall effect of an individual drug combination ($E_{A+B \text{ mix}}$) is greater than should be expected for two drugs with independent effects on the overall population ($E_A + E_B - E_A * E_B$). (G) The Bliss Index compares the ratio of the expected effect to the actual effect. Synergistic interactions have a Bliss Index < 0.85. (H) Excess over Bliss evaluates the magnitude of the difference between the actual and expected effects. Increasingly synergistic interactions show an excess over Bliss Index > 0. (I) Heat map of H1975 cells treated with the indicated doses of osimertinib and/or BAY-293 grown in either 2D (adherent) culture conditions or as 3D spheroids. Green indicates more cells, red indicates fewer cells. EC_{50} values for each individual drug are indicated by an *. (J) Heat map of Bliss Index assessing drug-drug synergy between osimertinib and BAY-293 at each dose combination from D. (K) Heat map of excess over Bliss assessing drug-drug synergy between osimertinib and BAY-293 at each dose combination from D. Bliss Index and excess-over Bliss are presented as the mean from three independent experiments. For each experiment, three technical replicates were assessed.

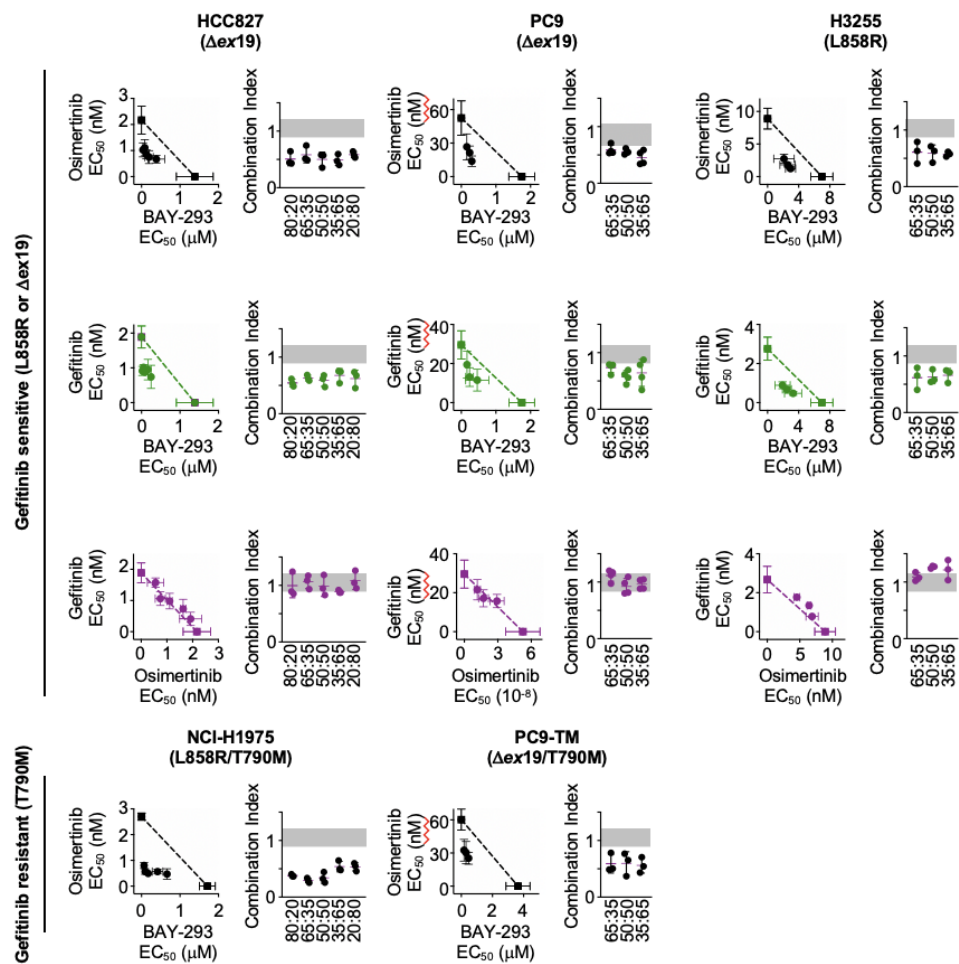


Figure 6 (LC160222). Isobologram analysis showing that SOS1 inhibition synergizes with EGFR-TKI treatment to inhibit survival in multiple EGFR-mutated NSCLC cell lines. Isobologram analysis and Combination Index (CI) from dose-equivalent treatments of the indicated EGFR-mutated gefitinib-sensitive (L858R or Dex19, top) or gefitinib-resistant (T790M, bottom) NSCLC cell lines with combinations of gefitinib, osimertinib, and BAY-293. Additive effects occur on the dashed lines of the isobologram plot and have a CI 0.8-1.2 (gray box), whereas synergistic interactions fall below the dashed lines and have a CI < 0.8. Data are presented as mean \pm s.d. from three independent experiments. For each experiment, three technical replicates were assessed.

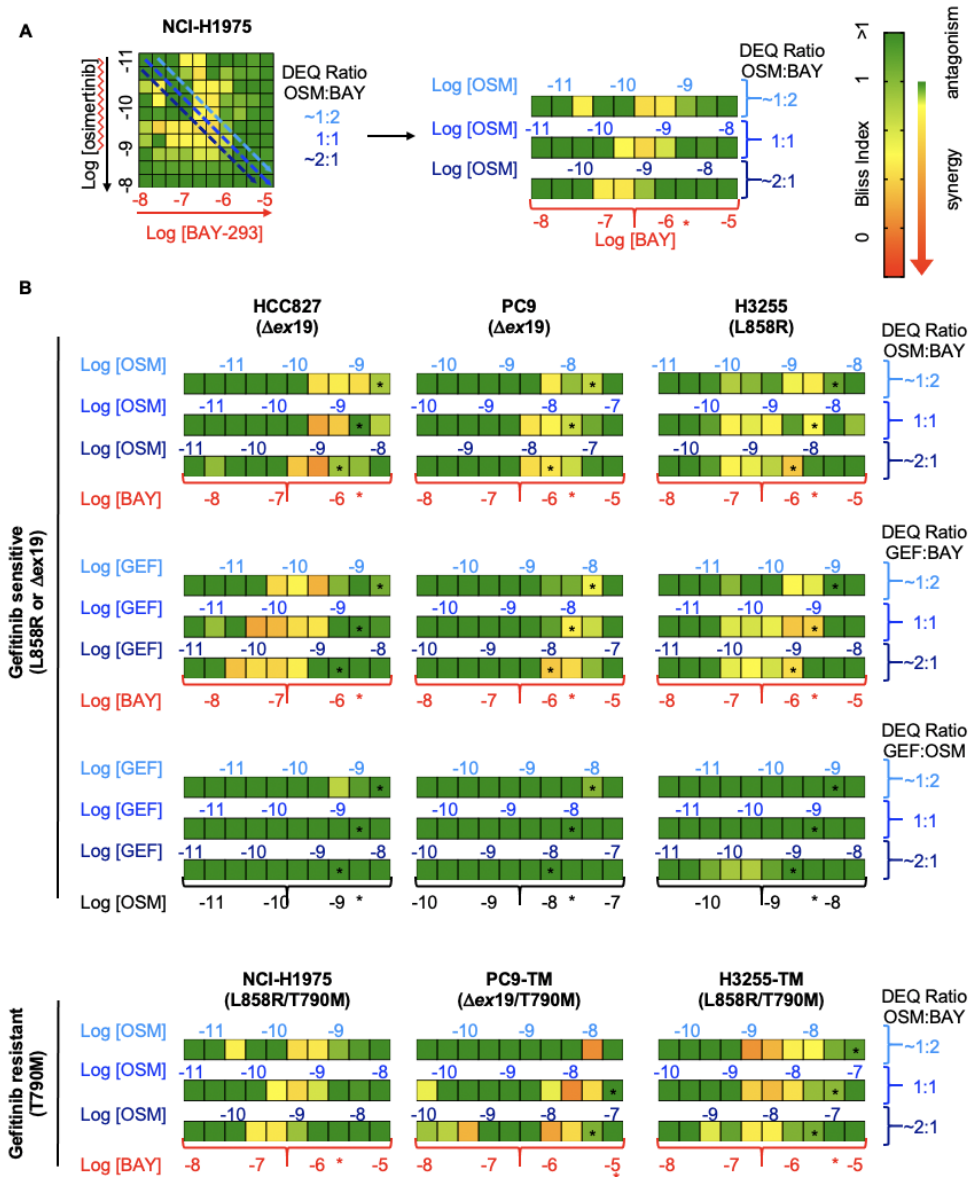


Figure7 (LC160222). Bliss Independence analysis showing that SOS1 inhibition synergizes with EGFR-TKI treatment to inhibit survival in multiple EGFR-mutated NSCLC cell lines. (A) Bliss Index heatmap from 3D spheroid cultured NCI-H1975 cells Fig. 2A (left) and horizontal projections of Bliss Indices of drug treatments at 2:1, 1:1, and 1:2 ratios of osimertinib:BAY-293 based on dose equivalencies (right). Increasingly synergistic interactions (Bliss index < 0.85) are indicated by the corresponding heat map. The concentration of BAY-293 (held constant, bottom) and of osimertinib (above each horizontal projection) are given. The IC₅₀ for each individual drug are shown (*). (B) Bliss Index heatmaps based on A for the indicated gefitinib-sensitive and gefitinib-resistant cell lines at 2:1, 1:1, and 1:2 ratios of osimertinib, gefitinib, and BAY-293 based on dose equivalencies. Data for NCI-H1975 cells are the same as in A. Data are presented as the mean from three independent experiments. For each experiment, three technical replicates were assessed.

We first assessed the role of Sos2 deletion on EGFR-TKI sensitivity in MEFs, and found that, similar to the data we originally saw using gefitinib, Sos2 deletion synergizes with osimertinib to inhibit transformation in MEFs expressing EGFR (L858R/T790M) (Fig. 8).

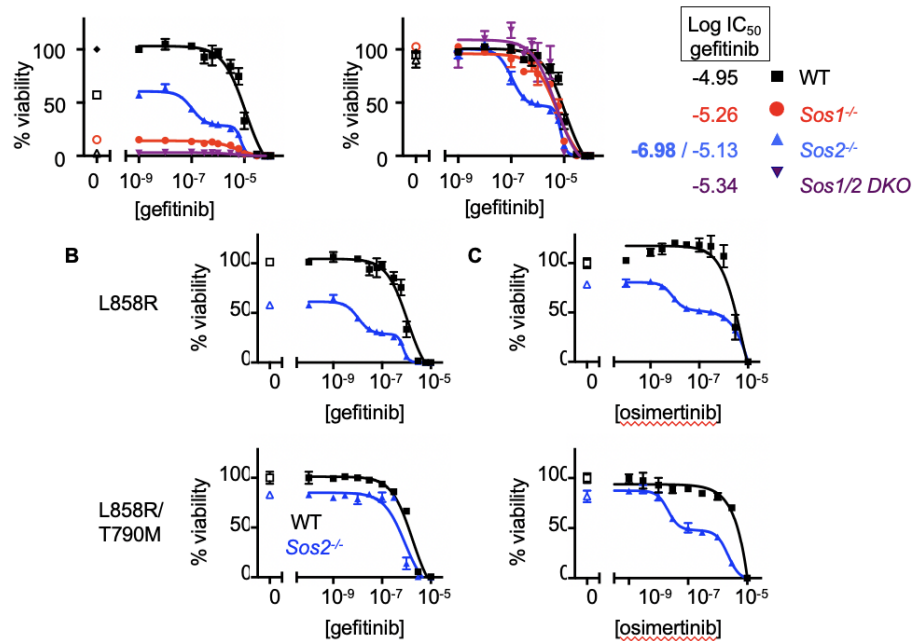


Fig 8 (LC160222). *Sos2* deletion synergizes with EGFR-TKI treatment to inhibit mutant EGFR-driven transformation. **A.** Dose-response curve to the 1st generation EGFR-TKI gefitinib in *Sos1* KO, *Sos2* KO, or combined *Sos1/2* DKO MEFs expressing a gefitinib-sensitive (L858R) EGFR mutant. **B-C.** Dose-response curve to the 1st generation EGFR-TKI gefitinib **B** or the 3rd generation EGFR-TKI osimertinib **C** in *Sos2* KO cells. *Sos2*^{-/-} MEFs showed a biphasic dose response to EGFR-TKI treatment in responsive cells. This was due to blocking the transforming capacity of mutant EGFR.

We have assessed the dose-response curve for Osimertinib in NT versus *SOS2* KO cells in all of the cell lines over a four day period. We found that in 10% serum, *SOS2* deletion does not alter osimertinib-induced killing in either 2D or 3D culture after 4 days of treatment (see Fig. 3 as an example in H1975 cells and Fig. 9 as an example in PC9 cells).

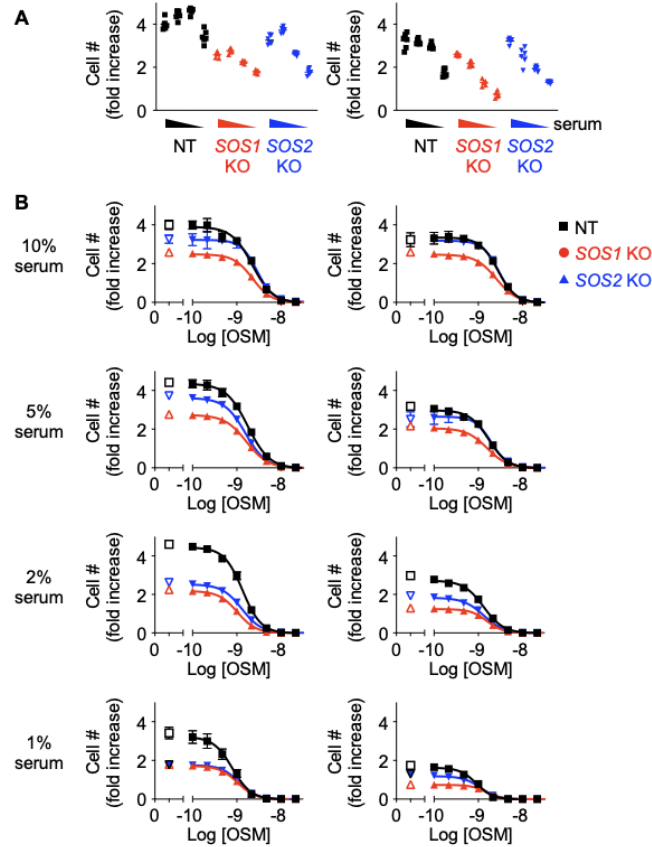


Fig. 9 (LC160222). *SOS1* and *SOS2* deletion enhances osimertinib-induced inhibition of transformation in PC9 cells. NT controls, *SOS1* KO or *SOS2* KO PC9 cells were cultured under 3D conditions in decreasing doses of serum (10%, 5%, 2%, or 1%). Cells were either left untreated (A) or were treated with increasing doses of osimertinib, and cell number was assessed at day 0, day 4, and day 7. We had previously found that *SOS1* KO inhibits transformation. Strikingly, we also found that *SOS2* KO inhibits transformation at limiting serum conditions (A) and may enhance the ability of osimertinib to inhibit transforming growth (B). Western blots confirming deletion are in Fig. 1.

Further, *SOS2* deletion does not enhance the marked synergy we observe between Osimertinib and the *SOS1* inhibitor BAY-293 in three different NSCLC cell lines (Fig. 10). This data was published in 2020 (Theard et al., *eLife*, 2020).

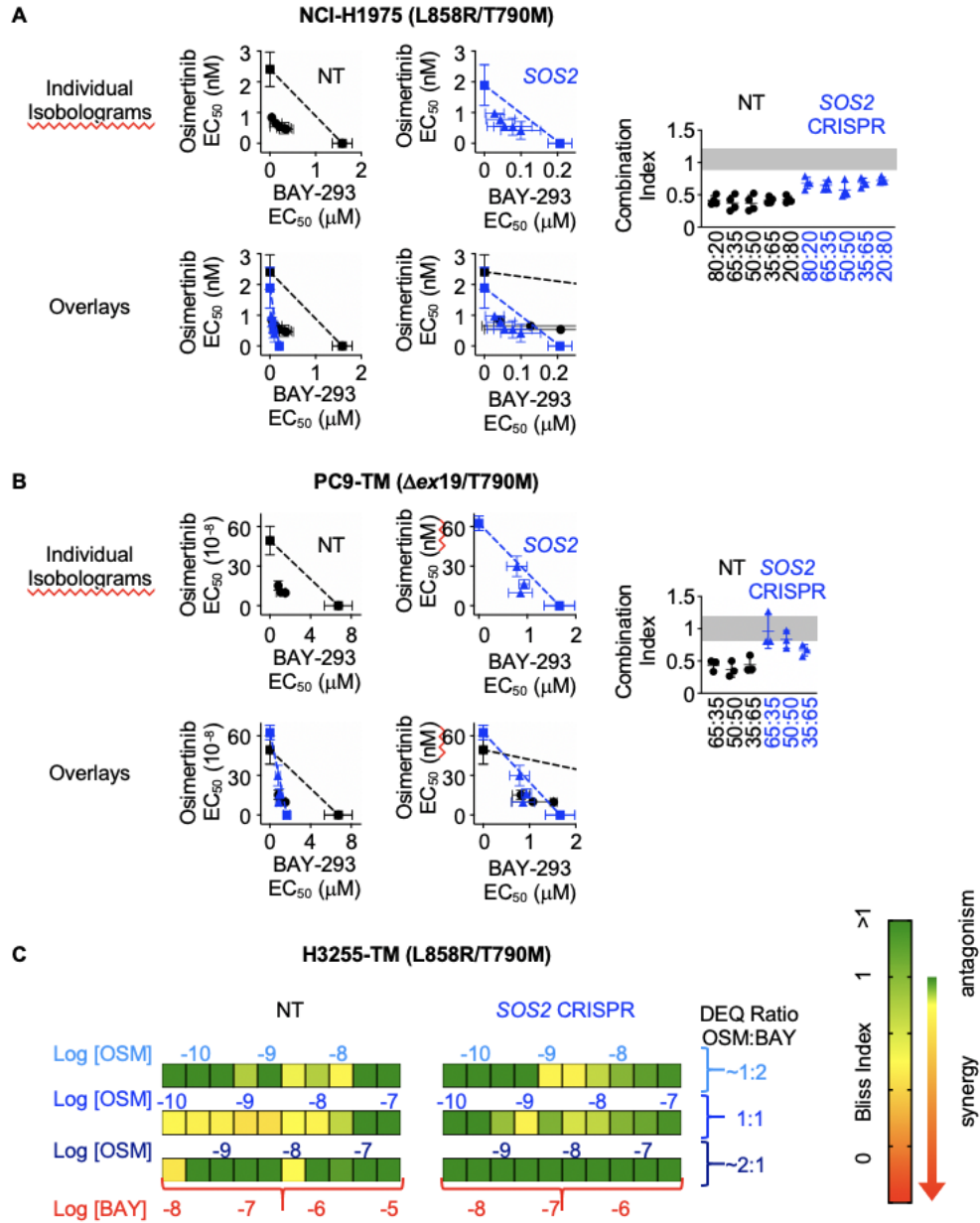


Figure 10 (LC160222). SOS2 deletion does not enhance the synergistic interaction between SOS1 inhibition and EGFR-TKI treatment.

(A-B) Isobologram analysis (left) and Combination Index (right) from dose-equivalent treatments of osimertinib and BAY-293 in H1975 (A) or PC9-TM (B) cells where SOS2 has been deleted (blue) versus NT controls (black). Overlay plots on two different BAY-293 dosing scales are shown below the individual isobologram plots. Additive effects occur on the dashed lines of the isobologram plot and have a CI 0.8-1.2 (gray box), whereas synergistic interactions fall below the dashed lines and have a CI < 0.8.

(C) Bliss Index heatmaps for H3255-TM cells where SOS2 has been deleted versus NT controls treated at at 1:2, 1:1, and 2:1 ratios of osimertinib and BAY-293 based on dose equivalencies.

Data are presented as mean +/- s.d. from three independent experiments.

For each experiment, three technical replicates were assessed.

However, we have found that *SOS2* deletion has a significant effect on the ability of osimertinib to inhibit transformation in 3D culture. These experiments require that cells be cultured long enough for transformation to be observed. First, when modeling HGF-stimulated osimertinib resistance in H1975 cells, we found that either *SOS1* or *SOS2* deletion reduced the dose of osimertinib required to inhibit transformation (Fig. 3). Further, under reduced serum conditions (2%), *SOS2* deletion reduces overall transforming growth and enhances osimertinib-induced killing in PC9 cells (Fig. 9).

3. Assessment of EGFR-TKI resistance following *Sos1* or *Sos2* re-introduction.
4. Assessment of EGFR-TKI resistance in WT and *SOS* KO MEFs using 96 well plate assay.

Since we are using CRISPR/Cas9 to delete *SOS1* and *SOS2* (rather than shRNA knockdowns), we are able to fully delete *SOS1* and *SOS2* in lung cancer cell lines and assess the emergence of EGFR-TKI resistance. Using these cells, we have assessed the generation of Osimertinib resistance in NCI-H1975 cells after either *SOS1* or *SOS2* deletion. Excitingly, we have found that deletion of *SOS2* delays the formation of resistance, and reduces the overall number of resistant colonies that form in a 96-well plate assay (Fig. 7). We also found that *SOS1* deletion or, in very preliminary data *SOS1* inhibition using BAY-293 or BI-3406, blocks osimertinib resistance in H1975 cells (Fig. 8). This exciting finding is the basis for the CDMRP/LCRP 2020 Idea Award that I submitted August 2020.

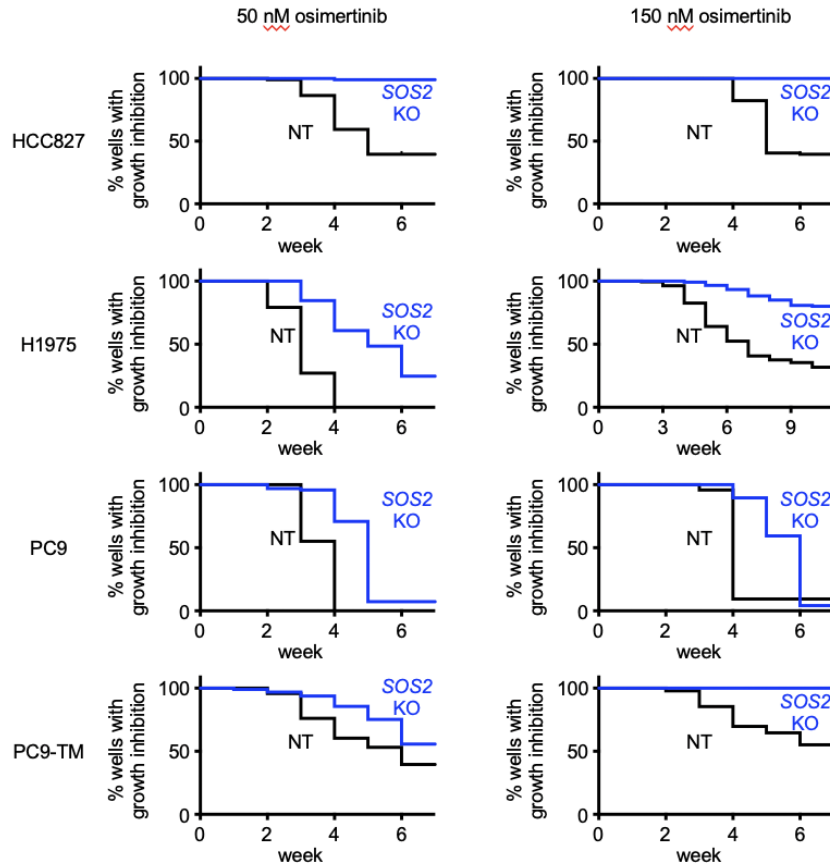


Figure 11 (LC160222). *SOS2* deletion limits osimertinib resistance in cell culture models
 Multi-well resistance experiments showing that *SOS2* deletion delays the development of osimertinib resistance and reduces the overall number of osimertinib resistant colonies in EGFR-mutated NSCLC cell lines treated with 50 nM (left) or 150 nM (right) osimertinib when compared to NT control.

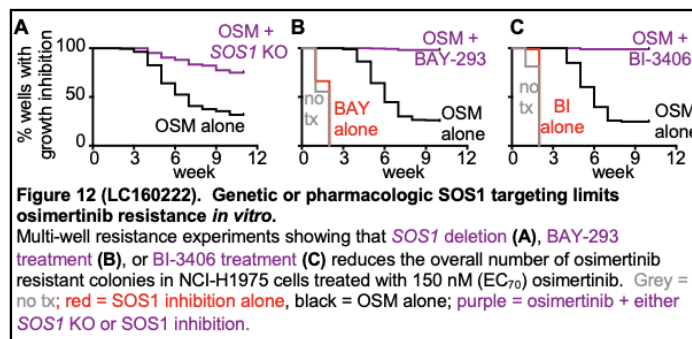


Figure 12 (LC160222). Genetic or pharmacologic *SOS1* targeting limits osimertinib resistance *in vitro*.
 Multi-well resistance experiments showing that *SOS1* deletion (A), BAY-293 treatment (B), or BI-3406 treatment (C) reduces the overall number of osimertinib resistant colonies in NCI-H1975 cells treated with 150 nM (EC_{70}) osimertinib. Grey = no tx; red = *SOS1* inhibition alone, black = OSM alone; purple = osimertinib + either *SOS1* KO or *SOS1* inhibition.

Aim 1, Major Task 3: Determine whether *Sos1* or *Sos2* are required for mutant EGFR-driven tumorigenesis *in vivo*

1. No animal use will be initiated until ACURO approval has been obtained.
2. Crossing of *Sos1^{fl/fl}* and *Sos1^{fl/fl}Sos2^{-/-}* mice separately onto each of three transgenic backgrounds (tetO-EGFR, CC10^{rtTA}, and Nkx2.1-CRE^{ERT2}).
3. Getting the first “informative mice” out of the above crosses.
4. Preliminary assessment of tumor development in above mice.

Unfortunately, the experiments were being done in the colony of my mentor for this grant, Dr. Udayan Guha. Dr. Guha did not get tenure and was forced to close his laboratory and animal

colony. We have since focused our efforts on obtaining preliminary data that allowed us to get CRADA funding from Boehringer Ingelheim to assess their SOS1 inhibitor in EGFR-mutant xenograft studies (cell lines). We are also seeking funding to do similar experiments in PDX models through the CDMRP.

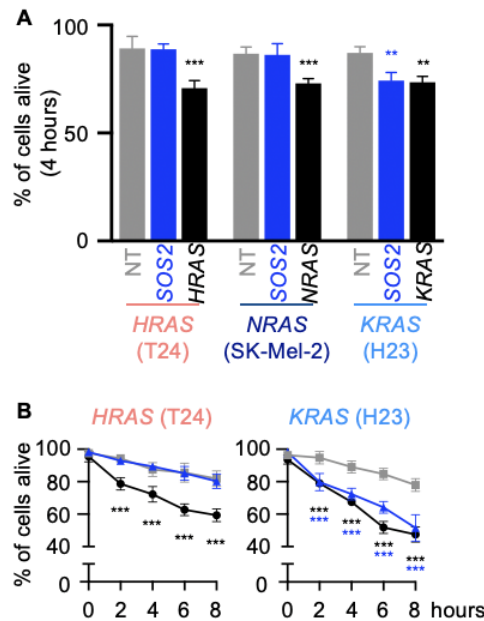
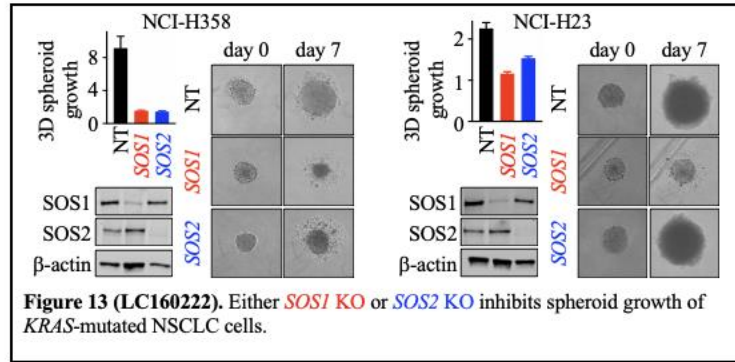
Aim 2, Major Task 1: Determine if inhibiting K-Ras–Sos–Ras positive feedback signaling can synergize with targeted therapeutics to kill KRAS–mutated lung cancer cells

1. Successful knockdown (or knockout) of *Sos1* and *Sos2* in *KRAS* NSCLC cells.

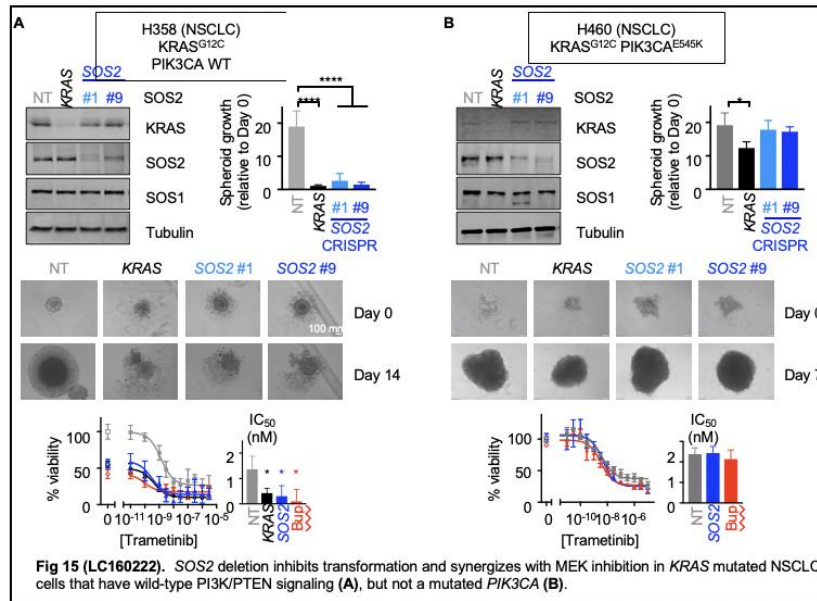
We have decided to use CRISPR/Cas9 to delete *SOS1* and *SOS2* in lung cancer lines, as we have found that this completely removes the gene in a majority of cells rather than reducing expression in all cells. We have designed and tested several sgRNAs that target *SOS1* or *SOS2*, and have found at least 3 sgRNAs that delete *SOS1* or *SOS2* in >80% of cells.

2. Assessment of proliferation and apoptosis, in above cells.

We assessed proliferation, transformation, and apoptosis in *KRAS* mutated NSCLC cell lines where we have deleted *SOS1* or *SOS2* using CRISPR/Cas9. We found that either *SOS1* or *SOS2* deletion reduces *KRAS*-driven transformation (Fig. 13). Further, we found that *SOS2* was required to protect *KRAS*-mutated LUAD cells from anoikis, or detachment-induced cell death (Fig. 14). *SOS2* transformation data were published in 2018 (Sheffels et al., *Sci Signaling*, 2018) and the effects on anoikis were published in 2019 (Sheffels et al., *Small GTPases*, 2019). .

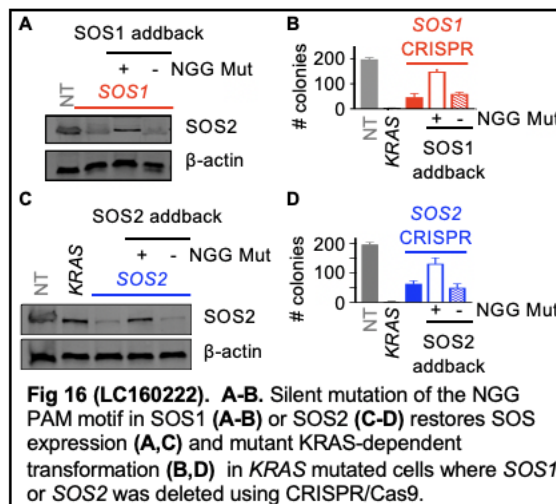


We have also found that in NCI-H460 cells (*KRAS* and *PIK3CA* mutated), *SOS2* deletion does not reduce oncogenic transformation or synergize with MEK inhibition to limit survival. We hypothesized that this is due to a bypass of *SOS2*-WT RAS-PI3K signaling by the *PIK3CA* mutation. This exciting finding has directly led to a new study assessing *SOS2* as a therapeutic target in NSCLC that was funded by the LCRP as an IDEA Award in 2018. These data are shown in Fig. 15.



3. Successful re-introduction of Sos1 or Sos2 mutants.

We generated SOS1 and SOS2 silent mutations in the PAM (NGG) motif necessary for CRISPR/Cas9 deletion to allow us to reintroduce WT or mutated SOS1 or SOS2. Reintroduction of WT SOS1 or SOS2 rescues transformation in KRAS mutated cells (Fig. 16).



4. Assessment of proliferation and apoptosis, in above cells.
5. Test KRAS “synthetic lethal” inhibitors treatment in NSCLC cells.
6. Assessment of synergy between *sos1* or *sos2* deletion and inhibitor treatments in above cells.

We found significant synergy between *SOS2* deletion and MEK inhibition in blocking transformation (3D growth) of KRAS mutated cancer cells (Sheffels et al., *Science*

Signaling (2018). Our data showed that *SOS2* deletion substitutes for a PI3K inhibitor, cooperating with a MEK inhibitor to block transformation. This is a seminal finding. We further found that this synergy only occurs when PI3K/AKT signaling is WT. This formed the basis of aim 2 of our 2018 CDMRP/LCRP grant.

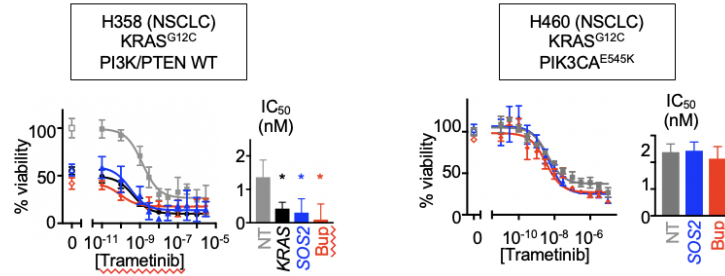


Figure 17 (LC160222). *SOS2* deletion synergizes with the MEK inhibitor trametinib in *KRAS*-mutated NSCLC cell lines with WT PI3K/PTEN. *SOS2* was deleted in H358 (*KRAS*-mutated/*PIK3CA* WT) and H460 (*KRAS*-mutated/*PIK3CA*-mutated) NSCLC cells using CRISPR/Cas9. *SOS2* KO cells and NT control cells were treated with increasing doses of trametinib. NT cells were also treated with trametinib + an IC_{50} dose of buparlisib as a control for inhibiting PI3K. We found that *SOS2* deletion synergized with MEK inhibition to inhibit growth of *KRAS*-mutated/*PIK3CA* WT cells as well as the combination of MEK + PI3K inhibition. In contrast, this synergy was lost in cells with mutated *PIK3CA*.

Further, we found that *SOS1* deletion or *SOS1* inhibition synergizes with *KRAS*^{G12C} inhibitors in *KRAS*^{G12C}-mutated LUAD cells (Fig. 18 and Fig. 19). These data are exciting, and are a seminal part of our CDMRP 2020 proposal and the R01 we are writing for October 2020 submission.

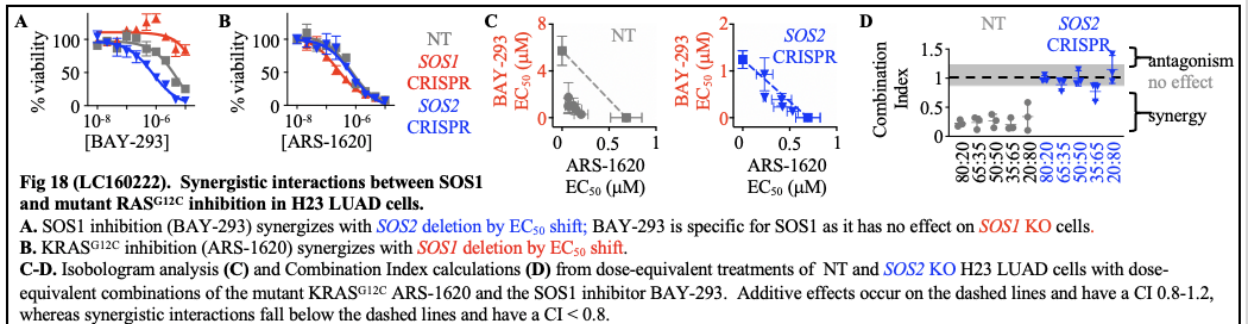


Fig 18 (LC160222). Synergistic interactions between *SOS1* and mutant *RAS*^{G12C} inhibition in H23 LUAD cells.

A. *SOS1* inhibition (BAY-293) synergizes with *SOS2* deletion by EC_{50} shift; BAY-293 is specific for *SOS1* as it has no effect on *SOS1* KO cells.

B. *KRAS*^{G12C} inhibition (ARS-1620) synergizes with *SOS1* deletion by EC_{50} shift.

C-D. Isobologram analysis (**C**) and Combination Index calculations (**D**) from dose-equivalent treatments of NT and *SOS2* KO H23 LUAD cells with dose-equivalent combinations of the mutant *KRAS*^{G12C} ARS-1620 and the *SOS1* inhibitor BAY-293. Additive effects occur on the dashed lines and have a CI 0.8-1.2, whereas synergistic interactions fall below the dashed lines and have a CI < 0.8.

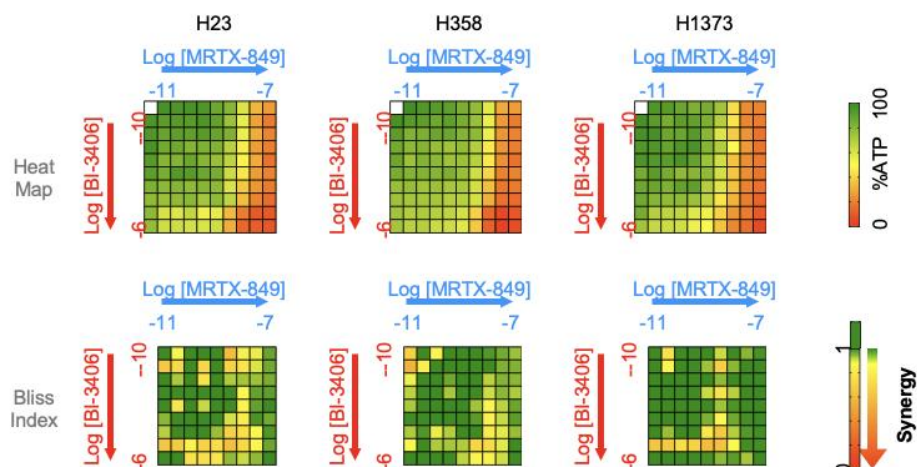


Fig. 19 (LC160222). The clinical $KRAS^{G12C}$ inhibitors MRTX849 synergizes with BI-3406 to inhibit $KRAS^{G12C}$ -mutated cell growth in 3D spheroid culture.

Aim 2, Major Task 2: Determine the potential for targeting Sos–dependent feedback signaling to treat $KRAS$ –driven lung adenocarcinoma *in vivo*

1. No animal use will be initiated until ACURO approval has been obtained.
2. Successful cloning of shRNAs into a doxycycline-inducible lentiviral vector.

We have dox-inducible Cas9, and have cloned the sgRNAs for SOS1 and SOS2 into vectors lacking Cas9.

3. Successful introduction of doxycycline inducible shRNA constructs into $KRAS$ mutant NSCLC cell lines.
4. Successful knockdown of Sos1 and Sos2 in a doxycycline-inducible manner in the above cells.
5. Assessment of tumor xenograft growth in NSCLC cells where *sos1* or *sos2* have been knocked either prior to tumor cell injection, at the time of tumor injection, or after tumor formation occurs.

These experiments were not able to be started due to the COVID-19 shut down. We have further learned from our *in situ* work that SOS1 inhibition is a much better treatment than SOS1 KO for long-term animal studies. We are currently seeking funding for these important studies.

What opportunities for training and professional development has the project provided?

If the project was not intended to provide training and professional development opportunities or there is nothing significant to report during this reporting period, state “Nothing to Report.”

Describe opportunities for training and professional development provided to anyone who worked on the project or anyone who was involved in the activities supported by the project. “Training” activities are those in which individuals with advanced professional skills and experience assist others in attaining greater proficiency. Training activities may include, for

example, courses or one-on-one work with a mentor. “Professional development” activities result in increased knowledge or skill in one’s area of expertise and may include workshops, conferences, seminars, study groups, and individual study. Include participation in conferences, workshops, and seminars not listed under major activities.

I have presented this work at research seminars for three different departments at the NCI (Pediatric Oncology Branch, Laboratory of Cell and Developmental Signaling, Laboratory of Cancer Biology and Genetics.

How were the results disseminated to communities of interest?

If there is nothing significant to report during this reporting period, state “Nothing to Report.”

Describe how the results were disseminated to communities of interest. Include any outreach activities that were undertaken to reach members of communities who are not usually aware of these project activities, for the purpose of enhancing public understanding and increasing interest in learning and careers in science, technology, and the humanities.

The SOS2 findings were published in two manuscripts:

Sheffels E, Sealover NE, Wang C, Kim DH, Vazirani IA, Lee E, Tyrell E, Morrison DK, Luo J, and **Kortum RL** (2018). Oncogenic Ras isoforms show a hierarchical requirement for SOS2 to drive transformation. *Science Signaling*, **11**:eaar8371.

Sheffels E, Sealover NE, Theard PT, and **Kortum RL** (2019). Anchorage-independent growth conditions reveal a differential SOS2 dependence for transformation and survival in RAS-mutant cancer cells. *Small GTPases*, May 7:1-12.

The EGFR findings were published in the recently accepted manuscript:

Theard PT, Sheffels E, Sealover NE, Linke AJ, Pratico DJ, and **Kortum RL** (2020). Marked Synergy by Vertical Inhibition of EGFR signaling in NSCLC Spheroids: SOS1 as a therapeutic target in EGFR-mutated cancer. *eLife*, **9**:e58204.

We also contributed significantly to a manuscript understanding specificity in the RAS/RAF interaction important for KRAS-driven oncogenesis:

My graduate student Erin Sheffels has presented the KRAS research at two local meetings (USU Research Days Poster and NCI Signaling Retreat Poster) and one national (ASCB/EMBO Annual Meeting, Washington D.C.) meeting.

A fourth year medical student, David Prattico, did his CAPSTONE project working on the EGFR study with Patricia Theard. He presented his findings in a USU Research Days Poster.

Describe briefly what you plan to do during the next reporting period to accomplish the goals and objectives.

This is the final reporting period. We are currently writing a methods paper using this technique for Bio-Protocols and will submit this in September 2020. We plan to submit a SOS1/KRAS manuscript in either late 2020 or early 2021.

4. **IMPACT:** Describe distinctive contributions, major accomplishments, innovations, successes, or any change in practice or behavior that has come about as a result of the project relative to:

What was the impact on the development of the principal discipline(s) of the project?

If there is nothing significant to report during this reporting period, state “Nothing to Report.”

Describe how findings, results, techniques that were developed or extended, or other products from the project made an impact or are likely to make an impact on the base of knowledge, theory, and research in the principal disciplinary field(s) of the project. Summarize using language that an intelligent lay audience can understand (Scientific American style).

Most current studies of genes whose deletion may change oncogenic proliferation are done under anchorage-dependent (attached, 2D) conditions. Our approach, in which we use a combination of genetic and pharmacologic manipulations to understand the role of SOS1 and SOS2 in oncogenesis under anchorage-independent (3D) growth conditions, is highly innovative, as it has revealed novel aspects of RAS effector biology that could not be appreciated under 2D growth conditions. *EGFR*-mutated cells show differential RTK expression and phosphorylation in 3D versus 2D conditions and we and others have shown that they respond more robustly to *EGFR*-TKIs in 3D cultures compared to 2D settings (48); *KRAS*-mutated cell lines deemed “*KRAS*-independent” in 2D culture still require *KRAS* for anchorage-independent growth (54-57), and some *KRAS*^{G12C}-mutated NSCLC cell lines respond to *KRAS*(G12C) inhibitors in 3D culture and *in vivo* but not in 2D adherent culture. The relevance of 3D culture systems extends to the identification of novel therapeutic targets and therapeutic combinations. We found that cells expressing mutated RAS isoforms show differential sensitivity to pharmacologic PI3K/AKT or Raf/MEK/ERK effector pathway inhibition, but only under 3D growth conditions. In *KRAS*-mutated LUAD cells we showed that SOS2 is specifically required for PI3K-dependent protection from anoikis and *SOS2* deletion synergizes with MEK inhibition to kill *KRAS* mutated cells only under 3D culture conditions. In *EGFR*-mutated LUAD cells, we showed

marked synergy between vertical inhibition of EGFR and SOS1 in *EGFR* mutated cancer cells, but again only under 3D culture conditions. Further, specific SOS1 and SHP2 inhibitors are much more efficacious in 3D cultured cells compared to 2D adherent cultures, and we found that the SOS1 inhibitor BI-3406 can only inhibit ERK signaling under 3D, but not 2D culture condition. Notably, for each of these fundamental findings we only observed this differential sensitivity only in 3D growth assays, not in assays assessing 2D growth. This finding suggests that we must take care in choosing the appropriate culture system to identify and test novel therapeutic targets to treat *EGFR* or *KRAS* mutant tumors, and that anchorage-independent 3D growth screens should be used to supplement current 2D screening efforts.

What was the impact on other disciplines?

If there is nothing significant to report during this reporting period, state “Nothing to Report.”

Describe how the findings, results, or techniques that were developed or improved, or other products from the project made an impact or are likely to make an impact on other disciplines.

Nothing to report

What was the impact on technology transfer?

If there is nothing significant to report during this reporting period, state “Nothing to Report.”

Describe ways in which the project made an impact, or is likely to make an impact, on commercial technology or public use, including:

- *transfer of results to entities in government or industry;*
- *instances where the research has led to the initiation of a start-up company; or*
- *adoption of new practices.*

Our work has led directly to a CRADA (Cooperative Research And Development Agreement) between our lab and Boehringer Ingelheim assessing their clinical SOS1 inhibitors in *EGFR*-mutated NSCLC. These are already in phase 1 trials for *KRAS* mutated cancers.

What was the impact on society beyond science and technology?

If there is nothing significant to report during this reporting period, state “Nothing to Report.”

Describe how results from the project made an impact, or are likely to make an impact, beyond the bounds of science, engineering, and the academic world on areas such as:

- *improving public knowledge, attitudes, skills, and abilities;*
- *changing behavior, practices, decision making, policies (including regulatory policies), or social actions; or*
- *improving social, economic, civic, or environmental conditions.*

Nothing to report

- 5. CHANGES/PROBLEMS:** The PD/PI is reminded that the recipient organization is required to obtain prior written approval from the awarding agency grants official whenever there are significant changes in the project or its direction. If not previously reported in writing, provide the following additional information or state, "Nothing to Report," if applicable:

Nothing to report

Actual or anticipated problems or delays and actions or plans to resolve them

Describe problems or delays encountered during the reporting period and actions or plans to resolve them.

Nothing to report

Changes that had a significant impact on expenditures

Describe changes during the reporting period that may have had a significant impact on expenditures, for example, delays in hiring staff or favorable developments that enable meeting objectives at less cost than anticipated.

Nothing to report

Significant changes in use or care of human subjects, vertebrate animals, biohazards, and/or select agents

Describe significant deviations, unexpected outcomes, or changes in approved protocols for the use or care of human subjects, vertebrate animals, biohazards, and/or select agents during the reporting period. If required, were these changes approved by the applicable institution committee (or equivalent) and reported to the agency? Also specify the applicable Institutional Review Board/Institutional Animal Care and Use Committee approval dates.

Significant changes in use or care of human subjects

n/a

Significant changes in use or care of vertebrate animals

n/a

Significant changes in use of biohazards and/or select agents

n/a

6. **PRODUCTS:** List any products resulting from the project during the reporting period. If there is nothing to report under a particular item, state “Nothing to Report.”

- **Publications, conference papers, and presentations**

Report only the major publication(s) resulting from the work under this award.

Journal publications. *List peer-reviewed articles or papers appearing in scientific, technical, or professional journals. Identify for each publication: Author(s); title; journal; volume: year; page numbers; status of publication (published; accepted, awaiting publication; submitted, under review; other); acknowledgement of federal support (yes/no).*

1. Sheffels E, Sealover NE, Wang C, Kim DH, Vazirani IA, Lee E, Terrell E, Morrison DK, Luo J, and **Kortum RL** (2018). Oncogenic RAS isoforms show a hierarchical requirement for the guanine nucleotide exchange factor SOS2 to mediate cell transformation. *Science Signaling*, **11**:eaar8371.
PMID:30181243
2. Sheffels E, Sealover NE, Theard PT, and **Kortum RL** (2019). Oncogenic Ras isoforms show a hierarchical requirement for SOS2 to drive transformation. *Small GTPases*, May 7:1-12.
PMID: 31062644
3. Terrell EM, Durrant DE, Ritt DA, Sheffels E, Sealover NE, Esposito D, Zhou Z, Hancock J, **Kortum RL**, and Morrison DK (2019). Distinct Binding Preferences Between Individual Ras and Raf Family Members and the Impact on Oncogenic Ras Signaling. *Mol Cell*, **76**:872-84.
PMID:31606273
4. Theard PT, Sheffels E, Sealover NE, Linke AJ, Pratico DJ and **Kortum RL** (2020). Marked synergy by vertical inhibition of EGFR signaling in NSCLC spheroids shows SOS1 is a therapeutic target in EGFR-mutated cancer. *eLife*, **9**:e58204.
PMID:32897190

Books or other non-periodical, one-time publications. *Report any book, monograph, dissertation, abstract, or the like published as or in a separate publication, rather than a periodical or series. Include any significant publication in the proceedings of a one-time conference or in the report of a one-time study, commission, or the like. Identify for each one-time publication: author(s); title; editor; title of collection, if applicable; bibliographic information; year; type of publication (e.g., book, thesis or dissertation); status of publication (published; accepted, awaiting publication; submitted, under review; other); acknowledgement of federal support (yes/no).*

We were invited to write the June 2020 NCI RAS dialogue. There was no opportunity to cite support in this format:

Sheffels E and **Kortum RL** (2020). SOS Signaling in RAS-mutated cancers. *NCI RAS Initiative: RAS Dialogue*, June 2020.

<https://www.cancer.gov/research/key-initiatives/ras/ras-central/blog/2020/kortum-sos-proteins-in-kras-cancers>

My first student, Erin Sheffels, completed her PhD dissertation. CDMRP support was acknowledged:

Sheffels E (2020). The RasGEFs SOS1 and SOS2 are Potential Therapeutic Targets in RAS-Driven Cancers. USU MCB Program Doctoral Dissertation.

Other publications, conference papers and presentations. *Identify any other publications, conference papers and/or presentations not reported above. Specify the status of the publication as noted above. List presentations made during the last year (international, national, local societies, military meetings, etc.). Use an asterisk (*) if presentation produced a manuscript.*

This represents a list of all conference presentations between 06/2019 -05/2020. The publications have been listed above.

1. Sheffels E, Sealover NE, Theard PL, and **Kortum RL**, “3D culture conditions reveal therapeutic signaling vulnerabilities in RAS-mutant cancer cells” USUHS Research Days Graduate Student Colloquium, May 2020. Poster presentation.
2. Theard PL and **Kortum RL**, “Marked Synergy by Bivalent Inhibition of EGFR signaling in NSCLC Spheroids: SOS1 as a therapeutic target in EGFR-mutated cancer” USUHS Research Days Graduate Student Colloquium, May 2020. Poster presentation.
3. Sealover NE, Linke A, Theard PL, Sheffels E, Yohe M, and **Kortum RL**, “Assessing potential therapeutic approaches in Rhabdomyosarcoma” USUHS Research Days Graduate Student Colloquium, May 2020. Poster presentation.
4. Pratico D, Theard PL, and **Kortum RL**, “Investigation of Therapeutic Resistance of EGFR-driven NSCLC Cells Through Imaging and Dose Response Curves” USUHS Research Days Graduate Student Colloquium, May 2020. Poster presentation.
5. Sheffels E, Sealover NE, Theard PL, and **Kortum RL**, “3D culture conditions reveal therapeutic signaling vulnerabilities in RAS-mutant cancer cells” ASCB/EMBO Annual Meeting, Washington D.C., December 2019. Poster presentation.
6. Theard PL and **Kortum RL**, “SOS1 and SOS2 are therapeutic targets that play unique roles in mutant EGFR-driven NSCLC cells” ASCB/EMBO Annual Meeting, Washington D.C., December 2019. Poster presentation.

7. Sheffels E, Sealover NE, Theard PL, and **Kortum RL**, “Anchorage-independent growth conditions reveal a differential SOS2 dependence for transformation and survival in RAS-mutant cancer cells” 12th Annual Combined Signaling Retreat, NCI, NIH. November 2019. Poster presentation.
8. Theard PL and **Kortum RL**, “SOS1 and SOS2 are therapeutic targets that play unique roles in mutant EGFR-driven NSCLC cells” 12th Annual Combined Signaling Retreat, NCI, NIH. November 2019. Poster presentation.
9. Sealover NE, Sheffels E, and **Kortum RL**, “Toward a comprehensive understanding of how RasGEF-WT RAS signaling influences mutant RAS-driven transformation” 12th Annual Combined Signaling Retreat, NCI, NIH. November 2019. Poster presentation.

- **Website(s) or other Internet site(s)**

List the URL for any Internet site(s) that disseminates the results of the research activities. A short description of each site should be provided. It is not necessary to include the publications already specified above in this section.

We were invited to write the June 2020 NCI RAS dialogue. There was no opportunity to cite support in this format:

Sheffels E and **Kortum RL** (2020). SOS Signaling in RAS-mutated cancers. *NCI RAS Initiative: RAS Dialogue*, June 2020.

<https://www.cancer.gov/research/key-initiatives/ras/ras-central/blog/2020/kortum-sos-proteins-in-kras-cancers>

- **Technologies or techniques**

Identify technologies or techniques that resulted from the research activities. Describe the technologies or techniques were shared.

The use of 3D spheroid cultures to assess the combined genetic and pharmacologic inhibition of transformation in EGFR mutated cells. This technique is in the published *eLife* manuscript. We are currently writing a methods paper using this technique for Bio-Protocols.

- **Inventions, patent applications, and/or licenses**

Identify inventions, patent applications with date, and/or licenses that have resulted from the research. Submission of this information as part of an interim research performance progress report is not a substitute for any other invention reporting required under the terms and conditions of an award.

Not applicable.

- **Other Products**

Identify any other reportable outcomes that were developed under this project. Reportable outcomes are defined as a research result that is or relates to a product, scientific advance, or research tool that makes a meaningful contribution toward the understanding, prevention, diagnosis, prognosis, treatment and /or rehabilitation of a disease, injury or condition, or to improve the quality of life. Examples include:

- *data or databases;*
- *physical collections;*
- *audio or video products;*
- *software;*
- *models;*
- *educational aids or curricula;*
- *instruments or equipment;*
- *research material (e.g., Germplasm; cell lines, DNA probes, animal models);*
- *clinical interventions;*
- *new business creation; and*
- *other.*

Not applicable.

7. PARTICIPANTS & OTHER COLLABORATING ORGANIZATIONS

What individuals have worked on the project?

Provide the following information for: (1) PDs/PIs; and (2) each person who has worked at least one person month per year on the project during the reporting period, regardless of the source of compensation (a person month equals approximately 160 hours of effort). If information is unchanged from a previous submission, provide the name only and indicate “no change”.

Name:	Robert Kortum, MD/PhD
Project Role:	PI
Researcher Identifier (e.g. ORCID ID):	
Nearest person month worked:	4.8

Contribution to Project:	Dr. Kortum has performed many of the experiments with graduate students and technicians and has analyzed all the data.
--------------------------	--

Funding Support:	
------------------	--

Name: Dr. Regina M. Day
Project Role: Mentor
Researcher Identifier (e.g. ORCID ID):
Nearest person month worked: 0.60

Contribution to Project: Provided mentoring on the successful running of a research program and helped focus Dr. Kortum's research toward important pre-clinical and clinical questions in lung cancer.

Name: Dr. Corey A. Carter
Project Role: Mentor
Researcher Identifier (e.g. ORCID ID):
Nearest person month worked: 0.60

Contribution to Project: Provided mentoring on understanding the pathophysiology of lung cancer and the critical clinical questions surrounding lung cancer treatment. Dr. Carter helped in the interpretation of data and the planning of experiments that involve combining SOS deletion with current therapeutics being used to treat EGFR- and KRAS-driven lung cancer

Name: Dr. Udayan Guha
Project Role: Mentor
Researcher Identifier (e.g. ORCID ID):
Nearest person month worked: 0.60

Contribution to Project: Provided mentoring on how to perform experiments using clinically relevant mouse models for lung cancer, and how to design experiments to understand the evolution of EGFR-TKI resistance. Dr. Guha helped in the interpretation of data and the planning of experiments that involve combining SOS deletion EGFR-TKIs, and on understanding EGFR-TKI resistance

Name: Nancy Sealover
Project Role: Graduate Student
Researcher Identifier (e.g. ORCID ID):
Nearest person month worked: 3

Contribution to Project: Ms. Sealover and Ms. Sheffels performed all of the KRAS experiments described in Aim 2 with the help of Dr. Kortum.

Funding Support:

Name: Erin Sheffels
Project Role: Graduate Student
Researcher Identifier (e.g. ORCID ID):
Nearest person month worked: 1

Contribution to Project: Ms. Sealover and Ms. Sheffels performed all of the KRAS experiments described in Aim 2 with the help of Dr. Kortum.

Funding Support:

Name: Patricia Theard
Project Role: MD/PhD Student
Researcher Identifier (e.g. ORCID ID):
Nearest person month worked: 3

Contribution to Project: Ms. Theard is performing all of the EGFR experiments with the help of Dr. Kortum outlined in Aim 1.

Funding Support:

Has there been a change in the active other support of the PD/PI(s) or senior/key personnel since the last reporting period?

If there is nothing significant to report during this reporting period, state “Nothing to Report.”

If the active support has changed for the PD/PI(s) or senior/key personnel, then describe what the change has been. Changes may occur, for example, if a previously active grant has closed and/or if a previously pending grant is now active. Annotate this information so it is clear what has changed from the previous submission. Submission of other support information is not necessary for pending changes or for changes in the level of effort for active support reported previously. The awarding agency may require prior written approval if a change in active other support significantly impacts the effort on the project that is the subject of the project report.

Nothing to report

If there is nothing significant to report during this reporting period, state “Nothing to Report.”

Describe partner organizations – academic institutions, other nonprofits, industrial or commercial firms, state or local governments, schools or school systems, or other organizations (foreign or domestic) – that were involved with the project. Partner organizations may have

provided financial or in-kind support, supplied facilities or equipment, collaborated in the research, exchanged personnel, or otherwise contributed.

Provide the following information for each partnership:

Organization Name:

Location of Organization: (if foreign location list country)

Partner's contribution to the project (identify one or more)

- *Financial support;*
- *In-kind support (e.g., partner makes software, computers, equipment, etc., available to project staff);*
- *Facilities (e.g., project staff use the partner's facilities for project activities);*
- *Collaboration (e.g., partner's staff work with project staff on the project);*
- *Personnel exchanges (e.g., project staff and/or partner's staff use each other's facilities, work at each other's site); and*
- *Other.*

Nothing to report

8. SPECIAL REPORTING REQUIREMENTS

COLLABORATIVE AWARDS: For collaborative awards, independent reports are required from BOTH the Initiating Principal Investigator (PI) and the Collaborating/Partnering PI. A duplicative report is acceptable; however, tasks shall be clearly marked with the responsible PI and research site. A report shall be submitted to <https://ers.amedd.army.mil> for each unique award.

QUAD CHARTS: If applicable, the Quad Chart (available on <https://www.usamraa.army.mil>) should be updated and submitted with attachments.

9. APPENDICES: Please see attached

Marked synergy by vertical inhibition of EGFR signaling in NSCLC spheroids shows SOS1 is a therapeutic target in EGFR-mutated cancer

Patricia L Theard, Erin Sheffels, Nancy E Sealover, Amanda J Linke, David J Pratico, Robert L Kortum*

Department of Pharmacology and Molecular Therapeutics, Uniformed Services University of the Health Sciences, Bethesda, United States

Abstract Drug treatment of 3D cancer spheroids more accurately reflects in vivo therapeutic responses compared to adherent culture studies. In EGFR-mutated lung adenocarcinoma, EGFR-TKIs show enhanced efficacy in spheroid cultures. Simultaneous inhibition of multiple parallel RTKs further enhances EGFR-TKI effectiveness. We show that the common RTK signaling intermediate SOS1 was required for 3D spheroid growth of EGFR-mutated NSCLC cells. Using two distinct measures of pharmacologic synergy, we demonstrated that SOS1 inhibition strongly synergized with EGFR-TKI treatment only in 3D spheroid cultures. Combined EGFR- and SOS1-inhibition markedly inhibited Raf/MEK/ERK and PI3K/AKT signaling. Finally, broad assessment of the pharmacologic landscape of drug-drug interactions downstream of mutated EGFR revealed synergy when combining an EGFR-TKI with inhibitors of proximal signaling intermediates SOS1 and SHP2, but not inhibitors of downstream RAS effector pathways. These data indicate that vertical inhibition of proximal EGFR signaling should be pursued as a potential therapy to treat EGFR-mutated tumors.

*For correspondence:
robert.kortum@usuhs.edu

Competing interests: The authors declare that no competing interests exist.

Funding: See page 25

Received: 23 April 2020

Accepted: 14 August 2020

Published: 08 September 2020

Reviewing editor: Seth J Corey, Cleveland Clinic, United States

© This is an open-access article, free of all copyright, and may be freely reproduced, distributed, transmitted, modified, built upon, or otherwise used by anyone for any lawful purpose. The work is made available under the [Creative Commons CC0 public domain dedication](https://creativecommons.org/licenses/by/4.0/).

Introduction

Lung cancer is the leading cause of cancer-related death worldwide; adenocarcinomas are the most common subtype of lung cancer. Oncogenic driver mutations in the RTK/RAS pathway are found in over 75% of lung adenocarcinomas (*Cancer Genome Atlas Research Network, 2014*). Activating EGFR mutations occur in 10–30% of lung adenocarcinomas and are the major cause of lung cancer in never-smokers. In patients whose tumors harbor either an L858R mutation or an exon 19 deletion (85% of EGFR mutated tumors), first-generation EGFR-tyrosine kinase inhibitors (TKIs) erlotinib and gefitinib enhance progression-free survival (*Mok et al., 2009; Yang et al., 2017; Eberhard et al., 2005*). However, resistance to first generation EGFR-TKIs invariably occurs. In most cases, acquired resistance to first generation EGFR-TKIs occurs via either a secondary EGFR ‘gatekeeper mutation’ (T790M, 50–60% of cases) that renders the receptor insensitive to first generation EGFR-TKIs or oncogenic shift to alternative RTKs (15–30%). To treat patients with T790M-mutated resistant tumors, the third generation EGFR-TKI osimertinib, which selectively targets activating EGFR mutant proteins including T790M but spares wild-type EGFR, was developed (*Jänne et al., 2015; Cross et al., 2014*). However, despite further enhancing survival of patients with EGFR-mutant tumors, resistance again emerges.

Unlike first-generation EGFR-TKIs, mechanisms driving osimertinib resistance are more variable, including both EGFR-dependent (10–30%) and EGFR-independent mechanisms (*Mancini et al., 2018; Romaniello et al., 2018; La Monica et al., 2017; Eberlein et al., 2015*). The most common

eLife digest Lung cancer is the leading cause of cancer-related deaths worldwide. In non-smokers, this disease is usually caused by a mutation in a protein found on the surface of a cell, called EGFR. In healthy lung cells, these proteins trigger a chain of chemical signals that tell the cells to multiply. However, faulty forms of EGFR make the cells grow uncontrollably, leading to the formation of tumors.

Current treatments use EGFR inhibitors that block the activity of these proteins. But cancer cells often become resistant to these treatments by activating other types of growth proteins. One way to overcome this resistance has been by targeting the signaling pathways within individual tumors. But since those pathways differ between tumors, it has been challenging to find a single therapy that can treat all drug-resistant cancer cells.

Now, Theard et al. assessed the therapeutic effects of blocking a specific protein inside lung cells, called SOS1, which is involved in growth signaling in all tumor cells. Six different types of human lung cancer cells were used, all of which had faulty forms of EGFR, with three of the cell types showing drug resistance to current therapies. The cancer cells were either exposed to EGFR inhibitors only or to a combination of EGFR and SOS1 inhibitors. The most effective treatment was found to be through combinational therapy, with enhanced killing of drug-resistant cells.

Theard et al. further assessed the effect of combinational therapy using cells kept in two different ways. Cancer cells were either grown in a two-dimensional format, with cells forming a single cell layer, or in a three-dimensional format, where cells were multi-layered and grew on top of each other as self-aggregating spheroids. Combinational therapy treatment was only successful when the cells were grown in a three-dimensional format.

These findings highlight that future drug development studies should give consideration to the way cells are grown, as it can impact the results. They also provide a steppingstone towards tackling drug resistance in lung cancers that arise from EGFR mutations.

EGFR-independent resistance mechanisms involve reactivation of the RTK/RAS/effector pathway (Eberlein et al., 2015), often via enhanced signaling through parallel RTKs (Mancini et al., 2018; Romaniello et al., 2018; La Monica et al., 2017; Shi et al., 2016; Park et al., 2016; Kim et al., 2019; Taniguchi et al., 2019; Jimbo et al., 2019; Namba et al., 2019). Here, combining osimertinib with individual RTK inhibitors can both inhibit the development of resistance through the inhibited RTK and kill cancer cells with resistance driven by the specific RTK being inhibited. However, simultaneous inhibition of multiple RTKs with osimertinib may be required to eliminate oncogenic shift to alternative RTKs (Romaniello et al., 2018). Downstream of RAS, co-targeting intermediates of the RAF/MEK/ERK and PI3K/AKT pathways enhances osimertinib effectiveness, however, signaling through the uninhibited effector pathway may drive resistance (Tricker et al., 2015; Jacobsen et al., 2017; Ku et al., 2018; Ichihara et al., 2017). Thus, it may be important for therapeutic combinations including osimertinib to stifle all downstream RTK/RAS signaling to be effective.

Recent studies suggest that pharmacologic assessments of targeted therapeutics should be performed under 3D culture conditions rather than in 2D adherent cultures (Nunes et al., 2019; Langhans, 2018). 3D spheroids show altered growth characteristics, changes in cell surface proteins, altered metabolism, changes in activation of signaling pathways or altered responses to targeted pathway inhibitors, and are more resistant to drug-induced apoptosis compared to 2D adherent cultures signaling (Hao et al., 2019; Kim et al., 2011; Riedl et al., 2017; Jones et al., 2019). These differences may be particularly relevant in EGFR-mutated NSCLC. EGFR-mutated cells show differential RTK expression and phosphorylation in 3D versus 2D conditions (Ekert et al., 2014). Further, EGFR-mutated cells respond more robustly to first-generation EGFR-TKIs in 3D cultures, and these responses more closely resemble responses seen in vivo (Jacobi et al., 2017). These data highlight the need for pharmacologic assessment of therapeutics designed to treat EGFR-mutated NSCLC under 3D culture conditions.

The ubiquitously expressed RasGEFs (guanine nucleotide exchange factors) SOS1 and SOS2 (son of sevenless 1 and 2) are common signaling intermediates of RTK-mediated RAS activation. Although not initially considered as drug targets because of the low oncogenic potential of SOS

(Vigil et al., 2010), there has been renewed interest in SOS proteins as therapeutic targets for cancer treatment. We and others have shown that SOS1 and SOS2 may be important therapeutic targets in KRAS-mutated cancer cells (Jeng et al., 2012; Sheffels et al., 2018; Sheffels et al., 2019), and a specific SOS1 inhibitor (BAY-293) has recently been identified (Hillig et al., 2019). Here, we investigate SOS1 and SOS2 as potential therapeutic targets in EGFR-mutated lung adenocarcinoma cells. Using two distinct measures of pharmacologic synergy, we demonstrate that SOS1 inhibition using BAY-293 synergizes with osimertinib only under 3D spheroid culture conditions, and in doing so add to the growing evidence that pharmacologic assessment of novel therapeutics designed to treat cancer must be performed under 3D culture conditions (Ekert et al., 2014; Sheffels et al., 2018; Nunes et al., 2019; Janes et al., 2018; Jacobi et al., 2017). By assessing the pharmacologic landscape of EGFR/RAS pathway inhibitors, we demonstrate that inhibition of proximal signaling is required to synergize with osimertinib, and that combined EGFR and SOS1 inhibition synergizes to inhibit RAS effector signaling in 3D culture. These findings have significant therapeutic implications for the development of combination therapies to treat EGFR-mutated lung adenocarcinoma.

Results

SOS1 deletion inhibits transformation in EGFR-mutated NSCLC cells

Previous studies showed that EGFR-mutated NSCLC cell lines show much more robust responsiveness to first-generation EGFR-TKIs in 3D culture (monoculture cancer cell line spheroids or monoculture or mixed culture organoids in ECM/Matrigel) compared to 2D adherent culture, and further that 3D conditions more readily mirror EGFR-TKI responses seen in vivo (Jacobi et al., 2017). To confirm these findings and extend them to third-generation EGFR-TKIs, we assessed dose-dependent survival of both first-generation EGFR-TKI sensitive (HCC827, exon 19 deletion [Δ ex19]) or resistant (NCI-H1975, L858R/T790M) NSCLC cell lines to either gefitinib or osimertinib treatment under both adherent (2D) or spheroid (3D) culture conditions (Figure 1A). HCC827 and H1975 cells were plated in either adherent or spheroid cultures, allowed to rest for 48 hr, and then treated with increasing doses of either the first-generation EGFR-TKI gefitinib or the third-generation EGFR-TKI osimertinib for 4 days. HCC827 cells showed responsiveness to both EGFR-TKIs under 2D and 3D culture conditions, however in both cases 3D spheroid cultures showed a > 1 log enhancement in EGFR-TKI efficacy and enhanced overall growth inhibition. While NCI-H1975 cells were not sensitive to gefitinib, osimertinib treatment of H1975 cells showed enhanced efficacy and increased overall growth inhibition in 3D spheroids over 2D adherent cultures.

SOS1 and SOS2 are ubiquitously expressed RasGEFs responsible for transmitting EGFR signaling to downstream effector pathways. To determine whether SOS1 or SOS2 were required for 2D anchorage-dependent proliferation or 3D spheroid growth in EGFR-mutated NSCLC cells, SOS1 (Figure 1—figure supplement 1 and Munoz et al., 2016) or SOS2 (31) were deleted in pooled populations of HCC827 and H1975 cells to avoid clonal effects, and both proliferation and spheroid growth were assessed versus NT controls (Figure 1B and C). In adherent culture, neither SOS1 nor SOS2 deletion altered proliferation (Figure 1B). In contrast, SOS1 deletion completely inhibited spheroid growth in both HCC827 and H1975 cells, indicating that SOS1 was required to maintain the transformed phenotype in both cell lines. To determine whether SOS1 was generally required for mutant EGFR-driven transformation, we further deleted SOS1 or SOS2 in both first-generation sensitive NCI-H3255 (L858R) and PC9 (Δ ex19) cells and in subcultures of these cell lines that had acquired T790M mutations after continuous EGFR-TKI treatment (PC9-TM [de Bruin et al., 2014] and H3255-TM [Engelman et al., 2006]). In all cases, SOS1 deletion significantly diminished oncogenic transformation, whereas SOS2 deletion had variable effects on transformation depending on the EGFR mutated cell line examined (Figure 1D). These data indicate that SOS1 is the major Ras-GEF responsible for oncogenesis downstream of mutated EGFR.

BAY-293 was recently described as a specific inhibitor for SOS1 (Hillig et al., 2019). To determine whether SOS1 inhibition was similarly more effective in 3D spheroids over 2D adherent culture, we assessed dose-dependent survival of H1975 cells after BAY-293 treatment under both 2D and 3D culture conditions (Figure 1E). Similar to what we observed after either EGFR-TKI treatment (Figure 1A) or SOS1 deletion (Figure 1C and D), BAY-293 showed enhanced efficacy and increased overall growth inhibition in 3D spheroids over 2D adherent cultures. To confirm the specificity of

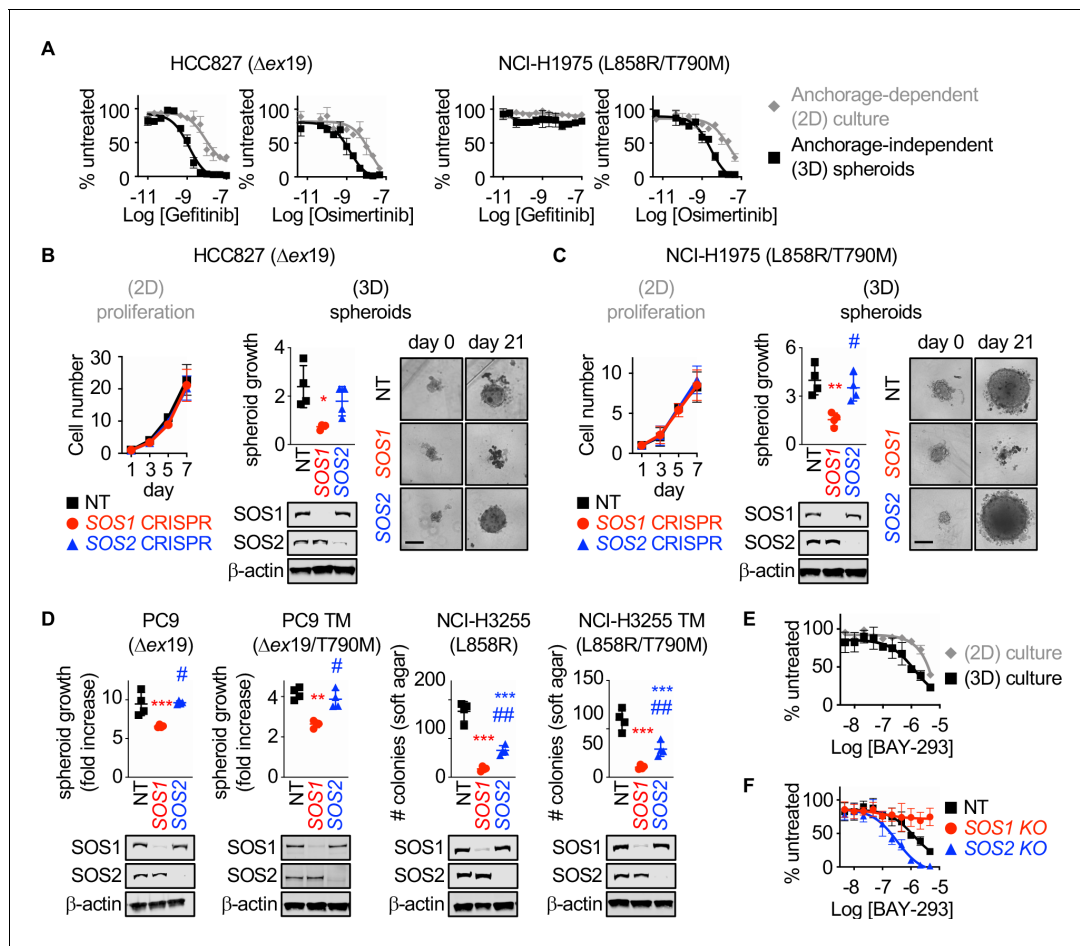


Figure 1. SOS1 deletion inhibits anchorage-dependent (3D) transformation in EGFR-mutated NSCLC cell lines. (A) Dose-response curves of EGFR-mutated HCC827 (Δ ex19) (left) or NCI-H1975 (L858R/T790M) (right) cells treated with gefitinib or osimertinib under 2D anchorage-dependent (gray diamonds) or 3D spheroid (black squares) culture conditions. (B-C) 2D proliferation (left) or 3D spheroid growth (right) in pooled populations of (B) HCC827 or (C) NCI-H1975 cells where *SOS1* or *SOS2* has been deleted using CRISPR/Cas9 vs NT controls. 10x images of representative spheroids at day 0 and 21 are shown, scale bar = 250 μ m. (D) 3D transformation in pooled populations of the indicated EGFR-mutated NSCLC cell lines where *SOS1* or *SOS2* has been deleted using CRISPR/Cas9 vs NT controls. (E) Dose-response curve cells of NCI-H1975 cells treated with the *SOS1* inhibitor BAY-293 under 2D anchorage-dependent (gray diamonds) or 3D spheroid (black squares) culture conditions. Data are represented as cell # versus untreated for each individual cell line. (F) Dose-response curves of NCI-H1975 cells where *SOS1* (red circles) or *SOS2* (blue triangles) has been deleted using CRISPR/Cas9 vs NT controls (black squares) treated with BAY-293 under 3D spheroid culture conditions. For each condition, the untreated sample was set to 100%, and drug-treated samples were compared to untreated for each cell line. Dose-response curves and 2D proliferation are presented as mean \pm s.d. from a least three independent experiments. For transformation studies, data are from four independent experiments. Each individual experiment was performed using populations (not clones) of independently CRISPR'd cells. For each experiment, three technical replicates were assessed. Statistical significance was determined by ANOVA using Tukey's method for multiple comparisons. * $p < 0.05$, ** $p < 0.01$, *** $p < 0.001$ vs. NT cells. # $p < 0.05$, ## $p < 0.01$ vs. *SOS1* KO cells.

The online version of this article includes the following source data and figure supplement(s) for figure 1:

Source data 1. The *SOS1* inhibitor BAY-293 is specific for *SOS1* and is enhanced by *SOS2* deletion in EGFR (T790M) mutated NSCLC cell lines.

Figure supplement 1. Deletion of *SOS1* using CRISPR/Cas9.

Figure supplement 2. The *SOS1* inhibitor BAY-293 is specific for *SOS1* and is enhanced by *SOS2* deletion in EGFR (T790M) mutated NSCLC cell lines.

BAY-293 for *SOS1*, we further treated 3D spheroid cultured H1975, PC9-TM, and H3255-TM cells where either *SOS1* or *SOS2* had been deleted versus NT controls with increasing doses of BAY-293 for four days, and assessed cell viability within the spheroids using Cell Titre Glo (Figure 1F and Figure 1—figure supplement 2). BAY-293 treatment did not inhibit survival of spheroids where *SOS1* had been deleted, indicating the specificity of BAY-293 for *SOS1*. Further, cells where *SOS2* had been deleted showed an approximately 1-log enhancement in BAY-293 efficacy and enhanced

overall growth inhibition compared to NT controls, indicating that SOS1 and SOS2 have some overlapping functions in supporting survival of spheroid cultured EGFR-mutated NSCLC cells. For these experiments, the untreated sample cell number at day four of treatment for each cell line (NT, SOS1 KO, SOS2 KO) was set to 100%, so differences in transformation (see **Figure 1B–D**) will not be appreciated. Further, for NCI-H1975 and NCI-H3255-TM cells, SOS1 deletion does not show transformation differences after four days. Overall, these data suggest that EGFR-mutated NSCLC cells are more sensitive to either mutant EGFR or SOS1 inhibition in 3D spheroid culture compared to traditional 2D adherent conditions.

SOS1 inhibition synergizes with EGFR-TKIs to inhibit cell survival under anchorage independent (3D) culture conditions

Previous studies reported that combining osimertinib with an alternative RTK inhibitor may inhibit or treat the development of resistance driven by that specific RTK (*Mancini et al., 2018; Romaniello et al., 2018; La Monica et al., 2017*), whereas simultaneous inhibition of multiple parallel RTKs with osimertinib may be required to effectively potentiate osimertinib action (*Romaniello et al., 2018*). Further, while many studies show enhanced drug activity in combination therapies versus osimertinib treatment alone, they do not assess whether the effects of the two-drug combinations are truly synergistic; synergistic interactions between therapeutics allow for maximization of the therapeutic effect while minimizing adverse events and may be required for effective therapeutic combinations with targeted agents (*Roell et al., 2017*).

SOS1 is a common downstream mediator of RTK signaling. We hypothesized that SOS1 could be an effective drug target to synergize with EGFR-TKI inhibition to treat EGFR-mutated lung adenocarcinoma. To directly assess synergy between osimertinib and SOS1 inhibition, we use two distinct methods based on the most widely established reference models of drug additivity. The first method, isobologram analysis, assesses changes in the dose-response curves for mixtures of two drugs compared to sham mixtures of each individual drug with itself. The second method, Bliss independence analysis, assesses whether a mixture of two individual drug doses has a greater effect than would be expected if the two drugs acted independently. We will first describe and then use each method in turn to determine the whether SOS1 inhibition using BAY-293 could synergize with the EGFR-TKI osimertinib in EGFR-mutated lung adenocarcinoma cells.

Isobologram analysis is a dose-effect analysis based on the principle of Loewe additivity, which states that a drug mixed with itself, and by extension a mixture of two or more similar drugs, will show additive effects. For two drugs (Drug A and Drug B) that have parallel dose-response curves so that a constant potency ratio is maintained at all doses of A and B (**Figure 2A**), treatment using any dose-equivalent (DEQ) mixture of Drugs A and B will show a similar effect to treatment with either Drug A or Drug B alone if the effects of the two drugs are additive. In contrast, if the two drugs show synergism, then the effect seen by treatment with DEQ mixtures of A and B will be greater than the effect for either drug alone. By generating dose-response curves for different DEQ mixtures of Drugs A and B (**Figure 2B**), one can compare the EC₅₀ of each DEQ mixture to the EC₅₀ of Drug A or Drug B alone on an isobologram plot (**Figure 2C**). The EC₅₀ of each individual drug is plotted as the x- or y-intercept, and the calculated contribution of each drug to the overall EC₅₀ for each DEQ mix is plotted as a single point (EC_{50,A}, EC_{50,B}) on the graph. If the EC₅₀ values for each DEQ mix fall along the straight line (isobole) that connects the individual drug EC₅₀ values, then the drug-drug interaction is additive. In contrast, points that fall above or below the isobole indicate antagonism or synergy. The extent to which two drugs interact can be further quantified from the EC₅₀ data as a combination index (CI) (**Figure 2D**). A CI between 0.8 and 1.2 indicates the two drugs have additive effects when combined, a CI <0.8 indicates synergy, and a CI >1.2 indicates antagonism.

To assess drug-drug synergy between osimertinib and BAY-293 via isobologram analysis, NCI-H1975 cells were cultured under 2D adherent or 3D spheroid conditions for 48 hr, and were treated with varying DEQ combinations of osimertinib:BAY-293 (see **Figure 2B**) for four days. Cell viability data was assessed using CellTiter-Glo and EC₅₀ values from each DEQ mixture were used to generate isobologram plots and calculate combination indices (**Figure 2E**). When cells were cultured under 2D conditions, osimertinib and BAY-293 showed additive effects, as DEQ EC₅₀ values fell on the isobole and CI values were between 0.8 and 1.2. In contrast, when cells were cultured as 3D

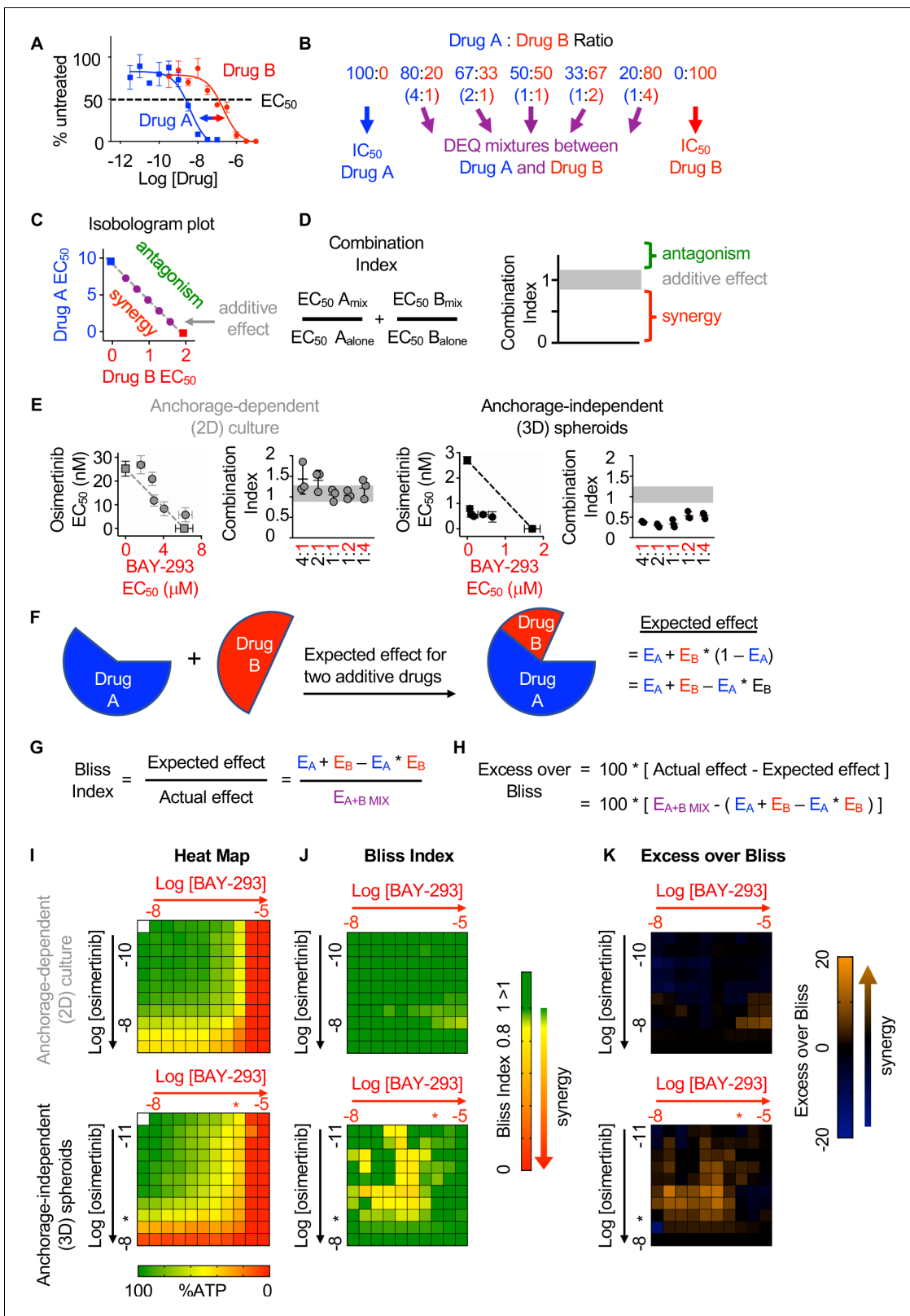


Figure 2. SOS1 inhibition synergizes with the EGFR-TKI inhibitor osimertinib to inhibit cell survival under anchorage-independent (3D) culture conditions. (A-D) Isobologram analysis examines drug-drug synergy by comparing dose equivalent (DEQ) mixtures of two drugs based on their EC₅₀ values to treatment with either drug alone (A and B). From the dose-response curves of the DEQ mixtures, plotting the fractional EC₅₀ for each drug in the combination (purple) relative to the individual drug EC₅₀ values (blue, red) on an isobologram plot (C) and calculation of the combination index (CI), Figure 2 continued on next page

Figure 2 continued

D and E allows assessment of drug-drug synergy. Additive effects occur on the dashed lines of the isobologram plot and have a CI 0.8–1.2 (gray box), whereas synergistic interactions fall below the dashed lines and have a CI <0.8. **(E)** Isobologram plots and CI from dose-equivalent treatments of H1975 EGFR-mutated NSCLC cells treated with DEQ combinations of osimertinib and BAY-293. Isobologram and CI data are presented as mean +/- s.d. from three independent experiments. **(F)** Bliss additivity evaluates whether the overall effect of an individual drug combination ($E_{A+B_{mix}}$) is greater than should be expected for two drugs with independent effects on the overall population ($E_A + E_B - E_A * E_B$). **(G)** The Bliss Index compares the ratio of the expected effect to the actual effect. Synergistic interactions have a Bliss Index < 0.85. **(H)** Excess over Bliss evaluates the magnitude of the difference between the actual and expected effects. Increasingly synergistic interactions show an excess over Bliss Index > 0. **(I)** Heat map of H1975 cells treated with the indicated doses of osimertinib and/or BAY-293 grown in either 2D (adherent) culture conditions or as 3D spheroids. Green indicates more cells, red indicates fewer cells. EC₅₀ values for each individual drug are indicated by an *. **(J)** Heat map of Bliss Index assessing drug-drug synergy between osimertinib and BAY-293 at each dose combination from **D**. **(K)** Heat map of excess over Bliss assessing drug-drug synergy between osimertinib and BAY-293 at each dose combination from **D**. Bliss Index and excess-over Bliss are presented as the mean from three independent experiments. For each experiment, three technical replicates were assessed.

The online version of this article includes the following source data for figure 2:

Source data 1. SOS1 inhibition synergizes with the EGFR-TKI inhibitor osimertinib to inhibit cell survival under anchorage-independent (3D) culture conditions.

spheroids, osimertinib and BAY-293 showed significant synergy, as DEQ EC₅₀ values were well below the isobole and CI <0.8.

Bliss independence analysis is an effect-based analysis based on the principle of Bliss additivity, which assumes that two drugs will act independently of each other so that their combined effect can be assessed by assessing the effect of each drug sequentially (**Figure 2F**). Unlike isobologram analysis, this method does not require that two drugs being assessed have parallel dose-response curves and can be calculated based as few as three drug treatments, the effect each drug has on its own on the cell population, and the effect of combining the two drug treatments together. By representing the effect of each drug treatment as a probabilistic outcome between 0 (no effect) and 1 (100% effect), we can compare the observed effect of the drug-drug combination to the expected effect if each drug acted independently (**Figure 2E**). The ratio of the expected effect to the observed effect is the Bliss Index (BI), where a BI <1 indicates synergy (**Figure 2G**). Alternatively, the magnitude of the difference between the observed and expected result can be reported as the excess over Bliss (**Figure 2H**). While excess over Bliss is the most widely reported synergy metric, the Bliss Index can be directly compared with the combination index in isobologram experiments and should be used when both synergy methods are used to assess a given drug-drug interaction.

To assess drug-drug synergy between osimertinib and BAY-293 via Bliss Independence analysis, NCI-H1975 cells were cultured under 2D adherent or 3D spheroid conditions for 48 hr and were treated with increasing doses of BAY-293, osimertinib, or combinations of the two drugs over a 3-log scale for four days. Cell viability was determined using CellTiter-Glo and overall viability (**Figure 2I**), Bliss index (**Figure 2J**), and excess over Bliss (**Figure 2K**) were represented as heat-maps. Similar to what we observed for isobologram analysis, osimertinib and BAY-293 did not show significant synergy in cells cultured under 2D adherent conditions. In contrast, we observed significant synergy between osimertinib and BAY-293, mostly at dose combinations of osimertinib and BAY-293 falling just below the individual drug EC₅₀ values. Overall, the data presented in **Figure 2** indicate that osimertinib and BAY-293 show significant drug-drug synergy in EGFR-mutated H1975 cells, but only in 3D spheroid culture conditions.

To determine whether the SOS1 inhibitor BAY-293 could generally synergize with EGFR-TKIs in EGFR-mutated lung adenocarcinoma cells, we extended our assessment of drug-drug synergy to isobologram analysis (**Figure 3**) and Bliss independence analysis (**Figure 4**) in six different EGFR-mutated lung adenocarcinoma cell lines. In cells that were sensitive to first-generation EGFR-TKIs (HCC827, PC9, H3255; T790 wild-type), we assess drug-drug synergy between BAY-293 and either a first-generation (gefitinib) or third-generation (osimertinib) EGFR-TKI. In cells that were resistant to first-generation EGFR-TKIs (H1975; PC9-TM, H3255-TM; T790M) we limited our assessment to synergy between BAY-293 and osimertinib. To first determine the individual EC₅₀ values for gefitinib, osimertinib, and BAY-293 in each cell line, cells were cultured as 3D spheroids for 48–72 hr, and then treated with increasing doses of drug for four days followed by assessment of cell viability by CellTiter-Glo (**Figure 3—figure supplement 1**). In five of six cell lines, the individual dose-response

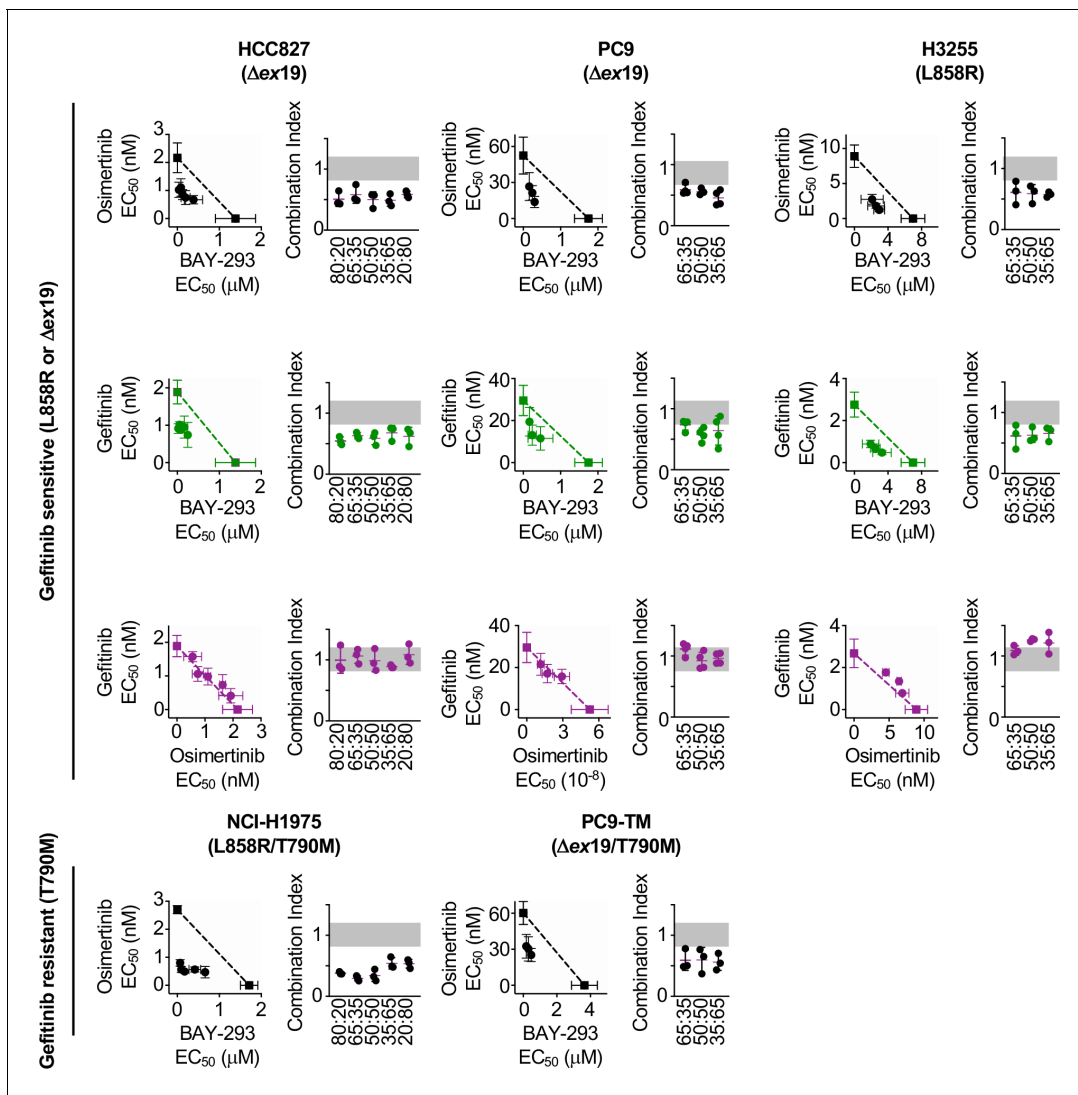


Figure 3. Isobologram analysis showing that *SOS1* inhibition synergizes with EGFR-TKI treatment to inhibit survival in multiple EGFR-mutated NSCLC cell lines. Isobologram analysis and Combination Index (CI) from dose-equivalent treatments of the indicated EGFR-mutated gefitinib-sensitive (L858R or Δ ex19, top) or gefitinib-resistant (T790M, bottom) NSCLC cell lines with combinations of gefitinib, osimertinib, and BAY-293. Additive effects occur on the dashed lines of the isobologram plot and have a CI 0.8–1.2 (gray box), whereas synergistic interactions fall below the dashed lines and have a CI < 0.8. Data are presented as mean \pm s.d. from three independent experiments. For each experiment, three technical replicates were assessed. The online version of this article includes the following source data and figure supplement(s) for figure 3:

Source data 1. EGFR mutated NSCLC cell lines are responsive to osimertinib, BAY-293, and gefitinib in 3D spheroid cultures.

Figure supplement 1. EGFR mutated NSCLC cell lines are responsive to osimertinib, BAY-293, and gefitinib in 3D spheroid cultures.

curves for BAY-293, osimertinib, and gefitinib (where appropriate) showed similar maximal effects and Hill coefficients, and were thus appropriate for linear isobologram analysis for each two-drug combination of BAY-293, osimertinib, and gefitinib (Tallarida, 2011). In contrast, H3255-TM cells were only moderately sensitive to osimertinib, showing at most a 50% reduction in viability at high doses. Therefore, we limited our assessment of drug-drug synergy in H3255-TM cells to Bliss independence analysis. Further, to simplify our assessment of Bliss independence across multiple drugs and cell lines, we limited our drug treatments to 1:2, 1:1, and 2:1 mixtures of each drug combination based on dose equivalence (see Figure 4A).

For each first-generation EGFR-TKI sensitive cell line (HCC827, PC9, H3255), gefitinib and osimertinib did not show any synergy with each other by either isobologram analysis (Figure 3) or Bliss Independence analysis (Figure 4), instead showing additive effects (CI and BI \sim 1) as would be

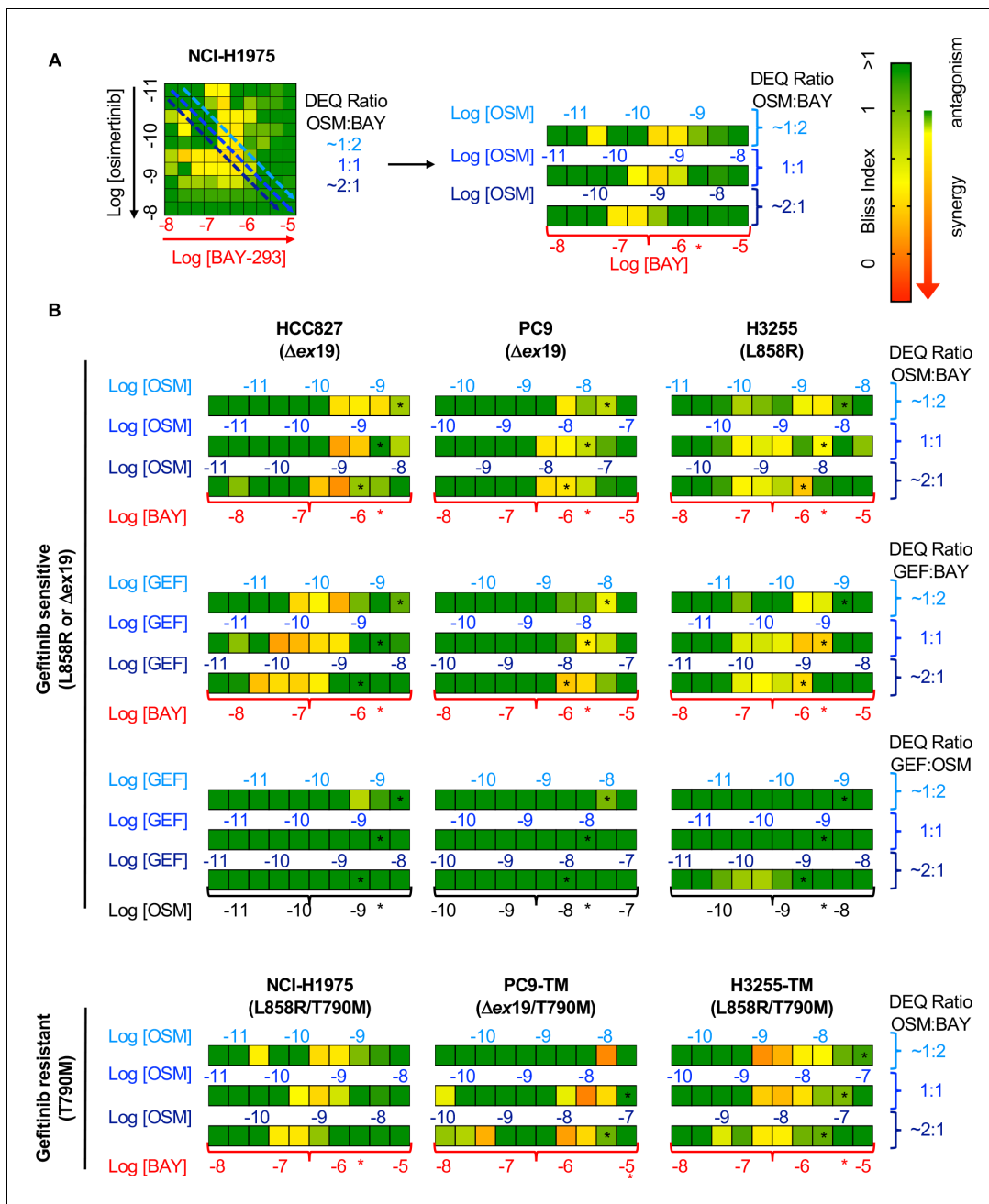


Figure 4. Bliss Independence analysis showing that SOS1 inhibition synergizes with EGFR-TKI treatment to inhibit survival in multiple EGFR-mutated NSCLC cell lines. (A) Bliss Index heatmap from 3D spheroid cultured NCI-H1975 cells **Figure 2A** (left) and horizontal projections of Bliss Indices of drug treatments at 2:1, 1:1, and 1:2 ratios of osimertinib:BAY-293 based on dose equivalencies (right). Increasingly synergistic interactions (Bliss index <0.85) are indicated by the corresponding heat map. The concentration of BAY-293 (held constant, bottom) and of osimertinib (above each horizontal projection) are given. The IC₅₀ for each individual drug are shown (*). (B) Bliss Index heatmaps based on A for the indicated gefitinib-sensitive and gefitinib-resistant cell lines at 2:1, 1:1, and 1:2 ratios of osimertinib, gefitinib, and BAY-293 based on dose equivalencies. Data for NCI-H1975 cells are the same as in A. Data are presented as the mean from three independent experiments. For each experiment, three technical replicates were assessed. The online version of this article includes the following source data for figure 4:

Source data 1. Bliss Independence analysis showing that SOS1 inhibition synergizes with EGFR-TKI treatment to inhibit survival in multiple EGFR-mutated NSCLC cell lines.

expected for two drugs with the same molecular target. In contrast, BAY-293 showed significant synergy with gefitinib and osimertinib by both isobologram analysis (**Figure 3**) and Bliss Independence analysis (**Figure 4**), suggesting that SOS1 inhibition can act as a secondary treatment for all EGFR-TKIs. Further, in all three T790M mutated cell lines (H1975, PC9-TM, H3255-TM), BAY-293 again showed synergy with osimertinib. These data suggest that combined SOS1 and EGFR inhibition is a robust therapeutic combination that synergize to inhibit EGFR-mutated lung adenocarcinoma cell growth.

Synergy between BAY-293 and osimertinib is independent of SOS2

We showed that SOS2 deletion sensitized NCI-H1975 cells to the SOS1 inhibitor BAY-293 (**Figure 1F**). We wanted to determine whether the synergy we observed between EGFR- and SOS1-inhibition (**Figures 3** and **4**) was enhanced by SOS2 deletion in EGFR-mutated NSCLC cell lines. To examine whether SOS2 deletion alters the synergy between osimertinib and BAY-293 in EGFR (T790M) mutated cells, SOS2 was deleted in H1975, PC9-TM, and H3255-TM cells. For H1975 and PC9-TM cells, SOS2 KO cells vs NT controls were cultured under 3D spheroid conditions for 48–72 hr, and were then treated with varying DEQ combinations of osimertinib:BAY-293 for 4 days. Cell viability data was assessed using CellTiter-Glo and EC₅₀ values from each DEQ mixture were used to generate Isobologram plots and calculate confidence intervals (**Figure 5A and B**). For both cell lines, SOS2 deletion sensitized cells to BAY-293, decreasing EC₅₀ by 5–10-fold compared to NT controls without altering the EC₅₀ to osimertinib treatment alone. However, unlike what we observed in the NT control cells, osimertinib and BAY-293 showed only mild synergy in EGFR-mutated cells where SOS2 was deleted as assessed by the distance of the interaction points to the isobole and the increased combination index vs. NT controls. Further, when we overlaid the NT and SOS2 KO isobologram plots at two different scales of BAY-293, the drug combination data points were overlapping between NT and SOS2 KO cells, suggesting that SOS2 deletion did not enhance synergy between osimertinib and BAY-293.

Since H3255-TM cells are not appropriate for linear isobologram analysis between BAY-293 and osimertinib, we instead performed Bliss independence analysis to assess potential synergy between osimertinib and BAY-293 in the presence or absence of SOS2. H3255-TM cells where SOS2 had been deleted vs NT controls were cultured under 3D spheroid conditions for 48–72 hr, and were then treated with increasing doses of osimertinib alone, BAY-293 alone, or mixtures of each drug dose at 1:2, 1:1, and 2:1 mixtures of osimertinib and BAY-293 based on dose equivalence for four days. Cell viability data was assessed using CellTiter-Glo, and the Bliss index was calculated for each drug mixture as shown in **Figure 2C** and **Figure 4**. As was the case in H1975 and PC9-TM cells, while the SOS2 deletion sensitized H3255-TM cells to BAY-293 we observed less overall synergy between osimertinib and BAY-293 H3255-TM cells where we had deleted SOS2 vs NT controls. These data suggest that although osimertinib and BAY-293 synergize to limit viability of EGFR-mutated lung adenocarcinoma cells, the synergy between osimertinib and BAY-293 is independent of SOS2.

BAY-293 and osimertinib synergize to inhibit RAS effector signaling

Mutated EGFR signals through downstream RAF/MEK/ERK and PI3K/AKT effector pathways to promote proliferation, transformation, and survival. Since SOS2 deletion did not further enhance synergy between BAY-293 and osimertinib, we hypothesized that SOS1 inhibition specifically enhanced EGFR-TKI-dependent inhibition of downstream signaling in 3D culture. To perform signaling experiments on 3D cultured spheroids, cells were seeded in 24-well micropatterned low-attachment culture plates (Aggrewell, StemCell) containing ~1200 individual spheroids per condition. To determine the extent to which SOS1 inhibition and/or SOS2 deletion altered osimertinib-dependent inhibition of downstream effector signaling in 3D culture, H1975 or PC9-TM cells where SOS2 was deleted vs. NT controls were cultured as spheroids for 48–72 hr and then treated with increasing doses of osimertinib +/- BAY-293 prior to spheroid collection, lysis, and western blotting for phosphorylated ERK and AKT (**Figure 6**). In both NT and SOS2 knockout cells, BAY-293 reduced the dose of osimertinib required to inhibit both ERK and AKT phosphorylation (**Figure 6**). For Raf/MEK/ERK signaling, Bliss Independence analysis of pERK quantitation revealed that either SOS1 inhibition or SOS2 deletion independently synergized with osimertinib to inhibit Raf/MEK/ERK signaling, and the combination of inhibiting SOS1/2 signaling further enhanced this synergy. In contrast, for PI3K/AKT signaling

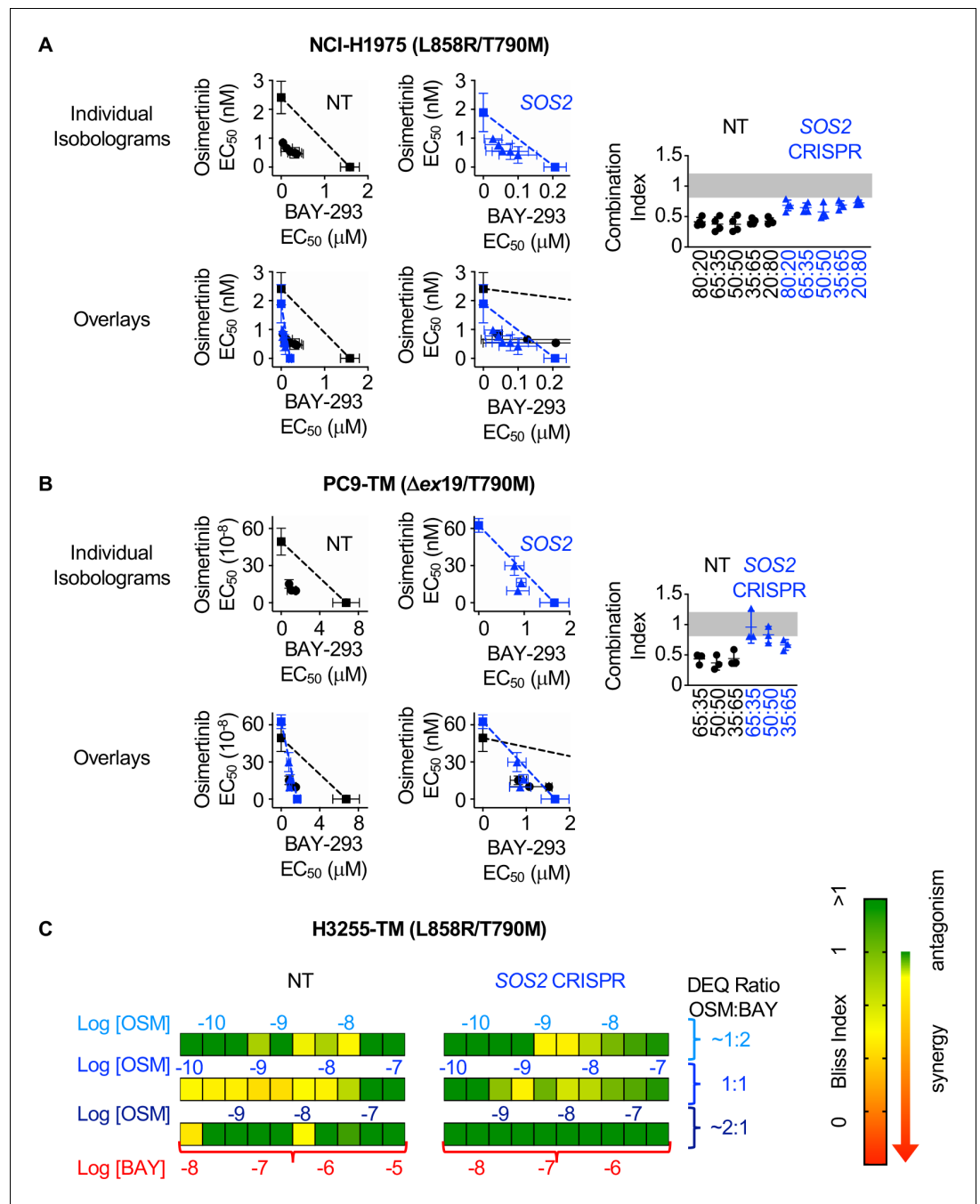


Figure 5. SOS2 deletion does not enhance the synergistic interaction between SOS1 inhibition and EGFR-TKI treatment. (A-B) Isobologram analysis (left) and Combination Index (right) from dose-equivalent treatments of osimertinib and BAY-293 in H1975 (A) or PC9-TM (B) cells where SOS2 has been deleted (blue) versus NT controls (black). Overlay plots on two different BAY-293 dosing scales are shown below the individual isobologram plots. Additive effects occur on the dashed lines of the isobologram plot and have a CI 0.8–1.2 (gray box), whereas synergistic interactions fall below the dashed lines and have a CI <0.8. (C) Bliss Index heatmaps for H3255-TM cells where SOS2 has been deleted versus NT controls treated at 1:2, 1:1, and 2:1 ratios of osimertinib and BAY-293 based on dose equivalencies. Data are presented as mean +/- s.d. from three independent experiments. For each experiment, three technical replicates were assessed. The online version of this article includes the following source data for figure 5:

Source data 1. SOS2 deletion does not enhance the synergistic interaction between SOS1 inhibition and EGFR-TKI treatment.

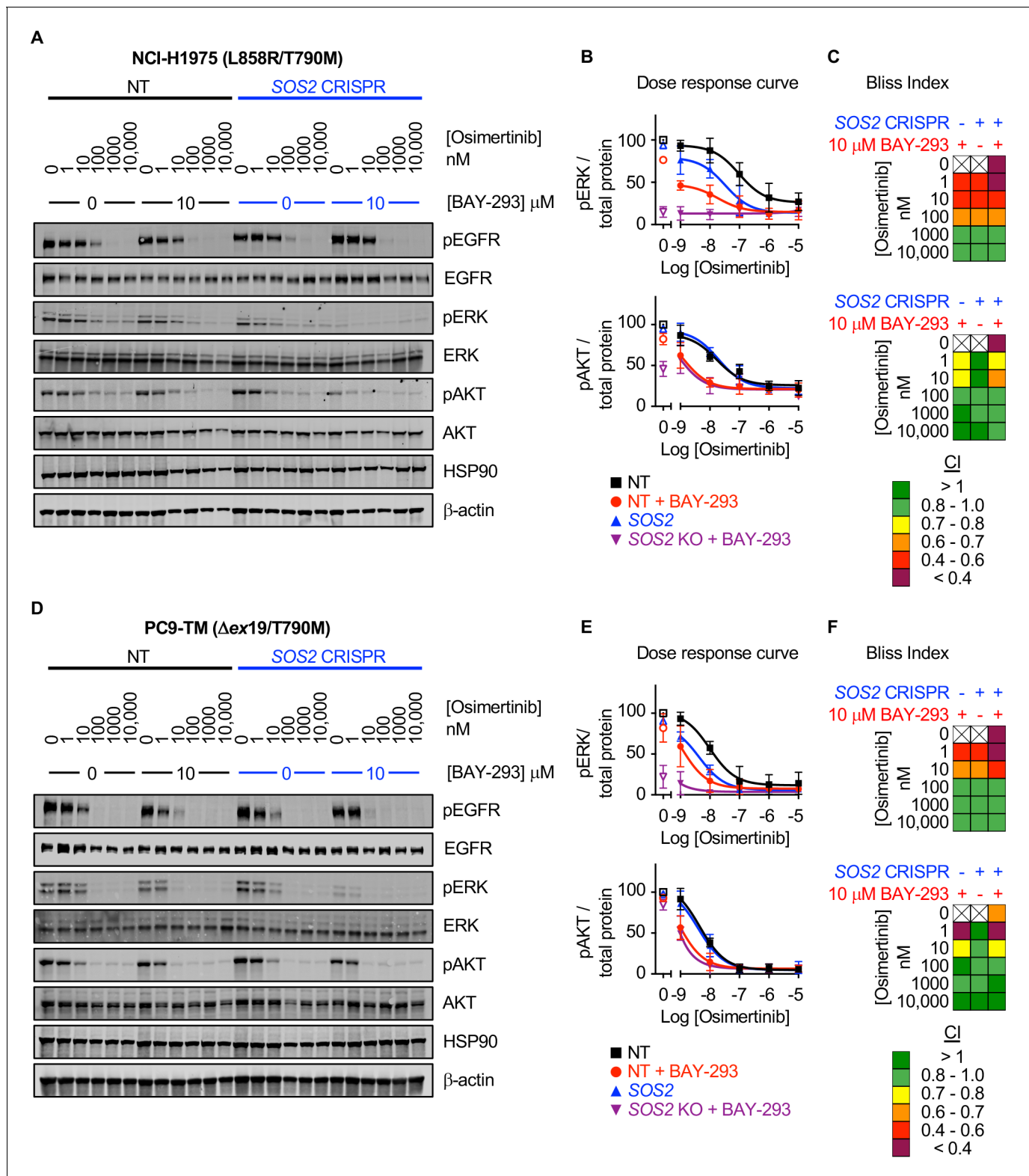


Figure 6. SOS1 inhibition synergizes with mutant EGFR inhibition to inhibit downstream effector signaling. Western blots (A, D), pERK and pAKT quantitation (B, E), and Bliss Indices (C, F) of WCLs of NCI-H1975 cells (A-C, top) or PC9-TM cells (D-F, bottom) cultured under 3D spheroid conditions for 48 hr and then treated with the indicated concentrations of the EGFR-TKI osimertinib and/or the SOS1 inhibitor BAY-293 for 6 hr. Western blots are for pEGFR, EGFR, pAKT, AKT, pERK1/2, ERK1/2, HSP90, and β -actin. pERK and pAKT quantifications were calculated using a weighted average of total protein western blots. Combination Indices are based on pERK/Total protein and pAKT/Total protein quantitations. Increasingly synergistic
Figure 6 continued on next page

Figure 6 continued

combinations are indicated in yellow, orange, red, or purple. Phosphoprotein quantitations are presented as mean \pm s.d. from three independent experiments. Bliss indices are presented as mean from three independent experiments. For each experiment, three technical replicates were assessed. The online version of this article includes the following source data for figure 6:

Source data 1. SOS1 inhibition synergizes with mutant EGFR inhibition to inhibit downstream effector signaling.

SOS2 deletion did not enhance the synergy between osimertinib and BAY-293. While either osimertinib treatment or SOS2 deletion independently synergized with BAY-293 to inhibit AKT phosphorylation, SOS2 deletion did not further enhance the ability osimertinib to inhibit PI3K/AKT signaling in the presence or absence of BAY-293. These data strongly suggest that vertical inhibition of EGFR and SOS1 limits cell viability by inhibiting activation of both RAF/MEK/ERK and PI3K/AKT effector pathways.

Assessment of inhibitor landscape in EGFR-mutated cells lines shows synergy upon inhibition of upstream pathway effectors

Since the most common EGFR-independent resistance mechanisms involve reactivation of RTK/RAS/effector pathways (Mancini et al., 2018; Romaniello et al., 2018; La Monica et al., 2017; Eberlein et al., 2015), we wanted to assess whether inhibition of different proteins within the EGFR/RAS signaling pathway could synergize to inhibit 3D survival of EGFR (T790M) mutated cancer cells. To determine drug-drug synergies after inhibition of EGFR-RAS pathway signaling at different levels, we assessed synergy between osimertinib, inhibitors of EGFR signaling intermediates upstream of RAS (BAY-293 for SOS1 and RMC-4450 for SHP2), and inhibitors of the Raf/MEK/ERK (trametinib) and PI3K/AKT (buparlisib) pathways (Figure 7A). H1975 and PC9-TM cells were treated with each individual inhibitor or 1:1 DEQ mixtures of every drug-drug combination, and the combination index was calculated to assess drug-drug synergy. Since H3255-TM cells are not suitable for isobologram analysis, these cells were treated with full-dose mixtures based on dose equivalence and the Bliss Index was calculated for each drug-drug combination (Figure 7B). Intriguingly, all three cell lines showed drug-drug synergy with any combination of EGFR, SOS1, and SHP2 inhibition. In contrast, inhibition of downstream Raf/MEK/ERK or PI3K/AKT pathways failed to consistently synergize with either osimertinib or any other inhibitor (Figure 7B, top). These data support the premise that combined vertical inhibition of proximal EGFR signaling may constitute an effective strategy to treat EGFR-mutated lung adenocarcinomas.

SHP2 is important for the stabilization of the GRB2:SOS1/2 complexes on EGFR (Dance et al., 2008), and the mechanism of allosteric SHP2 inhibitors depends on SOS1 (Nichols et al., 2018), although the contribution of SOS2 to SHP2 inhibitors was not assessed. To determine whether SOS2 deletion altered the spectrum of drug-drug synergies in EGFR-mutated cells, parallel studies were performed in EGFR-mutated cells where SOS2 was deleted (Figure 7B, bottom). Unlike what we observed for synergy between EGFR- and SOS1 inhibition, synergy between SOS1 and SHP2 inhibition was enhanced by SOS2 deletion. These data suggest that SOS2 plays a role in SHP2-dependent signaling. SOS1 inhibition also synergized with MEK inhibition in SOS2 KO cells. Given the strong synergy between SOS1 inhibition and SOS2 deletion in inhibiting Raf/MEK/ERK signaling (Figure 6), these data suggest that deep inhibition of MEK signaling is sufficient to inhibit survival in EGFR-mutated cells.

To further evaluate synergy between inhibitors of proximal EGFR signaling, we examined combinations of EGFR- SOS1- and SHP2 inhibition both by expanded evaluation of each two-drug combination and by assessing whether combined inhibition of EGFR, SOS1, and SHP2 would be more effective than two drug combinations of these inhibitors. To assess each two-drug combination, H1975 cells cultured under 3D spheroid conditions were treated with dose-equivalent combinations of osimertinib, BAY-293, and RMC-4550, assessed for cell viability, and subjected to isobologram analysis to assess drug-drug synergy. Each two-drug combination showed synergy at three different DEQ ratios (Figure 7C), suggesting that inhibition of any two proximal signaling proteins may be an effective therapeutic regimen to treat EGFR-mutated cancer. To assess whether adding a third proximal inhibitor to each two-drug combination would further enhance synergistic inhibition of spheroid survival, each two-drug combination was mixed at 1:1 ratio, and then a third proximal pathway

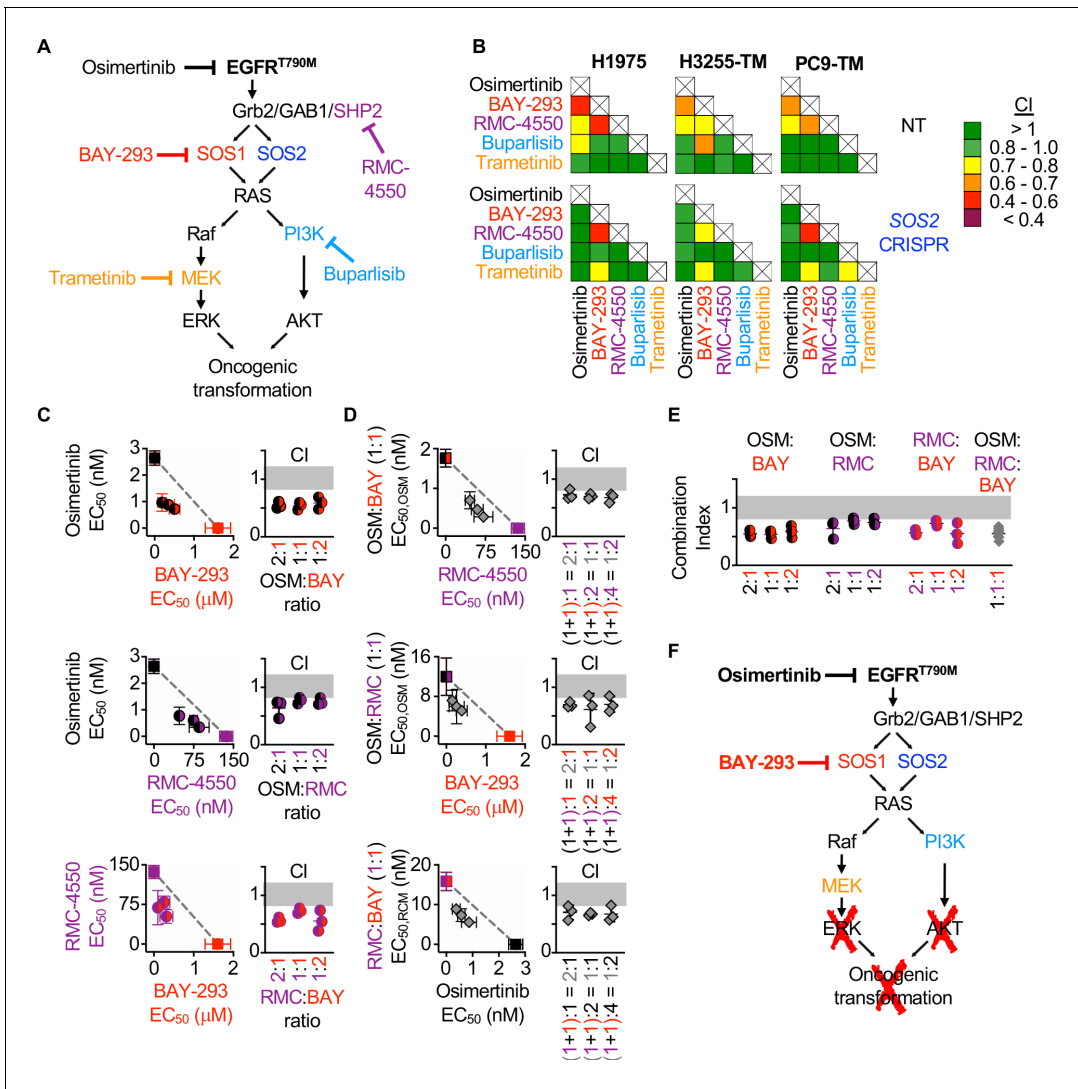


Figure 7. Assessment of the EGFR/RAS pathway ‘inhibitor landscape’ suggests that combination therapies inhibiting mutated EGFR, SOS1, and SHP2 have therapeutic potential in EGFR-mutated NSCLC. (A) Signaling diagram showing EGFR/RAS pathway inhibitors that were assessed for pairwise synergy by isobologram analysis using 50:50 dose-equivalent mixes of each drug pair. (B) Heat map of Combination Indices from isobologram analyses of the indicated drug-drug combinations in NT and *SOS2* KO NSCLC cell lines. Synergistic combinations are indicated in yellow, orange, or red. Data are presented as the mean from three independent experiments. (C-D) Isobologram analysis and Combination Index (CI) from dose-equivalent treatments of 3D spheroid cultured NCI-H1975 cells treated with the indicated two-drug (C) or three-drug (D) combinations of osimertinib (black), RMC-4550 (purple), and BAY-293 (red). For three drug combination, the two drugs indicated on the y-axis were held at a 1:1 ratio, and then mixed at dose equivalent ratio with the third drug. CI values indicate enhanced synergy beyond the two drug combination on the y-axis of the isobologram plot and are calculated based on the y-axis drug combination calculated as a single drug treatment. Additive effects occur on the dashed lines of the isobologram plot and have a CI 0.8–1.2 (gray box), whereas synergistic interactions fall below the dashed lines and have a CI <0.8. (E) Combination indices from two-drug combinations of osimertinib (black), RMC-4550 (purple), and BAY-293 (red) mixed at 2:1, 1:1, or 1:2 ratios or the three drug combination at a 1:1:1 ratio (grey). CI are calculated based on three individual drug treatments. (F) Signaling model based on data from Figures 1–7 showing that combined targeting of mutated EGFR and SOS1 provides sufficient vertical inhibition of upstream signaling to inhibit RAS effector signaling and block oncogenic transformation. This synergistic inhibition can be further enhanced by SHP2 inhibition, providing multiple potential drug combinations for therapeutic intervention in EGFR-mutated NSCLC. Isobologram and CI data are presented as mean +/- s.d. from three independent experiments. For each experiment, three technical replicates were assessed.

The online version of this article includes the following source data for figure 7:

Source data 1. Assessment of the EGFR/RAS pathway ‘inhibitor landscape’ suggests that combination therapies inhibiting mutated EGFR, SOS1, and SHP2 have therapeutic potential in EGFR-mutated NSCLC.

inhibitor was added to give the indicated three-drug mixtures (**Figure 7D**). Isobologram analysis of these three drug mixtures revealed that addition of a third proximal pathway inhibitor to any two-drug combination of osimertinib, BAY-293, and RMC-4550 further enhanced synergy above what was observed for each two-drug combination (**Figure 7D**). Finally, comparing the combination index for the three-drug combination at a 1:1:1 ratio when each drug is treated independently versus the two-drug combinations showed marked synergy for the three drug combination, but that this synergy was not significantly enhanced compared to the combination of osimertinib and BAY-293 (**Figure 7E**). These data indicate that vertical inhibition of proximal EGFR signaling with the combination of osimertinib and a SOS1 inhibitor may be the most effective therapeutic combination to treat *EGFR*-mutated NSCLC.

Discussion

Activating *EGFR* mutations are found in 10–30% of lung adenocarcinomas and are the major cause of lung cancer in never smokers. The third-generation *EGFR*-TKI osimertinib enhances both progression-free (*Soria et al., 2018*) and overall survival (*Ramalingam et al., 2020*) compared to first generation *EGFR*-TKIs and is now considered first-line treatment in *EGFR*-mutated NSCLC. Osimertinib resistance often develops via activation of parallel RTK pathways (*Mancini et al., 2018; Romaniello et al., 2018; La Monica et al., 2017*), and broad inhibition RTK signaling may enhance osimertinib efficacy and delay therapeutic resistance. Here, we demonstrate that inhibition of the common RTK signaling intermediate SOS1 using BAY-293 showed marked synergy with osimertinib in 3D spheroid-cultured *EGFR*-mutated NSCLC cells. Our observations that (i) osimertinib–BAY-293 synergy was only observed in 3D spheroids but not in adherent (2D) cultures and (ii) synergy between RTK-signaling intermediates and osimertinib was not broadly applicable to *EGFR* downstream signaling components but was limited to proteins upstream of RAS reveal novel insights into pharmacologic studies assessing therapeutics designed to treat NSCLC.

While most studies designed to identify or test therapeutic targets to treat cancer are done in 2D adherent culture, a growing body of evidence suggests that pharmacologic assessment of novel therapeutics must be performed in 3D culture systems (*Nunes et al., 2019*). Here, there are many different 3D model systems available that vary in both ease-of-use and complexity of the system. The simplest systems employ non-scaffold-dependent monoculture of cancer cell lines where spheroids are either generated using hanging-drop methodology, magnetic levitation, or using ultra-low attachment plates. More complex systems include embedding spheroids in an extracellular matrix (Matrigel, collagen, gelatin, or a synthetic hydrogel) either as a cancer cell line monoculture or in combination with cancer-derived fibroblasts, or using specialized microfluidics or culturing cancer-derived organoids. These methods have been thoroughly reviewed elsewhere (*Langhans, 2018*). In the current study, we use ultra-low attachment plates of monoculture NSCLC cell lines as these have the advantage of recapitulating in vivo findings while allowing for dose-response studies done at scale (*Mittler et al., 2017*).

In NSCLC, multiple studies have now revealed the importance of 3D culture systems in order to recapitulate in vivo findings. *EGFR*-mutated cells show differential RTK expression and phosphorylation in 3D versus 2D conditions (*Ekert et al., 2014*) and respond more robustly to *EGFR*-TKIs in 3D cultures compared to 2D settings (**Figure 1** and *Jacobi et al., 2017*); *KRAS*-mutated cell lines deemed 'KRAS-independent' in 2D culture (*Balbin et al., 2013; Singh et al., 2009; Singh et al., 2012; Scholl et al., 2009; Lamba et al., 2014*) still require *KRAS* for anchorage-independent growth (*Fujita-Sato et al., 2015; Rotem et al., 2015; Zhang et al., 2006; McCormick, 2015*), and some *KRAS*^{G12C}-mutated NSCLC cell lines respond to *KRAS*(G12C) inhibitors in 3D culture and in vivo but not in 2D adherent culture (*Janes et al., 2018*). The relevance of 3D culture systems extends to the identification of novel therapeutic targets and therapeutic combinations. We recently showed that SOS2 is specifically required for PI3K-dependent protection from anoikis in *KRAS*-mutated NSCLC cells (*Sheffels et al., 2019*) and SOS2 deletion synergizes with MEK inhibition to kill *KRAS* mutated cells only under 3D culture conditions (*Sheffels et al., 2018*). Here, we show marked synergy between vertical inhibition of *EGFR* and SOS1 in *EGFR* mutated cancer cells, but only under 3D culture conditions (**Figure 2**). CRISPR screens performed in spheroid cultures of *KRAS*- and *EGFR*-mutated NSCLC cell lines more accurately reproduce in vivo findings and identify drivers of oncogenic growth compared to screens performed in 2D cultures (*Han et al., 2020*). Intriguingly, in this

study SOS1 was essential for 3D spheroid survival but not 2D spheroid growth of both EGFR- and KRAS-mutated cells, and a recently accepted publication assessing a novel SOS1 inhibitor showed that it was more effective in 3D compared to 2D culture (Hofmann et al., 2020). These data are in complete agreement with our data from **Figure 1** showing the requirement for SOS1 in 3D transformation but not 2D proliferation, and support our conclusion that SOS1 is an important therapeutic target in EGFR-mutated NSCLC. We hypothesize the requirement for SOS1 (and SOS2) to promote oncogenic growth in 3D versus proliferation in 2D culture are due to the requirement for PI3K signaling to promote cell survival in 3D but not 2D. Downstream of EGFR activation, the threshold for Raf/MEK/ERK versus PI3K/AKT pathway activation are drastically different, so small amounts of EGFR signaling (in the presence of either SOS1 or SOS2) promote Raf/MEK/ERK signaling, whereas high levels of EGFR signaling are required to activate the PI3K/AKT pathway (Fortian and Sorkin, 2014). While this hypothesis remains to be tested, we speculate that depending on the specific oncogenic contexts, either SOS1 or SOS2 inhibition will be sufficient to modulate RTK signaling and change the threshold for PI3K signaling, thereby affecting oncogenic growth. These data suggest that future studies assessing novel therapeutics to treat lung adenocarcinomas must be performed in a 3D setting, and that SOS1 and SOS2 might be ubiquitous therapeutic targets in RTK-driven tumors.

Osimertinib resistant can occur via oncogenic shift to alternative RTKs including c-MET (Shi et al., 2016), HER2 and/or HER3 (Mancini et al., 2018; Romaniello et al., 2018; La Monica et al., 2017), IGF1R (Park et al., 2016), and AXL (Kim et al., 2019; Taniguchi et al., 2019; Jimbo et al., 2019; Namba et al., 2019). The variety of RTK bypass pathways that can lead to osimertinib resistance suggests that broad inhibition of RTK signaling may be a more effective therapeutic strategy than any individual RTK inhibitor to limit osimertinib resistance, whereas once resistance via oncogenic shift to an alternative RTK occurs then inhibition of the upregulated RTK would have therapeutic benefit. Toward this end, Phase I and II clinical trials are currently examining whether combining osimertinib with inhibitors of AXL (DS-1205c, NCT03255083) or c-MET (teponitib, NCT03940703; savolitinib, NCT03778229) are effective in patients who have progressed on osimertinib treatment.

Combining osimertinib with a MEK inhibitor can enhance osimertinib efficacy (Eberlein et al., 2015; Tricker et al., 2015; Ichihara et al., 2017; Shi et al., 2017; Della Corte et al., 2018) and Phase II clinical trials are currently underway to assess combining osimertinib with the MEK inhibitor selumetinib in EGFR-mutated NSCLC (NCT03392246), although resistance to combined osimertinib and MEK inhibition still occurs (Tricker et al., 2015). In a recent study designed to understand resistance to combined osimertinib and MEK inhibition, Kurppa et al., 2020 show that combining osimertinib with the MEK inhibitor trametinib results in EGFR-mutated cells entering a senescent state that is dependent on the activation of the Hippo pathway effector YAP and its transcription-factor-binding partner TEAD (Kurppa et al., 2020). Inhibition of YAP/TEAD signaling overcame this senescence and enhanced killing of EGFR-mutated cells (Kurppa et al., 2020). EGFR-signaling drives YAP nuclear translocation and transcriptional regulation through PI3K-PDK1 signaling (Fan et al., 2013; Xia et al., 2018; Tumaneng et al., 2012). This suggest that therapeutic combinations able to synergistically inhibit both Raf/MEK/ERK and PI3K/AKT effector signaling should overcome YAP-dependent senescence and treat EGFR-mutated NSCLC.

Here, we show that osimertinib does not broadly synergize with inhibitors of downstream EGFR/RAS/RAS effector signaling. Instead, we found that synergy was limited to combinations of osimertinib with inhibitors of proximal EGFR signaling intermediates SOS1 and SHP2 (**Figure 7**). Further, SOS1 inhibition significantly enhanced osimertinib-dependent inhibition of both Raf/MEK/ERK and PI3K/AKT signaling (**Figure 6**), whereas inhibition of individual downstream Raf/MEK/ERK or PI3K/AKT effector pathways did not synergize with osimertinib (**Figure 7**) to inhibit 3D spheroid growth. We hypothesize that these two findings are inexorably linked, so that any potential therapeutic must synergize with osimertinib to inhibit all downstream RAS effector signaling to show drug-drug synergy in 3D culture. In support of this idea, previous studies showed inhibition of SRC family kinases (SFK) potentiated osimertinib to a much greater extent than either MEK or PI3K inhibition (Ichihara et al., 2017), and that SFK inhibition synergized with osimertinib to inhibit both Raf/MEK/ERK and PI3K/AKT signaling (Ichihara et al., 2017; Watanabe et al., 2017).

There remain several open questions regarding SOS1 inhibition as a therapeutic strategy to limit osimertinib resistance. First, does SOS1 inhibition enhance osimertinib efficacy in vivo using xenograft studies? While BAY-293 shows tremendous specificity toward SOS1 (**Figure 1—figure supplement 1 and 2**, and Hillig et al., 2019) and is a very useful tool compound for in vitro studies, it has

limited bioavailability making it unsuitable for in vivo use. Thus, new SOS1 inhibitors that can be used in vivo are needed to move SOS1 forward as a therapeutic target. Intriguingly, while this paper was under review Boehringer Ingelheim reported two orally available SOS1 inhibitors suitable for in vivo studies (*Hofmann et al., 2020*). They found that SOS1 inhibition could overcome MEK inhibitor resistance in KRAS-mutated cell lines and that the combination of SOS1 and MEK inhibition showed marked show efficacy in KRAS-mutated cell lines and xenograft models. They are now moving one of these compounds into Phase I safety trials for KRAS mutated solid tumors (BI-1701963, NCT04111458). It will be exciting to assess whether these new SOS1 inhibitors work in combination with osimertinib to limit the growth EGFR-mutated tumors. Further, these studies will be necessary to translate SOS1-targeted therapies for use in EGFR-mutated lung adenocarcinoma. Second, does SOS1 inhibition actually limit the development of osimertinib resistance? While outside the scope of the current paper, it will be intriguing to use in vitro models of EGFR-TKI resistance (*Tricker et al., 2015*) to assess whether SOS1 inhibition can block the development of osimertinib resistance. Third, while we have focused on the RAF/MEK/ERK and PI3K/AKT effector pathways as the major contributors to mutant EGFR-driven NSCLC, there are many different effector pathways downstream of RAS that may be SOS1-dependent and contribute to the oncogenic phenotype. Here, and unbiased approach at understanding the individual and combined effects of osimertinib and SOS1 inhibition on RAS activation (to validate relatively new SOS1 inhibitors) and RAS effector signaling would provide valuable insight into how these therapies alter EGFR-driven signaling in NSCLC.

Overall, our data suggest that inhibitors of proximal signaling may be the most efficacious therapeutics to combine with osimertinib to treat EGFR-mutated tumors. Toward this end, Phase I trials are currently underway assessing the combination of osimertinib and the SRC inhibitor dasatinib (NCT02954523) in EGFR-mutated NSCLC, and recently developed SOS1 (BI-1701963, NCT04111458) and SHP2 (JAB-3068, NCT03565003; RMC-4630, NCT03634982) inhibitors have entered Phase I safety trials. Our study provides a framework for the systematic, preclinical assessment of therapeutic combinations designed to treat EGFR-mutated cancer cells. We show both how to use basic pharmacologic principles to assess drug-drug synergy and that these combinations must be assessed under 3D culture conditions. Using this framework, we show that the combination of osimertinib and the SOS1 inhibitor BAY-293 shows marked efficacy in 3D spheroid culture and should be pursued as a therapeutic option to treat EGFR-mutated lung adenocarcinoma.

Materials and methods

Key resources table

Reagent type (species) or resource	Designation	Source or reference	Identifiers	Additional information
Cell line (<i>Homo sapiens</i>)	Lung; adenocarcinoma; non-small cell lung cancer	Obtained from Udayan Guha, available at ATCC	NCI-H1975 CRL-5908 RRID:CVCL_UE30	
Cell line (<i>Homo sapiens</i>)	Lung; adenocarcinoma; epithelial	Obtained from Udayan Guha, available at ATCC	HCC827 CRL-2868 RRID:CVCL_DH92	
Cell line (<i>Homo sapiens</i>)	Lung; adenocarcinoma; non-small cell lung cancer	Obtained from Udayan Guha, available at NCI-DTP or ATCC	NCI-H3255 CRL-2882NCI-DTP Cat# NCI-H3255, RRID:CVCL_6831	
Cell line (<i>Homo sapiens</i>)	Lung; adenocarcinoma; non-small cell lung cancer	<i>de Bruin et al., 2014</i>	NCI-H3255TM	
Cell line (<i>Homo sapiens</i>)	Dermal fibroblast (normal, Adult)	Obtained from Udayan Guha, available at Millipore Sigma or BCRJ	PC9 #90071810 BCRJ_Cat# 0331, RRID:CVCL_B260	
Cell line (<i>Homo sapiens</i>)	Lung; adenocarcinoma; non-small cell lung cancer	<i>Engelman et al., 2006</i>	PC9-TM	

Continued on next page

Continued

Reagent type (species) or resource	Designation	Source or reference	Identifiers	Additional information
Cell line (<i>Homo sapiens</i>)	Kidney; epithelial fibroblast (fetus)	ATCC	HEK-293T ATCC Cat# CRL-3216, RRID:CVCL_0063	
Other	TransIT-Lenti	Mirus	Catalogue # MIR 6605	Lentiviral transduction reagent
Other	MISSION Lentiviral packaging mix	Millipore Sigma	Catalogue # SHP001	
Other	Bovine Serum Albumin	Millipore Sigma	Catalogue # A8022	Cell culture reagent for ACL-4 media
Other	apo-Transferrin (human)	Millipore Sigma	Catalogue # T5391	Cell culture reagent for ACL-4 media
Other	Sodium Selenite	Millipore Sigma	Catalogue # S9133	Cell culture reagent for ACL-4 media
Other	Hydrocortisone	Millipore Sigma	Catalogue # H0135	Cell culture reagent for ACL-4 media
Other	Ethanolamine	Millipore Sigma	Catalogue # E0135	Cell culture reagent for ACL-4 media
Other	O-Phosphoryl ethanolamine	Millipore Sigma	Catalogue # P0503	Cell culture reagent for ACL-4 media
Other	3,3',5-Triiodo-L-thyronine [T3]	Millipore Sigma	Catalogue # T5516	Cell culture reagent for ACL-4 media
Other	Sodium Pyruvate	Millipore Sigma	Catalogue # P4562	Cell culture reagent for ACL-4 media
Other	HEPES	Invitrogen	Catalogue # 15630-080	Cell culture reagent for ACL-4 media
Other	Epidermal Growth Factor [EGF]	Millipore Sigma	Catalogue # E4127	Cell culture reagent for ACL-4 media
Other	Recombinant Human Insulin	Millipore Sigma	Catalogue # I9278	Cell culture reagent for ACL-4 media
Other	AggreWell 400 low-attachment culture plates	Stem Cell	Catalogue # 34415	
Other	ultra-low attachment 96-well round bottomed plates	Corning Corstar	Catalogue # 7007	
Other	Nunc Nucleon Sphera microplates	ThermoFisher	Catalogue # 174929	
Other	coated 96-well white-walled CulturePlates	Perken Elmer	Catalogue # 6005688	
Antibody	anti-Sos 1 Antibody (C-23): sc-256, rabbit polyclonal	Santa Cruz	sc-256	(1:500)
Antibody	anti-SOS2 antibody (C-19): sc-258, rabbit polyclonal	Santa Cruz	sc-258	(1:500)
Antibody	anti- β -actin antibody AC15, mouse monoclonal	Millipore Sigma	#A1978	(1:5000)
Antibody	anti-Phospho-EGF Receptor (Tyr1068) (D7A5) XP Rabbit mAb #3777	Cell Signaling Technology	#3777	(1:1000)
Antibody	anti-phospho p44/42 MAPK (Erk1/2) (Thr202/Tyr204) (D13.14.4E) XP Rabbit mAb #4370	Cell Signaling Technology	#4370	(1:1000)

Continued on next page

Continued

Reagent type (species) or resource	Designation	Source or reference	Identifiers	Additional information
Antibody	anti-p44/42 MAPK (Erk1/2) (L34F12) Mouse mAb #4696	Cell Signaling Technology	#4696	(1:1000)
Antibody	anti- Phospho-Akt (Ser473) (D9E) XP Rabbit mAb #4060	Cell Signaling Technology	#4060	(1:1000)
Antibody	anti- Akt (pan) (40D4) Mouse mAb #2920	Cell Signaling Technology	#2920	(1:1000)
Antibody	anti-HSP 90 α / β Antibody (H-114): sc-7947	Santa Cruz	#sc-7947	(1:1000)
Antibody	anti-EGF Receptor (D38B1) XP Rabbit mAb #4267	Cell Signaling Technology	#4267	(1:1000)
Recombinant DNA Reagent	pLentiCrispr v2	<i>Sanjana et al., 2014</i>		
Other	CellTiter-Glo 2.0	Promega	G9243	
Recombinant DNA reagent	pLentiCrispr. NT	<i>Sheffels et al., 2018</i>	NT	sgRNA: CCATATCG GGGCGAGACATG
Recombinant DNA reagent	pLentiCrispr. SOS2-9	<i>Sheffels et al., 2018</i>	SOS2-9	sgRNA: GAGAACA GTCCGAAATGGCG
Recombinant DNA reagent	pLentiCrispr. SOS1-1	This manuscript	SOS1-1	sgRNA: GGGCAGC TGCTGCGCCTGCA
Recombinant DNA reagent	pLentiCrispr. SOS1-2	This manuscript	SOS1-2	sgRNA: GCATCCT TTCCAGTGTACTC
Recombinant DNA reagent	pLentiCrispr. SOS1-3	This manuscript	SOS1-3	sgRNA: TATTCTG CATTGCTAGCAC
Recombinant DNA reagent	pLentiCrispr. SOS1-4	This manuscript	SOS1-4	sgRNA: AGTGGCA TATAAGCAGACCT
Recombinant DNA reagent	pLentiCrispr. SOS1-5	This manuscript	SOS1-5	sgRNA: ATTGCAA GAGACAATGGACC
Recombinant DNA reagent	pLentiCrispr. SOS1-6	This manuscript	SOS1-6	sgRNA: GCTTATAT GCCACTCACTG
Recombinant DNA reagent	pLentiCrispr. SOS1-7	This manuscript	SOS1-7	sgRNA: GAAGGAA CTCTTACACGTGT
Recombinant DNA reagent	pLentiCrispr. SOS1-8	This manuscript	SOS1-8	sgRNA: CTATTGG GTGTAAGGTGAGC

Cell culture

Cell lines were cultured at 37°C and 5% CO₂. HCC827, NCI-H1975, PC9, and PC9-TM cells were maintained in Roswell Park Memorial Institute medium (RPMI), each supplemented with 10% fetal bovine serum and 1% penicillin-streptomycin. Cell lines were authenticated by STR profiling and confirmed as mycoplasma negative. EGFR mutations were confirmed by Sanger sequencing. H3255 and H3255-TM were maintained in ACL4 medium formulated in DMEM:F-12 including: Bovine Serum Albumin 0.5% (w/v) (Sigma cat no. A8022), apo-Transferrin (human) (Sigma cat no. T5391) 0.01 mg/mL, Sodium Selenite (Sigma cat no. S9133) 25 nM, Hydrocortisone (Sigma cat no. H0135) 50 nM, Ethanolamine (Sigma cat no. E0135) 0.01 mM, O-Phosphorylethanolamine (Sigma cat no. P0503) 0.01 mM, 3,3',5-Triiodo-L-thyronine [T3] (Sigma cat no. T5516) 100pM, Sodium Pyruvate (Sigma cat no. P4562), HEPES (Invitrogen cat no 15630-080) 10 mM, Epidermal Growth Factor [EGF] 1 ng/mL, Recombinant Human Insulin (Sigma cat no. I9278) 0.02 mg/mL, and 1% penicillin-streptomycin. For signaling experiments, cells were seeded in 24-well micropatterned AggreWell 400 low-attachment culture plates (Stem Cell # 34415) at 1.2 × 10⁶ cells/well in 2 mL of medium. 24 hr post-plating, half of the media was carefully replaced with fresh media to not disturb the spheroids. At 48 hr, 1 mL

media was removed and replaced with 2 x inhibitor. Cells were treated with inhibitor for 6 hr and then collected for cell lysis and western blot analysis.

Cell lysis and western blot analysis

Cells were lysed in RIPA buffer (1% NP-40, 0.1% SDS, 0.1% Na-deoxycholate, 10% glycerol, 0.137 M NaCl, 20 mM Tris pH [8.0], protease (Biotool #B14002) and phosphatase (Biotool #B15002) inhibitor cocktails) for 20 min at 4°C and spun at 10,000 RPM for 10 min. Clarified lysates were boiled in SDS sample buffer containing 100 mM DTT for 10 min prior to western blotting. Proteins were resolved by sodium dodecyl sulfate-polyacrylamide (Criterion TGX precast) gel electrophoresis and transferred to nitrocellulose membranes. Western blots were developed by multiplex Western blotting using anti-SOS1 (Santa Cruz sc-256; 1:500), anti-SOS2 (Santa Cruz sc-258; 1:500), anti- β -actin (Sigma AC-15; 1:5,000), anti-pEGFR (Cell Signaling 3777; 1:1000), anti-EGFR (Cell Signaling 4267; 1:1000), anti-pERK1/2 (Cell Signaling 4370; 1:1,000), anti-ERK1/2 (Cell Signaling 4696; 1:1000), anti-pAKT Ser⁴⁷³ (Cell Signaling 4060; 1:1000), anti-AKT (Cell Signaling 2920; 1:1000), anti-HSP90 (Santa Cruz sc-7947, 1:1000), primary antibodies. Anti-mouse and anti-rabbit secondary antibodies conjugated to IRDye680 or IRDye800 (LI-COR; 1:10,000) were used to probe primary antibodies. Western blot protein bands were detected and quantified using the Odyssey system (LI-COR). For quantification of SOS1 and SOS2 abundance, samples were normalized to either β -actin or HSP90. For quantification of pERK and pAKT, samples were normalized to a weighted average of HSP90, β -actin, total ERK1/2, total AKT, and total EGFR (Janes, 2015).

Proliferation studies

For 2D proliferation assays, 5×10^2 cells were seeded on cell culture-coated 96-well white-walled CulturePlates (Perkin Elmer #6005688). Cells were lysed with CellTiter-Glo 2.0 Reagent (Promega), and luminescence was read using a Bio-Tek Cytation five multi-mode plate reader. Cell number was assessed 24 hr after plating to account for any discrepancies in plating (Day 1), and then on days 3, 5, and 7. Data were analyzed as an increase in luminescence over Day 1.

Transformation studies

H3255 and H3255-TM cells were seeded in 0.32% Nobel agar at 2×10^4 cells per 35 mm dish to assess anchorage-independent. Soft agar colonies were counted 28 days after seeding. For all other cell lines spheroid growth assessed in ultra-low attachment 96-well round bottomed plates (Corning Costar #7007), cells were seeded at 500 cells per well. Images were taken 24 hr after plating to assess initial spheroid size, and then 7, 14, and 21 days later to assess transformation. Cell number was assessed in parallel plates at 0, 7, 14, and 21 days using CellTiter-Glo 2.0 reagent.

sgRNA studies

A non-targeting (NT) single guide RNA (sgRNA), a SOS2-targeted sgRNA (Sheffels et al., 2018), and eight potential SOS1-targeted sgRNAs previously used to target SOS1 in a genome-wide CRISPR screen (Munoz et al., 2016) were each cloned into pLentiCRISPRv2 as previously described (Sanjana et al., 2014). SOS1-2 was chosen as the SOS1 sgRNA for the study, and SOS2-9 was chosen as previously described (Sheffels et al., 2018). For studies in Figure 1, cells were infected lentivirus to express the given sgRNA with Cas9, and cells were selected for 10 days with puromycin prior to Western blotting. Cell lysates were probed for SOS1 or SOS2, and only cell populations showing greater than 80% SOS deletion within the overall population were used. Importantly, cell clones were not used, rather cell populations where > 80% of cells showed SOS deletion were used to minimize clonal effects. Independent infections were used for each experiment.

Construct	sgRNA
NT	CCATATCGGGGCGAGACATG
SOS2-9	GAGAACAGTCCGAAATGGCG
SOS1-1	GGGCAGCTGCTGCGCCTGCA

Continued on next page

Continued

Construct	sgRNA
SOS1-2	GCATCCTTTCCAGTGTACTC
SOS1-3	TATTCTGCATTGCTAGCACC
SOS1-4	AGTGCCATATAAGCAGACCT
SOS1-5	ATTGCAAGAGACAATGGACC
SOS1-6	GCTTATATGCCACTCAACTG
SOS1-7	GAAGGAACTCTTACACGTGT
SOS1-8	CTATTGGGTGTAAGGTGAGC

Production of recombinant lentiviruses

Lentiviruses were produced by co-transfecting MISSION lentiviral packaging mix (Sigma) into 293 T cells using Mirus TransIT-Lenti transfection reagent (Mirus Bio # MIR6605) in Opti-MEM (Thermo Scientific #31-985-062). At 48 hr post-transfection, viral supernatants were collected and filtered. Viral supernatants were then either stored at -80°C or used immediately to infect cells in combination with polybrene at $8\ \mu\text{g}/\text{mL}$. 48 hr post-infection, cells were selected in $4\ \mu\text{g}/\text{mL}$ Puromycin (Invitrogen). Twelve days after selection, cells were analyzed for SOS1 and SOS2 expression and plated for proliferation and transformation assays.

Inhibitor studies

- 2D adherent studies – Cells were seeded at 500–1,000 cells per well in $100\ \mu\text{L}$ in the inner-60 wells of 96-well white-walled culture plates (Perkin Elmer) and allowed to attach for 48 hr prior to drug treatment. Cells were treated with drug for 72 hr prior to assessment of cell viability using CellTiter-Glo 2.0.
- 3D adherent studies – Cells were seeded at 500–1,000 cells per well in $100\ \mu\text{L}$ in the inner-60 wells of 96-well ultra-low attachment round bottomed plates (Corning #7007) or Nunc Nucleon Sphera microplates (ThermoFisher # 174929) and allowed to coalesce as spheroids for 48–72 hr prior to drug treatment. Cells were treated with drug for 96 hr prior to assessment of cell viability using CellTiter-Glo 2.0.

For all studies, outer wells (rows A and H, columns 1 and 12) were filled with $200\ \mu\text{L}$ of PBS to buffer inner cells from temperature and humidity fluctuations. Triplicate wells of cells were then treated with increasing concentrations $100\ \mu\text{L}$ of $2 \times$ inhibitor at either a semilog (single drug dose response curves to determine EC_{50}) or a 1/3-log scale (isobologram and Bliss independence experiments) for 72 (adherent cultures) or 96 (spheroids) hr. Cell viability was assessed using CellTiter-Glo 2.0 ($30\ \mu\text{L}/\text{well}$). Luminescence was assessed using a Bio-Tek Cytation five multi-mode plate reader. Data were normalized to the maximum luminescence reading of untreated cells, and individual drug EC_{50} values were calculated using Prism eight by non-linear regression using $\log(\text{inhibitor})$ vs. response with a variable slope (four parameters) to assess for differences in the Hill Coefficient between different drug treatments. For all drug-treatment studies, the untreated sample for each cell line was set to 100%. This would mask any differences in 3D cell proliferation seen between cell lines.

Isobologram analysis

Dose equivalence was first determined by assessing individual-drug EC_{50} values; individual-drug Hill Coefficients were determined to assure that the two drugs could be assessed for synergy by Lowe additivity. To generate dose-equivalent dose-response curves, the dose for each drug closest to the EC_{50} on a 1/3-log scale was set as equivalent, and 10-point dose response curves were generated for each individual drug on either side of the equivalent dose to ensure the top (no drug effect) and bottom (maximal drug effect) were represented on the dose-response curve. $100\ \mu\text{L}$ of drug each drug dose was added as outlined above. To generate dose-equivalent mixtures for isobologram analysis, equivalent doses of the two drugs were mixed at different ratios so that the total dose ($100\ \mu\text{L}$) would be expected to have an equivalent effect on the cells if the two drugs were additive.

Drugs were mixed at either five (4:1, 2:1, 1:1, 1:2, and 1:4) or three (2:1, 1:1, and 1:2) different drug mixtures depending on the experiment. Cells were treated and EC₅₀ values for each individual drug or drug mixture based on each drug's dosing were determined for as outlined above. To generate an isobologram plot, the EC₅₀ of each individual drug was plotted as the x- or y-intercept, and the calculated contribution of each drug to the overall EC₅₀ for each DEQ mix is plotted as a single point (EC_{50,A}, EC_{50,B}) on the graph.

$$\text{Combination Index} = \frac{EC_{50}A_{\text{mix}}}{EC_{50}A_{\text{alone}}} + \frac{EC_{50}B_{\text{mix}}}{EC_{50}B_{\text{alone}}}$$

To calculate the combination index for each dose equivalent mixture, the calculated contribution of each drug to the overall EC₅₀ were used in the equation:

As an example, we will show data for one trial analyzing the combination of osimertinib and BAY-293 in 3D spheroid cultured H1975 cells in **Figure 2B**. The EC₅₀ values for each individual drug were first determined: -8.57 for osimertinib and -5.73 for BAY-293. Based on these EC₅₀ values, the dose equivalence was set at -8.67 for osimertinib -5.67 for BAY-293 (approximated EC₅₀ for each drug in bold), and the following 10-point dose response curves were generated:

Osimertinib	-11	-10.67	-10.33	-10	-9.67	-9.33	-9	-8.67	-8.33	-8
BAY-293	-8	-7.67	-7.33	-7	-6.67	-6.33	-6	-5.67	-5.33	-5

Cells were then treated with the following volumes of each drug to generate seven dose-equivalent dose response curves:

		4:1 mixture	2:1 mixture	1:1 mixture	1:2 mixture	1:4 mixture	
osimertinib	100 μL	80 μL	66 μL	50 μL	34 μL	20 μL	0 μL
BAY-293	0 μL	20 μL	34 μL	50 μL	66 μL	80 μL	100 μL

EC₅₀ values for each dose-response curve were then determined based on each drug's dosing:

	OSM alone	4:1 mixture	2:1 mixture	1:1 mixture	1:2 mixture	1:4 mixture	BAY alone
osimertinib EC ₅₀ (nM)	2.62	0.84	0.70	0.92	1.49	1.19	2.40
BAY-293 EC ₅₀ (μM)	2.14	1.01	0.83	1.09	1.49	1.04	1.82

EC₅₀ values were then adjusted based on the amount of each drug that was put in the mixture to determine the contribution of each drug in the mixture to the overall EC₅₀. For example, the 4:1 mixture was 80% osimertinib, so the osimertinib EC₅₀ for that mixture is multiplied by 0.8. The corresponding corrected EC₅₀ values and combination indices were:

	OSM alone	4:1 mixture	2:1 mixture	1:1 mixture	1:2 mixture	1:4 mixture	BAY alone
osimertinib EC ₅₀ (nM)	2.62	0.67	0.45	0.46	0.52	0.24	0
BAY-293 EC ₅₀ (μM)	0	0.20	0.29	0.54	0.97	0.84	1.82
Combination Index		0.40	0.34	0.44	0.65	0.46	

Bliss independence analysis

Unlike Isobologram analysis, individual drug doses are not reduced for drug-drug combinations when performing Bliss independence analysis. For data in **Figure 2**, wells were treated with a full dose of each individual drug or drug combination in a 10×10 matrix of dose combinations for osimertinib and BAY-293 on a 1/3-log scale. Data were normalized to the maximum luminescence reading of untreated cells, and a heat-map depicting cell viability was generated using Prism 8. The Bliss index was calculated by first converting viability (on a scale of 0 to 1) for each treatment to the effect of each drug or drug combination, where 0 represents no effect and 1 represents 100% effect (no viable cells).

$$\text{effect} = 1 - \text{viability}$$

From the effect data, the expected effect for each drug combination is calculated:

$$\text{Expected effect} = E_A + E_B * (1 - E_A)$$

$$\text{Expected effect} = E_A + E_B - E_A * E_B$$

The Bliss Index is the ratio of the expected effect/actual effect:

$$\text{Bliss Index} = (\text{expected effect}) / (\text{actual effect})$$

$$\text{Bliss Index} = (E_A + E_B - E_A * E_B) / (E_{A+B\text{MIX}})$$

A Bliss Index of 1 indicates that the actual and expected effects are equivalent, and the effects of the two drugs are additive. Bliss Index < 1 indicates increasing synergy, whereas Bliss Index > 1 indicates antagonism.

Excess over Bliss is calculated by determining how much greater the actual effect of the drug combination is versus the expected effect, and is calculated as:

$$\text{Excess over Bliss} = 100 * [\text{actual effect} - \text{expected effect}]$$

$$\text{Excess over Bliss} = 100 * [E_{A+B\text{MIX}} - (E_A + E_B - E_A * E_B)]$$

An excess over Bliss of 0 indicates that the actual and expected effects are equivalent, and the effects of the two drugs are additive; values > 0 indicate increasing synergy, whereas values < 0 indicate antagonism.

Since synergy occurred at drug combinations at or just below the EC₅₀ values for each individual drug, Bliss experiments in **Figures 4** and **5**, drug mixtures were limited to 3×10 drug mixtures based on dose equivalence with mixtures at approximately 2:1, 1:1, and 1:2 mixes of the two drugs based on dose equivalence. Here, the doses used for one drug were held constant, and the second drug dose was shifted by 1/3 log up or down to generate 2:1 and 1:2 mixtures. For example, for the combination of osimertinib and BAY-293 in H1975 cells, the following drug doses were used:

Osimertinib (1:2 ratio of OSM:BAY)	-11.33	-11	-10.67	-10.33	-10	-9.67	-9.33	-9	-8.67	-8.33
Osimertinib (1:1 ratio of OSM:BAY)	-11	-10.67	-10.33	-10	-9.67	-9.33	-9	-8.67	-8.33	-8
Osimertinib (2:1 ratio of OSM:BAY)	-10.67	-10.33	-10	-9.67	-9.33	-9	-8.67	-8.33	-8	-7.67
BAY-293 (constant)	-8	-7.67	-7.33	-7	-6.67	-6.33	-6	-5.67	-5.33	-5

Three-drug isobologram analysis

For three-drug isobologram studies with osimertinib ($EC_{50} = -8.57$), BAY-293 ($EC_{50} = -5.74$), and RCM-4550 ($EC_{50} = -6.84$), drugs were again mixed based on dose equivalency. The dose-equivalent 10-point dose-response curves for these drugs in 3D cultured H1975 cells were (approximated EC_{50} for each drug in bold):

Osimertinib	-11	-10.67	-10.33	-10	-9.67	-9.33	-9	-8.67	-8.33	-8
BAY-293	-8	-7.67	-7.33	-7	-6.67	-6.33	-6	-5.67	-5.33	-5
RCM-4550	-9	-8.67	-8.33	-8	-7.67	-7.33	-7	-6.67	-6.33	-6

Each two-drug combination was set as a single 'drug mixture' at a 1:1 ratio, and the third drug was combined with this drug mixture at 2:1, 1:1, and 1:2 drug ratios. To generate the proper two and three-drug mixtures for analysis, 21 total dose response curves were generated. The five dose-response curves on the right represent the mixtures used to generate the isobologram plots in **Figure 7D**. The other two two-drug mixtures in **bold** (two-drug 2:1 and 1:2 mixtures) were used to generate the isobologram plots in **Figure 7C**. Combination indices were calculated based on whether addition of the third drug to each two-drug 1:1 mixture further enhanced synergy when added to the two-drug mixture.

[osimertinib:BAY-293] mixture vs. RCM-4550:

	OSM:BAY 2:1	OSM:BAY 1:2	Osm:BAY 1:1	(1+1):1 2:1 mixture	(1+1):2 1:1 mixture	(1+1):4 1:2 mixture	RCM alone
osimertinib	66 μ L	34 μ L	50 μ L	33 μ L	25 μ L	17 μ L	0 μ L
BAY-293	34 μ L	66 μ L	50 μ L	33 μ L	25 μ L	17 μ L	0 μ L
RCM-4550	0 μ L	0 μ L	0 μ L	34 μ L	50 μ L	66 μ L	100 μ L

$$\text{Combination Index} = \frac{EC_{50} \text{ OSM} + BAY_{3\text{-drug mix}}}{EC_{50} \text{ OSM} + BAY_{50:50}} + \frac{EC_{50} \text{ RCM}_{3\text{-drug mix}}}{EC_{50} \text{ RCM}_{\text{alone}}}$$

[osimertinib:RCM-4550] mixture vs. BAY-293:

	OSM:RCM 2:1	OSM:RCM 1:2	Osm:RCM 1:1	(1+1):1 2:1 mixture	(1+1):2 1:1 mixture	(1+1):4 1:2 mixture	RCM alone
osimertinib	66 μ L	34 μ L	50 μ L	33 μ L	25 μ L	17 μ L	0 μ L
BAY-293	0 μ L	0 μ L	0 μ L	34 μ L	50 μ L	66 μ L	100 μ L
RCM-4550	34 μ L	66 μ L	50 μ L	33 μ L	25 μ L	17 μ L	0 μ L

$$\text{Combination Index} = \frac{EC_{50} \text{ OSM} + RCM_{3\text{-drug mix}}}{EC_{50} \text{ OSM} + RCM_{50:50}} + \frac{EC_{50} \text{ BAY}_{3\text{-drug mix}}}{EC_{50} \text{ BAY}_{\text{alone}}}$$

[BAY-293:RCM-4550] mixture vs. osimertinib:

	BAY:RCM 2:1	BAY:RCM 1:2	Bay:RCM 1:1	(1+1):1 2:1 mixture	(1+1):2 1:1 mixture	(1+1):4 1:2 mixture	RCM alone
osimertinib	0 μ L	0 μ L	0 μ L	34 μ L	50 μ L	66 μ L	100 μ L
BAY-293	66 μ L	34 μ L	50 μ L	33 μ L	25 μ L	17 μ L	0 μ L
RCM-4550	34 μ L	66 μ L	50 μ L	33 μ L	25 μ L	17 μ L	0 μ L

$$\text{Combination Index} = \frac{EC_{50} \text{BAY} + RCM_{3\text{-drug mix}}}{EC_{50} \text{BAY} + RCM_{50:50}} + \frac{EC_{50} \text{OSM}_{3\text{-drug mix}}}{EC_{50} \text{OSM}_{\text{alone}}}$$

To calculate the three-drug combination index where each drug was considered independently (**Figure 7E**), the following equation was used:

$$\text{Combination Index} = \frac{EC_{50} \text{OSM}_{3\text{-drug mix}}}{EC_{50} \text{OSM}_{50:50}} + \frac{EC_{50} \text{BAY}_{3\text{-drug mix}}}{EC_{50} \text{BAY}_{\text{alone}}} + \frac{EC_{50} \text{RCM}_{3\text{-drug mix}}}{EC_{50} \text{RCM}_{\text{alone}}}$$

Acknowledgements

We thank Udayan Guha for NCI-H1975, HCC827, PC9, H3255 and H3255-TM cells and for helpful discussions throughout the project. We thank Julian Downward for PC9-TM cells. Funding: This work was supported by grants from the Congressionally Directed Medical Research Program to RLK (LC160222 and LC180213).

Additional information

Funding

Funder	Grant reference number	Author
Congressionally Directed Medical Research Programs	LC160222	Robert L Kortum
Congressionally Directed Medical Research Programs	LC180213	Robert L Kortum

The funders had no role in study design, data collection and interpretation, or the decision to submit the work for publication.

Author contributions

Patricia L Theard, Robert L Kortum, Conceptualization, Resources, Data curation, Formal analysis, Supervision, Funding acquisition, Investigation, Methodology, Writing - original draft, Project administration, Writing - review and editing; Erin Sheffels, Conceptualization, Data curation, Formal analysis, Investigation, Writing - original draft, Writing - review and editing; Nancy E Sealover, Conceptualization, Investigation, Writing - review and editing; Amanda J Linke, David J Pratico, Investigation, Writing - review and editing

Author ORCIDs

Robert L Kortum  <https://orcid.org/0000-0002-1634-4882>

Decision letter and Author response

Decision letter <https://doi.org/10.7554/eLife.58204.sa1>

Author response <https://doi.org/10.7554/eLife.58204.sa2>

Additional files

Supplementary files

- Source data 1. Supplemental raw data.
- Transparent reporting form

Data availability

All data generated or analysed during this study are included in the manuscript and supporting files. Source data files have been provided for Figures 1, 2, 3, 4, 5, 6, 7, and Figure 1—figure supplement 2 and Figure 3—figure supplement 1.

References

- Balbin OA**, Prensner JR, Sahu A, Yocum A, Shankar S, Malik R, Fermin D, Dhanasekaran SM, Chandler B, Thomas D, Beer DG, Cao X, Nesvizhskii AI, Chinnaiyan AM. 2013. Reconstructing targetable pathways in lung Cancer by integrating diverse omics data. *Nature Communications* **4**:2617. DOI: <https://doi.org/10.1038/ncomms3617>, PMID: 24135919
- Cancer Genome Atlas Research Network**. 2014. Comprehensive molecular profiling of lung adenocarcinoma. *Nature* **511**:543–550. DOI: <https://doi.org/10.1038/nature13385>, PMID: 25079552
- Cross DA**, Ashton SE, Ghiorghiu S, Eberlein C, Nebhan CA, Spitzler PJ, Orme JP, Finlay MR, Ward RA, Mellor MJ, Hughes G, Rahi A, Jacobs VN, Red Brewer M, Ichihara E, Sun J, Jin H, Ballard P, Al-Kadhimi K, Rowlinson R, et al. 2014. AZD9291, an irreversible EGFR TKI, overcomes T790M-mediated resistance to EGFR inhibitors in lung Cancer. *Cancer Discovery* **4**:1046–1061. DOI: <https://doi.org/10.1158/2159-8290.CD-14-0337>, PMID: 24893891
- Dance M**, Montagner A, Salles JP, Yart A, Raynal P. 2008. The molecular functions of Shp2 in the ras/Mitogen-activated protein kinase (ERK1/2) pathway. *Cellular Signalling* **20**:453–459. DOI: <https://doi.org/10.1016/j.cellsig.2007.10.002>, PMID: 17993263
- de Bruin EC**, Cowell C, Warne PH, Jiang M, Saunders RE, Melnick MA, Gettinger S, Walther Z, Wurtz A, Heynen GJ, Heideman DA, Gómez-Román J, García-Castaño A, Gong Y, Ladanyi M, Varmus H, Bernards R, Smit EF, Politi K, Downward J. 2014. Reduced NF1 expression confers resistance to EGFR inhibition in lung Cancer. *Cancer Discovery* **4**:606–619. DOI: <https://doi.org/10.1158/2159-8290.CD-13-0741>, PMID: 24535670
- Della Corte CM**, Ciaramella V, Cardone C, La Monica S, Alfieri R, Petronini PG, Malapelle U, Vigliar E, Pepe F, Troncione G, Castellone MD, Troiani T, Martinelli E, Ciardiello F, Morgillo F. 2018. Antitumor efficacy of dual blockade of EGFR signaling by osimertinib in combination with selumetinib or cetuximab in activated EGFR human NCLC tumor models. *Journal of Thoracic Oncology* **13**:810–820. DOI: <https://doi.org/10.1016/j.jtho.2018.02.025>, PMID: 29526823
- Eberhard DA**, Johnson BE, Amler LC, Goddard AD, Heldens SL, Herbst RS, Ince WL, Jänne PA, Januario T, Johnson DH, Klein P, Miller VA, Ostland MA, Ramies DA, Sebisano D, Stinson JA, Zhang YR, Seshagiri S, Hillan KJ. 2005. Mutations in the epidermal growth factor receptor and in KRAS are predictive and prognostic indicators in patients with non-small-cell lung Cancer treated with chemotherapy alone and in combination with erlotinib. *Journal of Clinical Oncology* **23**:5900–5909. DOI: <https://doi.org/10.1200/JCO.2005.02.857>, PMID: 16043828
- Eberlein CA**, Stetson D, Markovets AA, Al-Kadhimi KJ, Lai Z, Fisher PR, Meador CB, Spitzler P, Ichihara E, Ross SJ, Ahdesmaki MJ, Ahmed A, Ratcliffe LE, O'Brien EL, Barnes CH, Brown H, Smith PD, Dry JR, Beran G, Thress KS, et al. 2015. Acquired resistance to the Mutant-Selective EGFR inhibitor AZD9291 is associated with increased dependence on RAS signaling in preclinical models. *Cancer Research* **75**:2489–2500. DOI: <https://doi.org/10.1158/0008-5472.CAN-14-3167>, PMID: 25870145
- Ekert JE**, Johnson K, Strake B, Pardin J, Jarantow S, Perkinson R, Colter DC. 2014. Three-dimensional lung tumor microenvironment modulates therapeutic compound responsiveness in vitro—implication for drug development. *PLOS ONE* **9**:e92248. DOI: <https://doi.org/10.1371/journal.pone.0092248>, PMID: 24638075
- Engelman JA**, Mukohara T, Zejnullahu K, Lifshits E, Borrás AM, Gale CM, Naumov GN, Yeap BY, Jarrell E, Sun J, Tracy S, Zhao X, Heymach JV, Johnson BE, Cantley LC, Jänne PA. 2006. Allelic dilution obscures detection of a biologically significant resistance mutation in EGFR-amplified lung Cancer. *Journal of Clinical Investigation* **116**:2695–2706. DOI: <https://doi.org/10.1172/JCI28656>, PMID: 16906227
- Fan R**, Kim NG, Gumbiner BM. 2013. Regulation of hippo pathway by mitogenic growth factors via phosphoinositide 3-kinase and phosphoinositide-dependent kinase-1. *PNAS* **110**:2569–2574. DOI: <https://doi.org/10.1073/pnas.1216462110>, PMID: 23359693
- Fortian A**, Sorkin A. 2014. Live-cell fluorescence imaging reveals high stoichiometry of Grb2 binding to the EGF receptor sustained during endocytosis. *Journal of Cell Science* **127**:432–444. DOI: <https://doi.org/10.1242/jcs.137786>, PMID: 24259669
- Fujita-Sato S**, Galeas J, Truitt M, Pitt C, Urisman A, Bandyopadhyay S, Ruggero D, McCormick F. 2015. Enhanced MET translation and signaling sustains K-Ras-Driven proliferation under Anchorage-Independent growth conditions. *Cancer Research* **75**:2851–2862. DOI: <https://doi.org/10.1158/0008-5472.CAN-14-1623>, PMID: 25977330
- Han K**, Pierce SE, Li A, Spees K, Anderson GR, Seoane JA, Lo YH, Dubreuil M, Olivias M, Kamber RA, Wainberg M, Kostyrko K, Kelly MR, Yousefi M, Simpkins SW, Yao D, Lee K, Kuo CJ, Jackson PK, Sweet-Cordero A, et al. 2020. CRISPR screens in Cancer spheroids identify 3D growth-specific vulnerabilities. *Nature* **580**:136–141. DOI: <https://doi.org/10.1038/s41586-020-2099-x>, PMID: 32238925
- Hao HX**, Wang H, Liu C, Kovats S, Velazquez R, Lu H, Pant B, Shirley M, Meyer MJ, Pu M, Lim J, Fleming M, Alexander L, Farsidjani A, LaMarche MJ, Moody S, Silver SJ, Caponigro G, Stuart DD, Abrams TJ, et al. 2019. Tumor intrinsic efficacy by SHP2 and RTK inhibitors in KRAS-Mutant cancers. *Molecular Cancer Therapeutics* **18**:2368–2380. DOI: <https://doi.org/10.1158/1535-7163.MCT-19-0170>, PMID: 31439712
- Hillig RC**, Sautier B, Schroeder J, Moosmayer D, Hilpmann A, Stegmann CM, Werbeck ND, Briem H, Boemer U, Weiske J, Badock V, Mastouri J, Petersen K, Siemeister G, Kahmann JD, Wegener D, Böhnke N, Eis K, Graham K, Wortmann L, et al. 2019. Discovery of potent SOS1 inhibitors that block RAS activation via disruption of the RAS-SOS1 interaction. *PNAS* **116**:2551–2560. DOI: <https://doi.org/10.1073/pnas.1812963116>, PMID: 30683722
- Hofmann MH**, Gmachl M, Ramharter J, Savarese F, Gerlach D, Marszalek JR, Sanderson MP, Kessler D, Trapani F, Arnhof H, Rumpel K, Botesteanu DA, Ettmayer P, Gerstberger T, Kofink C, Wunberg T, Zoepfel A, Fu SC,

- Teh JL, Bottcher J, et al. 2020. BI-3406, a potent and selective SOS1::KRAS interaction inhibitor, is effective in KRAS-driven cancers through combined MEK inhibition. *Cancer Discovery*:CD-20-0142. DOI: <https://doi.org/10.1158/2159-8290.CD-20-0142>, PMID: 32816843
- Ichihara E, Westover D, Meador CB, Yan Y, Bauer JA, Lu P, Ye F, Kulick A, de Stanchina E, McEwen R, Ladanyi M, Cross D, Pao W, Lovly CM. 2017. SFK/FAK signaling attenuates osimertinib efficacy in both Drug-Sensitive and Drug-Resistant models of EGFR-Mutant lung Cancer. *Cancer Research* **77**:2990–3000. DOI: <https://doi.org/10.1158/0008-5472.CAN-16-2300>, PMID: 28416483
- Jacobi N, Seeboeck R, Hofmann E, Schweiger H, Smolinska V, Mohr T, Boyer A, Sommergruber W, Lechner P, Pichler-Huebschmann C, Önder K, Hundsberger H, Wiesner C, Eger A. 2017. Organotypic three-dimensional Cancer cell cultures mirror drug responses *in vivo*: lessons learned from the inhibition of EGFR signaling. *Oncotarget* **8**:107423–107440. DOI: <https://doi.org/10.18632/oncotarget.22475>, PMID: 29296175
- Jacobsen K, Bertran-Alamillo J, Molina MA, Teixidó C, Karachaliou N, Pedersen MH, Castellví J, Garzón M, Codony-Servat C, Codony-Servat J, Giménez-Capitán A, Drozdowskyj A, Viteri S, Larsen MR, Lassen U, Felip E, Bivona TG, Ditzel HJ, Rosell R. 2017. Convergent akt activation drives acquired EGFR inhibitor resistance in lung Cancer. *Nature Communications* **8**:410. DOI: <https://doi.org/10.1038/s41467-017-00450-6>, PMID: 28871105
- Janes KA. 2015. An analysis of critical factors for quantitative immunoblotting. *Science Signaling* **8**:rs2. DOI: <https://doi.org/10.1126/scisignal.2005966>, PMID: 25852189
- Janes MR, Zhang J, Li LS, Hansen R, Peters U, Guo X, Chen Y, Babbar A, Firdaus SJ, Darjania L, Feng J, Chen JH, Li S, Li S, Long YO, Thach C, Liu Y, Zariah A, Ely T, Kucharski JM, et al. 2018. Targeting KRAS mutant cancers with a covalent G12C-Specific inhibitor. *Cell* **172**:578–589. DOI: <https://doi.org/10.1016/j.cell.2018.01.006>, PMID: 29373830
- Jänne PA, Yang JC, Kim DW, Planchard D, Ohe Y, Ramalingam SS, Ahn MJ, Kim SW, Su WC, Horn L, Haggstrom D, Felip E, Kim JH, Frewer P, Cantarini M, Brown KH, Dickinson PA, Ghiorghiu S, Ranson M. 2015. AZD9291 in EGFR inhibitor-resistant non-small-cell lung Cancer. *New England Journal of Medicine* **372**:1689–1699. DOI: <https://doi.org/10.1056/NEJMoa1411817>, PMID: 25923549
- Jeng HH, Taylor LJ, Bar-Sagi D. 2012. Sos-mediated cross-activation of wild-type ras by oncogenic ras is essential for tumorigenesis. *Nature Communications* **3**:1168. DOI: <https://doi.org/10.1038/ncomms2173>, PMID: 23132018
- Jimbo T, Hatanaka M, Komatsu T, Taira T, Kumazawa K, Maeda N, Suzuki T, Ota M, Haginoya N, Ioyama T, Fujiwara K. 2019. DS-1205b, a novel selective inhibitor of AXL kinase, blocks resistance to EGFR-tyrosine kinase inhibitors in a non-small cell lung Cancer xenograft model. *Oncotarget* **10**:5152–5167. DOI: <https://doi.org/10.18632/oncotarget.27114>, PMID: 31497246
- Jones GG, Del Río IB, Sari S, Sekerim A, Young LC, Hartig N, Areso Zubiaur I, El-Bahrawy MA, Hynds RE, Lei W, Molina-Arcas M, Downward J, Rodriguez-Viciano P. 2019. SHOC2 phosphatase-dependent RAF dimerization mediates resistance to MEK inhibition in RAS-mutant cancers. *Nature Communications* **10**:2532. DOI: <https://doi.org/10.1038/s41467-019-10367-x>, PMID: 31182717
- Kim JW, Ho WJ, Wu BM. 2011. The role of the 3D environment in hypoxia-induced drug and apoptosis resistance. *Anticancer Research* **31**:3237–3245. PMID: 21965731
- Kim D, Bach D-H, Fan Y-H, Luu T, Hong J-Y, Park HJ, Lee SK. 2019. AXL degradation in combination with EGFR-TKI can delay and overcome acquired resistance in human non-small cell lung Cancer cells. *Cell Death & Disease* **10**:361. DOI: <https://doi.org/10.1038/s41419-019-1601-6>
- Ku BM, Choi MK, Sun JM, Lee SH, Ahn JS, Park K, Ahn MJ. 2018. Acquired resistance to AZD9291 as an upfront treatment is dependent on ERK signaling in a preclinical model. *PLOS ONE* **13**:e0194730. DOI: <https://doi.org/10.1371/journal.pone.0194730>, PMID: 29641535
- Kurppa KJ, Liu Y, To C, Zhang T, Fan M, Vajdi A, Knelson EH, Xie Y, Lim K, Cejas P, Portell A, Lizotte PH, Ficarro SB, Li S, Chen T, Haikala HM, Wang H, Bahcall M, Gao Y, Shalhout S, et al. 2020. Treatment-Induced tumor dormancy through YAP-Mediated transcriptional reprogramming of the apoptotic pathway. *Cancer Cell* **37**:104–122. DOI: <https://doi.org/10.1016/j.ccell.2019.12.006>
- La Monica S, Cretella D, Bonelli M, Fumarola C, Cavazzoni A, Digiacomo G, Flammini L, Barocelli E, Minari R, Naldi N, Petronini PG, Tiseo M, Alfieri R. 2017. Trastuzumab emtansine delays and overcomes resistance to the third-generation EGFR-TKI osimertinib in NSCLC EGFR mutated cell lines. *Journal of Experimental & Clinical Cancer Research* **36**:174. DOI: <https://doi.org/10.1186/s13046-017-0653-7>, PMID: 29202823
- Lamba S, Russo M, Sun C, Lazzari L, Cancelliere C, Grennum W, Liefink C, Bernards R, Di Nicolantonio F, Bardelli A. 2014. RAF suppression synergizes with MEK inhibition in KRAS mutant Cancer cells. *Cell Reports* **8**:1475–1483. DOI: <https://doi.org/10.1016/j.celrep.2014.07.033>, PMID: 25199829
- Langhans SA. 2018. Three-Dimensional *in vitro* Cell Culture Models in Drug Discovery and Drug Repositioning. *Frontiers in Pharmacology* **9**:6. DOI: <https://doi.org/10.3389/fphar.2018.00006>, PMID: 29410625
- Mancini M, Gal H, Gaborit N, Mazzeo L, Romaniello D, Salame TM, Lindzen M, Mahlknecht G, Erika Y, Burton DG, Roth L, Noronha A, Marrocco I, Adreka D, Altstadter RE, Bousquet E, Downward J, Maraver A, Krizhanovsky V, Yarden Y. 2018. An oligoclonal antibody durably overcomes resistance of lung Cancer to third-generation EGFR inhibitors. *EMBO Molecular Medicine* **10**:294–308. DOI: <https://doi.org/10.15252/emmm.201708076>, PMID: 29212784
- McCormick F. 2015. KRAS as a therapeutic target. *Clinical Cancer Research* **21**:1797–1801. DOI: <https://doi.org/10.1158/1078-0432.CCR-14-2662>, PMID: 25878360

- Mittler F**, Obeid P, Rulina AV, Haguët V, Gidrol X, Balakirev MY. 2017. High-Content monitoring of drug effects in a 3D spheroid model. *Frontiers in Oncology* **7**:293. DOI: <https://doi.org/10.3389/fonc.2017.00293>, PMID: 29322028
- Mok TS**, Wu YL, Thongprasert S, Yang CH, Chu DT, Saijo N, Sunpaweravong P, Han B, Margono B, Ichinose Y, Nishiwaki Y, Ohe Y, Yang JJ, Chewaskulyong B, Jiang H, Duffield EL, Watkins CL, Armour AA, Fukuoka M. 2009. Gefitinib or carboplatin-paclitaxel in pulmonary adenocarcinoma. *New England Journal of Medicine* **361**: 947–957. DOI: <https://doi.org/10.1056/NEJMoa0810699>, PMID: 19692680
- Munoz DM**, Cassiani PJ, Li L, Billy E, Korn JM, Jones MD, Golji J, Ruddy DA, Yu K, McAllister G, DeWeck A, Abramowski D, Wan J, Shirley MD, Neshat SY, Rakiec D, de Beaumont R, Weber O, Kauffmann A, McDonald ER, et al. 2016. CRISPR screens provide a comprehensive assessment of Cancer vulnerabilities but generate False-Positive hits for highly amplified genomic regions. *Cancer Discovery* **6**:900–913. DOI: <https://doi.org/10.1158/2159-8290.CD-16-0178>, PMID: 27260157
- Namba K**, Shien K, Takahashi Y, Torigoe H, Sato H, Yoshioka T, Takeda T, Kurihara E, Ogoshi Y, Yamamoto H, Soh J, Tomida S, Toyooka S. 2019. Activation of AXL as a preclinical acquired resistance mechanism against osimertinib treatment in EGFR-Mutant Non-Small Cell Lung Cancer Cells. *Molecular Cancer Research* **17**:499–507. DOI: <https://doi.org/10.1158/1541-7786.MCR-18-0628>, PMID: 30463991
- Nichols RJ**, Haderk F, Stahlhut C, Schulze CJ, Hemmati G, Wildes D, Tzitzilonis C, Mordec K, Marquez A, Romero J, Hsieh T, Zaman A, Olivás V, McCoach C, Blakely CM, Wang Z, Kiss G, Koltun ES, Gill AL, Singh M, et al. 2018. RAS nucleotide cycling underlies the SHP2 phosphatase dependence of mutant BRAF-, NF1- and RAS-driven cancers. *Nature Cell Biology* **20**:1064–1073. DOI: <https://doi.org/10.1038/s41556-018-0169-1>, PMID: 30104724
- Nunes AS**, Barros AS, Costa EC, Moreira AF, Correia IJ. 2019. 3d tumor spheroids as in vitro models to mimic in vivo human solid tumors resistance to therapeutic drugs. *Biotechnology and Bioengineering* **116**:206–226. DOI: <https://doi.org/10.1002/bit.26845>, PMID: 30367820
- Park JH**, Choi YJ, Kim SY, Lee JE, Sung KJ, Park S, Kim WS, Song JS, Choi CM, Sung YH, Rho JK, Lee JC. 2016. Activation of the IGF1R pathway potentially mediates acquired resistance to mutant-selective 3rd-generation EGF receptor tyrosine kinase inhibitors in advanced non-small cell lung Cancer. *Oncotarget* **7**:22005–22015. DOI: <https://doi.org/10.18632/oncotarget.8013>, PMID: 26980747
- Ramalingam SS**, Vansteenkiste J, Planchard D, Cho BC, Gray JE, Ohe Y, Zhou C, Reungwetwattana T, Cheng Y, Chewaskulyong B, Shah R, Cobo M, Lee KH, Cheema P, Tiseo M, John T, Lin MC, Imamura F, Kurata T, Todd A, et al. 2020. Overall survival with osimertinib in Untreated, EGFR-Mutated Advanced NSCLC. *New England Journal of Medicine* **382**:41–50. DOI: <https://doi.org/10.1056/NEJMoa1913662>, PMID: 31751012
- Riedl A**, Schleder M, Pudelko K, Stadler M, Walter S, Unterleuthner D, Unger C, Kramer N, Hengstschläger M, Kenner L, Pfeiffer D, Krupitza G, Dolznig H. 2017. Comparison of Cancer cells in 2D vs 3D culture reveals differences in AKT-mTOR-S6K signaling and drug responses. *Journal of Cell Science* **130**:203–218. DOI: <https://doi.org/10.1242/jcs.188102>, PMID: 27663511
- Roell KR**, Reif DM, Motsinger-Reif AA. 2017. An introduction to terminology and methodology of chemical Synergy-Perspectives from across disciplines. *Frontiers in Pharmacology* **8**:158. DOI: <https://doi.org/10.3389/fphar.2017.00158>, PMID: 28473769
- Romaniello D**, Mazzeo L, Mancini M, Marrocco I, Noronha A, Kreitman M, Srivastava S, Ghosh S, Lindzen M, Salame TM, Onn A, Bar J, Yarden Y. 2018. A combination of approved antibodies overcomes resistance of lung Cancer to osimertinib by blocking bypass pathways. *Clinical Cancer Research* **24**:5610–5621. DOI: <https://doi.org/10.1158/1078-0432.CCR-18-0450>, PMID: 29967248
- Rotem A**, Janzer A, Izar B, Ji Z, Doench JG, Garraway LA, Struhl K. 2015. Alternative to the soft-agar assay that permits high-throughput drug and genetic screens for cellular transformation. *PNAS* **112**:5708–5713. DOI: <https://doi.org/10.1073/pnas.1505979112>, PMID: 25902495
- Sanjana NE**, Shalem O, Zhang F. 2014. Improved vectors and genome-wide libraries for CRISPR screening. *Nature Methods* **11**:783–784. DOI: <https://doi.org/10.1038/nmeth.3047>
- Scholl C**, Fröhling S, Dunn IF, Schinzel AC, Barbie DA, Kim SY, Silver SJ, Tamayo P, Wadlow RC, Ramaswamy S, Döhner K, Bullinger L, Sandy P, Boehm JS, Root DE, Jacks T, Hahn WC, Gilliland DG. 2009. Synthetic lethal interaction between oncogenic KRAS dependency and STK33 suppression in human Cancer cells. *Cell* **137**: 821–834. DOI: <https://doi.org/10.1016/j.cell.2009.03.017>, PMID: 19490892
- Sheffels E**, Sealover NE, Wang C, Kim DH, Vazirani IA, Lee E, M Terrell E, Morrison DK, Luo J, Kortum RL. 2018. Oncogenic RAS isoforms show a hierarchical requirement for the guanine nucleotide exchange factor SOS2 to mediate cell transformation. *Science Signaling* **11**:eaar8371. DOI: <https://doi.org/10.1126/scisignal.aar8371>, PMID: 30181243
- Sheffels E**, Sealover NE, Theard PL, Kortum RL. 2019. Anchorage-independent growth conditions reveal a differential SOS2 dependence for transformation and survival in RAS -mutant cancer cells. *Small GTPases* **2**:1–12. DOI: <https://doi.org/10.1080/21541248.2019.1611168>
- Shi P**, Oh YT, Zhang G, Yao W, Yue P, Li Y, Kanteti R, Riehm J, Salgia R, Owonikoko TK, Ramalingam SS, Chen M, Sun SY. 2016. Met gene amplification and protein hyperactivation is a mechanism of resistance to both first and third generation EGFR inhibitors in lung Cancer treatment. *Cancer Letters* **380**:494–504. DOI: <https://doi.org/10.1016/j.canlet.2016.07.021>, PMID: 27450722
- Shi P**, Oh YT, Deng L, Zhang G, Qian G, Zhang S, Ren H, Wu G, Legendre B, Anderson E, Ramalingam SS, Owonikoko TK, Chen M, Sun SY. 2017. Overcoming acquired resistance to AZD9291, A Third-Generation EGFR inhibitor, through modulation of MEK/ERK-Dependent bim and Mcl-1 degradation. *Clinical Cancer Research* **23**:6567–6579. DOI: <https://doi.org/10.1158/1078-0432.CCR-17-1574>, PMID: 28765329

- Singh A**, Greninger P, Rhodes D, Koopman L, Violette S, Bardeesy N, Settleman J. 2009. A gene expression signature associated with "K-Ras addiction" reveals regulators of EMT and tumor cell survival. *Cancer Cell* **15**: 489–500. DOI: <https://doi.org/10.1016/j.ccr.2009.03.022>, PMID: 19477428
- Singh A**, Sweeney MF, Yu M, Burger A, Greninger P, Benes C, Haber DA, Settleman J. 2012. TAK1 inhibition promotes apoptosis in KRAS-dependent Colon cancers. *Cell* **148**:639–650. DOI: <https://doi.org/10.1016/j.cell.2011.12.033>, PMID: 22341439
- Soria JC**, Ohe Y, Vansteenkiste J, Reungwetwattana T, Chewaskulyong B, Lee KH, Dechaphunkul A, Imamura F, Nogami N, Kurata T, Okamoto I, Zhou C, Cho BC, Cheng Y, Cho EK, Voon PJ, Planchard D, Su WC, Gray JE, Lee SM, et al. 2018. Osimertinib in untreated EGFR-Mutated advanced Non-Small-Cell lung Cancer. *The New England Journal of Medicine* **378**:113–125. DOI: <https://doi.org/10.1056/NEJMoa1713137>, PMID: 29151359
- Tallarida RJ**. 2011. Quantitative methods for assessing drug synergism. *Genes & Cancer* **2**:1003–1008. DOI: <https://doi.org/10.1177/1947601912440575>, PMID: 22737266
- Taniguchi H**, Yamada T, Wang R, Tanimura K, Adachi Y, Nishiyama A, Tanimoto A, Takeuchi S, Araujo LH, Boroni M, Yoshimura A, Shiotsu S, Matsumoto I, Watanabe S, Kikuchi T, Miura S, Tanaka H, Kitazaki T, Yamaguchi H, Mukae H, et al. 2019. AXL confers intrinsic resistance to osimertinib and advances the emergence of tolerant cells. *Nature Communications* **10**:259. DOI: <https://doi.org/10.1038/s41467-018-08074-0>, PMID: 30651547
- Tricker EM**, Xu C, Uddin S, Capelletti M, Ercan D, Ogino A, Pratilas CA, Rosen N, Gray NS, Wong KK, Jänne PA. 2015. Combined EGFR/MEK inhibition prevents the emergence of resistance in EGFR-Mutant lung Cancer. *Cancer Discovery* **5**:960–971. DOI: <https://doi.org/10.1158/2159-8290.CD-15-0063>, PMID: 26036643
- Tumaneng K**, Schlegelmilch K, Russell RC, Yimlamai D, Basnet H, Mahadevan N, Fitamant J, Bardeesy N, Camargo FD, Guan KL. 2012. YAP mediates crosstalk between the hippo and PI(3)K–TOR pathways by suppressing PTEN via miR-29. *Nature Cell Biology* **14**:1322–1329. DOI: <https://doi.org/10.1038/ncb2615>, PMID: 23143395
- Vigil D**, Cherfils J, Rossman KL, Der CJ. 2010. Ras superfamily GEFs and GAPs: validated and tractable targets for Cancer therapy? *Nature Reviews Cancer* **10**:842–857. DOI: <https://doi.org/10.1038/nrc2960>, PMID: 21102635
- Watanabe S**, Yoshida T, Kawakami H, Takegawa N, Tanizaki J, Hayashi H, Takeda M, Yonesaka K, Tsurutani J, Nakagawa K. 2017. T790M-Selective EGFR-TKI combined with dasatinib as an optimal strategy for overcoming EGFR-TKI resistance in T790M-Positive Non-Small cell lung Cancer. *Molecular Cancer Therapeutics* **16**:2563–2571. DOI: <https://doi.org/10.1158/1535-7163.MCT-17-0351>, PMID: 28839001
- Xia H**, Dai X, Yu H, Zhou S, Fan Z, Wei G, Tang Q, Gong Q, Bi F. 2018. EGFR-PI3K-PDK1 pathway regulates YAP signaling in hepatocellular carcinoma: the mechanism and its implications in targeted therapy. *Cell Death & Disease* **9**:269. DOI: <https://doi.org/10.1038/s41419-018-0302-x>, PMID: 29449645
- Yang JJ**, Zhou Q, Yan HH, Zhang XC, Chen HJ, Tu HY, Wang Z, Xu CR, Su J, Wang BC, Jiang BY, Bai XY, Zhong WZ, Yang XN, Wu YL. 2017. A phase III randomised controlled trial of erlotinib vs gefitinib in advanced non-small cell lung Cancer with EGFR mutations. *British Journal of Cancer* **116**:568–574. DOI: <https://doi.org/10.1038/bjc.2016.456>
- Zhang Z**, Jiang G, Yang F, Wang J. 2006. Knockdown of mutant K-ras expression by adenovirus-mediated siRNA inhibits the in vitro and in vivo growth of lung Cancer cells. *Cancer Biology & Therapy* **5**:1481–1486. DOI: <https://doi.org/10.4161/cbt.5.11.3297>, PMID: 17172815



Anchorage-independent growth conditions reveal a differential SOS2 dependence for transformation and survival in *RAS*-mutant cancer cells

Erin Sheffels, Nancy E. Sealover, Patricia L. Theard & Robert L. Kortum

To cite this article: Erin Sheffels, Nancy E. Sealover, Patricia L. Theard & Robert L. Kortum (2019): Anchorage-independent growth conditions reveal a differential SOS2 dependence for transformation and survival in *RAS*-mutant cancer cells, *Small GTPases*, DOI: 10.1080/21541248.2019.1611168

To link to this article: <https://doi.org/10.1080/21541248.2019.1611168>



Published online: 07 May 2019.



Submit your article to this journal [↗](#)



Article views: 3



View Crossmark data [↗](#)

RESEARCH PAPER



Anchorage-independent growth conditions reveal a differential SOS2 dependence for transformation and survival in *RAS*-mutant cancer cells

Erin Sheffels , Nancy E. Sealover *, Patricia L. Theard, and Robert L. Kortum

Department of Pharmacology and Molecular Therapeutics, Uniformed Services University of the Health Sciences, Bethesda, MD, USA

ABSTRACT

The *RAS* family of genes (*HRAS*, *NRAS*, and *KRAS*) is mutated in around 30% of human tumours. Wild-type *RAS* isoforms play an important role in mutant *RAS*-driven oncogenesis, indicating that RasGEFs may play a significant role in mutant *RAS*-driven transformation. We recently reported a hierarchical requirement for SOS2 in mutant *RAS*-driven transformation in mouse embryonic fibroblasts, with *KRAS*>*NRAS*>*HRAS* (Sheffels et al., 2018). However, whether SOS2 deletion differentially affects mutant *RAS* isoform-dependent transformation in human tumour cell lines has not been tested. After validating sgRNAs that efficiently deleted *HRAS* and *NRAS*, we showed that the differential requirement for SOS2 to support anchorage-independent (3D) growth, which we previously demonstrated in MEFs, held true in cancer cells. *KRAS*-mutant cells showed a high dependence on SOS2 for 3D growth, as previously shown, whereas *HRAS*-mutant cells did not require SOS2 for 3D growth. This differential requirement was not due to differences in RTK-stimulated WT *RAS* activation, as SOS2 deletion reduced RTK-stimulated WT *RAS*/PI3K/AKT signalling in both *HRAS* and *KRAS* mutated cell lines. Instead, this differential requirement of SOS2 to promote transformation was due to the differential sensitivity of *RAS*-mutated cancer cells to reductions in WT *RAS*/PI3K/AKT signalling. *KRAS* mutated cancer cells required SOS2/PI3K signalling to protect them from anoikis, whereas survival of both *HRAS* and *NRAS* mutated cancer cells was not altered by SOS2 deletion. Finally, we present an integrated working model of SOS signaling in the context of mutant *KRAS* based on our findings and those of others.

ARTICLE HISTORY

Received 12 December 2018
Revised 15 April 2019
Accepted 20 April 2019

KEYWORDS

RAS; SOS2; cancer; son of sevenless; MAPK; PI3K; anoikis

RAS in cancer

The RTK–*RAS* pathway is among the most commonly mutated pathways in cancer^[1]. The three *RAS* genes, *HRAS*, *NRAS*, and *KRAS*, are the most commonly mutated gene family, with mutations found in around 30% of human tumours [2]. Within the *RAS* gene family, *KRAS* is the most frequently mutated, accounting for 85% of *RAS*-driven cancers [2], including 95% of pancreatic cancers [3], 42% of colon cancers [4], and 20–30% of lung cancers [5], which are the top three causes of cancer-related death in the United States [2,6]. *H*- and *NRAS* mutations are common in other cancer types, including bladder cancers and skin cancers, respectively [7]. Due to their prevalence in tumours, many efforts have been made to develop therapies to directly target *RAS*. Thus far, no effective *KRAS* inhibitors have been developed, with the exception of cross-linking compounds targeting the *KRAS* (G12C) mutant [5,8–10]. Targeting other RTK pathway members has also had limited success in *RAS*-driven

cancers, due to high toxicities and resistance arising from the disruption of feedback mechanisms in the RTK–*RAS*–*RAF* pathway [11]. Together, these difficulties in developing treatments for *RAS*-driven tumours indicate a need for novel therapeutic strategies.

Several studies have found that non-mutated wild-type *RAS* proteins play an important role in modulating downstream effector signalling during mutant *RAS*-driven tumorigenesis, but this role differs for the wild-type allele of the mutated *RAS* gene versus the other two non-mutated *RAS* family members. Cancers driven by mutant *KRAS* often show loss of the wild-type *KRAS* allele [12–14]; in *KRAS*-mutant tumours loss of heterozygosity (LOH) at the *KRAS* locus correlates with increased tumour growth and shortened overall survival [15]. These data suggest that in *KRAS*-mutant tumours, wild-type *KRAS* may have a tumour suppressor role [16–18], a hypothesis which has been supported by observations *in vitro* [19,20] and *in vivo* with mouse models [20–22].

CONTACT Robert L. Kortum  robert.kortum@usuhs.edu  Department of Pharmacology and Molecular Therapeutics, Uniformed Services University of the Health Sciences, Bethesda, MD, USA

*E.S. and N.E.S. contributed equally to this manuscript

© 2019 Informa UK Limited, trading as Taylor & Francis Group

In contrast, the two non-mutated RAS family members may play a tumour-promoting role in RAS-mutant tumours. In RAS-mutated cancer cell lines, wild-type RAS isoforms promote mutant RAS-driven proliferation and transformation [23–26]. Wild-type RAS isoforms may contribute to oncogenic signalling through their ability to activate effector pathways that the mutant isoform does not strongly activate, making the cellular outcome a product of combined signalling by wild-type and mutant RAS [27]. Activation of wild-type RAS requires interaction with a RasGEF (guanine nucleotide exchange factor), such as Son of Sevenless 1 and 2 (SOS1 and SOS2), which are required for normal RTK-dependent RAS activation [28]. SOS1 can also be activated by allosteric binding of RAS-GTP [29], providing a potential link between constitutively active mutant RAS and wild-type RAS activation. The importance of wild-type RAS in mutant RAS-driven cancer indicates that SOS1 and SOS2 may be novel therapeutic targets for RAS-driven tumours. Defining their independent and combined roles in mutant RAS-dependent oncogenesis is key to determining the value of SOS1 and SOS2 as therapeutic targets in RAS-mutated tumours.

SOS2 is hierarchically required for transformation in RAS-mutant cancer cells

We recently showed that in immortalized mouse embryo fibroblasts (MEFs) there was a hierarchical requirement for SOS2 in RAS-driven transformation (KRAS > NRAS > HRAS), with KRAS being the most SOS2-dependent RAS isoform [30]. We also demonstrated that KRAS-mutant lung and pancreatic cancer cell lines required SOS2 to fully maintain their transformed phenotype. To complement our recent findings in KRAS-mutant cancer cells, we investigated whether HRAS- and NRAS-mutant cancer cell lines were dependent on SOS2 to maintain their transformed phenotype. We began our investigation using the HRAS (G12V) mutant T24 bladder cancer cell line and the NRAS (Q61H) mutant RD rhabdomyosarcoma line, as they were previously used to establish the contribution of wild-type RAS signalling to anchorage-dependent proliferation of RAS-mutant cancer lines by Young et al. [24].

Before testing HRAS and NRAS mutated cancer cell lines for SOS2 dependence, we first established the dependence of these cell lines on oncogenic RAS expression for both proliferation and transformation. To identify sgRNAs that would allow us to efficiently delete oncogenic HRAS or NRAS using CRISPR/Cas9, we tested four putative targeting sgRNAs for each RAS

isoform from a previously published genome-wide CRISPR screen, which used 18–20 sgRNAs per gene [31]. To target HRAS, we selected four sgRNAs that showed specific growth inhibition in a MET-amplified cancer cell line that showed a strong HRAS dependence, and for NRAS sgRNAs we tested four sgRNAs that showed specific growth inhibition in an NRAS-mutant cancer cell line.

Out of the four HRAS-targeting sgRNAs we tested, three (#1, #2, and #3) successfully deleted HRAS in >90% of cells, as indicated by the decrease in protein abundance compared to a non-targeting (NT) sgRNA construct (Figure 1). We next examined whether HRAS deletion by each sgRNA would inhibit anchorage-dependent (2D) proliferation and anchorage-independent (3D) transformation in HRAS-mutant T24 cells. For each sgRNA that successfully deleted HRAS, we observed a significant decrease in anchorage-dependent (2D) proliferation, as expected, though proliferation was not completely blocked. HRAS deletion also led to the reversion of the transformed phenotype, as measured by a cancer stem cell (CSC) frequency assay [32]. Here, serially diluted T24 cells were seeded in ultra-low attachment 96-well flat-bottomed plates (1–1000 cells/well), cultured for 7–10 days, and scored for the formation of cancer spheres. Wells containing cancer spheres that had grown to a diameter greater than 100 µm were scored as positive, and the frequency of cancer stem cells in the population of T24 cells was then calculated by extreme limiting dilution analysis [33]. When HRAS was deleted, the frequency of cancer stem cells decreased, indicating a dependence on HRAS for transformation. As sgRNA #3 had the most consistent effect on HRAS abundance and HRAS-dependent proliferation and transformation, we chose this sgRNA for further studies.

In NRAS-mutant RD cells, three out of four of the NRAS sgRNAs tested (#1, #2, and #4) successfully deleted NRAS, again as assessed by protein abundance compared to a non-targeting construct. Similar to what we observed in T24 cells following HRAS deletion, NRAS deletion reduced anchorage-dependent proliferation in RD cells. Furthermore, NRAS deletion also reduced, but did not completely block, anchorage-independent (3D) growth of cancer spheroids, indicating that in RD cells, transformation is not fully dependent on mutant NRAS expression. For NRAS, sgRNA #4 showed the most consistent decrease in protein abundance and so was chosen for further studies. These results indicate that HRAS-mutant T24 cells and NRAS-mutant RD cells are both dependent on mutant RAS expression for full 2D and 3D growth.

Having established sgRNAs that allow us to efficiently delete HRAS and NRAS to use as positive controls, we then investigated the effect of deleting SOS2 using one of two

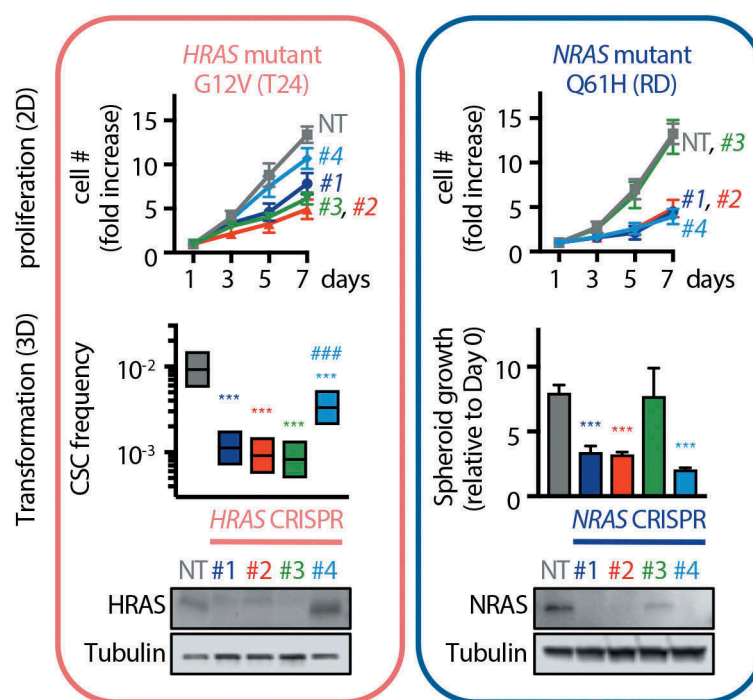


Figure 1. Mutant RAS is required for 2D and 3D growth in *HRAS* and *NRAS*-mutant cancer cells. (a) *HRAS* (G12V) mutant T24 bladder cancer cells were transduced with lentiviruses expressing Cas9 and either a non-targeting sgRNA (NT) or one of four sgRNAs designed to target *HRAS*. Infected cells were assessed for 2D proliferation (top) and cancer stem cell frequency as a measure of transformation (middle). Whole cell lysates (WCLs) were analyzed by Western blotting with antibodies specific for *HRAS* and β -actin (bottom). (b) *NRAS* (Q61H) mutant RD rhabdomyosarcoma cells were transduced with lentiviruses with Cas9 and either a non-targeting sgRNA (NT) or one of four sgRNAs designed to target *NRAS*. Infected cells were assessed for 2D proliferation (top) and 3D spheroid growth (middle). Whole cell lysates (WCLs) were analyzed by Western blotting with antibodies specific for *NRAS* and β -actin (bottom). Data are mean \pm SD from three independent experiments. Blots and images are representative of 3 independent experiments. Statistical significance was determined by ANOVA using the Tukey's method to correct for multiple comparisons. * $P < 0.05$, *** $P < 0.001$ versus NT; #### $P < 0.001$ versus *HRAS* #1, #2, #3.

different sgRNAs on proliferation and transformation in T24 cells, RD cells, and H358 cells, a *KRAS*-mutated cancer cell line. We first confirmed efficient *SOS2* and mutant RAS deletion by the appropriate sgRNA constructs by Western blot (Figure 2, bottom), which did not alter the expression of *SOS1* or β -actin. In each cell line, deletion of the mutated RAS gene significantly reduced both anchorage-dependent (2D) proliferation and anchorage-independent (3D) transformation, confirming the RAS dependence of each cell line for both 2D and 3D growth. Consistent with our previous observations using MEFs, *SOS2* deletion had no effect on 2D proliferation in cells expressing mutated *HRAS*, *NRAS*, or *KRAS* (Figure 2, top), indicating that mutant RAS-driven anchorage-dependent growth is independent of *SOS2*.

When we assessed anchorage-independent transformation, we observed a differential effect of *SOS2* deletion on cellular transformation that was again similar to our previous observations in MEFs. *SOS2* deletion had no effect on 3D growth in *HRAS*-mutant T24 cells, consistent with our previous observations in MEFs (Figure 2, middle). In *NRAS*-mutant RD cells, *SOS2*

deletion led to a non-significant decrease in 3D growth compared to the non-targeting sgRNA construct, indicating *NRAS*-mutant cancer cells do not require *SOS2* for 3D growth, but may have an intermediate dependence between *HRAS*- and *KRAS*-mutant cells similar to the intermediate dependence established in MEFs. In *KRAS*-mutated H358 cells, *SOS2* deletion significantly reduced transformation, as we had previously observed in *KRAS* mutated YAPC pancreatic cancer cells [30].

To confirm that the differential requirement for *SOS2* in promoting RAS isoform-dependent transformation in human cancer cell lines was generalizable across multiple RAS mutated cancer cell lines, we tested the effects of *SOS2* deletion on anchorage-independent growth in six more cancer cell lines, two each expressing mutated *HRAS*, *NRAS*, or *KRAS* (Figure 3, see Table 1 for cell line information). As expected, we found that *SOS2* was necessary for full anchorage-independent growth for in each of the additional *KRAS*-mutated cell lines we tested (H23 and SW620) but that *SOS2* deletion had no effect on anchorage-independent growth in either of the *HRAS*-mutant

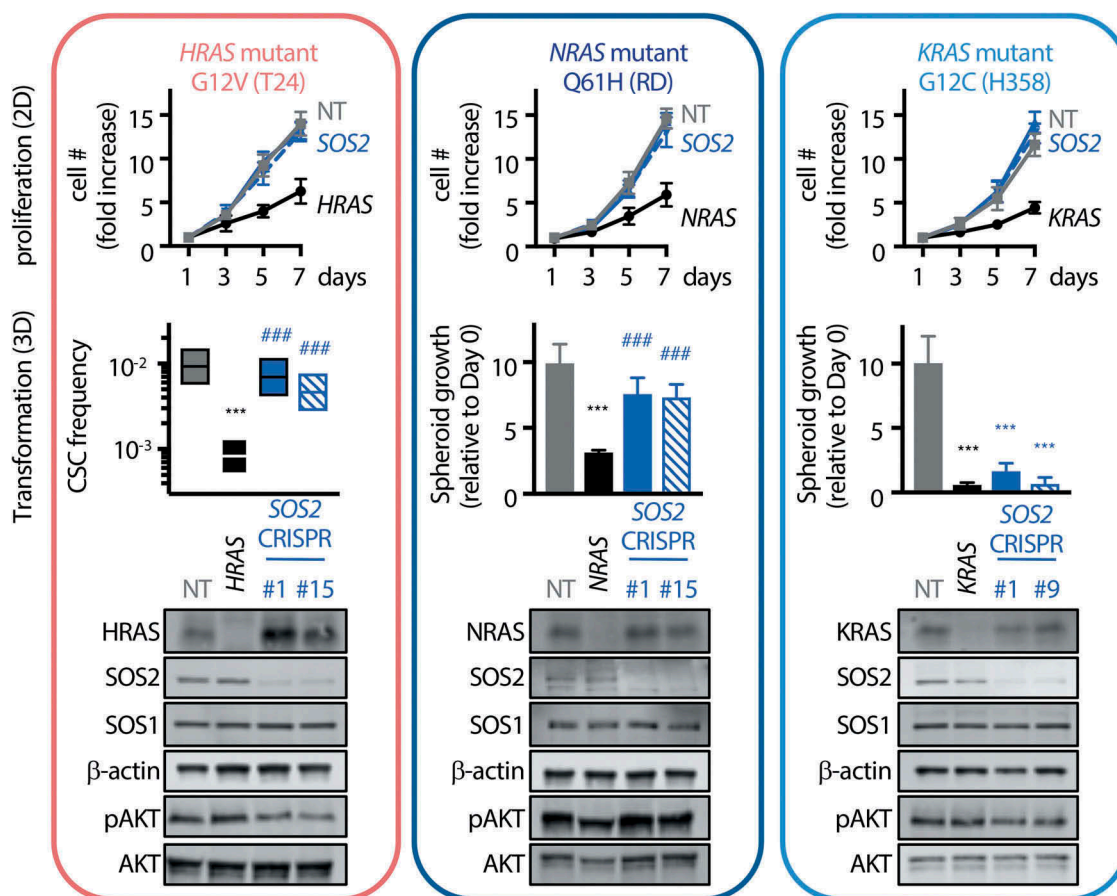


Figure 2. *KRAS*-mutant cancer cells depend on *SOS2* for anchorage-independent, but not anchorage-dependent, growth. *HRAS* (G12V) mutant T24 bladder cancer cells (salmon), *NRAS* (Q61H) mutant RD rhabdomyosarcoma cells (dark blue), or *KRAS* (G12C) mutant H358 non-small cell lung cancer (NSCLC) cells (light blue) were transduced with lentiviruses expressing Cas9 and either an NT sgRNA, an sgRNA targeting mutant *RAS*, or one of two sgRNAs targeting *SOS2*. Post-selection, cells were assessed for 2D proliferation (top) and 3D transformation (middle). WCLs were analysed by Western blotting with antibodies specific for *SOS1*, *SOS2*, *HRAS*, *NRAS*, *KRAS*, β -actin, pAKT, and AKT (bottom). Data are mean \pm SD from three independent experiments. Blots and images are representative of three independent experiments. Statistical significance was determined by ANOVA using the Tukey's method to correct for multiple comparisons. * $P < 0.05$, *** $P < 0.001$ versus NT; ### $P < 0.001$ versus mutant *RAS* deletion.

cell lines (RL95-2 and NCI-H1915). We again saw an intermediate *SOS2* dependence in *NRAS*-mutant cell lines. While *SOS2* deletion showed no effect on oncogenic transformation in SK-Mel-2 cells, we observed a significant decrease in anchorage-independent growth in NCI-H1299 NSCLC cells. These data are consistent with the intermediate *SOS2* dependence on *NRAS*-driven transformation we had originally observed in MEFs.

We had previously described an RTK/*SOS2*/WT *RAS*/*PI3K* signalling pathway that was important for transformation in MEFs expressing mutated *KRAS*, and demonstrated that in *KRAS* mutated YAPC pancreatic cancer cells *SOS2* is necessary for full RTK-dependent *PI3K*/*AKT* pathway activation. To determine whether this held generally true in *RAS* mutated cancer cells, we assessed *AKT* phosphorylation in cycling T24, RD, and H358 cells. We found a significant decrease in *AKT*

phosphorylation in both *HRAS* mutated T24 cells and in *KRAS* mutated H358 cells (Figure 2). In contrast, *AKT* phosphorylation was not reduced by *SOS2* deletion in RD cells, perhaps due to their already high levels of *AKT* phosphorylation (Figure 2, middle) and consistent with previous reports where *AKT* phosphorylation was shown to be independent of WT *RAS* in RD cells [24]. To determine whether the decreased *AKT* phosphorylation we observed was due to reduced RTK signalling, we assessed EGF-stimulated *PI3K*/*AKT* signalling in T24 and H358 cells after overnight serum deprivation. We found that in both T24 and H358 cells, EGF-stimulated *AKT* phosphorylation was significantly reduced after *SOS2* deletion (Figure 4).

We further assessed whether *SOS2* was required for RTK-stimulated WT *RAS* activation in *HRAS* mutated (T24) and in *KRAS* (H23) mutated cancer cells (Figure 5) using *RAS*-binding domain (RBD) pull-downs after

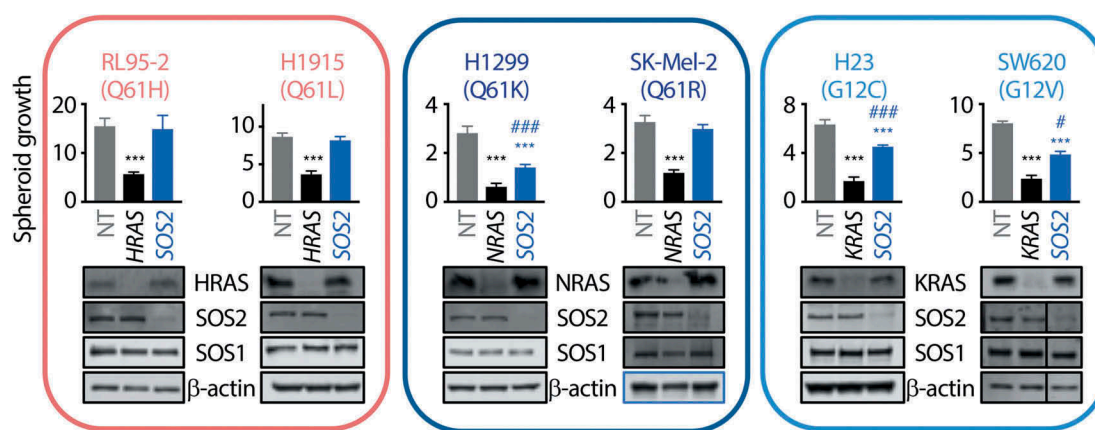


Figure 3. There is a differential requirement for SOS2 to promote anchorage-independent growth in *RAS*-mutant cancer cell lines. *HRAS* (Q61H) mutant RL95-2 endometrial carcinoma cells and *HRAS* (Q61L) mutant NCI-H1915 NSCLC cells (salmon), *NRAS* (Q61K) mutant NCI-H1299 NSCLC cells and *NRAS* (Q61R) mutant SK-Mel-2 melanoma cells (dark blue), or *KRAS* (G12C) mutant H358 NSCLC cells and *KRAS* (G12V) mutant SW620 colorectal adenocarcinoma cells (lite blue) were transduced with lentiviruses expressing Cas9 and either an NT sgRNA, an sgRNA targeting mutant *RAS*, or an sgRNA targeting *SOS2*. Post-selection, cells were assessed for 3D transformation. WCLs were analysed by Western blotting with antibodies specific for *SOS1*, *SOS2*, *HRAS*, *NRAS*, *KRAS*, and β -actin. Data are mean \pm SD from three independent experiments. Blots and images are representative of three independent experiments. Images of *SOS1*, *SOS2*, and β -actin Western blots for SW620 cells were assembled from separate parts of the same image, as these samples were separated on the original Western blots (black line). Statistical significance was determined by ANOVA using the Tukey's method to correct for multiple comparisons. *** $P < 0.001$ versus NT; ### $P < 0.05$, ### $P < 0.001$ versus mutant *RAS* deletion.

Table 1. *RAS* mutation status and tissue of origin of the cancer cell lines studied.

Cell line	<i>RAS</i> mutation	Origin
T24	<i>HRAS</i> G12V	Transitional cell carcinoma
RL95-2	<i>HRAS</i> Q61H	Endometrial carcinoma
NCI-H1915	<i>HRAS</i> Q61L	NSCLC
RD	<i>NRAS</i> Q61H	Muscle rhabdomyosarcoma
NCI-H1299	<i>NRAS</i> Q61K	NSCLC
SK-MEL-2	<i>NRAS</i> Q61R	Melanoma
NCI-H358	<i>KRAS</i> G12C	NSCLC
NCI-H23	<i>KRAS</i> G12C	NSCLC
SW620	<i>KRAS</i> G12V	Colorectal adenocarcinoma

overnight serum deprivation. In *KRAS* mutated cancer cells, we found that *SOS2* deletion inhibited RTK-stimulated *HRAS* activation and reduced RTK-stimulated *NRAS* activation, showing the requirement for *SOS2* in WT *RAS* activation in the setting of mutated *KRAS*. Furthermore, in *HRAS* mutated cancer cells, we observed a reduction in RTK-stimulated *KRAS* activation following *SOS2* deletion. In contrast, *SOS2* deletion had no effect on basal WT *RAS* activation in cells expressing either mutated *KRAS* or *HRAS*. These data confirm the importance of *SOS2* to RTK-stimulated WT *RAS* activation in *RAS* mutated cancer cells.

During oncogenic transformation, one of the major roles of the PI3K/AKT pathway is to promote survival by protecting cancer cells from anoikis, a form of apoptosis associated with loss of extracellular matrix (ECM) contact which must be overcome by cancer cells in order for them to grow in an anchorage-

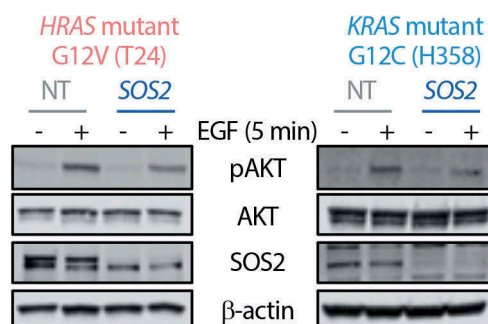


Figure 4. *SOS2* is required for full RTK-stimulated AKT phosphorylation in *RAS* mutated cancer cells. *HRAS* (G12V) mutant T24 bladder cancer cells or *KRAS* (G12C) mutant H358 NSCLC cells were transduced with lentiviruses expressing Cas9 and either an NT sgRNA, an sgRNA targeting mutant *RAS*, or an sgRNA targeting *SOS2*. Post-selection, cells were starved overnight and then stimulated with EGF 100 ng/mL for 5 min prior to lysis. Multiplex western blotting for pAKT (Ser⁴⁷²), AKT, *SOS2*, and β -actin was performed on a LI-COR Odyssey machine.

independent environment and to invade and metastasize [34,35]. To determine whether *SOS2* was required for anchorage-independent survival, *HRAS*, *NRAS*, or *KRAS* mutated cancer cells expressing either a NT sgRNA or sgRNAs that deleted either *SOS2* or oncogenic *RAS* were seeded as spheroids in 96-well ultra-low attachment round-bottomed plates and counted using trypan blue to assess cell viability 4 h after plating. As expected, oncogenic *RAS* deletion reduced cell

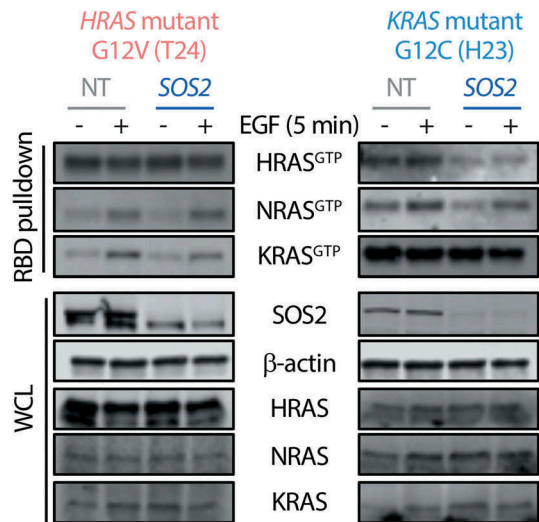


Figure 5. SOS2 is required for full RTK-stimulated WT RAS activation in *RAS* mutated cancer cells. *HRAS* (G12V) mutant T24 bladder cancer cells or *KRAS* (G12C) mutant H23 NSCLC cells were transduced with lentiviruses expressing Cas9 and either an NT sgRNA, an sgRNA targeting mutant *RAS*, or an sgRNA targeting *SOS2*. Post-selection, cells were starved overnight and then stimulated with EGF 100 ng/mL for 5 min prior to lysis. Lysates were subjected to GST-RAS binding domain pull-downs and were analysed by Western blotting with an antibody specific for HRAS, NRAS, or KRAS to assess activation (GTP loading) of endogenous RAS. WCLs were subjected to Multiplex Western blotting for HRAS, NRAS, KRAS, SOS2, and β -actin on a LI-COR Odyssey machine.

viability for all RAS mutated cancer cells. In contrast, *SOS2* deletion reduced cell viability in *KRAS* mutated cancer cells, but not *HRAS* or *NRAS* mutated cancer cells (Figure 6(a)). These data are consistent with the differential requirement for *SOS2* to support the transformation of *KRAS* mutated cancer cells (see Figures 2 and 3). We further assessed the effect of *SOS2* deletion over time on anchorage-independent cell survival in *HRAS* versus *KRAS* mutated cancer cells, and found not only that *SOS2* was preferentially required for anchorage-independent survival in *KRAS* mutated cancer cells, but that *SOS2* deletion reduced cell survival under anchorage-independent conditions similar to *KRAS* deletion (Figure 6(b)).

Taken together, these results demonstrate the differential dependence on *SOS2* for RAS-dependent transformation originally established in MEFs [30] is also generally applicable in *RAS*-mutated cancer cell lines. The ability of *HRAS* and *NRAS*-mutant cells to grow in 3D conditions in the absence of *SOS2* indicates that *SOS2* is likely not an effective therapeutic target in *HRAS*- and *NRAS*-mutant tumours. It also indicates that promising drug targets like *SOS2* [33], RTKs [36–39], or Shp2 [40–42], which synergize with MEK inhibition in *KRAS*-mutant cancer cells, may not have the same effect in *HRAS* and *NRAS*-driven cancers, suggesting a continued need for new therapeutic strategies for these tumours.

In addition to demonstrating the differential requirement for *SOS2* in *RAS*-mutant cancer cell

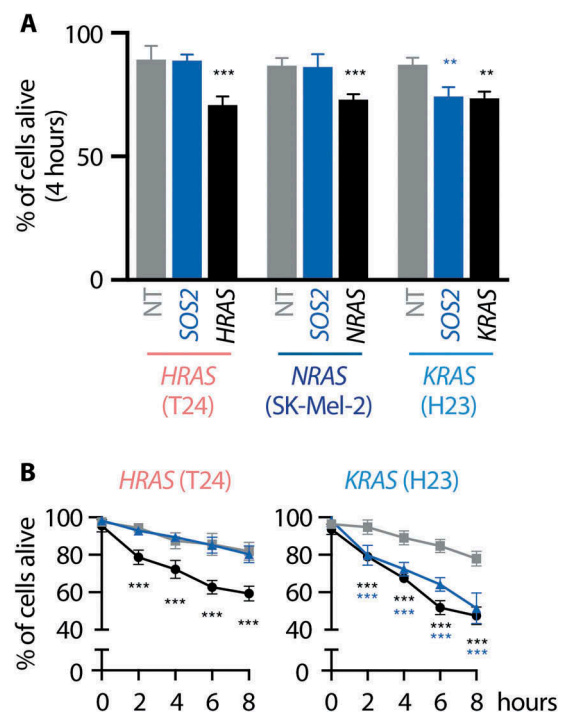


Figure 6. *HRAS* (G12V) mutant T24 bladder cancer cells, and *NRAS* (Q61R) mutant SK-Mel-2 melanoma cells, or *KRAS* (G12C) mutant H23 NSCLC cells were transduced with lentiviruses expressing Cas9 and either an NT sgRNA, an sgRNA targeting mutant *RAS*, or an sgRNA targeting *SOS2*. Post-selection, cells were counted using trypan blue to assess cell viability at time 0, and then, plated in 96-well ultra-low attachment plates for 4 h (a) or for 0, 2, 4, 6, or 8 h (b). Forming spheroids were dislodged into a single cell suspension by pipetting, and cells were counted using trypan blue to assess cell viability. ** $P < 0.01$, *** $P < 0.001$ versus NT.

lines, our findings also emphasize the importance of using 3D growth assays to screen for vulnerabilities in cancers. Though all three RAS-mutant cell lines used here were dependent on their oncogene for both 2D and 3D growth, the dependence of *KRAS*-mutant cells on *SOS2* was only revealed in 3D growth conditions. Here, our data indicate that RTK/*SOS2*/WT RAS/PI3K signalling is a critical survival signal in *KRAS* mutated cancer cells. New approaches for treating RAS-driven cancers, such as synergistic inhibition of MEK and upstream RTK signaling, are still needed to improve patient survival, and screens using assays that more closely mimic the tumor environment are more likely to detect effective therapeutic targets.

Toward an integrated working model of SOS signalling in mutant RAS-driven cancers

Previous studies have shown that RAS isoforms have differing abilities to activate the two major RAS effectors, RAF and PI3K. *KRAS* has a higher ability to activate RAF than *HRAS*, and conversely, *HRAS* has a higher ability to activate PI3K than *KRAS*; in each case, *NRAS* is intermediate between the other two isoforms (Figure 7(a)) [23,43–45]. *BRAF* and *KRAS* mutations are generally mutually exclusive in cancer (cBioPortal) [46,47], suggesting that mutant *KRAS* optimally activates the RAF pathway for proliferation and transformation, and higher levels of RAF–MEK–ERK pathway activation that would come from additional *BRAF* mutations may lead to senescence and apoptosis. In contrast, *HRAS* and *BRAF* mutations significantly co-occur, as do *NRAS* and *BRAF* mutations, indicating that additional activation of the RAF pathway may improve the survival or transformation in *HRAS* or *NRAS*-driven cancers.

Unlike *BRAF* mutations, PI3K activating mutations are not mutually exclusive with *KRAS* or *HRAS* mutations in tumours, suggesting that neither activated RAS isoform activates PI3K optimally (cBioPortal) [46,47]. In fact, *PIK3CA* mutations and *HRAS* or *KRAS* mutations co-occur in cancers more frequently than would be expected by random mutation (cBioportal) [46,47], indicating that RAS-independent PI3K activation may play an important role in driving RAS-mutant cancers. However, *HRAS* does have a higher ability to activate PI3K than *KRAS*, with *NRAS* again intermediate [43] (Figure 7(a)), suggesting that *HRAS* may be less reliant on other sources of PI3K pathway activation. Indeed, we previously established that MEFs expressing mutated *HRAS* are less sensitive to PI3K inhibition than those expressing mutated *KRAS* in anchorage-independent growth conditions. On the other hand,

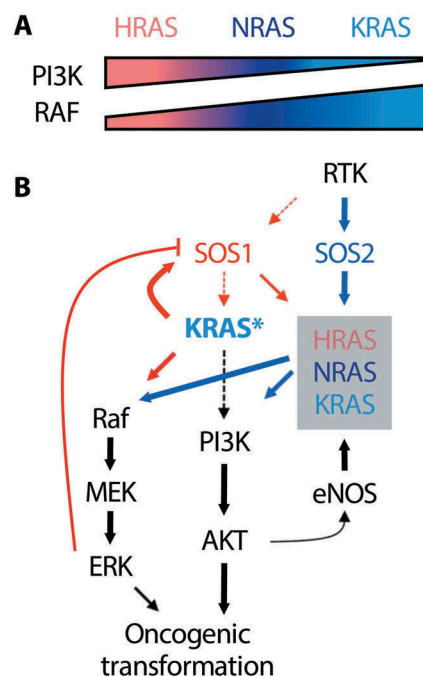


Figure 7. An integrated working model of SOS signalling in RAS-mutated cancer cells. (a) The three RAS isoforms have different relative abilities to activate key downstream effectors RAF and PI3K. *KRAS* activates RAF more strongly than *HRAS*, whereas *HRAS* activates PI3K more strongly than *KRAS*. *NRAS* has intermediate activation ability for both effectors. (b) Schematic of SOS-dependent signalling in mutant *KRAS*-driven cancers.

mutant *HRAS*-expressing cells were more sensitive to MEK inhibition than mutant *KRAS*-expressing cells [30]. These patterns in downstream effector pathway activation and sensitivity to effector inhibition suggest that mutant RAS-driven cancers may be vulnerable to therapeutic strategies targeting effector pathways that are not fully engaged by mutant RAS.

These differences in mutant RAS-dependent effector signalling help explain why *SOS2* deletion specifically affects transformation by *KRAS*, but not *HRAS*. We previously showed that at the level of effector signalling, *Sos2* deletion reduced RTK-dependent AKT phosphorylation in MEFs expressing all mutant RAS isoforms [30], and here we show that this holds true in *HRAS* and *KRAS* mutated cancer cell lines. However, when we examined the effect of PI3K inhibition on MEFs expressing mutant RAS isoforms or in RAS mutated cancer cell lines, we found that there was a hierarchical requirement for PI3K signalling in promoting RAS-driven transformation ($KRAS \geq NRAS > HRAS$) that mirrored the hierarchical requirement for *SOS2*. We hypothesize this is due to the relative inability of *KRAS* to activate the PI3K pathway, making cells expressing mutated *KRAS* more sensitive to alterations in PI3K signalling than cells expressing mutated *NRAS* or *HRAS*. Furthermore, *KRAS*-driven transformation could be

rescued in *Sos2*^{-/-} MEFs by the introduction of an activated PI3K catalytic subunit, suggesting that *Sos2* deletion specifically reduced PI3K–AKT signalling to block oncogenic transformation.

Based on our previous results [30] and those of others, we propose a working model of SOS signalling in mutant KRAS-driven cancers (Figure 7(b)). In cells expressing mutated KRAS, SOS proteins can be activated by two distinct mechanisms: (i) RKT-dependent recruitment of SOS to the plasma membrane by Grb2 and (ii) allosteric binding of SOS by mutant KRAS setting up a mutant KRAS^{GTP}–SOS1–wild-type RAS positive feedback loop. For SOS1, KRAS-dependent RAF–MEK–ERK signalling sets up a signalling environment where competing signals titrate the activity of SOS1. Mutant KRAS binds an allosteric pocket on SOS1 [29], relieving SOS1 autoinhibition [48] and thereby activating a mutant KRAS^{GTP}–SOS1–wild-type RAS positive feedback loop that helps drive cell proliferation [49]. In parallel, constitutive RAF–MEK–ERK signalling causes multiple ERK- and RSK-dependent negative feedback phosphorylation events [50–60] including phosphorylation of SOS1 that result in both ERK-dependent dissociation of the Grb2/SOS1 complex [53–56] and RSK-dependent cytoplasmic sequestration of SOS1 by 14–3–3 [50,51]. This ERK- and RSK-dependent feedback phosphorylation may remove a portion of SOS1 from the pool of Grb2-associated SOS, making SOS1 less available for RTK-dependent signalling to wild-type RAS.

In contrast to SOS1, these feedback mechanisms do not seem to regulate the activity of SOS2. SOS2 cannot be phosphorylated by ERK [54] or RSK [50], so the activity of SOS2 is not curtailed by RAF–MEK–ERK feedback inactivation. Furthermore, we have shown that the allosteric (RAS^{GTP}-dependent) SOS2 signalling does not contribute to wild-type HRAS activation or mutant KRAS-dependent transformation [30]. Because of this, the entire pool of SOS2 is available for RTK signalling, where SOS2 plays a critical role in RTK-dependent PI3K–AKT pathway activation [30]. Interestingly, while SOS2 deletion has a marked effect on RTK-stimulated AKT phosphorylation, it does not alter RTK-stimulated RAF–MEK–ERK pathway activation. We hypothesize that this is due to the markedly differing thresholds of RTK stimulation required to fully activate the PI3K–AKT versus RAF–MEK–ERK cascades, where a much stronger stimulus is required to activate PI3K–AKT than ERK [61]. Because of this difference, we posit that after SOS2 deletion the ‘active’ pool of SOS1, those SOS1 molecules not phosphorylated and inhibited by ERK and RSK, remains sufficient to support full RAF–MEK–ERK pathway activation but

is insufficient to activate PI3K–AKT signalling. Alternatively, the specificity of signalling from SOS2 to PI3K through RAS may also be influenced either (i) by colocalization of specific signalling components at the membrane [62–66] which has been proposed as a mechanism of regulation for RAS signalling or (ii) by activation of Rac/p110β signalling downstream of SOS2. Previous studies have shown that in addition to its RasGEF activity, the combined DH/PH domain of SOS1 can act as a RacGEF in some settings [28,67,68]. Functionally, association of the proline-rich (PR) regions of SOS1 with different signalling complexes may regulate Ras/ERK (SOS1/Grb2) versus Rac/JNK (SOS1/E3b1/Abi-1) signalling [69]. In primary MEFs, combined deletion of SOS1 and SOS2 is required to reduce RTK-stimulated RAC activation [70]. Furthermore, activating mutations in the DH domain of SOS2 are associated with Noonan Syndrome, indicating the functional importance of this domain in SOS2 [71,72]. However, whether either of these mechanisms can fully explain the differential effect of SOS2 deletion on PI3K–AKT versus RAF–MEK–ERK pathway activation requires further study.

Combined inhibition of PI3K and MEK effectively blocks *KRAS*-mutant cancer growth, but inhibiting these two key pathways has high toxicity in patients, necessitating alternative approaches. *SOS2* deletion reduces RTK-dependent PI3K pathway signalling, indicating that *SOS2* is a potential alternative therapeutic target to direct PI3K inhibition. We previously demonstrated that deletion of *SOS2* synergized with the MEK inhibitor trametinib to block the transformed phenotype in *KRAS*-mutant tumor cell lines [30]. These results indicate that *SOS2*-dependent PI3K signalling plays an important role in mutant *KRAS*-driven transformation, and that *SOS2* may be a therapeutic target in *KRAS*-driven cancers. While *SOS2* is a potential therapeutic target in *KRAS*-drive cancer, the lack of effect of *SOS2* deletion on anchorage-independent growth in *HRAS* or *NRAS*-mutant cancer cell lines indicates that *SOS2* is unlikely to be a viable therapeutic in these cancers. Additionally, *SOS2* is likely only a therapeutic target in *KRAS* mutated tumours that have wild-type PI3K/Pten signalling, since the expression of an activated p110α catalytic subunit restored *KRAS*-dependent transformation in *Sos2*^{-/-} MEFs. Therefore, further study on *RAS*-mutated cancer cell lines with different origin sites and co-mutations will need to be done to determine the range of applicability of *SOS2* inhibition as a therapeutic strategy.

In addition to further defining the potential for *SOS2* as a therapeutic target, our data presented here also

indicates the importance of using anchorage-independent growth assays to investigate potential therapeutic vulnerabilities in RAS-mutated cancer cells. The differential dependence on SOS2 for promoting RAS-dependent transformation is only revealed in anchorage-independent conditions (Figures 2 and 3), which more closely model the in vivo tumour environment, and the synergistic effects of MEK inhibition and SOS2 deletion are only revealed under anchorage-independent conditions [30]. These data suggest a new paradigm where future large-scale screens that search for therapeutic vulnerabilities/synthetic lethal interactions to inhibit cancer growth should be performed under anchorage-independent conditions in order to reveal novel, tractable therapeutic vulnerabilities that would not be identified in anchorage-dependent screens.

Materials and methods

Cell culture

RD and RL95-2 cells were maintained in Dulbecco's modified Eagle's medium (DMEM); NCI-H358, NCI-H1915, NCI-H1299, and NCI-H23 cells were maintained in Roswell Park Memorial Institute medium (RPMI); SK-MEL-2 cells were maintained in Eagle's Minimal Essential medium (EMEM); and T24 cells were maintained in McCoy's 5A (Modified) medium. Each medium was supplemented with 10% fetal bovine serum, 2 mM l-glutamine, 0.1 mM minimum essential medium with non-essential amino acids, and 1% penicillin-streptomycin.

Production of recombinant lentiviruses

Lentiviruses were produced by co-transfecting MISSION lentiviral packaging mix (Sigma) into 293 T cells using calcium phosphate. At 48 to 72 h post-transfection, viral supernatants were collected and filtered. Viral supernatants were then either stored at -80°C or used immediately to infect cells in combination with polybrene at 8 $\mu\text{g}/\text{mL}$. All cell lines were selected with 4 $\mu\text{g}/\text{mL}$ Puromycin (Invitrogen).

sgRNA studies

A non-targeting (NT) single guide RNA (sgRNA), a KRAS-targeted sgRNA, the three confirmed SOS2-targeted sgRNAs, the four potential HRAS-targeted sgRNAs, and the four potential NRAS-targeted sgRNAs were each cloned into pLentiCRISPRv2 as previously described. sgRNA sequences are given in supplemental table S1. Lentiviruses were produced as described above. Forty-eight hours post-infection, cells were selected in 4 $\mu\text{g}/\text{mL}$

Puromycin. Ten days after selection, cells were analysed for KRAS, HRAS, NRAS, and/or SOS2 expression and plated for proliferation and transformation assays.

Cell lysis and western blot analysis

Cells were lysed in RIPA buffer (1% NP-40, 0.1% SDS, 0.1% Na-deoxycholate, 10% glycerol, 0.137 M NaCl, 20 mM Tris pH [8.0], protease and phosphatase inhibitor cocktails (Biotool)) for 20 min at 4°C and spun at 10,000 RPM for 10 min. Clarified lysates were boiled in SDS sample buffer containing 100 mM DTT for 10 min prior to Western blotting. Proteins were resolved by sodium dodecyl sulfate-polyacrylamide gel electrophoresis and transferred to nitrocellulose or PVDF membranes. Western blots were developed by multiplex Western blotting using anti-SOS1 (Santa Cruz sc-256; 1:500), anti-SOS2 (Santa Cruz sc-258; 1:500), anti-b-actin (Sigma AC-15; 1:5,000), anti-KRAS (Sigma WH0003845M1; 1:100), anti-HRAS (Santa Cruz sc-250; 1:100), anti-NRAS (Santa Cruz sc-31; 1:100), anti-pERK1/2 (Cell Signaling 4370; 1:1,000), anti-ERK1/2 (Cell Signaling 4696; 1:1000), anti-pAKT Ser⁴⁷² (Cell Signaling 4060; 1:1000), or anti-AKT (Cell Signaling 4691; 1:1000) primary antibodies. Anti-mouse and anti-rabbit secondary antibodies conjugated to IRDye680 or IRDye800 (LI-COR; 1:10,000) were used to probe primary antibodies. Protein bands were detected and quantified by Western blotting with the Odyssey system (LI-COR).

RAS pull-downs

For RAS pull-downs, cells were lysed on ice for 20 min in RAS-PD lysis buffer (1% NP-40, 50 mM Tris pH 7.5, 200 mM NaCl, 2.5 mM MgCl₂, protease and phosphatase inhibitor cocktails (Biotool)), and spun at 10,000 RPM for 10 min. GST-RBD bound to glutathione-sepharose beads (Millipore) was used to isolate RAS-GTP from lysates by rotating incubation for 1 h at 4°C . Samples were washed four times in RAS-PD lysis buffer. All samples were boiled in 2 \times SDS sample buffer containing 40 mM DTT for 10 min prior to Western blotting.

Proliferation studies

For growth assays, 2×10^3 cells were seeded on cell culture-coated 96-well plates (CellTreat). Cells were lysed with CellTiter-Glo 2.0 reagent (Promega), and luminescence was read using a Synergy H1 Hybrid Reader (BioTek). Cell number was assessed 24 h after plating to account for any discrepancies in plating, and then every 48 h for 7 days. Data were analysed as an increase in luminescence over Day 0.

Transformation studies

For spheroid growth in ultra-low attachment 96-well round-bottomed plates (Corning Costar #7007), cells were seeded at 500–1000 cells per well. Cell number was assessed 18 h after plating to allow spheroids to form (day 0), and then at day 7 or 14 using CellTiter-Glo 2.0 reagent (Promega), which measures ATP content as a surrogate of overall cell number. Spheroid growth for each cell line was normalized to the CellTiter Glo signal at day 0 and is expressed as a fold-increase over day 0.

To determine the cancer stem cell (CSC) frequency, serially diluted T24 cells were seeded in ultra-low attachment 96 well flat-bottomed plates (1–1000 cells/well), cultured for 7–10 days, and scored for the formation of cancer spheres [32]. Wells containing cancer spheres that had grown to a diameter greater than 100 μm were scored as positive, and the frequency of cancer stem cells in the population of T24 cells was then calculated by extreme limiting dilution analysis [33].

Anoikis studies

Cells were plated in ultra-low attachment 96-well round-bottomed plates (Corning Costar #7007) at 10,000 cells per well. At the times indicated, cells were counted using trypan blue to indicate cell death. Percentage of live cells was calculated by dividing the live cell count by the combined living and dead cell counts.

Disclosure statement

No potential conflict of interest was reported by the authors.

Funding

This work was supported by the Congressionally Directed Medical Research Programs [LC160222].

ORCID

Erin Sheffels  <http://orcid.org/0000-0001-8356-6517>

Nancy E. Sealover  <http://orcid.org/0000-0002-6463-5836>

References

- [1] Lemmon MA, Schlessinger J. Cell signaling by receptor-tyrosine kinases. *Cell*. 2010;141:1117–1134.
- [2] Papke B, Der CJ, Drugging RAS. Know the enemy. *Science*. 2017;355:1158–1163.
- [3] Jaffee EM, Hruban RH, Canto M, et al. Focus on pancreas cancer. *Cancer Cell*. 2002;2:25–28.
- [4] Grady WM, Markowitz SD. Genetic and epigenetic alterations in colon cancer. *Annu Rev Genomics Hum Genet*. 2002;3:101–128.
- [5] Riely GJ, Marks J, Pao W. KRAS mutations in non-small cell lung cancer. *Proc Am Thorac Soc*. 2009;6:201–205.
- [6] Jemal A, Siegel R, Xu J, et al. Cancer statistics, 2010. *CA Cancer J Clin*. 2010;60:277–300.
- [7] Pylayeva-Gupta Y, Grabocka E, Bar-Sagi D. RAS oncogenes: weaving a tumorigenic web. *Nat Rev Cancer*. 2011;11:761–774.
- [8] Cox AD, Fesik SW, Kimmelman AC, et al. Drugging the undruggable Ras: mission possible? *Nat Rev Drug Discov*. 2014;13:828–851.
- [9] Stephen AG, Esposito D, Bagni RK, et al. Dragging Ras back in the ring. *Cancer Cell*. 2014;25:272–281.
- [10] Janes MR, Zhang J, Li L-S, et al. Targeting KRAS mutant cancers with a covalent G12C-specific inhibitor. *Cell*. 2018;172:578–589 e517.
- [11] Chandarlapaty S. Negative feedback and adaptive resistance to the targeted therapy of cancer. *Cancer Discov*. 2012;2:311–319.
- [12] Zhou B, Der CJ, Cox AD. The role of wild type RAS isoforms in cancer. *Semin Cell Dev Biol*. 2016;58:60–69.
- [13] Burgess MR, Hwang E, Mroue R, et al. KRAS allelic imbalance enhances fitness and modulates MAP kinase dependence in cancer. *Cell*. 2017;168:817–829 e815.
- [14] Mueller S, Engleitner T, Maresch R, et al. Evolutionary routes and KRAS dosage define pancreatic cancer phenotypes. *Nature*. 2018;554:62–68.
- [15] Yu CC, Qiu W, Juang CS, et al. Mutant allele specific imbalance in oncogenes with copy number alterations: occurrence, mechanisms, and potential clinical implications. *Cancer Lett*. 2017;384:86–93.
- [16] Diaz, R., Ahn D, Lopez-Barcons L, et al. The N-ras proto-oncogene can suppress the malignant phenotype in the presence or absence of its oncogene. *Cancer Res*. 2002;62:4514–4518.
- [17] Li J, Zhang Z, Dai Z, et al. LOH of chromosome 12p correlates with Kras2 mutation in non-small cell lung cancer. *Oncogene*. 2003;22:1243–1246.
- [18] Guerrero I, Villasante A, Corces V, et al. Loss of the normal N-ras allele in a mouse thymic lymphoma induced by a chemical carcinogen. *Proc Natl Acad Sci U S A*. 1985;82:7810–7814.
- [19] Diaz R, Lue J, Mathews J, et al. Inhibition of Ras oncogenic activity by Ras protooncogenes. *Int J Cancer*. 2005;113:241–248.
- [20] Ambrogio C, Köhler J, Zhou Z-W, et al. KRAS dimerization impacts MEK inhibitor sensitivity and oncogenic activity of mutant KRAS. *Cell*. 2018;172:857–868 e815.
- [21] To MD, Perez-Losada J, Mao J-H, et al. A functional switch from lung cancer resistance to susceptibility at the Pas1 locus in Kras2LA2 mice. *Nat Genet*. 2006;38:926–930.
- [22] Zhang Z, Wang Y, Vikis HG, et al. Wildtype Kras2 can inhibit lung carcinogenesis in mice. *Nat Genet*. 2001;29:25–33.
- [23] Hamilton M, Wolfman A. Oncogenic Ha-Ras-dependent mitogen-activated protein kinase activity requires signaling through the epidermal growth factor receptor. *J Biol Chem*. 1998;273:28155–28162.

- [24] Young A, Lou D, McCormick F. Oncogenic and wild-type Ras play divergent roles in the regulation of mitogen-activated protein kinase signaling. *Cancer Discov.* 2013;3:112–123.
- [25] Lim KH, Ancrile BB, Kashatus DF, et al. Tumour maintenance is mediated by eNOS. *Nature.* 2008;452:646–649.
- [26] Bentley C, Jurinka SS, Kljavin NM, et al. A requirement for wild-type Ras isoforms in mutant KRAS-driven signalling and transformation. *Biochem J.* 2013;452:313–320.
- [27] Castellano E, Santos E. Functional specificity of ras isoforms: so similar but so different. *Genes Cancer.* 2011;2:216–231.
- [28] Buday L, Downward J. Many faces of Ras activation. *Biochim Biophys Acta.* 2008;1786:178–187.
- [29] Margarit SM, Sondermann H, Hall BE, et al. Structural evidence for feedback activation by Ras.GTP of the Ras-specific nucleotide exchange factor SOS. *Cell.* 2003;112:685–695.
- [30] Sheffels E, Sealover NE, Wang C, et al. Oncogenic RAS isoforms show a hierarchical requirement for the guanine nucleotide exchange factor SOS2 to mediate cell transformation. *Sci Signal.* 2018;11. doi:10.1126/sci-signal.aar8371.
- [31] Munoz DM, Cassiani PJ, Li L, et al. CRISPR screens provide a comprehensive assessment of cancer vulnerabilities but generate false-positive hits for highly amplified genomic regions. *Cancer Discov.* 2016;6:900–913.
- [32] Inoue R, Hirohashi Y, Kitamura H, et al. GRIK2 has a role in the maintenance of urothelial carcinoma stem-like cells, and its expression is associated with poorer prognosis. *Oncotarget.* 2017;8:28826–28839.
- [33] Hu Y, Smyth GK. ELDA: extreme limiting dilution analysis for comparing depleted and enriched populations in stem cell and other assays. *J Immunol Methods.* 2009;347:70–78.
- [34] Paoli P, Giannoni E, Chiarugi P. Anoikis molecular pathways and its role in cancer progression. *Biochim Biophys Acta, Mol Cell Res.* 2013;1833:3481–3498.
- [35] Castellano E, Downward J. RAS interaction with PI3K: more than just another effector pathway. *Genes Cancer.* 2011;2:261–274.
- [36] Manchado E, Weissmueller S, Morris JP, et al. A combinatorial strategy for treating KRAS-mutant lung cancer. *Nature.* 2016;534:647–651.
- [37] Ebi H, Corcoran RB, Singh A, et al. Receptor tyrosine kinases exert dominant control over PI3K signaling in human KRAS mutant colorectal cancers. *J Clin Invest.* 2011;121:4311–4321.
- [38] Sun C, Hobor S, Bertotti A, et al. Intrinsic resistance to MEK inhibition in KRAS mutant lung and colon cancer through transcriptional induction of ERBB3. *Cell Rep.* 2014;7:86–93.
- [39] Pettazoni P, Viale A, Shah P, et al. Genetic events that limit the efficacy of MEK and RTK inhibitor therapies in a mouse model of KRAS-driven pancreatic cancer. *Cancer Res.* 2015;75:1091–1101.
- [40] Fedele C, Ran H, Diskin B, et al. SHP2 inhibition prevents adaptive resistance to MEK inhibitors in multiple cancer models. *Cancer Discov.* 2018;8:1237–1249.
- [41] Mainardi S, Mulero-Sánchez A, Prahallad A, et al. SHP2 is required for growth of KRAS-mutant non-small-cell lung cancer in vivo. *Nat Med.* 2018;24:961–967.
- [42] Ruess DA, Heynen GJ, Ciecieski KJ, et al. Mutant KRAS-driven cancers depend on PTPN11/SHP2 phosphatase. *Nat Med.* 2018;24:954–960.
- [43] Yan J, Roy S, Apolloni A, et al. Ras isoforms vary in their ability to activate Raf-1 and phosphoinositide 3-kinase. *J Biol Chem.* 1998;273:24052–24056.
- [44] Voice JK, Klemke RL, Le A, et al. Four human ras homologs differ in their abilities to activate Raf-1, induce transformation, and stimulate cell motility. *J Biol Chem.* 1999;274:17164–17170.
- [45] Li W, Zhu T, Guan KL. Transformation potential of Ras isoforms correlates with activation of phosphatidylinositol 3-kinase but not ERK. *J Biol Chem.* 2004;279:37398–37406.
- [46] Cerami E, Gao J, Dogrusoz U, et al. The cBio cancer genomics portal: an open platform for exploring multi-dimensional cancer genomics data. *Cancer Discov.* 2012;2:401–404.
- [47] Gao J, Aksoy BA, Dogrusoz U, et al. Integrative analysis of complex cancer genomics and clinical profiles using the cBioPortal. *Sci Signal.* 2013;6:pl1.
- [48] Sondermann H, Soisson SM, Boykevich S, et al. Structural analysis of autoinhibition in the Ras activator Son of sevenless. *Cell.* 2004;119:393–405.
- [49] Jeng HH, Taylor LJ, Bar-Sagi D. Sos-mediated cross-activation of wild-type Ras by oncogenic Ras is essential for tumorigenesis. *Nat Commun.* 2012;3:1168.
- [50] Saha M, Carriere A, Cheerathodi M, et al. RSK phosphorylates SOS1 creating 14-3-3-docking sites and negatively regulating MAPK activation. *Biochem J.* 2012;447:159–166.
- [51] Douville E, Downward J. EGF induced SOS phosphorylation in PC12 cells involves P90 RSK-2. *Oncogene.* 1997;15:373–383.
- [52] Hennig A, Markwart R, Wolff K, et al. Feedback activation of neurofibromin terminates growth factor-induced Ras activation. *Cell Commun Signal.* 2016;14:5.
- [53] Langlois WJ, Sasaoka T, Saltiel AR, et al. Negative feedback regulation and desensitization of insulin- and epidermal growth factor-stimulated p21ras activation. *J Biol Chem.* 1995;270:25320–25323.
- [54] Corbalan-Garcia S, Yang SS, Degenhardt KR, et al. Identification of the mitogen-activated protein kinase phosphorylation sites on human Sos1 that regulate interaction with Grb2. *Mol Cell Biol.* 1996;16:5674–5682.
- [55] Dong C, Waters SB, Holt KH, et al. SOS phosphorylation and disassociation of the Grb2-SOS complex by the ERK and JNK signaling pathways. *J Biol Chem.* 1996;271:6328–6332.
- [56] Kamioka Y, Yasuda S, Fujita Y, et al. Multiple decisive phosphorylation sites for the negative feedback regulation of SOS1 via ERK. *J Biol Chem.* 2010;285:33540–33548.
- [57] Catalanotti F, Reyes G, Jesenberger V, et al. A Mek1-Mek2 heterodimer determines the strength and duration of the Erk signal. *Nat Struct Mol Biol.* 2009;16:294–303.

- [58] Dougherty MK, Müller J, Ritt DA, et al. Regulation of Raf-1 by direct feedback phosphorylation. *Mol Cell Biol.* [2005](#);17:215–224.
- [59] Ritt DA, Monson DM, Specht SI, et al. Impact of feedback phosphorylation and Raf heterodimerization on normal and mutant B-Raf signaling. *Mol Cell Biol.* [2010](#);30:806–819.
- [60] McKay MM, Ritt DA, Morrison DK. Signaling dynamics of the KSR1 scaffold complex. *Proc Natl Acad Sci U S A.* [2009](#);106:11022–11027.
- [61] Fortian A, Sorkin A. Live-cell fluorescence imaging reveals high stoichiometry of Grb2 binding to the EGF receptor sustained during endocytosis. *J Cell Sci.* [2014](#);127:432–444.
- [62] Casar B, Arozarena I, Sanz-Moreno V, et al. Ras subcellular localization defines extracellular signal-regulated kinase 1 and 2 substrate specificity through distinct utilization of scaffold proteins. *Mol Cell Biol.* [2009](#);29:1338–1353.
- [63] Casar, B., Badrock AP, Jiménez I, et al. RAS at the Golgi antagonizes malignant transformation through PTPK κ -mediated inhibition of ERK activation. *Nat Commun.* [2018](#);9:3595.
- [64] Cheng C-M, Li H, Gasman S, et al. Compartmentalized Ras proteins transform NIH 3T3 cells with different efficiencies. *Mol Cell Biol.* [2011](#);31:983–997.
- [65] Hancock JF. Ras proteins: different signals from different locations. *Nat Rev Mol Cell Biol.* [2003](#);4:373–384.
- [66] Henis YI, Hancock JF, Prior IA. Ras acylation, compartmentalization and signaling nanoclusters (Review). *Mol Membr Biol.* [2009](#);26:80–92.
- [67] Nimnual AS, Yatsula BA, Bar-Sagi D. Coupling of Ras and Rac guanosine triphosphatases through the Ras exchanger Sos. *Science.* [1998](#);279:560–563.
- [68] Scita G, Nordstrom J, Carbone R, et al. EPS8 and E3B1 transduce signals from Ras to Rac. *Nature.* [1999](#);401:290–293.
- [69] Innocenti M, Tenca P, Frittoli E, et al. Mechanisms through which Sos-1 coordinates the activation of Ras and Rac. *J Cell Biol.* [2002](#);156:125–136.
- [70] Licerias-Boillos P, García-Navas R, Ginel-Picardo A, et al. Sos1 disruption impairs cellular proliferation and viability through an increase in mitochondrial oxidative stress in primary MEFs. *Oncogene.* [2016](#);35:6389–6402.
- [71] Cordeddu V, Yin JC, Gunnarsson C, et al. Activating mutations affecting the Dbl homology domain of SOS2 cause noonan syndrome. *Hum Mutat.* [2015](#);36:1080–1087.
- [72] Yamamoto GL, Agüena M, Gos M, et al. Rare variants in SOS2 and LZTR1 are associated with Noonan syndrome. *J Med Genet.* [2015](#);52:413–421.

CANCER

Oncogenic RAS isoforms show a hierarchical requirement for the guanine nucleotide exchange factor SOS2 to mediate cell transformation

Erin Sheffels¹, Nancy E. Sealover¹, Chenyue Wang¹, Do Hyung Kim¹, Isabella A. Vazirani¹, Elizabeth Lee¹, Elizabeth M. Terrell², Deborah K. Morrison², Ji Luo³, Robert L. Kortum^{1*}

Copyright © 2018
The Authors, some
rights reserved;
exclusive licensee
American Association
for the Advancement
of Science. No claim
to original U.S.
Government Works

About a third of tumors have activating mutations in *HRAS*, *NRAS*, or *KRAS*, genes encoding guanosine triphosphatases (GTPases) of the RAS family. In these tumors, wild-type RAS cooperates with mutant RAS to promote downstream effector activation and cell proliferation and transformation, suggesting that upstream activators of wild-type RAS are important modulators of mutant RAS-driven oncogenesis. The guanine nucleotide exchange factor (GEF) SOS1 mediates *KRAS*-driven proliferation, but little is understood about the role of SOS2. We found that RAS family members have a hierarchical requirement for the expression and activity of SOS2 to drive cellular transformation. In mouse embryonic fibroblasts (MEFs), SOS2 critically mediated mutant *KRAS*-driven, but not *HRAS*-driven, transformation. *Sos2* deletion reduced epidermal growth factor (EGF)-dependent activation of wild-type *HRAS* and phosphorylation of the kinase AKT in cells expressing mutant RAS isoforms. Assays using pharmacological inhibitors revealed a hierarchical requirement for signaling by phosphoinositide 3-kinase (PI3K) in promoting RAS-driven cellular transformation that mirrored the requirement for SOS2. *KRAS*-driven transformation required the GEF activity of SOS2 and was restored in *Sos2*^{-/-} MEFs by expression of constitutively activated PI3K. Finally, CRISPR/Cas9-mediated deletion of *SOS2* reduced EGF-stimulated AKT phosphorylation and synergized with MEK inhibition to revert the transformed phenotype of human *KRAS* mutant pancreatic and lung tumor cells. These results indicate that SOS2-dependent PI3K signaling mediates mutant *KRAS*-driven transformation, revealing therapeutic targets in *KRAS*-driven cancers. Our data also reveal the importance of three-dimensional culture systems in investigating the mediators of mutant *KRAS*.

INTRODUCTION

The RAS family of small guanosine triphosphatases (GTPases) includes three genes—*HRAS*, *NRAS*, and *KRAS*—whose protein products (*HRAS*, *NRAS*, *KRAS4A*, and *KRAS4B*) are activated by multiple physiological inputs to regulate different cellular outcomes depending on the specific context, including proliferation, differentiation, growth, apoptosis, and cell survival (1, 2). RAS proteins are molecular switches that are active when they are guanosine 5'-triphosphate (GTP)-bound and inactive when they are guanosine diphosphate (GDP)-bound. They are activated by RAS guanine nucleotide exchange factors (RASGEFs) that exchange GDP for GTP on RAS and are inactivated by their own intrinsic GTPase activity, which is facilitated by RAS GTPase-activating proteins (RASGAPs). Receptor tyrosine kinase (RTK) engagement recruits the RASGEFs Son of Sevenless 1 and 2 (SOS1 and SOS2, respectively) to the plasma membrane, where they induce nucleotide exchange and activate RAS. Active RAS then signals through multiple effectors to initiate downstream signaling cascades important for proliferation and survival, including the Raf/MEK [MAPK (mitogen-activated protein kinase) kinase]/ERK (extracellular signal-regulated kinase) kinase cascade and the phosphoinositide 3-kinase (PI3K)/AKT pathway.

In addition to the role of RAS in RTK-dependent signaling, somatic mutations in *HRAS*, *NRAS*, or *KRAS* drive oncogenesis in about 30% of human tumors. These oncogenic RAS mutations, which

most commonly cause amino acid substitutions at codon 12, 13, or 61, impair RASGAP-mediated GTP hydrolysis, leading to constitutive GTP binding and activation. Although this constitutive RAS activation was originally thought to make RAS mutant tumors independent of upstream signaling, we now know that activation of nonmutated wild-type RAS plays an important role in modulating downstream effector signaling during mutant RAS-driven tumorigenesis. The wild-type allele of the corresponding mutated RAS isoform is frequently deleted in RAS-driven tumors, suggesting that it may have a tumor suppressor role (3–5). This hypothesis is supported by observations in vitro (6) and in vivo with mouse models (7, 8). In contrast, the other two nonmutated wild-type RAS family members are necessary for mutant RAS-driven proliferation and transformation in some contexts (9–12). The wild-type RAS isoforms potentially contribute through their ability to activate effector pathways that the mutant isoform does not strongly activate, making the cellular outcome a product of signaling by both wild-type and mutant RAS (13).

Two models have been proposed to explain how wild-type RAS signaling cooperates with mutant RAS to promote downstream effector activation and RAS-driven oncogenesis. In the first model, RTK-dependent activation of wild-type RAS supplements the basal oncogenic signaling from mutant RAS to fully activate downstream effector pathways and promote proliferation in RAS mutant tumor cell lines (11, 14, 15). In the second model, GTP-bound RAS (RAS^{GTP}) binds an allosteric pocket on the RASGEF SOS1 that relieves SOS1 autoinhibition, increasing its catalytic activity up to 80-fold (16). Relief of SOS1 autoinhibition then sets up a positive feedback loop from mutant RAS^{GTP} through SOS1 to wild-type RAS that enhances activation of downstream effectors and is important for proliferation of *KRAS* mutant pancreatic cancer cells (17).

¹Department of Pharmacology and Molecular Therapeutics, Uniformed Services University of the Health Sciences, Bethesda, MD 20814, USA. ²Laboratory of Cell and Developmental Signaling, National Cancer Institute (NCI)—Frederick, Frederick, MD 21702, USA. ³Laboratory of Cancer Biology and Genetics, Center for Cancer Research, NCI, National Institutes of Health, Bethesda, MD 20892, USA.

*Corresponding author. Email: robert.kortum@usuhs.edu

Whereas a role for SOS1 in *KRAS* mutant pancreatic cancer proliferation has been established, a role for SOS2 in mutant *RAS*-driven oncogenesis is not yet understood. Here, we used immortalized *Sos2*^{-/-} mouse embryonic fibroblasts (MEFs) to determine the role of SOS2 in HRAS-, NRAS-, and KRAS-driven transformation. We found that there was a hierarchical requirement for SOS2 in *RAS*-driven transformation (*KRAS* > *NRAS* > *HRAS*), with *KRAS* being the most SOS2-dependent *RAS* isoform. Using mutant SOS2 constructs, we found that *KRAS*-driven transformation was dependent on SOS2 RASGEF activity, but not on putative SOS2 allosteric activation. SOS2 was required for epidermal growth factor (EGF)-stimulated, but not basal, wild-type HRAS activation in cells expressing mutant *KRAS*. At the level of effector signaling, *Sos2* deletion reduced RTK-dependent AKT phosphorylation in cells expressing all mutant *RAS* isoforms. However, we also found that there was a hierarchical requirement for PI3K signaling in promoting *RAS*-driven transformation (*KRAS* ≥ *NRAS* > *HRAS*) that mirrored the hierarchical requirement for SOS2. Furthermore, *KRAS*-driven transformation could be rescued in *Sos2*^{-/-} MEFs by introduction of an activated PI3K catalytic subunit. Finally, deletion of *SOS2* reduced RTK-dependent AKT phosphorylation and synergized with the MEK inhibitor trametinib to block transformation of *KRAS* mutant tumor cell lines. These results indicate that SOS2-dependent PI3K signaling plays an important role in mutant *KRAS*-driven transformation and that SOS2 may be a therapeutic target in *KRAS*-driven cancers. In addition, the specific requirement for SOS2 to promote mutant *KRAS*-driven proliferation in three-dimensional (3D), but not 2D, culture suggests that anchorage-independent screens must be used to supplement current 2D screening efforts when investigating therapeutic interventions to treat *KRAS* mutant tumors.

RESULTS

Mutant *RAS* isoforms show a hierarchical requirement for *Sos2* to drive transformation

Previous work has shown that activation of wild-type *RAS* promotes mutant *RAS*-dependent oncogenesis by at least two mechanisms. First, RTK-dependent wild-type *RAS* activation, presumably via the RASGEFs SOS1 and/or SOS2, cooperates with mutant HRAS, NRAS, and *KRAS* to promote *RAS* effector activation and cancer cell proliferation (11, 15). Second, mutant *KRAS* allosterically activates SOS1 (16), generating a feedback loop from GTP-bound *KRAS* (*KRAS*^{GTP}) through SOS1 to wild-type *RAS* that critically mediated proliferation of pancreatic cancer cells (17). Although this contribution of SOS1 in mutant *KRAS*-driven cancer cell proliferation has been established, the specific role of SOS2 in *RAS* mutant tumors is not yet clear.

Previous work has shown a role for SOS1, but not SOS2, in anchorage-dependent (2D) proliferation in primary MEFs (18); however, we wanted to specifically assess the role of SOS2 in mutant *RAS*-dependent transformation. Because primary MEFs require cooperating oncogenes in addition to mutant *RAS* to promote transformation (19), we first generated immortalized MEFs that can be transformed by mutant *RAS* alone (20). To establish a model system to allow us to examine the specific role of SOS2 in oncogenic transformation, we immortalized *Sos1*^{fl/fl} and *Sos1*^{fl/fl}*Sos2*^{-/-} MEFs by a 3T6 protocol (21, 22) to generate stable cell lines (hereafter referred to as *Sos2*^{+/+} and *Sos2*^{-/-} MEFs). To assess the role of SOS2 in mutant *RAS*-driven proliferation and transformation, we then stably expressed hemagglutinin (HA)-tagged HRAS^{G12V}, NRAS^{G12V}, or KRAS4B^{G12V} (hereafter referred to as KRAS^{G12V}) in the

Sos2^{+/+} and *Sos2*^{-/-} MEFs at 0.2 to 3 times total endogenous *RAS* protein abundance (Fig. 1A). Whereas neither *Sos2* deletion nor mutant *RAS* expression altered SOS1 protein abundance, expression of mutant *RAS* family members did decrease the expression of EGF receptor (EGFR) to variable extents, potentially due to feedback regulation on the signaling pathway (Fig. 1A).

As expected, expression of oncogenic HRAS^{G12V}, NRAS^{G12V}, or KRAS^{G12V} enhanced cell proliferation over vector controls in immortalized MEFs (fig. S1), and *Sos2* deletion did not affect GTP loading of the mutant *RAS* protein (Fig. 1A), did not alter proliferation driven by mutant NRAS or *KRAS*, and only modestly reduced proliferation stimulated by mutant HRAS on the last day of a 5-day growth curve (Fig. 1B and fig. S1). These data suggest that SOS2 is not a critical mediator of mutant *KRAS*- or *NRAS*-driven proliferation and has a minimal effect on proliferation driven by HRAS, in agreement with a previous study in primary MEFs showing that SOS1, but not SOS2, is a critical mediator of proliferation (18). To assess *RAS*-driven transformation, we examined two common features of transformed cells: anchorage-independent growth (soft agar assay; Fig. 1C) and loss of contact inhibition (focus-forming assay; Fig. 1D). The effect of *Sos2* deletion on *RAS*-driven transformation differed depending on which mutant *RAS* isoform was expressed. *Sos2* deletion did not affect HRAS^{G12V}-induced anchorage-independent growth (Fig. 1C), loss of contact inhibition (Fig. 1D), or morphologic transformation (Fig. 1E), indicating that SOS2 was dispensable for HRAS^{G12V}-induced transformation. In contrast, *Sos2* deletion reduced the transforming capacity of NRAS^{G12V} and critically mediated transformation driven by KRAS^{G12V} (Fig. 1, C to E). *Sos2*^{-/-} MEFs expressing NRAS^{G12V} showed a 50% reduction in colony formation in soft agar (Fig. 1C) and qualitatively reduced the proportion of cells showing loss of contact inhibition (Fig. 1D), indicating that SOS2 promoted, but was not required for, transformation by NRAS^{G12V}. *Sos2*^{-/-} MEFs expressing KRAS^{G12V} exhibited minimal anchorage-independent growth (Fig. 1C), remained contact-inhibited (Fig. 1D), and did not show any signs of morphologic transformation (Fig. 1E). These data suggest that there is a hierarchical requirement for SOS2 in mutant *RAS*-driven transformation.

Within the pool of *RAS* mutant tumors, *KRAS* is the most frequently mutated *RAS* family member (85%). Most *KRAS* mutations occur at codon G12, G13, or Q61, with the frequency of specific mutations varying depending on the tumor type (23, 24). Because our data indicated that *Sos2* deletion has a larger effect on transformation driven by mutant *KRAS* compared to mutant HRAS or NRAS, we further investigated the requirement of SOS2 in mutant *KRAS*-driven transformation. To determine whether this requirement is mutation-specific, we expressed either wild-type *KRAS* or one of six common *KRAS* oncogenic mutants (G12C, G12D, G12V, G13D, Q61L, or Q61R) in *Sos2*^{+/+} and *Sos2*^{-/-} MEFs (Fig. 2A). For all *KRAS* G12 and G13 oncogenic mutants examined, SOS2 critically mediated mutant *KRAS*-induced anchorage-independent growth (Fig. 2B) and loss of contact inhibition (Fig. 2C). In contrast, for the *KRAS* Q61 mutants, low amounts of *KRAS*-induced loss of contact inhibition were detectable in the absence of SOS2, indicating that, although Q61 mutants require SOS2 for full transformation, they can induce some transformation without SOS2. These data suggest that SOS2 critically mediates full *KRAS*-driven transformation in MEFs, regardless of the specific *KRAS* oncogenic mutation, although it is only partially required for Q61 mutants.

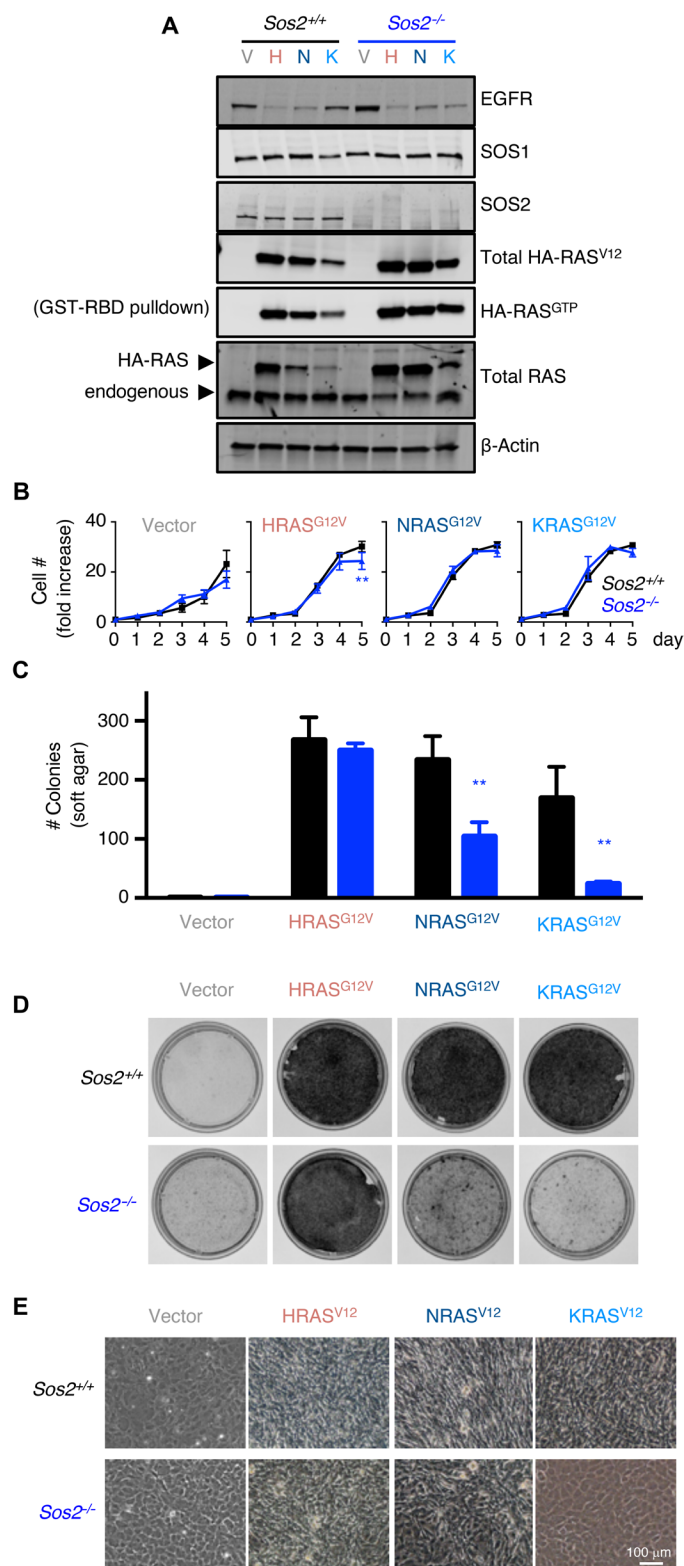


Fig. 1. Oncogenic mutant RAS isoforms show a hierarchical requirement for SOS2 to drive transformation in MEFs. (A) *Sos2*^{+/+} and *Sos2*^{-/-} MEFs were transduced with lentiviruses expressing either empty vector (V) or the indicated HA-tagged mutant RAS isoform (HRAS, NRAS, and KRAS: HRAS^{G12V}, NRAS^{G12V}, and KRAS^{G12V}, respectively). Whole-cell lysates (WCLs) were analyzed by Western blotting with antibodies specific for EGFR, SOS1, SOS2, HA (for RAS^{G12V}), total RAS, or β-actin to assess total protein. Glutathione S-transferase (GST)-RAS binding domain (RBD) pull-downs (PDs) were analyzed by Western blotting with an antibody specific for the HA epitope to assess activation of mutant HA-RAS^{G12V}. Blots are representative of three independent experiments. (B to D) *Sos2*^{+/+} and *Sos2*^{-/-} MEFs expressing the indicated mutant RAS isoform were assessed for (B) proliferation in 2D culture plates, (C) colony growth in soft agar to assess anchorage-independent growth, and (D) loss of contact inhibition as assessed by a focus-forming assay. Data are means ± SD from three independent experiments. ***P* < 0.01 by analysis of variance (ANOVA) using the Tukey's method to correct for multiple comparisons. (E) Representative 10× images of post-confluent MEFs from (D). Scale bar, 100 μm. See also fig. S1 for an overlay of the proliferation curves in (B).

making them less dependent on GEF activity to restore GTP binding (25). Because of this, we first assessed whether KRAS GTP loading was dependent on SOS2 for KRAS^{G12C}, KRAS^{G12V}, and KRAS^{Q61R} mutant proteins. We did not observe any significant alterations in KRAS^{GTP} abundance upon *Sos2* deletion for any of the mutant KRAS proteins (fig. S2), indicating that the activation of mutant KRAS is not dependent on SOS2.

Next, we examined the mechanism by which SOS2 contributes to KRAS-driven transformation by restoring SOS2 expression in *Sos2*^{-/-} MEFs, using either wild-type or mutant SOS2 constructs to distinguish the relative contributions of RTK-SOS2-wild-type RAS and KRAS^{GTP}-SOS2-wild-type RAS signaling. However, because of the hypothesized dynamics of SOS signaling, we first created a construct that would allow us to restore SOS2 in *Sos2*^{-/-} MEFs at near endogenous (*Sos2*^{+/+}) protein abundance. In a quantitative proteomic analysis of the core components in the RTK/RAS/MAPK signaling pathway, Shi *et al.* (26) showed that the absolute abundances of SOS1 and SOS2 are extremely low relative to the other core proteins in the RTK/RAS signaling pathway, leading them to hypothesize that SOS1 and SOS2 may be “stoichiometric bottlenecks” for signal transduction through this pathway. Their findings suggest that exogenous introduction of SOS2 at superphysiologic protein abundance could result in aberrant RAS-dependent signaling, making rescue experiments difficult to interpret. To circumvent this, SOS2 was cloned into lentiviral vectors containing one of five different promoters, each with different predicted expression levels, and then stably expressed in *Sos2*^{-/-} MEFs (fig. S3A). The high-activity EF1α and UbC promoters, and the moderate-activity phosphoglycerate kinase (PGK) promoter, lead to SOS2 protein abundance >30- and 18-fold higher than endogenous SOS2 found in *Sos2*^{+/+} MEFs, respectively, indicating that these promoters are not optimal for expressing SOS2 at physiologic protein abundances. In contrast, using either an SV40 or a minimal cytomegalovirus (mCMV) promoter to drive SOS2 expression leads to SOS2 abundance at only two- to fivefold above that of endogenous SOS2. This near-endogenous SOS2 abundance restored transformation in *Sos2*^{-/-} MEFs expressing KRAS^{G12V} (fig. S3B). Because the SV40 promoter gave more consistent near-endogenous SOS2 abundance across multiple experiments, we used this promoter for subsequent SOS2 rescue experiments.

Bentley *et al.* (15) previously showed that wild-type NRAS and HRAS critically mediate transformation of KRAS mutant cancer cells. We hypothesized that SOS2 potentially promotes KRAS-driven

SOS2 RASGEF activity is required for KRAS-driven transformation

KRAS Q61 mutants have lower amounts of GTPase activity than the already reduced activity in G12 and G13 mutants, potentially

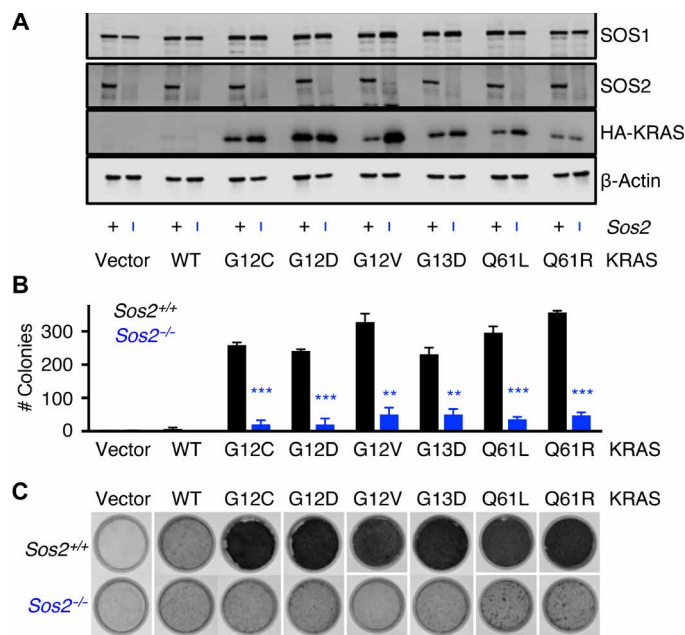


Fig. 2. SOS2 critically mediates mutant KRAS-driven transformation in MEFs. (A) *Sosl2*^{+/+} (+) and *Sosl2*^{-/-} (-) MEFs were transduced with lentiviruses expressing either empty vector, wild-type (WT) KRAS, or the indicated HA-tagged mutant KRAS constructs. WCLs were analyzed by Western blotting with antibodies specific for SOS2, HA (KRAS), or β -actin. Blots are representative of three independent experiments. (B and C) *Sosl2*^{+/+} and *Sosl2*^{-/-} MEFs expressing the indicated KRAS constructs were assessed for (B) colony growth in soft agar to assess anchorage-independent growth, and (C) loss of contact inhibition as assessed by focus-forming assay. Data are means \pm SD from three independent experiments. ** $P < 0.01$, *** $P < 0.001$ by ANOVA using the Tukey's method to correct for multiple comparisons.

transformation by one of two mechanisms: either by RTK-dependent activation of downstream effectors or as a part of an allosteric KRAS^{GTP}-SOS2-wild-type RAS feedback loop similar to the one previously described for SOS1 (16, 17). To differentiate between these two possibilities, we made constructs with point mutations in SOS2 that are homologous to mutations previously identified in SOS1: SOS2^{F927A}, which is homologous to the SOS1^{F929A} mutant that ablates RASGEF activity (27), and SOS2^{W727E}, which is homologous to the SOS1^{W729E} mutant that renders SOS1 unable to be allosterically activated by RAS^{GTP} (16, 28). If the major contribution of SOS2 is to promote RTK-SOS2-wild-type RAS signaling, then only the SOS2^{F927A} mutant will fail to restore transformation in *Sosl2*^{-/-} MEFs expressing mutant KRAS. In contrast, if KRAS^{GTP}-SOS2-wild-type RAS signaling is important for mutant KRAS-driven transformation, then neither the SOS2^{F927A} nor the SOS2^{W727E} mutants will restore transformation in *Sosl2*^{-/-} MEFs expressing mutant KRAS (Fig. 3A).

We stably introduced wild-type SOS2, SOS2^{F927A}, or SOS2^{W727E} into *Sosl2*^{-/-} MEFs expressing KRAS^{G12C}, KRAS^{G12V}, or KRAS^{Q61R} (Fig. 3B). Wild-type SOS2 restored KRAS-driven anchorage-independent growth (Fig. 3C), loss of contact inhibition (Fig. 3D), and morphologic transformation (Fig. 3E) in *Sosl2*^{-/-} MEFs expressing each of the mutant RAS constructs. In contrast, RASGEF-dead SOS2 (SOS2^{F927A}) could not restore KRAS-driven transformation in cells expressing either KRAS^{G12C} or KRAS^{G12V} (Fig. 3, C to E). In cells expressing KRAS^{Q61R}, however, we observed that SOS2^{F927A} enhanced the small incidence of transformation we had observed in *Sosl2*^{-/-} MEFs expressing KRAS^{Q61R}, suggesting that, although *Sosl2* deletion did not

alter the global GTP loading of KRAS^{Q61R}, the GTPase activity of different oncogenic KRAS mutants may modulate their dependence on SOS2. However, although KRAS^{Q61R} exhibited lower dependence on SOS2 for transformation than either KRAS^{G12C} or KRAS^{G12V} did, SOS2 GEF activity still mediated full KRAS^{Q61R}-driven transformation. On the other hand, a SOS2 mutant construct resistant to RAS^{GTP}-dependent feedback activation (SOS2^{W727E}) restored KRAS-driven transformation similarly to wild-type SOS2. Because SOS2 RASGEF activity, but not allosteric RAS^{GTP}-dependent SOS2 activation, was required for mutant KRAS to fully transform MEFs, these data suggest that RTK-dependent SOS2 signaling to wild-type RAS cooperates with basal signaling from mutant KRAS to promote the transformed phenotype.

To directly examine the role of SOS2 in activation of wild-type RAS, we expressed V5-tagged wild-type HRAS in *Sosl2*^{+/+} and *Sosl2*^{-/-} MEFs expressing HA-KRAS^{G12C} and performed GST-RBD PDs to directly assess HRAS^{GTP} in both actively cycling cells and upon EGF stimulation after an overnight starve (Fig. 3F). Activation of wild-type HRAS was significantly decreased in actively cycling *Sosl2*^{-/-} MEFs compared to the *Sosl2*^{+/+} MEFs, indicating that SOS2 is important for full wild-type HRAS activation (Fig. 3F, left). In serum-starved cells, the abundance of HRAS^{GTP} was unchanged upon *Sosl2* deletion, indicating that basal KRAS^{G12C}-dependent activation of wild-type HRAS was independent of SOS2. EGF stimulation after an overnight starve showed increased wild-type HRAS activation in *Sosl2*^{+/+} MEFs, but not *Sosl2*^{-/-} MEFs, suggesting that SOS2-dependent activation of wild-type HRAS is downstream of RTK signaling in cells with mutant KRAS (Fig. 3F, right). Furthermore, assessment of V5-HRAS activation in KRAS^{G12C} *Sosl2*^{-/-} MEFs expressing wild-type SOS2, SOS2^{F927A}, or SOS2^{W727E} showed that activation of wild-type HRAS was increased in *Sosl2*^{-/-} MEFs expressing wild-type SOS2 and SOS2^{W727E} compared to either vector controls or *Sosl2*^{-/-} MEFs expressing SOS2^{F927A} (Fig. 3G). These data indicate that SOS2 GEF activity, but not allosteric feedback activation of SOS2 by oncogenic KRAS, is key to SOS2-dependent activation of wild-type HRAS downstream of RTKs.

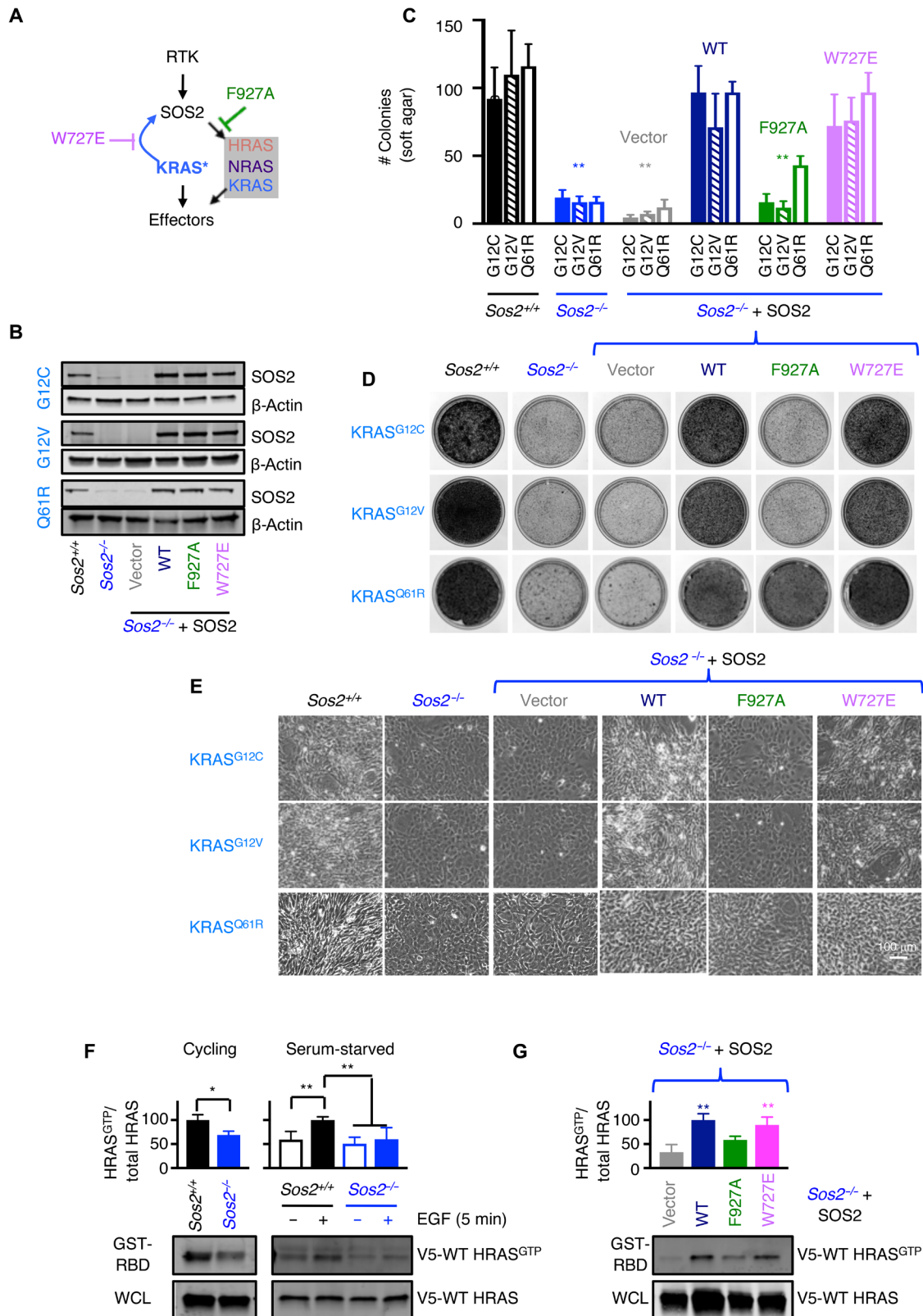
SOS2 promotes EGF-stimulated AKT phosphorylation in cells expressing mutant RAS

The data presented in Fig. 3 suggest that RTK-SOS2 signaling through wild-type RAS to downstream Raf/MEK/ERK and PI3K/AKT effector pathways augments basal KRAS^{G12V} signaling to promote oncogenic transformation. To test this possibility, we assessed EGF-stimulated phosphorylation of ERK and AKT in *Sosl2*^{+/+} and *Sosl2*^{-/-} MEFs expressing each RAS^{G12V} isoform (Fig. 4). Although mutant RAS expression reduced EGFR expression (Fig. 1A), *Sosl2* deletion did not have any further effects on EGFR protein abundance, so comparisons of EGF-stimulated signaling in *Sosl2*^{+/+} or *Sosl2*^{-/-} MEFs expressing any individual mutant RAS isoform were not confounded by alterations in EGFR abundance (Fig. 4A). *Sosl2* deletion did not significantly alter EGF-stimulated ERK phosphorylation in cells expressing mutant HRAS, NRAS, or KRAS as shown by the lack of reduction in both peak ERK phosphorylation and prolonged Raf/MEK/ERK signaling upon *Sosl2* deletion (Fig. 4, A and B). In contrast, *Sosl2* deletion significantly reduced EGF-stimulated AKT phosphorylation in cells expressing mutant HRAS, NRAS, or KRAS (Fig. 4, A and B). Loss of SOS2 reduced peak AKT phosphorylation and blocked prolonged PI3K/AKT signaling. These data suggest that SOS2 is important for RTK-stimulated PI3K/AKT, but not Raf/MEK/ERK, signaling. However, these data do not sufficiently explain the differential requirement for

Fig. 3. SOS2 RASGEF activity contributes to KRAS-driven transformation.

(A) Schematic showing potential routes of SOS2-dependent WT RAS activation in the presence of mutant KRAS. SOS2 point mutants block either RASGEF activity (F927A) or putative allosteric SOS2 activation by KRAS (W727E).

(B) *Sos2*^{-/-} MEFs expressing KRAS^{G12C}, KRAS^{G12V}, or KRAS^{Q61R} were transduced with lentiviruses expressing either empty vector, WT SOS2, RASGEF-deficient (F927A) SOS2, or feedback-defective (W727E) SOS2. WCLs were analyzed by Western blotting with antibodies specific for SOS2 or β -actin. **(C and D)** *Sos2*^{+/+} MEFs, *Sos2*^{-/-} MEFs, or *Sos2*^{-/-} MEFs expressing the indicated SOS2 constructs along with either KRAS^{G12C} (closed), KRAS^{G12V} (hashed), or KRAS^{Q61R} (open) were assessed for **(C)** colony growth in soft agar to assess anchorage-independent growth, and **(D)** loss of contact inhibition by a focus-forming assay. **(E)** Representative 10 \times images of post-confluent MEFs from **(D)**. Scale bar, 100 μ m. **(F and G)** Western blotting for activated V5-HRAS from GST-RBD PDs (middle, quantified above) or for total V5-HRAS from WCLs (below) from **(F)** *Sos2*^{+/+} or *Sos2*^{-/-} MEFs expressing HA-KRAS^{G12C} and V5-WT HRAS in either actively cycling cells (left) or cells serum-starved overnight and then lysed or stimulated with EGF (100 μ g/ml) for 5 min (right) or **(G)** *Sos2*^{-/-} MEFs expressing HA-KRAS^{G12C}, V5-WT HRAS, and the indicated SOS2 construct. All data are means \pm SD from three independent experiments; all blots and images are representative of three independent experiments. **P* < 0.05, ***P* < 0.01 [for **(C)**, versus *Sos2*^{+/+} and WT; for **(G)**, versus vector and SOS2^{F927A}] by ANOVA using the Tukey's method to correct for multiple comparisons.



Downloaded from <http://stke.sciencemag.org/> on September 18, 2018

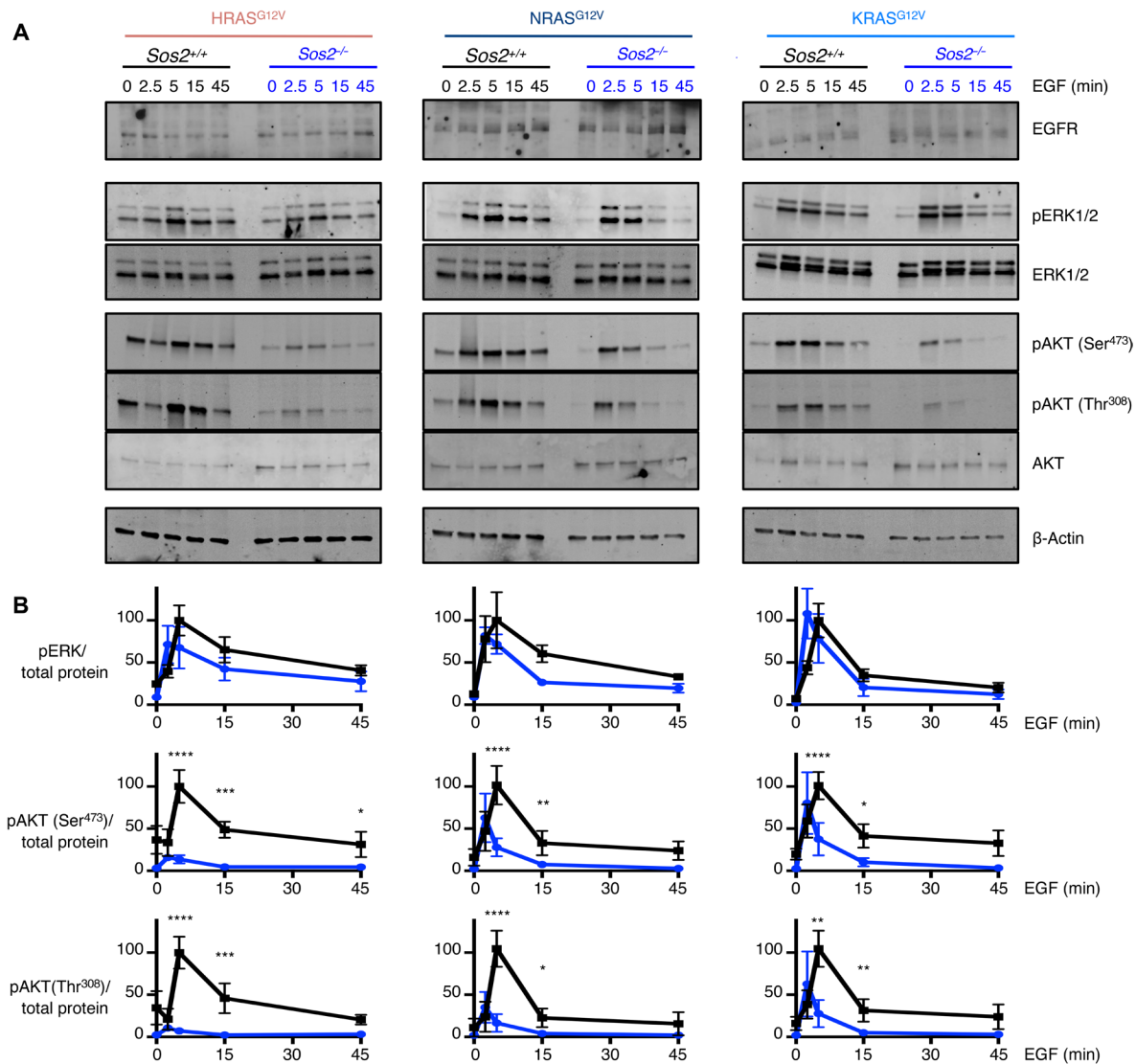


Fig. 4. SOS2 mediates RTK-dependent AKT phosphorylation in cells expressing mutant RAS. *Sos2*^{+/+} and *Sos2*^{-/-} MEFs expressing the indicated mutant RAS isoforms were placed in serum-free media overnight and then stimulated with EGF (100 μg/ml) for the indicated times. (A) WCLs were analyzed by multiplex Western blotting for pERK1/2, ERK1/2, pAKT (Ser⁴⁷³), pAKT (Thr³⁰⁸), AKT, and β-actin on a LI-COR Odyssey machine. Blots are representative of three independent experiments. (B) Quantification of pERK1/2, pAKT (Ser⁴⁷³), and pAKT (Thr³⁰⁸) abundance versus a weighted average of total proteins (ERK1/2, AKT, and β-actin). Data are means ± SD from three independent experiments. **P* < 0.05, ***P* < 0.01, ****P* < 0.001, *****P* < 0.0001 by ANOVA using the Tukey's method to correct for multiple comparisons.

SOS2 in RAS isoform-driven transformation because the reduction in AKT phosphorylation was similar in cells expressing each of the mutant RAS isoforms.

Mutant RAS isoforms show a differential requirement for PI3K for transformation

To reconcile the hierarchical effect of *Sos2* deletion on mutant RAS-dependent transformation with the equivalent decrease in RTK-stimulated AKT phosphorylation, we examined whether MEFs expressing each mutant RAS isoform showed differential sensitivity to PI3K/AKT or Raf/MEK/ERK effector pathway inhibition. Because our initial observation showed that *Sos2* deletion altered transformation but not proliferation, we assessed effector pathway inhibition under both anchorage-dependent and anchorage-independent (transforming) conditions. *Sos2*^{+/+} MEFs expressing HRAS^{G12V}, NRAS^{G12V}, or KRAS^{G12V} were seeded on cell culture-treated (anchorage-dependent)

and ultra-low attachment (anchorage-independent) 96-well plates and treated with increasing doses of the PI3K inhibitor LY294002 (Fig. 5A), the AKT inhibitor AZD5363 (Fig. 5B), or the MEK inhibitor trametinib (Fig. 5C). We confirmed that these inhibitors blocked signaling downstream of their intended target by comparing the phosphorylation of downstream targets in treated and untreated MEFs (fig. S4). We then assessed two measurements of drug potency: the median inhibitory concentration (IC₅₀), which measures the drug concentration at half-maximal inhibition, and the area under the viability curve (AUC), which takes into account both the potency and total amount of growth inhibition by a given compound. Cells expressing the different mutant RAS isoforms did not show any differences in their responses to PI3K, AKT, or MEK inhibition under anchorage-dependent growth conditions (Fig. 5, A to C, left). These data suggest that mutant HRAS-, NRAS-, and KRAS-driven anchorage-dependent proliferation depends on these RAS effector pathways to a similar extent.

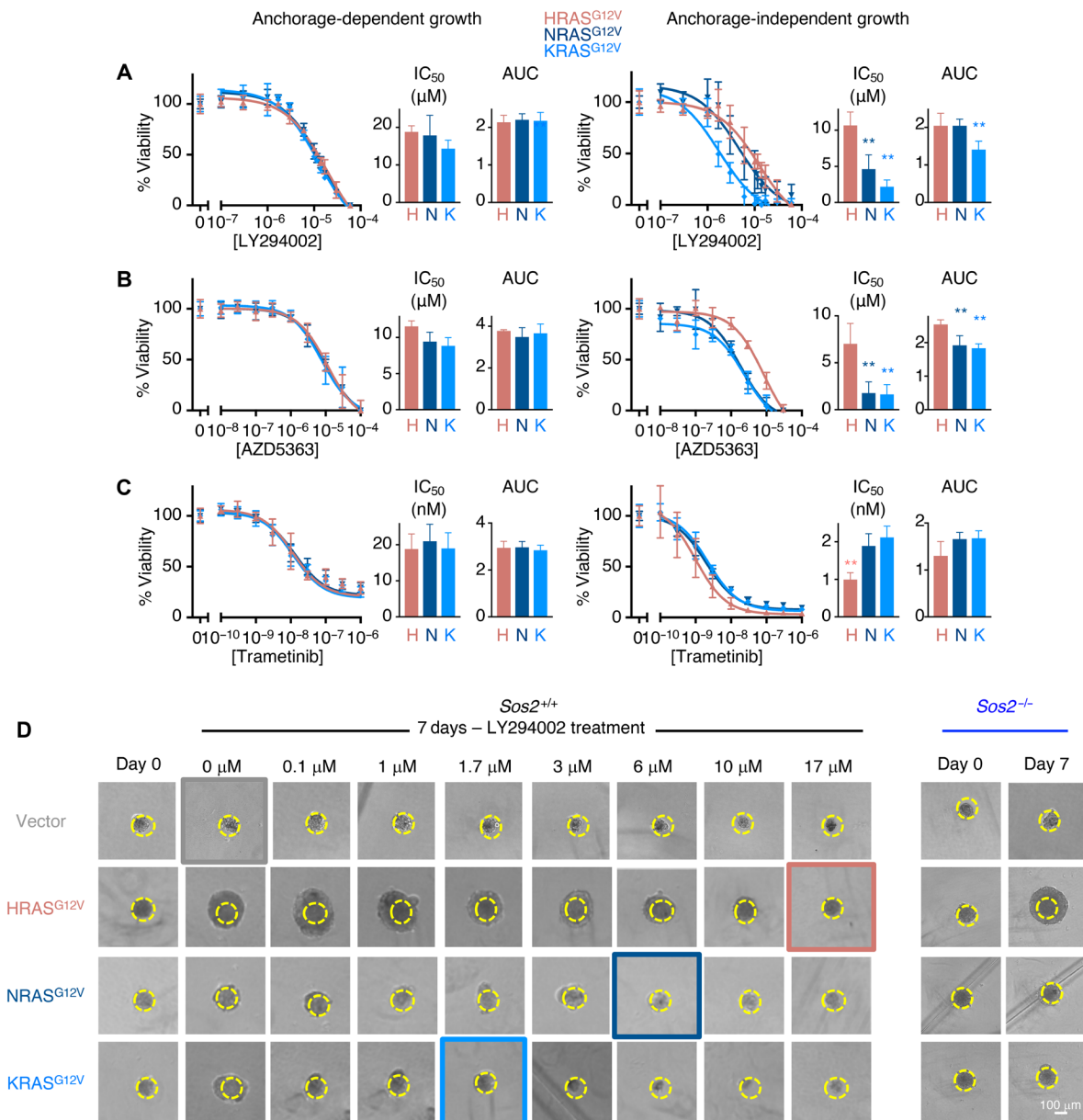


Fig. 5. Mutant RAS isoforms show a hierarchical requirement for PI3K signaling to drive transformation in MEFs. (A to C) *Sos2*^{+/+} MEFs expressing the indicated mutant RAS isoforms were seeded onto either tissue culture–treated 96-well plates to assess anchorage-dependent growth or low-attachment 96-well plates to assess anchorage-independent growth. Cells were treated with the indicated concentrations of (A) the PI3K inhibitor LY294002, (B) the AKT inhibitor AZD5363, or (C) the MEK1/2 inhibitor trametinib for 4 days, and cell number was assessed. IC₅₀ values and AUC measurements are shown. Data are means ± SD from four independent experiments, presented relative to vehicle-treated controls. ***P* < 0.01 versus HRAS^{G12V}. HRAS^{G12V} (salmon triangles), NRAS^{G12V} (dark blue inverted triangles), and KRAS^{G12V} (light blue diamonds) by ANOVA using the Tukey’s method to correct for multiple comparisons. (D) *Sos2*^{+/+} MEFs expressing the indicated mutant RAS isoform were seeded in low-attachment 96-well round-bottomed plates and treated with the indicated concentrations of the PI3K inhibitor LY294002 to assess the effects of PI3K inhibition on RAS-induced cancer spheroid formation (left). *Sos2*^{-/-} MEFs expressing the indicated mutant RAS isoforms were seeded in parallel and left untreated for comparison (right). Images of spheroids were taken 16 hours after plating (day 0) and again 7 days later, and are representative of three independent experiments. Scale bar, 100 μm. The outlined image for each cell line represents the LY294002 concentration where cancer spheroid size did not increase relative to day 0. Images are representative of three independent experiments. See fig. S4 for inhibition of downstream protein phosphorylation by specific inhibitors, and fig. S5 for quantification of spheroid growth between *Sos2*^{+/+} and *Sos2*^{-/-} MEFs expressing mutant RAS.

In contrast to the equivalent effects of effector pathway inhibition on mutant RAS-driven anchorage-dependent growth, RAS-expressing cells showed a hierarchical requirement for PI3K (Fig. 5A, right) to promote anchorage-independent growth, mirroring the requirement for SOS2, with KRAS ≥ NRAS > HRAS. When mutant RAS-expressing

MEFs were treated with increasing concentrations of LY294002, anchorage-independent proliferation was inhibited at lower drug concentrations in KRAS^{G12V}-expressing MEFs compared to HRAS^{G12V}-expressing MEFs, with a significant shift in the dose response curve to lower drug concentrations, resulting in significant decrease in the

AUC and a fivefold decrease in the IC_{50} for LY294002 (Fig. 5A). Furthermore, NRAS^{G12V}-expressing MEFs show an intermediate phenotype between MEFs expressing the other two RAS family members. NRAS^{G12V}-expressing MEFs showed a twofold decrease in the IC_{50} for LY294002 but no difference in the AUC compared to HRAS^{G12V}-expressing MEFs.

To confirm that these differences were due to inhibition of the PI3K/AKT pathway and not off-target effects of LY294002, RAS^{G12V}-expressing MEFs were treated with the AKT inhibitor AZD5363 (Fig. 5B). Similar to what was observed for PI3K inhibition, RAS isoform-expressing MEFs showed a differential requirement for AKT to promote anchorage-independent growth, with KRAS = NRAS > HRAS. Here again, KRAS^{G12V}-expressing MEFs showed a decrease in the AUC and a fivefold decrease in the IC_{50} for the AKT inhibitor AZD5363 compared to HRAS^{G12V}-expressing MEFs. However, unlike the intermediate phenotype the NRAS^{G12V}-expressing cells showed for PI3K inhibition, NRAS^{G12V}-expressing MEFs were as sensitive to AKT inhibition as KRAS^{G12V}-expressing cells.

In contrast to the increased sensitivity of KRAS^{G12V}-expressing cells to PI3K/AKT inhibition, treatment of mutant RAS-expressing MEFs with the MEK inhibitor trametinib revealed that HRAS^{G12V}-expressing MEFs were more sensitive to MEK inhibition compared to either NRAS^{G12V}- or KRAS^{G12V}-expressing MEFs. HRAS^{G12V}-expressing MEFs showed a twofold decrease in the IC_{50} for trametinib compared to NRAS^{G12V}- and KRAS^{G12V}-expressing MEFs. These data suggest that mutant HRAS may have a slightly increased reliance on Raf/MEK/ERK signaling to drive transformation compared to mutant NRAS- or KRAS-expressing cells (Fig. 5C).

To further examine the role of PI3K in mutant RAS isoform-driven transformation, we assessed cancer spheroid formation in *Sos2*^{+/+} MEFs expressing HRAS^{G12V}, NRAS^{G12V}, or KRAS^{G12V} treated with increasing doses of LY294002 (Fig. 5D). Cells were seeded in 96-well ultra-low attachment round-bottomed plates and imaged 16 hours after plating (day 0) and again 7 days later. In untreated cells, spheroid size increased in all RAS^{G12V}-expressing MEFs over the 7-day period but not in vector controls (Fig. 5D), indicating the RAS^{G12V} can induce cancer spheroid growth in MEFs. Mutant RAS-dependent spheroid growth showed the same hierarchical dependence on SOS2 that had been observed in other transformation assays (Fig. 5D, right, and fig. S5). Furthermore, when we assessed the effects of LY294002 treatment on cancer spheroid growth in *Sos2*^{+/+} MEFs, we observed a similar hierarchical requirement for PI3K signaling to the one observed in the anchorage-independent proliferation assay, with KRAS > NRAS > HRAS. The LY294002 concentration that inhibited spheroid growth for each mutant RAS isoform corresponded to the IC_{50} value that we observed for inhibiting anchorage-independent proliferation. These data further support the existence of a hierarchical requirement for PI3K signaling to promote RAS-driven transformation that correlates with the requirement for SOS2 expression.

Activated PI3K rescues KRAS-driven transformation in *Sos2*^{-/-} MEFs

The data presented up to this point suggest that RTK-SOS2-dependent PI3K signaling critically mediates mutant KRAS-induced transformation in MEFs. To determine whether restoring PI3K/AKT signaling is sufficient to restore mutant KRAS-dependent transformation in *Sos2*^{-/-} MEFs, we expressed an activated form of the p110 α catalytic subunit (p110 α ^{H1047R}) at near-endogenous levels, alone or in com-

bination with KRAS^{G12V}, in *Sos2*^{+/+} and *Sos2*^{-/-} MEFs (Fig. 6A). We then assessed transformation using focus-forming assays (Fig. 6, B and C) and by assessing morphologic transformation (fig. S6). Expression of activated p110 α ^{H1047R} alone modestly transformed *Sos2*^{+/+} MEFs, as previously reported (29). This p110 α ^{H1047R}-driven transformation was unaffected by *Sos2* deletion (Fig. 6B), suggesting that PI3K is downstream of, or parallel to, SOS2 in these cells. KRAS^{G12V} robustly transformed immortalized *Sos2*^{+/+} MEFs (Fig. 6B), and this transformation was further enhanced by combining p110 α ^{H1047R} with KRAS^{G12V} (Fig. 6, B and C), confirming previous reports of synergic transformation between KRAS^{G12V} and either p110 α (30) or AKT (31). As shown previously, KRAS^{G12V} was unable to transform *Sos2*^{-/-} MEFs alone (Figs. 1 and 6, B and C). In contrast, combined p110 α ^{H1047R} and KRAS^{G12V} expression robustly transformed *Sos2*^{-/-} MEFs similar to the transformation observed in *Sos2*^{+/+} MEFs (Fig. 6B). These data suggest that constitutively activated PI3K can substitute for SOS2 to promote KRAS-driven transformation.

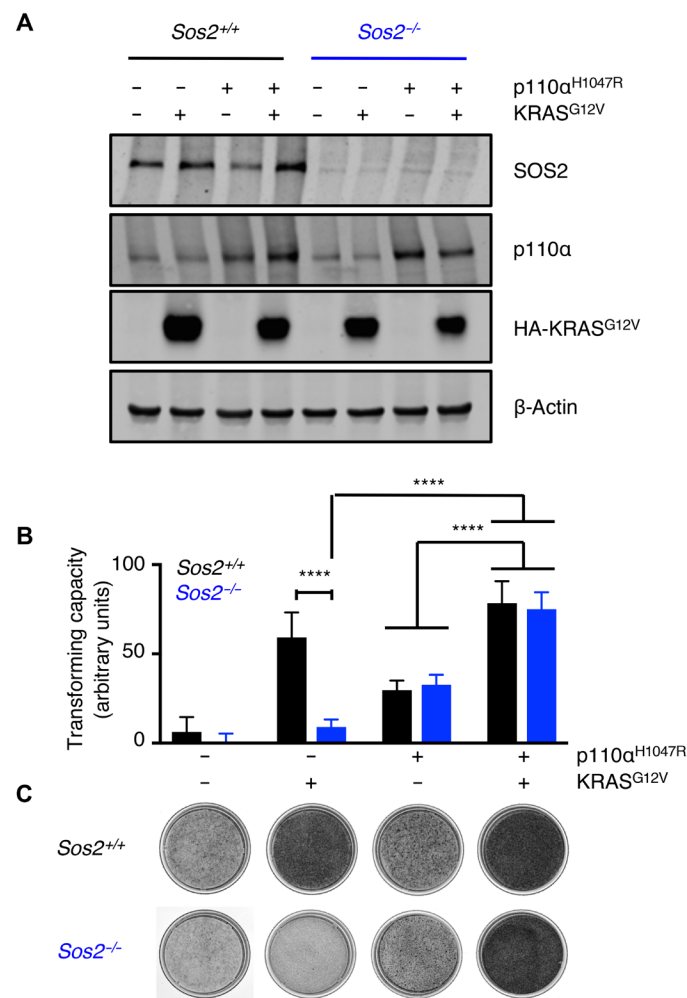


Fig. 6. Activated PI3K (p110 α) cooperates with mutant KRAS to transform *Sos2*^{-/-} MEFs. (A) *Sos2*^{+/+} and *Sos2*^{-/-} MEFs were transduced with lentiviruses expressing KRAS^{G12V} \pm p110 α ^{H1047R}. WCLs were analyzed by Western blotting with antibodies specific for SOS2, p110 α , HA (KRAS^{G12V}), or β -actin. Blots are representative of three independent experiments. (B and C) *Sos2*^{+/+} and *Sos2*^{-/-} MEFs expressing KRAS^{G12V} \pm p110 α ^{H1047R} were assessed for loss of contact inhibition by focus-forming assay (stained dishes below, quantified above). Images are representative from three independent experiments. See fig. S6 for 10 \times images of cells from (B).

SOS2 promotes transformation of KRAS mutant tumor cells

We next tested whether the requirement of *Sos2* for mutant *KRAS*-driven transformation in MEFs could be replicated in *KRAS* mutant human tumor cells. Because transformation assays typically assess growth for 2 to 4 weeks, we used clustered regularly interspaced short palindromic repeats (CRISPR)/CRISPR-associated protein 9 (Cas9) to delete *SOS2* rather than using a transient small interfering RNA approach. We cloned several candidate single-guide RNAs (sgRNAs) that were previously used to target *SOS2* in a genome-wide CRISPR/Cas9 screen (32) into the lentiCRISPRv2 vector, which allows for simultaneous expression of the sgRNA and Cas9 (33). Lentiviruses were then produced from these constructs and used to evaluate the efficiency of *SOS2* deletion by each sgRNA in 293T cells. We found seven different sgRNAs that deleted *SOS2* in >80% of 293T cells (fig. S7). Three of these sgRNAs that target nonoverlapping regions of *SOS2* (#1, #9, and #16) were selected and used to examine the role of *SOS2* in transformation in *KRAS*^{G12V} mutant YAPC pancreatic cancer cells.

YAPC cells were infected with either a nontargeting (NT) sgRNA, an sgRNA targeting *KRAS*, or one of three sgRNAs targeting *SOS2* (#1, #9, or #16). The resulting cells then underwent selection for 10 days after infection to allow for CRISPR/Cas9-mediated gene deletion. The effect of *SOS2* deletion was examined in pooled cultures to avoid any effects of clonal selection. *KRAS* sgRNA expression reduced *KRAS* abundance by >95%, and each *SOS2* sgRNA reduced *SOS2* protein abundance by >80% compared to NT controls, indicating that *SOS2* had been deleted in at least 80% of cells (Fig. 7A). *KRAS* deletion blocked anchorage-independent growth of YAPC pancreatic cancer cells, confirming the *KRAS* dependence of this cell line. Each of the three *SOS2* sgRNAs reduced the number of anchorage-independent colonies by >70%, and the colonies that did form were generally smaller than the colonies in NT controls, indicating a reversion from the transformed phenotype. These data suggest that *SOS2* critically mediated full mutant *KRAS*-driven oncogenic transformation in *KRAS* mutant pancreatic cancer cells.

To test whether the requirement for *SOS2* to promote mutant *KRAS*-driven transformation might hold true in a *KRAS* mutant tumor cell line from another anatomical site, we assessed whether *SOS2* mediated transformation in *KRAS*^{G12C} mutant H358 lung cancer cells. These cells have been used to show the specificity of covalent *KRAS*^{G12C}-specific inhibitors and are highly dependent on *KRAS* signaling for proliferation and transformation (34). Similar to what we observed in YAPC cells, *KRAS* deletion inhibited cancer spheroid growth in H358 lung cancer cells (Fig. 7B). Furthermore, deletion of *SOS2* using two different sgRNAs blocked spheroid growth to a similar extent as deleting *KRAS* itself. These data suggest that *SOS2* is an important modulator of mutant *KRAS*-driven transformation in human tumor cells from multiple anatomic sites.

To determine whether the mechanism of *SOS2* dependence in *KRAS* mutant cancer cells may be similar to the mechanism in mutant *KRAS*-expressing MEFs, we tested the activation of the Raf/MEK/ERK and the PI3K/AKT pathways in YAPC pancreatic cancer cells after deletion of *SOS2*. Deletion of *SOS2* with any of the three sgRNAs (#1, #9, or #16) had no effect on ERK phosphorylation in actively cycling cells (Fig. 7C) or after EGF stimulation (Fig. 7D). These data suggest that, similar to our assessment of the role of *Sos2* in MEFs, deletion of *SOS2* alone does not alter EGF-dependent ERK phosphorylation in *KRAS* mutant cancer cells. In contrast, deletion of *SOS2* significantly decreased AKT phosphorylation in actively cycling cells (Fig. 7C) and after EGF stimulation (Fig. 7D). These

data indicate that, similar to the mechanism that we had observed in *Sos2*^{-/-} MEFs, *SOS2* mediates RTK-stimulated AKT phosphorylation in a *KRAS* mutant cancer cell line.

With the notable exception of covalent *KRAS*^{G12C}-specific inhibitors (34), single-agent approaches have been broadly unsuccessful in limiting growth of *KRAS* mutant tumors. In contrast, combined inhibition of *KRAS* effector pathways, such as the combination of MEK and PI3K inhibitors, has shown marked benefit over single agents alone (35–37). Given that *SOS2* deletion reduced AKT phosphorylation in *KRAS* mutant pancreatic cancer cells (Fig. 7, C and D), we hypothesized that *SOS2* deletion might act similarly to a PI3K inhibitor and synergize with MEK inhibition to block proliferation and transformation in *KRAS* mutant tumor cells. To understand whether *SOS2* deletion would alter the response of *KRAS* mutant tumor cells to effector pathway inhibition, we assessed the combination of either *SOS2* or *KRAS* deletion with either the PI3K inhibitor buparlisib (Fig. 8, A and B) or the MEK inhibitor trametinib (Fig. 8, C and D) under both anchorage-dependent and anchorage-independent (transforming) conditions. We confirmed that these inhibitors blocked signaling downstream of their intended target by comparing the phosphorylation of downstream targets in treated and untreated YAPC cells (fig. S8). Deletion of *SOS2* had no significant effect on the IC₅₀ of buparlisib in either YAPC cells (Fig. 8A) or H358 cells (Fig. 8B), consistent with the idea that *SOS2* deletion and buparlisib treatment both act on the PI3K pathway. Although *SOS2* deletion did significantly decrease the AUC, especially under anchorage-independent conditions (Fig. 8, A and B, right), this was due to a decrease in the overall cell number after 5 days in culture in *SOS2*-deleted cells (see untreated cells). In contrast, we observed a synergistic effect between *SOS2* deletion and trametinib treatment in inhibiting both anchorage-dependent and anchorage-independent growth. *SOS2* deletion reduced the IC₅₀ for trametinib by two- to threefold under anchorage-dependent conditions (Fig. 8, C and D, left) and by fivefold under anchorage-independent growth conditions (Fig. 8, C and D, right).

To determine whether *SOS2* deletion had a similar effect to PI3K inhibition in synergizing with trametinib to block *KRAS* mutant tumor cell growth, YAPC or H358 cells expressing an NT sgRNA were treated with 100 nM buparlisib, a dose just below the threshold for inhibiting cell growth with buparlisib alone (Fig. 8, A and B), in combination with trametinib. The effects of combining trametinib with low-dose buparlisib were similar to the effects of combining trametinib with *SOS2* deletion (Fig. 8, C and D, compare red and blue curves). These data indicate that, similar to PI3K inhibition, *SOS2* deletion can synergize with MEK inhibition to block proliferation and transformation of *KRAS* mutant tumor cell lines. Furthermore, these data suggest that *SOS2* is an unappreciated therapeutic target for the treatment of *KRAS* mutant tumors.

DISCUSSION

Driver mutations in the RAS family of GTPases occur in ~30% of human tumors (38, 39). Although these tumors were originally thought to proliferate independently of upstream signaling inputs, we now know that signaling through wild-type RAS cooperates with mutant RAS to activate downstream effector pathways and drive oncogenic proliferation (12). Here, we demonstrated that there is a hierarchical requirement for the RASGEF *SOS2* in RAS isoform-driven transformation, with *KRAS* > *NRAS* > *HRAS*. This requirement for *SOS2* parallels a differential requirement for PI3K signaling to maintain the

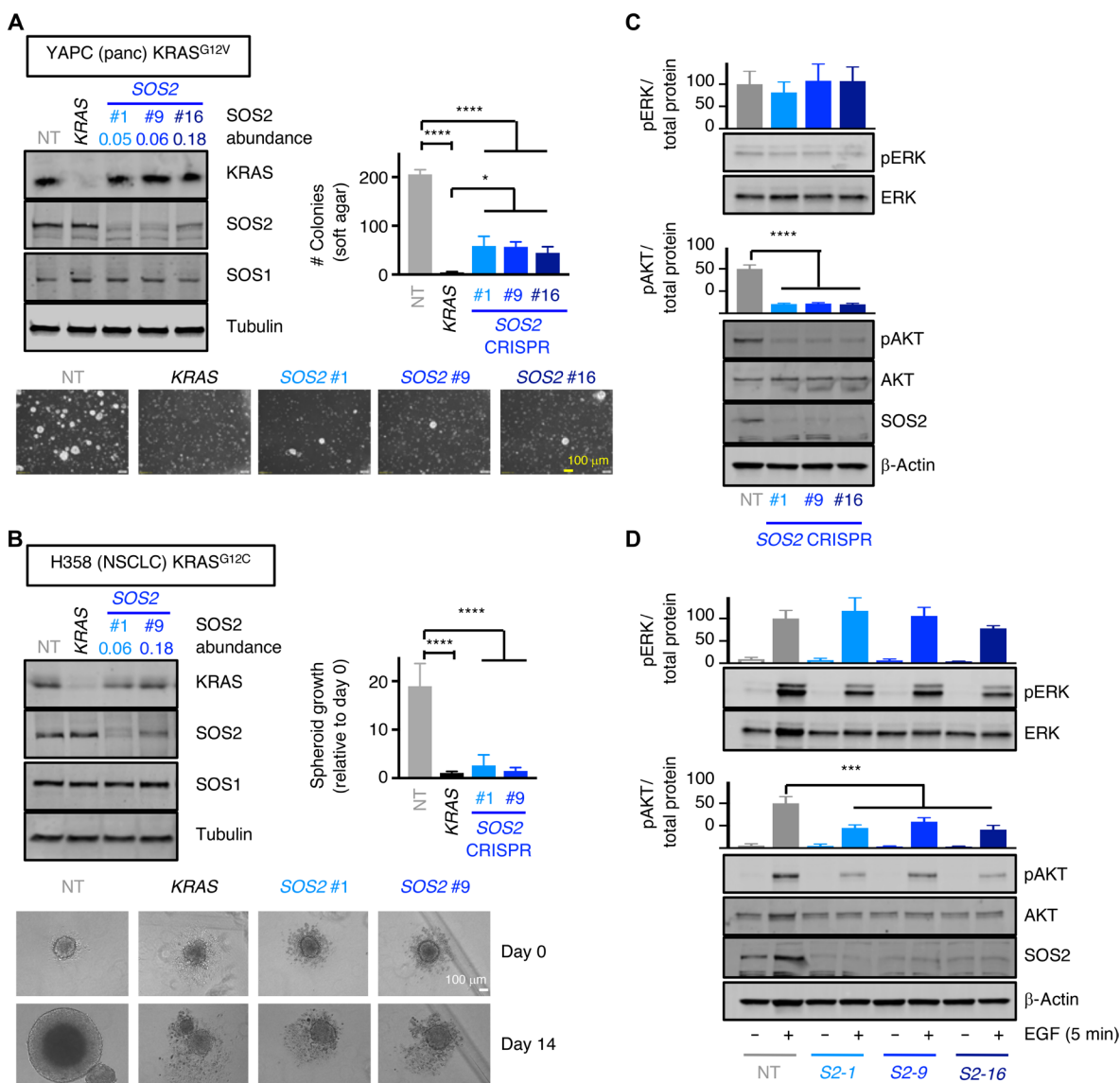


Fig. 7. SOS2 critically mediates transformation of KRAS mutant tumor cells. (A) YAPC pancreatic cancer cells (harboring a KRAS^{G12V} mutation) were transduced with lentiviruses expressing Cas9 and an NT sgRNA, an sgRNA targeting KRAS, or one of three different sgRNAs targeting SOS2. WCLs were analyzed by Western blotting with antibodies specific for KRAS, SOS2, SOS1, or tubulin (left). The SOS2 protein abundance relative to the NT sgRNA control in the SOS2 CRISPR samples is given. Cells were assessed for colony growth in soft agar 21 days after plating to assess anchorage-independent growth (right), and 10 \times images showing transformed colonies growing in soft agar were taken (bottom). Scale bars, 100 μ m. (B) H358 non-small cell lung cancer (NSCLC) cells (harboring a KRAS^{G12C} mutation) were transduced with lentiviruses expressing Cas9 and an NT sgRNA, an sgRNA targeting KRAS, or one of two different sgRNAs targeting SOS2. WCLs were analyzed by Western blotting with antibodies specific for KRAS, SOS2, SOS1, or tubulin (left). The SOS2 protein abundance relative to the NT sgRNA control in the SOS2 CRISPR samples is given. Cells were assessed for anchorage-independent growth by cancer spheroid assay (right) and cancer spheroid growth 16 hours after plating (day 0) or 14 days later (10 \times images below). Scale bar, 100 μ m. (C and D) YAPC cells from (A) were either lysed actively cycling (C) or starved overnight and then stimulated overnight and then stimulated with EGF (100 ng/ml) for 5 min (D) before lysis. Multiplex Western blotting for pERK1/2, ERK1/2, pAKT (Ser⁴⁷³), AKT, and β -actin was performed on a LI-COR Odyssey machine. Quantification of pERK1/2 and pAKT (Ser⁴⁷³) abundance versus a weighted average of total proteins (ERK1/2, AKT, and β -actin) is shown above. All data are means \pm SD from three independent experiments; all blots and images are representative of three independent experiments. * P < 0.05, *** P < 0.001, **** P < 0.0001 by ANOVA using the Tukey's method to correct for multiple comparisons.

RAS-transformed phenotype and, in doing so, reveals a previously unappreciated RTK-SOS2-RAS-PI3K signaling pathway that supplements mutant KRAS-driven PI3K activation to drive oncogenic transformation.

Wild-type RAS isoforms cooperate with oncogenic RAS mutants to promote downstream effector activation and cell proliferation, but the mechanistic underpinnings of this cooperation are unclear. Previous reports have shown two interconnected mechanisms of

wild-type RAS activation in cells expressing mutant RAS, and both mechanisms involve RASGEFs as the direct activators of wild-type RAS, which raises the question: Which mechanism underlies RASGEF-dependent wild-type RAS activation in the context of mutant RAS? In the first model, RTK-dependent activation of wild-type RAS acts in an interconnected network with basal mutant RAS^{GTP} signaling to promote G2 checkpoint integrity (40) and proliferation of RAS mutant cancer cells (11). Our data support this model and suggest

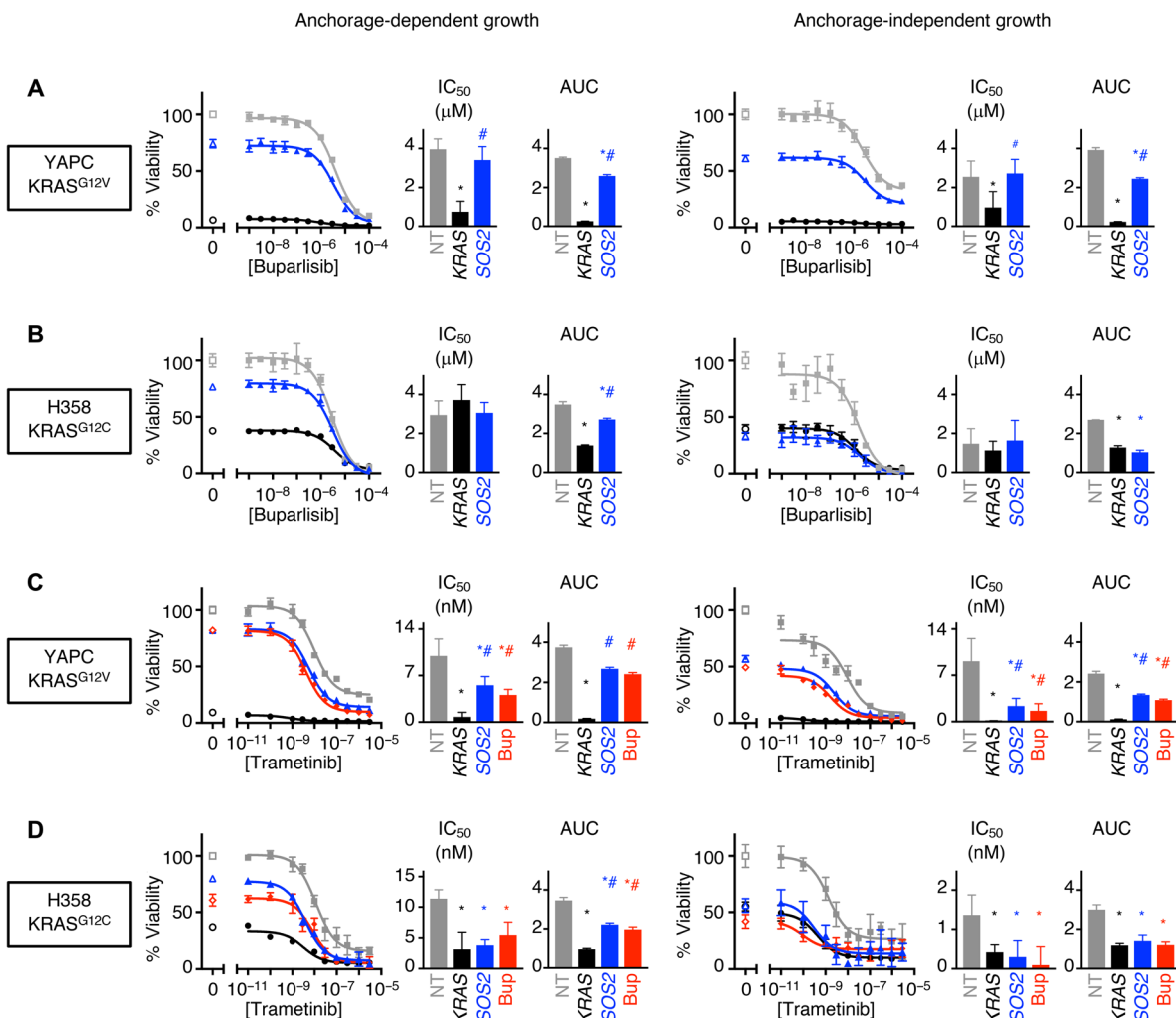


Fig. 8. SOS2 deletion synergizes with MEK inhibition to revert the transformed phenotype of KRAS mutant tumor cells. (A to D) KRAS mutant YAPC pancreatic cancer cells (A and C) or H358 NSCLC cells (B and D) transduced with lentiviruses expressing Cas9 and an NT sgRNA, a sgRNA targeting KRAS, or an sgRNAs targeting SOS2 were seeded onto either tissue culture–treated 96-well plates to assess anchorage-dependent growth (left) or low-attachment 96-well plates to assess anchorage-independent growth (right). Cells were treated with the indicated concentrations of the PI3K inhibitor buparlisib (A and B) or the MEK1/2 inhibitor trametinib (C and D) for 5 days, and cell number was assessed. For (C) and (D), NT cells were treated either with the indicated concentration of trametinib alone or in the presence of buparlisib (100 ng/ml). IC₅₀ values and AUC measurements are shown. Data are means ± SD from three independent experiments, presented relative to vehicle-treated controls. **P* < 0.05 (versus NT), #*P* < 0.05 [versus KRAS deletion; NT (gray squares), KRAS-deleted (black circles), SOS2-deleted (blue triangles), NT + buparlisib (100 ng/ml) (red diamonds)] by ANOVA using the Tukey's method to correct for multiple comparisons.

that, in cells expressing mutant RAS, robust RTK-dependent PI3K/AKT signaling is dependent on SOS2 and that this RTK-SOS2-AKT signaling is important for transformation driven by KRAS but not by HRAS. Alternatively, for the second model, crystallographic studies of the RAS-SOS1 complexes show that SOS1 contains an allosteric RAS^{GTP} binding site, distinct from its catalytic RASGEF domain, that relieves SOS1 autoinhibition when occupied (16). This allosteric binding of RAS^{GTP} to SOS1 sets up a potential RAS^{GTP}-SOS1-RAS positive feedback loop that can potentiate EGF signaling to downstream effectors (41), support prolonged T cell and B cell receptor-dependent RAS/ERK activation (28, 42), and promote proliferation of KRAS mutant cancer cells (17). Our data show that wild-type RAS is activated in cells expressing mutant KRAS independently of RTK signaling and SOS2 expression, suggesting that a SOS1-dependent positive feedback loop plays a role in basal mutant RAS signaling to wild-type RAS.

Mutant HRAS, NRAS, and KRAS can all interact with the major RAS effectors PI3K and Raf, thereby constitutively activating the PI3K/AKT and Raf/MEK/ERK pathways. Why, then, would wild-type RAS signaling be required to cooperate with mutant RAS to promote proliferation and oncogenic transformation? Although RAS isoforms interact with the same signaling effectors, they activate these effectors to different extents (43, 44), which are not correlated with a difference in binding affinity (45) or isoform stability (46). A potential role, then, for wild-type RAS is to activate the effector pathways that mutant RAS does not strongly activate, making the cellular outcome a product of signaling by wild-type and mutant RAS (13).

Our study revealed that cells expressing mutant RAS isoforms exhibit differential sensitivity to effector inhibition in maintaining their transformed phenotype. In cells expressing mutant NRAS or KRAS, isoforms that are relatively poor activators of PI3K (31, 43, 44),

anchorage-independent growth was inhibited at lower doses of either the PI3K or the AKT inhibitor than the dose required to inhibit growth in cells expressing mutant HRAS (Fig. 5). The converse was also true: In cells expressing mutant HRAS, an isoform that poorly activates Raf (31, 43, 44), anchorage-independent growth was inhibited at lower doses of the MEK inhibitor than the dose required in cells expressing mutant NRAS or KRAS. These data suggest that cells expressing mutant RAS isoforms are particularly sensitive to inhibition of RAS effectors that the oncogene poorly activates. Notably, this differential sensitivity to effector pathway inhibition was only observed in anchorage-independent growth assays, not in assays assessing anchorage-dependent (2D) growth, demonstrating that the appropriate culture system must be used to tease apart these drug sensitivities. Multiple studies have shown that *KRAS* mutant cancer cell lines show a range of *KRAS* dependency for survival in 2D culture (47–51). However, many of these “*KRAS*-independent” cell lines still require *KRAS* for anchorage-independent growth (52–55). This finding suggests that we must take care in choosing the appropriate culture system to identify and test novel therapeutic targets to treat *RAS* mutant tumors and that anchorage-independent 3D growth screens should be used to supplement current 2D screening efforts (53).

The differential sensitivity of 3D cultured cells expressing mutant *RAS* isoforms to PI3K inhibition may help explain why *Sos2* deletion showed a differential effect on *RAS* isoform-driven transformation. We found that cells ectopically expressing any of the three mutant *RAS* isoforms were reliant on *Sos2* expression for maximal RTK-stimulated AKT phosphorylation (Fig. 4). However, because *KRAS*-expressing MEFs were more reliant on PI3K signaling to promote transformation (Fig. 5), the reduced PI3K signaling that we observed upon *Sos2* deletion may have been sufficient to block transformation by ectopically expressed mutant *KRAS*, but not *HRAS* (Fig. 1); alternatively, the relatively high amount of ectopic *HRAS* in these experiments may mask any role that *SOS2*/PI3K signaling plays in *HRAS*-driven transformation. Extending these findings into *KRAS* mutant cancer cell lines, we found that *KRAS* mutant cancer cells were reliant on RTK-*SOS2*-AKT signaling pathway to supplement basal PI3K activation and promote oncogenic transformation, consistent with our MEF studies. However, whether *SOS2* deletion differentially affects the transformed phenotype in *HRAS* versus *KRAS* mutated cancer cell lines remains to be tested.

The importance of PI3K signaling in *KRAS* tumors is widely established (56), as is the efficacy of combined MEK and PI3K inhibition in blocking *KRAS*-driven transformation, because inhibiting either pathway alone leads to activation of the other through relief of negative feedback (36, 57). Unfortunately, this treatment strategy has a high risk of toxicity, because the Raf/MEK/ERK and PI3K/AKT pathways are both key players in normal cell function. To avoid this toxicity, many studies have investigated the efficacy of blocking the PI3K pathway indirectly or searched for other pathways that synergize with MEK or PI3K inhibition (35, 37). For example, Ebi *et al.* (35) show that PI3K signaling is downstream of insulin-like growth factor receptor (IGFR) in *KRAS* mutant colon cancer cells and that IGFR inhibition can indirectly block PI3K signaling. They also show that this indirect block coordinates with MEK inhibition to limit mutant tumor growth and promote apoptosis to the same extent as direct PI3K inhibition. When we compared the effects of *SOS2* deletion in combination with either PI3K inhibition (buparlisib) or MEK inhibition (trametinib) (Fig. 8), we found that *SOS2* deletion had the same effect as an intermediate dose of buparlisib when combined

with trametinib. Coupled with the decrease in AKT phosphorylation that we observed in the absence of *SOS2*, our findings point to *SOS2* as an alternate target to indirectly block RTK-mediated PI3K signaling in *KRAS* mutant cancer cells. *SOS2* inhibition may be more broadly applicable than inhibition of individual RTKs, because different RTKs are predominant in different types of *KRAS* mutant cancers. In addition, *SOS2* is not necessary for development and normal adult cell function in the presence of *SOS1* (58–60), so inhibition of *SOS2* may have lower toxicity in nontumor cells than inhibition of PI3K or RTKs. Overall, our findings point to a more complex role of RASGEF signaling in discriminating the effects of *RAS* isoform-driven transformation than has previously been appreciated and underline the importance of comprehensive examinations of the role of each RASGEF in *RAS*-driven transformation across *RAS* isoforms. In addition, our findings suggest that *SOS2* inhibition should be pursued as a potential therapeutic option in *KRAS*-driven cancers.

MATERIALS AND METHODS

Cell culture

MEFs were maintained in Dulbecco's modified Eagle's medium, and YAPC and H358 cells were maintained in RPMI 1640, each supplemented with 10% fetal bovine serum, 2 mM L-glutamine, 0.1 mM minimum essential medium with nonessential amino acids, and 1% penicillin-streptomycin.

RAS construct cloning

HA-*HRAS*^{G12V} was polymerase chain reaction (PCR)-amplified from pBabePuro and cloned into Eco RI/Bam HI-digested pCDH-CMV-MCS-EF1-Puro (System Biosciences) using the GeneArt Seamless Cloning and Assembly Kit (Invitrogen). To clone in wild-type *KRAS* and wild-type *NRAS*, pCDH-HA-*HRAS*^{G12V} was digested with Bam HI/Not I to remove *HRAS* but maintain the HA tag, and wild-type *KRAS* or *NRAS* was PCR-amplified and cloned using GeneArt. Oncogenic point mutations [*NRAS*^{G12V} and *KRAS* (G12C, G12D, G12V, G13D, Q61L, and Q61R)] were then introduced by site-directed mutagenesis. To produce V5-tagged wild-type *HRAS*, Hs.*HRAS* (attL1-attL2 clone R999-E10) was cloned into pDest-658 (blestidicin-resistant, attR4-attR2 lentiviral vector), along with the CMV51p promoter (C453-04, attL4-attL5 sites) and the V5 tag (C514-E24, attR5-attR1 sites) by Gateway Cloning (Invitrogen). All gateway clones were gifts from D. Esposito (RAS Project, Frederick National Laboratory).

SOS2 construct cloning

Hs.*SOS2* (attL1-attL2 clone 777-E319) was cloned into pDest-658 (blestidicin-resistant, attR4-attR2 lentiviral vector) along with one of five different promoters (attL4-attR1 clones C413-E15 EF1p, C413-E33 UbCp, C413-E21 PGKp, C413-E34 mCMVp, and C413-E26 SV40p) by Gateway Cloning (Invitrogen). All gateway clones were gifts from D. Esposito (RAS Project, Frederick National Laboratory). *SOS2* W727E and F927A point mutations were introduced by site-directed mutagenesis of the wild-type *SOS2* entry clone.

Production of recombinant lentiviruses

Lentiviruses were produced by cotransfecting MISSION lentiviral packaging mix (Sigma) into 293T cells using calcium phosphate. Ecotropic p110 α retrovirus was produced by calcium phosphate transfection of pBabePuro (p110 α ^{H1047}) into Phoenix-Eco cells. At 48 to 72 hours after transfection, viral supernatants were collected

and filtered. Viral supernatants were then either stored at -80°C or used immediately to infect cells in combination with polybrene at $8\ \mu\text{g}/\text{ml}$. MEFs were selected with puromycin ($4\ \mu\text{g}/\text{ml}$; Invitrogen) or blasticidin ($2.5\ \mu\text{g}/\text{ml}$; Invitrogen). YAPC and H358 cells were selected with puromycin ($6\ \mu\text{g}/\text{ml}$).

Generation of cell lines

Nonimmortalized MEFs were generated from 13.5-day *Sos1^{ff}* and *Sos1^{ff}Sos2^{-/-}* embryos using a previously described protocol. Cells were maintained in culture according to a 3T6 protocol until immortalized populations of cells emerged (21, 22).

Cell lysis and Western blot analysis

For WCL analysis, cells were either lysed while cycling or starved overnight before stimulation with EGF ($100\ \text{ng}/\text{ml}$) for the indicated times. Cells were then lysed in radioimmunoprecipitation assay buffer [1% NP-40, 0.1% SDS, 0.1% Na-deoxycholate, 10% glycerol, 0.137 M NaCl, 20 mM tris (pH 8.0), protease and phosphatase inhibitor cocktails (Biotool)] for 20 min at 4°C and spun at 10,000 rpm for 10 min. Clarified lysates were boiled in SDS sample buffer containing 100 mM dithiothreitol (DTT) for 10 min before Western blotting. Proteins were resolved by SDS-polyacrylamide gel electrophoresis and transferred to nitrocellulose or polyvinylidene difluoride membranes. Western blots were developed by multiplex Western blotting using anti-SOS1 (1:500; sc-256, Santa Cruz Biotechnology), anti-SOS2 (1:500; sc-258, Santa Cruz Biotechnology), anti- β -actin (1:5000; AC-15, Sigma), anti-HA (1:1000; sc-805, Santa Cruz Biotechnology), anti-RAS (1:500; 3965, Cell Signaling Technology), anti-V5 (1:1000; 13202, Cell Signaling Technology), anti-pERK1/2 (1:2000; 4370, Cell Signaling Technology), anti-ERK1/2 (1:1000; 4696, Cell Signaling Technology), anti-pAKT [Thr³⁰⁸ (1:1000; 2965, Cell Signaling Technology) or Ser⁴⁷³ (1:1000; 4060, Cell Signaling Technology)], anti-AKT (1:1000; 2920, Cell Signaling Technology), anti-p110 α PI3K (1:1000; 4249, Cell Signaling Technology), anti-KRAS (1:200; WH0003845M1, Sigma), or anti-tubulin (1:1000; Cell Signaling Technology) primary antibodies. Anti-mouse and anti-rabbit secondary antibodies conjugated to IRDye680 or IRDye800 (1:10,000; LI-COR Biosciences) were used to probe primary antibodies. Protein bands were detected and quantified by Western blotting with the Odyssey System (LI-COR Biosciences). For quantification of SOS2 abundance, samples were normalized to either β -actin or tubulin. For quantification of pERK and pAKT, samples were normalized to a weighted average of β -actin, total ERK1/2, and total AKT (61).

RAS pulldowns

For RAS PDs, cells were lysed on ice for 20 min in RAS-PD lysis buffer [1% NP-40, 50 mM tris (pH 7.5), 200 mM NaCl, 2.5 mM MgCl_2 , protease and phosphatase inhibitor cocktails (Biotool)] and spun at 10,000 rpm for 10 min. GST-RBD bound to glutathione-Sepharose beads was either prepared as previously described (62) or purchased (Millipore) and used to isolate RAS-GTP from lysates by rotating incubation for 1 hour at 4°C . Samples were washed four times in RAS-PD lysis buffer. All samples were boiled in 2 \times SDS sample buffer containing 100 mM DTT for 10 min before Western blotting.

Proliferation studies

For growth assays, 2×10^3 cells were seeded on cell culture-coated 96-well plates (CELLTREAT). Cells were lysed with CellTiter-Glo 2.0 Reagent (Promega), and luminescence was read using a GloMax

Discover plate reader (Promega). Cell number was assessed 2 hours after plating to account for any discrepancies in plating and then every 24 hours for 5 days. Data were analyzed as an increase in luminescence over day 0. For inhibitor studies, 4×10^3 cells were seeded on cell culture-treated 96-well plates (CELLTREAT) to assess anchorage-dependent growth and on ultra-low attachment 96-well plates (Corning Costar #3474) to assess anchorage-independent growth (52). On day 4, cells were assessed using CellTiter-Glo 2.0 Reagent as described. Inhibitor data are plotted as a scaled dose-response curve for each cell line $(E_{\text{drug}} - E_{\text{max}})/(E_0 - E_{\text{max}})$, where E_{drug} is the effect of the drug at a given concentration, E_{max} is the maximal effect of the drug, and E_0 is the effect seen in the dimethyl sulfoxide (DMSO) control (63, 64). Data were analyzed, and IC_{50} and AUC values were calculated using Prism 7.

Transformation studies

Cells were seeded in 0.32% Noble agar at 2×10^4 cells per 35-mm dish to assess anchorage-independent growth (soft agar assays) or at 10^5 cells per 6-cm dish to assess the loss of contact inhibition (focus-forming assays). Soft agar colonies were counted 21 to 28 days after seeding; 10 \times images of focus-forming assays were taken 14 to 21 days after seeding, and then the dishes were stained with 1% bromophenol blue (65). Stained focus-forming assay dishes were scanned on the Bio-Rad ChemiDoc Imaging System, and cell density was quantified using Image Lab software. For spheroid growth in ultra-low attachment 96-well round-bottom plates (Corning Costar #7007), cells were seeded at 500 cells per well with the indicated concentration of inhibitor or DMSO. Images were taken 16 hours after plating to assess initial spheroid size and then 7 or 14 days later to assess the effects of drug treatment on spheroid growth (66). Spheroid size was quantified using ImageJ. In parallel plates, cell number was assessed on days 0, 7, and 14 using CellTiter-Glo 2.0 reagent.

sgRNA studies

An NT sgRNA, a KRAS-targeted sgRNA, and the 16 potential SOS2-targeted sgRNAs were each cloned into pLentiCRISPRv2, as previously described (33). sgRNA sequences are given in table S1. Lentiviruses were produced as described above. Forty-eight hours after infection, cells were selected for 4 days in puromycin at $6\ \mu\text{g}/\text{ml}$ and then shifted into puromycin at $3\ \mu\text{g}/\text{ml}$ for an additional 6 days. Ten days after selection, cells were analyzed for KRAS and SOS2 expression and plated for signaling and transformation assays.

Statistical analysis

Statistical analysis was performed using GraphPad Prism 7 software. Data were analyzed by ANOVA using the Tukey's method to correct for multiple comparisons. IC_{50} and AUC values from dose-response studies were obtained from nonlinear regression analysis [log(inhibitor) versus response (three parameters)]. Data are represented as means \pm SD from a minimum of three independent experiments. Data were considered significant at $P < 0.05$ and are indicated by * $P < 0.05$, ** $P < 0.01$, *** $P < 0.001$, and **** $P < 0.0001$.

SUPPLEMENTARY MATERIALS

www.sciencesignaling.org/cgi/content/full/11/546/eaar8371/DC1

Fig. S1. *Sos2* deletion does not alter cellular proliferation in MEFs expressing oncogenic RAS.

Fig. S2. *Sos2* deletion does not alter GTP loading of mutant KRAS in MEFs.

Fig. S3. Introduction of SOS2 into *Sos2^{-/-}* MEFs using different promoters to drive *Sos2* expression.

Fig. S4. Inhibitor treatment of MEFs expressing mutant HRAS, NRAS, and KRAS blocks their corresponding downstream signaling pathways.

Fig. S5. There is a hierarchical requirement for SOS2 in promoting mutant RAS-driven cancer spheroid growth.

Fig. S6. Activated PI3K (p110 α) cooperates with KRAS^{G12V} to transform *Sos2*^{-/-} MEFs.

Fig. S7. Deletion of SOS2 using CRISPR/Cas9.

Fig. S8. Inhibitor treatment of YAPC cells blocks their corresponding downstream signaling pathways.

Table S1. sgRNA sequences used in this study.

REFERENCES AND NOTES

- T. G. Bivona, S. E. Quatela, B. O. Bodemann, I. M. Ahearn, M. J. Soskis, A. Mor, J. Miura, H. H. Wiener, L. Wright, S. G. Saba, D. Yim, A. Fein, I. Pérez de Castro, C. Li, C. B. Thompson, A. D. Cox, M. R. Phillips, PKC regulates a farnesyl-electrostatic switch on K-Ras that promotes its association with Bcl-XL on mitochondria and induces apoptosis. *Mol. Cell* **21**, 481–493 (2006).
- L. S. Steelman, R. A. Franklin, S. L. Abrams, W. Chappell, C. R. Kempf, J. Bäsecke, F. Stivala, M. Donia, P. Fagone, F. Nicoletti, M. Libra, P. Ruvolo, V. Ruvolo, C. Evangelisti, A. M. Martelli, J. A. McCubrey, Roles of the Ras/Raf/MEK/ERK pathway in leukemia therapy. *Leukemia* **25**, 1080–1094 (2011).
- R. Diaz, D. Ahn, L. Lopez-Barcos, M. Malumbres, I. Perez de Castro, J. Lue, N. Ferrer-Miralles, R. Mangues, J. Tsong, R. Garcia, R. Perez-Soler, A. Pellicer, The N-ras proto-oncogene can suppress the malignant phenotype in the presence or absence of its oncogene. *Cancer Res.* **62**, 4514–4518 (2002).
- J. Li, Z. Zhang, Z. Dai, C. Plass, C. Morrison, Y. Wang, J. S. Wiest, M. W. Anderson, M. You, LOH of chromosome 12p correlates with *Kras2* mutation in non-small cell lung cancer. *Oncogene* **22**, 1243–1246 (2003).
- I. Guerrero, A. Villasante, V. Corces, A. Pellicer, Loss of the normal N-ras allele in a mouse thymic lymphoma induced by a chemical carcinogen. *Proc. Natl. Acad. Sci. U.S.A.* **82**, 7810–7814 (1985).
- R. Diaz, J. Lue, J. Mathews, A. Yoon, D. Ahn, A. Garcia-España, P. Leonardi, M. P. Vargas, A. Pellicer, Inhibition of Ras oncogenic activity by Ras protooncogenes. *Int. J. Cancer* **113**, 241–248 (2005).
- M. D. To, J. Perez-Losada, J.-H. Mao, J. Hsu, T. Jacks, A. Balmain, A functional switch from lung cancer resistance to susceptibility at the *Pas1* locus in *Kras2*^{LA2} mice. *Nat. Genet.* **38**, 926–930 (2006).
- Z. Zhang, Y. Wang, H. G. Vikis, L. Johnson, G. Liu, J. Li, M. W. Anderson, R. C. Sills, H. L. Hong, T. R. Devereux, T. Jacks, K.-L. Guan, M. You, Wildtype *Kras2* can inhibit lung carcinogenesis in mice. *Nat. Genet.* **29**, 25–33 (2001).
- P. P. Fotiadou, C. Takahashi, H. N. Rajabi, M. E. Ewen, Wild-type NRas and KRas perform distinct functions during transformation. *Mol. Cell. Biol.* **27**, 6742–6755 (2007).
- K.-H. Lim, B. B. Anclire, D. F. Kashatus, C. M. Counter, Tumour maintenance is mediated by eNOS. *Nature* **452**, 646–649 (2008).
- A. Young, D. Lou, F. McCormick, Oncogenic and wild-type Ras play divergent roles in the regulation of mitogen-activated protein kinase signaling. *Cancer Discov.* **3**, 112–123 (2013).
- B. Zhou, C. J. Der, A. D. Cox, The role of wild type RAS isoforms in cancer. *Semin. Cell Dev. Biol.* **58**, 60–69 (2016).
- E. Castellano, E. Santos, Functional specificity of ras isoforms: So similar but so different. *Genes Cancer* **2**, 216–231 (2011).
- M. Hamilton, A. Wolfman, Oncogenic Ha-Ras-dependent mitogen-activated protein kinase activity requires signaling through the epidermal growth factor receptor. *J. Biol. Chem.* **273**, 28155–28162 (1998).
- C. Bentley, S. S. Jurinka, N. M. Kljavin, S. Vartanian, S. R. Ramani, L. C. Gonzalez, K. Yu, Z. Modrusan, P. Du, R. Bourgon, R. M. Neve, D. Stokoe, A requirement for wild-type Ras isoforms in mutant KRas-driven signalling and transformation. *Biochem. J.* **452**, 313–320 (2013).
- S. M. Margarit, H. Sondermann, B. E. Hall, B. Nagar, A. Hoelz, M. Pirruccello, D. Bar-Sagi, J. Kuriyan, Structural evidence for feedback activation by Ras.GTP of the Ras-specific nucleotide exchange factor SOS. *Cell* **112**, 685–695 (2003).
- H.-H. Jeng, L. J. Taylor, D. Bar-Sagi, Sos-mediated cross-activation of wild-type Ras by oncogenic Ras is essential for tumorigenesis. *Nat. Commun.* **3**, 1168 (2012).
- P. Licerias-Boillos, R. García-Navas, A. Ginel-Picardo, B. Anta, M. Pérez-Andrés, C. Lillo, C. Gómez, D. Jimeno, A. Fernández-Medarde, F. C. Baltanás, E. Santos, *Sos1* disruption impairs cellular proliferation and viability through an increase in mitochondrial oxidative stress in primary MEFs. *Oncogene* **35**, 6389–6402 (2016).
- H. Land, L. F. Parada, R. A. Weinberg, Tumorigenic conversion of primary embryo fibroblasts requires at least two cooperating oncogenes. *Nature* **304**, 596–602 (1983).
- R. F. Newbold, R. W. Overall, Fibroblast immortality is a prerequisite for transformation by EJ c-Ha-ras oncogene. *Nature* **304**, 648–651 (1983).
- G. J. Todaro, H. Green, Quantitative studies of the growth of mouse embryo cells in culture and their development into established lines. *J. Cell Biol.* **17**, 299–313 (1963).
- R. L. Kortum, H. J. Johnson, D. L. Costanzo, D. J. Volle, G. L. Razidlo, A. M. Fusello, A. S. Shaw, R. E. Lewis, The molecular scaffold kinase suppressor of Ras 1 is a modifier of Ras^{V12}-induced and replicative senescence. *Mol. Cell. Biol.* **26**, 2202–2214 (2006).
- A. D. Cox, S. W. Fesik, A. C. Kimmelman, J. Luo, C. J. Der, Drugging the undruggable RAS: Mission possible? *Nat. Rev. Drug Discov.* **13**, 828–851 (2014).
- K. M. Haigis, KRAS alleles: The devil is in the detail. *Trends Cancer* **3**, 686–697 (2017).
- J. C. Hunter, A. Manandhar, M. A. Carrasco, D. Gurbani, S. Gondi, K. D. Westover, Biochemical and structural analysis of common cancer-associated KRAS mutations. *Mol. Cancer Res.* **13**, 1325–1335 (2015).
- T. Shi, M. Niepel, J. E. McDermott, Y. Gao, C. D. Nicora, W. B. Chrisler, L. M. Markillie, V. A. Petyuk, R. D. Smith, K. D. Rodland, P. K. Sorger, W.-J. Qian, H. S. Wiley, Conservation of protein abundance patterns reveals the regulatory architecture of the EGFR-MAPK pathway. *Sci. Signal.* **9**, rs6 (2016).
- B. E. Hall, S. S. Yang, P. A. Boriack-Sjodin, J. Kuriyan, D. Bar-Sagi, Structure-based mutagenesis reveals distinct functions for Ras switch 1 and switch 2 in Sos-catalyzed guanine nucleotide exchange. *J. Biol. Chem.* **276**, 27629–27637 (2001).
- J. P. Roose, M. Mollenauer, M. Ho, T. Kurosaki, A. Weiss, Unusual interplay of two types of Ras activators, RasGRP and SOS, establishes sensitive and robust Ras activation in lymphocytes. *Mol. Cell. Biol.* **27**, 2732–2745 (2007).
- A. Denley, S. Kang, U. Karst, P. K. Vogt, Oncogenic signaling of class I PI3K isoforms. *Oncogene* **27**, 2561–2574 (2008).
- K. Oda, J. Okada, L. Timmerman, P. Rodriguez-Viciano, D. Stokoe, K. Shoji, Y. Taketani, H. Kuramoto, Z. A. Knight, K. M. Shokat, F. McCormick, PIK3CA cooperates with other phosphatidylinositol 3'-kinase pathway mutations to effect oncogenic transformation. *Cancer Res.* **68**, 8127–8136 (2008).
- W. Li, T. Zhu, K.-L. Guan, Transformation potential of Ras isoforms correlates with activation of phosphatidylinositol 3-kinase but not ERK. *J. Biol. Chem.* **279**, 37398–37406 (2004).
- D. M. Munoz, P. J. Cassiani, L. Li, E. Billy, J. M. Korn, M. D. Jones, J. Golji, D. A. Ruddy, K. Yu, G. McAllister, A. DeWeck, D. Abramowski, J. Wan, M. D. Shirley, S. Y. Neshat, D. Rakiec, R. de Beaumont, O. Weber, A. Kauffmann, E. R. McDonald III, N. Keen, F. Hofmann, W. R. Sellers, T. Schmelzle, F. Stegmeier, M. R. Schlabach, CRISPR screens provide a comprehensive assessment of cancer vulnerabilities but generate false-positive hits for highly amplified genomic regions. *Cancer Discov.* **6**, 900–913 (2016).
- N. E. Sanjana, O. Shalem, F. Zhang, Improved vectors and genome-wide libraries for CRISPR screening. *Nat. Methods* **11**, 783–784 (2014).
- M. R. Janes, J. Zhang, L.-S. Li, R. Hansen, U. Peters, X. Guo, Y. Chen, A. Babbar, S. J. Firdaus, L. Darjania, J. Feng, J. H. Chen, S. Li, S. Li, Y. O. Long, C. Thach, Y. Liu, A. Zariw, T. Ely, J. M. Kucharski, L. V. Kessler, T. Wu, K. Yu, Y. Wang, Y. Yao, X. Deng, P. P. Zarrinkar, D. Brehmer, D. Dhanak, M. V. Lorenzi, D. Hu-Lowe, M. P. Patricelli, P. Ren, Y. Liu, Targeting KRAS mutant cancers with a covalent G12C-specific inhibitor. *Cell* **172**, 578–589.e17 (2018).
- H. Ebi, R. B. Corcoran, A. Singh, Z. Chen, Y. Song, E. Lifshits, D. P. Ryan, J. A. Meyerhardt, C. Benes, J. Settleman, K.-K. Wong, L. C. Cantley, J. A. Engelman, Receptor tyrosine kinases exert dominant control over PI3K signaling in human KRAS mutant colorectal cancers. *J. Clin. Invest.* **121**, 4311–4321 (2011).
- J. A. Engelman, L. Chen, X. Tan, K. Crosby, A. R. Guimaraes, R. Upadhyay, M. Maira, K. McNamara, S. A. Perera, Y. Song, L. R. Chirieac, R. Kaur, A. Lightbown, J. Simendinger, T. Li, R. F. Padera, C. Garcia-Echeverria, R. Weissleder, U. Mahmood, L. C. Cantley, K.-K. Wong, Effective use of PI3K and MEK inhibitors to treat mutant *Kras* G12D and *PIK3CA* H1047R murine lung cancers. *Nat. Med.* **14**, 1351–1356 (2008).
- G. R. Anderson, P. S. Winter, K. H. Lin, D. P. Nussbaum, M. Cakir, E. M. Stein, R. S. Soderquist, L. Crawford, J. C. Leeds, R. Newcomb, P. Stepp, C. Yip, S. E. Wardell, J. P. Tingley, M. Ali, M. Xu, M. Ryan, S. J. McCall, A. J. McRee, C. M. Counter, C. J. Der, K. C. Wood, A landscape of therapeutic cooperativity in KRAS mutant cancers reveals principles for controlling tumor evolution. *Cell Rep.* **20**, 999–1015 (2017).
- I. A. Prior, P. D. Lewis, C. Mattos, A comprehensive survey of Ras mutations in cancer. *Cancer Res.* **72**, 2457–2467 (2012).
- A. G. Stephen, D. Esposito, R. K. Bagni, F. McCormick, Dragging Ras back in the ring. *Cancer Cell* **25**, 272–281 (2014).
- E. Grabocka, Y. Pylayeva-Gupta, M. J. Jones, V. Lubkov, E. Yemanaberhan, L. Taylor, H. H. Jeng, D. Bar-Sagi, Wild-type H- and N-Ras promote mutant K-Ras-driven tumorigenesis by modulating the DNA damage response. *Cancer Cell* **25**, 243–256 (2014).
- S. Boykevich, C. Zhao, H. Sondermann, P. Philippidou, S. Halegoua, J. Kuriyan, D. Bar-Sagi, Regulation of ras signaling dynamics by Sos-mediated positive feedback. *Curr. Biol.* **16**, 2173–2179 (2006).

42. J. Das, M. Ho, J. Zikherman, C. Govern, M. Yang, A. Weiss, A. K. Chakraborty, J. P. Roose, Digital signaling and hysteresis characterize Ras activation in lymphoid cells. *Cell* **136**, 337–351 (2009).
43. J. Yan, S. Roy, A. Apolloni, A. Lane, J. F. Hancock, Ras isoforms vary in their ability to activate Raf-1 and phosphoinositide 3-kinase. *J. Biol. Chem.* **273**, 24052–24056 (1998).
44. J. K. Voice, R. L. Klemke, A. Le, J. H. Jackson, Four human Ras homologs differ in their abilities to activate Raf-1, induce transformation, and stimulate cell motility. *J. Biol. Chem.* **274**, 17164–17170 (1999).
45. C. Herrmann, G. A. Martin, A. Wittinghofer, Quantitative analysis of the complex between p21^{ras} and the Ras-binding domain of the human Raf-1 protein kinase. *J. Biol. Chem.* **270**, 2901–2905 (1995).
46. J. Maher, D. A. Baker, M. Manning, N. J. Dibb, I. A. Roberts, Evidence for cell-specific differences in transformation by N-, H- and K-Ras. *Oncogene* **11**, 1639–1647 (1995).
47. O. A. Balbin, J. R. Prensner, A. Sahu, A. Yocum, S. Shankar, R. Malik, D. Fermin, S. M. Dhanasekaran, B. Chandler, D. Thomas, D. G. Beer, X. Cao, A. I. Nesvizhskii, A. M. Chinnaiyan, Reconstructing targetable pathways in lung cancer by integrating diverse omics data. *Nat. Commun.* **4**, 2617 (2013).
48. A. Singh, P. Greninger, D. Rhodes, L. Koopman, S. Violette, N. Bardeesy, J. Settleman, A gene expression signature associated with “K-Ras addiction” reveals regulators of EMT and tumor cell survival. *Cancer Cell* **15**, 489–500 (2009).
49. A. Singh, M. F. Sweeney, M. Yu, A. Burger, P. Greninger, C. Benes, D. A. Haber, J. Settleman, TAK1 inhibition promotes apoptosis in KRAS-dependent colon cancers. *Cell* **148**, 639–650 (2012).
50. C. Scholl, S. Frohling, I. F. Dunn, A. C. Schinzel, D. A. Barbie, S. Y. Kim, S. J. Silver, P. Tamayo, R. C. Wadlow, S. Ramaswamy, K. Dohner, L. Bullinger, P. Sandy, J. S. Boehm, D. E. Root, T. Jacks, W. C. Hahn, D. G. Gilliland, Synthetic lethal interaction between oncogenic KRAS dependency and STK33 suppression in human cancer cells. *Cell* **137**, 821–834 (2009).
51. S. Lamba, M. Russo, C. Sun, L. Lazzari, C. Cancelliere, W. Grenrum, C. Liefstink, R. Bernards, F. Di Nicolantonio, A. Bardelli, RAF suppression synergizes with MEK inhibition in KRAS mutant cancer cells. *Cell Rep.* **8**, 1475–1483 (2014).
52. S. Fujita-Sato, J. Galeas, M. Truitt, C. Pitt, A. Urisman, S. Bandyopadhyay, D. Ruggero, F. McCormick, Enhanced MET translation and signaling sustains K-Ras-driven proliferation under anchorage-independent growth conditions. *Cancer Res.* **75**, 2851–2862 (2015).
53. A. Rotem, A. Janzer, B. Izar, Z. Ji, J. G. Doench, L. A. Garraway, K. Struhl, Alternative to the soft-agar assay that permits high-throughput drug and genetic screens for cellular transformation. *Proc. Natl. Acad. Sci. U.S.A.* **112**, 5708–5713 (2015).
54. Z. Zhang, G. Jiang, F. Yang, J. Wang, Knockdown of mutant K-ras expression by adenovirus-mediated siRNA inhibits the in vitro and in vivo growth of lung cancer cells. *Cancer Biol. Ther.* **5**, 1481–1486 (2006).
55. F. McCormick, KRAS as a therapeutic target. *Clin. Cancer Res.* **21**, 1797–1801 (2015).
56. A. A. Krygowska, E. Castellano, PI3K: A crucial piece in the RAS signaling puzzle. *Cold Spring Harb. Perspect. Med.* **8**, a031450 (2018).
57. M. L. Sos, S. Fischer, R. Ullrich, M. Peifer, J. M. Heuckmann, M. Koker, S. Heynck, I. Stückrath, J. Weiss, F. Fischer, K. Michel, A. Goel, L. Regales, K. A. Politi, S. Perera, M. Getlik, L. C. Heukamp, S. Ansén, T. Zander, R. Beroukham, H. Kashkar, K. M. Shokat, W. R. Sellers, D. Rauh, C. Orr, K. P. Hoeflich, L. Friedman, K.-K. Wong, W. Pao, R. K. Thomas, Identifying genotype-dependent efficacy of single and combined PI3K- and MAPK-pathway inhibition in cancer. *Proc. Natl. Acad. Sci. U.S.A.* **106**, 18351–18356 (2009).
58. L. M. Esteban, A. Fernández-Medarde, E. López, K. Yienger, C. Guerrero, J. M. Ward, L. Tassarollo, E. Santos, Ras-guanine nucleotide exchange factor sos2 is dispensable for mouse growth and development. *Mol. Cell. Biol.* **20**, 6410–6413 (2000).
59. F. C. Baltanás, M. Pérez-Andrés, A. Ginel-Picardo, D. Diaz, D. Jimeno, P. Licerias-Boillos, R. L. Kortum, L. E. Samelson, A. Orfao, E. Santos, Functional redundancy of Sos1 and Sos2 for lymphopoiesis and organismal homeostasis and survival. *Mol. Cell. Biol.* **33**, 4562–4578 (2013).
60. R. L. Kortum, C. L. Sommers, J. M. Pinski, C. P. Alexander, R. K. Merrill, W. Li, P. E. Love, L. E. Samelson, Deconstructing Ras signaling in the thymus. *Mol. Cell. Biol.* **32**, 2748–2759 (2012).
61. K. A. Janes, An analysis of critical factors for quantitative immunoblotting. *Sci. Signal.* **8**, rs2 (2015).
62. A. F. Castro, J. F. Rebhun, L. A. Quilliam, Measuring Ras-family GTP levels in vivo—Running hot and cold. *Methods* **37**, 190–196 (2005).
63. R. P. Stephenson, A modification of receptor theory. *Br. J. Pharmacol. Chemother.* **11**, 379–393 (1956).
64. L. A. Harris, P. L. Frick, S. P. Garbett, K. N. Hardeman, B. B. Paudel, C. F. Lopez, V. Quaranta, D. R. Tyson, An unbiased metric of antiproliferative drug effect in vitro. *Nat. Methods* **13**, 497–500 (2016).
65. R. L. Kortum, R. E. Lewis, The molecular scaffold KSR1 regulates the proliferative and oncogenic potential of cells. *Mol. Cell. Biol.* **24**, 4407–4416 (2004).
66. M. Vinci, S. Gowan, F. Boxall, L. Patterson, M. Zimmermann, W. Court, C. Lomas, M. Mendiola, D. Hardisson, S. A. Eccles, Advances in establishment and analysis of three-dimensional tumor spheroid-based functional assays for target validation and drug evaluation. *BMC Biol.* **10**, 29 (2012).

Acknowledgments: We thank A. L. Snow and R. Day for helpful discussions throughout the project and R. Day for critical reading of the manuscript. We thank D. Esposito for Gateway Cloning reagents and helpful discussions throughout the project. **Funding:** This work was supported by start-up funds from the Uniformed Services University of the Health Sciences (to R.L.K.), a grant from the Congressionally Directed Medical Research Program (LC160222; to R.L.K.), and the Intramural Research Program of the Center for Cancer Research, National Cancer Institute, NIH (to J.L. and D.K.M.). **Author contributions:** E.S. and R.L.K. designed the experiments, analyzed the data, and performed most of the experiments. N.E.S. performed spheroid assays and assisted in inhibitor treatment assays. C.W. assisted with focus-forming and soft agar assays. D.H.K. assisted with CRISPR/Cas9 experiments. I.A.V. and E.L. performed promoter analysis for SOS2 protein abundance. E.M.T. and D.K.M. generated the mutant RAS constructs and prepared recombinant lentiviruses. J.L. helped with design of CRISPR experiments and generated the KRAS CRISPR sequences. E.S. and R.L.K. wrote the manuscript, and D.K.M. edited the manuscript. **Competing interests:** The authors declare that they have no competing interests. **Data and materials availability:** All data needed to evaluate the conclusions in the paper are present in the paper or the Supplementary Materials. Raw data and materials are available upon request from R.L.K.

Submitted 21 December 2017

Accepted 13 August 2018

Published 4 September 2018

10.1126/scisignal.aar8371

Citation: E. Sheffels, N. E. Sealover, C. Wang, D. H. Kim, I. A. Vazirani, E. Lee, E. M. Terrell, D. K. Morrison, J. Luo, R. L. Kortum, Oncogenic RAS isoforms show a hierarchical requirement for the guanine nucleotide exchange factor SOS2 to mediate cell transformation. *Sci. Signal.* **11**, eaar8371 (2018).

Oncogenic RAS isoforms show a hierarchical requirement for the guanine nucleotide exchange factor SOS2 to mediate cell transformation

Erin Sheffels, Nancy E. Sealover, Chenyue Wang, Do Hyung Kim, Isabella A. Vazirani, Elizabeth Lee, Elizabeth M. Terrell, Deborah K. Morrison, Ji Luo and Robert L. Kortum

Sci. Signal. **11** (546), eaar8371.
DOI: 10.1126/scisignal.aar8371

Finding alternatives to targeting RAS

Many tumors have mutations in the guanosine triphosphatases (GTPases) HRAS, NRAS, or KRAS. Pharmacologically targeting these proteins has so far been elusive; hence, targeting critical members of their signaling pathway(s) may be more successful. Sheffels *et al.* found that the guanine nucleotide exchange factor SOS2, in contrast to its family member SOS1, was dispensable for two-dimensional cell proliferation but mediated oncogenic and stem-like switches in the three-dimensional growth behavior of normal and tumor cells to varying degrees, most critically for cells expressing Gly^{12/13} mutants of KRAS. Further analysis of the differential downstream pathways suggested that SOS2 dependence and RAS mutant type may indicate whether individual inhibitors of the kinase PI3K, AKT, or MEK may be effective against the tumor.

ARTICLE TOOLS

<http://stke.sciencemag.org/content/11/546/eaar8371>

SUPPLEMENTARY MATERIALS

<http://stke.sciencemag.org/content/suppl/2018/08/30/11.546.eaar8371.DC1>

RELATED CONTENT

<http://stke.sciencemag.org/content/sigtrans/10/498/eaao3332.full>
<http://stke.sciencemag.org/content/sigtrans/10/494/eaak9702.full>

REFERENCES

This article cites 66 articles, 29 of which you can access for free
<http://stke.sciencemag.org/content/11/546/eaar8371#BIBL>

PERMISSIONS

<http://www.sciencemag.org/help/reprints-and-permissions>

Use of this article is subject to the [Terms of Service](#)



SOS signaling in RAS-mutated cancers

[Subscribe](#)

June 29, 2020, by Erin Sheffels and Rob Kortum

Rob Kortum earned his Ph.D. with Rob Lewis at the University of Nebraska Medical Center, and trained with both Larry Samelson and Deborah Morrison at NCI. He is an assistant professor of Pharmacology at Uniformed Services University in Bethesda, MD.

Erin Sheffels trained with Dr. Kortum and earned her Ph.D. in May 2020. She plans to do her postdoctoral work with Gina Razidlo at Mayo Clinic.



Rob Kortum, MD, PhD, and Erin Sheffels, PhD

RAS-mutated tumors were originally thought to proliferate independently of upstream signaling inputs, but we now know that receptor tyrosine kinase-dependent activation of both mutant RAS and non-mutated wild-type (WT) RAS plays an important role in modulating downstream effector signaling and driving therapeutic resistance in RAS-mutated cancers. The contributions of wild-type RAS to proliferation and transformation in RAS-mutated cancer cells places renewed interest in upstream signaling molecules, including the RasGEFs SOS1 and 2, as potential therapeutic targets in RAS-mutated cancers.

RAS isoforms have a hierarchy of abilities to activate RAS effectors

Mutant RAS-dependent transformation requires both Raf/MEK/ERK and PI3K/AKT effector pathway activation. However, while HRAS, NRAS, and KRAS can all interact with PI3K and RAF, a series of seminal papers showed that they activate these effectors to different extents, such that there is an inverse relationship in their ability to activate Raf and PI3K: mutant HRAS is a potent activator of PI3K but a poor activator of RAF, and conversely KRAS is a potent activator of Raf but a poor activator of PI3K (1-3). We are beginning to understand the mechanism for the differential activation of RAF proteins. The Morrison laboratory recently showed that BRAF preferentially interacts with KRAS via an interaction between the KRAS(4B) polybasic region and an acidic N-terminal region in BRAF (4). The ability to directly associate with both BRAF and CRAF makes KRAS a more potent activator of the RAF/MEK/ERK cascade. While the precise mechanism for differential PI3K activation between HRAS and KRAS remains unclear, a major contributor seems to be the polybasic stretch in the hypervariable region of KRAS; mutating basic residues in the KRAS(4B) HVR inhibits Raf/MEK/ERK

signaling but enhances PI3K/AKT phosphorylation (5). These differences in activation abilities impact the dependence of *RAS*-mutated cancers on upstream signals. For example, PI3K/AKT pathway activation is dependent on RTK signaling in *KRAS*-mutated colorectal (6) and lung (7) adenocarcinoma cells. A potential role for the WT RAS isoforms is to activate the effector pathways that mutant RAS does not strongly activate, making the cellular outcome a product of signaling by both WT and mutant RAS.

Mutant RAS can activate WT RAS via SOS

Mutant RAS can activate WT RAS independently of RTK input by at least two interdependent mechanisms. First, SOS1 can be allosterically activated by RAS, allowing increased activation of WT RAS. When assessing the crystal structure of SOS1, the Kuryian and Bar-Sagi labs found an allosteric RAS^{GTP} binding pocket distinct from the SOS1 catalytic domain that, when occupied, relieves SOS1 autoinhibition (8). This RAS^{GTP} binding increases SOS1 catalytic activity by up to 500-fold, setting up a RAS^{GTP}-SOS1-WT RAS positive feedback loop that allows for processive localized WT RAS activation at the plasma membrane. Further downstream, PI3K/AKT signaling can phosphorylate eNOS, which can nitrosylate and activate WT HRAS (9). RTK signaling can also activate WT RAS independently from mutant RAS. The McCormick laboratory built on previous work to show that canonical RTK-dependent WT RAS activation supplements basal signaling from mutated RAS to promote proliferation in *RAS*-mutated tumor cell lines, and combined inhibition of WT and mutated RAS is required to induce cell killing (3, 10). These mechanisms are not mutually exclusive and may cooperate in some contexts (11-13).

These models all indicate that SOS plays a role in activating WT RAS in mutant *RAS* cancers. Data from our lab and others suggests that SOS1 and SOS2 may play non-overlapping roles to promote WT RAS activation in *RAS* mutated tumor cells. For SOS1, allosteric signaling and RTK-dependent activation are both important for *KRAS*-mutated cancer cells depending on the cellular context: SOS1 is required for WT HRAS and NRAS activation in an animal model of *KRAS*-induced leukemia (14), mutant *KRAS*-SOS1-WT RAS allosteric signaling promotes growth of *KRAS* mutant pancreatic cancer cell xenografts (15), and both allosteric signaling and EGFR-SOS1 signaling contribute to growth of *KRAS*-mutated colorectal cancer cells (16). In contrast, we found that RTK-SOS2-WT RAS signaling, but not allosteric SOS2 activation, is a critical mediator of PI3K signaling in the context of mutant RAS (17) and protects *KRAS*-mutated cancer cells from anoikis (18).

SOS proteins as therapeutic targets in RAS-mutant cancers

In *KRAS*-mutated cancer cells, single agent MEK inhibitor treatment is ineffective because it relieves ERK-dependent negative feedback signaling, enhancing RTK-SOS-WT RAS signaling to the Raf/MEK/ERK and PI3K/AKT pathways and leading to therapeutic resistance (19-22). Similar relief of negative feedback signaling drives rapid resistance to *KRAS*^{G12C} inhibitors (23, 24). In both cases, this resistance is driven by multiple RTKs. CRISPR screens revealed that both *KRAS*^{G12C} inhibitors (25) and MEK inhibitors (26) require either broad inhibition of proximal RTK signaling or targeting of PI3K/mTOR survival signaling to enhance their efficacy and delay therapeutic resistance. Recent pre-clinical studies showed that co-treatment with allosteric SHP2 inhibitors can overcome both *KRAS*^{G12C} (23, 24) and MEK (27, 28) inhibitor resistance, leading to more durable responses. Furthermore, we

found that *SOS2* deletion inhibited RTK-WT RAS-PI3K signaling and synergized with MEK inhibitors in *KRAS* mutated cell lines (17).

While there are currently no *SOS2*-specific inhibitors, Bayer Pharmaceuticals published a *SOS1* inhibitor suitable for *in vitro* studies (29). Furthermore, Boehringer Ingelheim has developed orally available *SOS1* inhibitors (30) and started recruiting patients with advanced *KRAS*-mutated solid tumors in 2019 for a Phase 1 clinical trial (NCT04111458). *SOS1* inhibition is mechanistically most similar to *SHP2* inhibition (31), suggesting that *SOS1* inhibition could similarly enhance the efficacy of *KRAS*^{G12C}- and MEK-inhibitors. Indeed this appears to be true for combined *SOS1*/MEK inhibition, as preliminary data from Boehringer Ingelheim showed marked cooperativity between *SOS1*- and MEK-inhibition in multiple G12 and G13 *KRAS*-mutated PDX models (30). Furthermore, since *KRAS*^{G12C} allosteric inhibitors can only bind *KRAS*^{GDP}, inhibiting *SOS1* has the potential advantage of directly enhancing the efficacy of *KRAS*^{G12C} inhibitors by increasing the amount of mutant *KRAS*^{G12C} accessible to drug (29), in addition to inhibiting feedback activation of WT RAS. While further studies are required, the possibility of inhibiting *SOS1* has enormous clinical potential as a combination therapy.

WT RAS signaling is an important modifier of *KRAS*-mutated oncogenesis, and inhibition of WT RAS signaling may be required for effective treatment of *KRAS*-mutated cancers. Understanding the mechanisms by which the ubiquitously expressed RasGEFs *SOS1* and *SOS2* promote WT RAS activation is an important step in determining the best ways to limit WT RAS signaling. The ability to pharmacologically manipulate *SOS1/2* signaling may lead to optimized therapeutic combinations that can be used to treat *KRAS*-mutated cancers.

Selected References

1. Voice JK, Klemke RL, Le A, Jackson JH, 1999. **Four human ras homologs differ in their abilities to activate Raf-1, induce transformation, and stimulate cell motility.** J Biol Chem [PubMed Abstract]
2. Yan J, Roy S, Apolloni A, Lane A, Hancock JF, 1998. **Ras isoforms vary in their ability to activate Raf-1 and phosphoinositide 3-kinase.** J Biol Chem [PubMed Abstract]
3. Hamilton M, Wolfman A, 1998. **Oncogenic Ha-Ras-dependent mitogen-activated protein kinase activity requires signaling through the epidermal growth factor receptor.** J Biol Chem [PubMed Abstract]
4. Terrell EM, Durrant DE, Ritt DA, Sealover NE, Sheffels E, Spencer-Smith R, Esposito D, Zhou Y, Hancock JF, Kortum RL, Morrison DK, 2019. **Distinct Binding Preferences between Ras and Raf Family Members and the Impact on Oncogenic Ras Signaling.** Mol Cell [PubMed Abstract]
5. Zhou Y, Prakash P, Liang H, Cho KJ, Gorfe AA, Hancock JF, 2017. **Lipid-Sorting Specificity Encoded in K-Ras Membrane Anchor Regulates Signal Output.** Cell [PubMed Abstract]
6. Ebi H, Corcoran RB, Singh A, Chen Z, Song Y, Lifshits E, Ryan DP, Meyerhardt JA, Benes C, Settleman J, Wong KK, Cantley LC, Engelman JA, 2011. **Receptor tyrosine kinases exert dominant control over PI3K signaling in human *KRAS* mutant colorectal cancers.** J Clin

Invest [\[PubMed Abstract\]](#)

7. Molina-Arcas M, Hancock DC, Sheridan C, Kumar MS, Downward J, 2013. **Coordinate direct input of both KRAS and IGF1 receptor to activation of PI3 kinase in KRAS-mutant lung cancer.** *Cancer Discov* [\[PubMed Abstract\]](#)
8. Margarit SM, Sondermann H, Hall BE, Nagar B, Hoelz A, Pirruccello M, Bar-Sagi D, Kuriyan J, 2003. **Structural evidence for feedback activation by Ras.GTP of the Ras-specific nucleotide exchange factor SOS.** *Cell* [\[PubMed Abstract\]](#)
9. Lim KH, Ancrile BB, Kashatus DF, Counter CM, 2008. **Tumour maintenance is mediated by eNOS.** *Nature* [\[PubMed Abstract\]](#)
10. Young A, Lou D, McCormick F, 2013. **Oncogenic and wild-type Ras play divergent roles in the regulation of mitogen-activated protein kinase signaling.** *Cancer Discov* [\[PubMed Abstract\]](#)
11. Boykevisch S, Zhao C, Sondermann H, Philippidou P, Halegoua S, Kuriyan J, Bar-Sagi D, 2006. **Regulation of ras signaling dynamics by Sos-mediated positive feedback.** *Curr Biol* [\[PubMed Abstract\]](#)
12. Roose JP, Mollenauer M, Ho M, Kurosaki T, Weiss A, 2007. **Unusual interplay of two types of Ras activators, RasGRP and SOS, establishes sensitive and robust Ras activation in lymphocytes.** *Mol Cell* [\[PubMed Abstract\]](#)
13. Das J, Ho M, Zikherman J, Govern C, Yang M, Weiss A, Chakraborty AK, Roose JP, 2009. **Digital signaling and hysteresis characterize ras activation in lymphoid cells.** *Cell* [\[PubMed Abstract\]](#)
14. You X, Kong G, Ranheim EA, Yang D, Zhou Y, Zhang J, 2018. **Unique dependence on Sos1 in KrasG12D -induced leukemogenesis.** *Blood* [\[PubMed Abstract\]](#)
15. Jeng HH, Taylor LJ, Bar-Sagi D, 2012. **Sos-mediated cross-activation of wild-type Ras by oncogenic Ras is essential for tumorigenesis.** *Nat Commun* [\[PubMed Abstract\]](#)
16. Depeille P, Henricks LM, van de Ven RA, Lemmens E, Wang CY, Matli M, Werb Z, Haigis KM, Donner D, Warren R, Roose JP, 2015. **RasGRP1 opposes proliferative EGFR-SOS1-Ras signals and restricts intestinal epithelial cell growth.** *Nat Cell Biol* [\[PubMed Abstract\]](#)
17. Sheffels E, Sealover NE, Wang C, Kim DH, Vazirani IA, Lee E, M Terrell E, Morrison DK, Luo J, Kortum RL, 2018. **Oncogenic RAS isoforms show a hierarchical requirement for the guanine nucleotide exchange factor SOS2 to mediate cell transformation.** *Sci Signal* [\[PubMed Abstract\]](#)
18. Sheffels E, Sealover NE, Theard PL, Kortum RL, 2019. **Anchorage-independent growth conditions reveal a differential SOS2 dependence for transformation and survival in RAS-mutant cancer cells.** *Small GTPases* [\[PubMed Abstract\]](#)
19. Turke AB, Song Y, Costa C, Cook R, Arteaga CL, Asara JM, Engelman JA, 2012. **MEK inhibition leads to PI3K/AKT activation by relieving a negative feedback on ERBB receptors.** *Cancer Res* [\[PubMed Abstract\]](#)
20. Pettazzoni P, Viale A, Shah P, Carugo A, Ying H, Wang H, Genovese G, Seth S, Minelli R, Green T, Huang-Hobbs E, Corti D, Sanchez N, Nezi L, Marchesini M, Kapoor A, Yao W, Francesco ME,

- Petrocchi A, Deem AK, Scott K, Colla S, Mills GB, Fleming JB, Heffernan TP, Jones P, Toniatti C, DePinho RA, Draetta GF, 2015. **Genetic events that limit the efficacy of MEK and RTK inhibitor therapies in a mouse model of KRAS-driven pancreatic cancer.** *Cancer Res* [[PubMed Abstract](#)]
21. Sos ML, Fischer S, Ullrich R, Peifer M, Heuckmann JM, Koker M, Heynck S, Stückerath I, Weiss J, Fischer F, Michel K, Goel A, Regales L, Politi KA, Perera S, Getlik M, Heukamp LC, Ansén S, Zander T, Beroukhir R, Kashkar H, Shokat KM, Sellers WR, Rauh D, Orr C, Hoeflich KP, Friedman L, Wong KK, Pao W, Thomas RK, 2009. **Identifying genotype-dependent efficacy of single and combined PI3K- and MAPK-pathway inhibition in cancer.** [[PubMed Abstract](#)]
22. Manchado E, Weissmueller S, Morris JP 4th, Chen CC, Wullenkord R, Lujambio A, de Stanchina E, Poirier JT, Gainor JF, Corcoran RB, Engelman JA, Rudin CM, Rosen N, Lowe SW, 2016. **A combinatorial strategy for treating KRAS-mutant lung cancer.** *Nature* [[PubMed Abstract](#)]
23. Xue JY, Zhao Y, Aronowitz J, Mai TT, Vides A, Qeriqi B, Kim D, Li C, de Stanchina E, Mazutis L, Risso D, Lito P, 2020. **Rapid non-uniform adaptation to conformation-specific KRAS(G12C) inhibition.** *Nature* [[PubMed Abstract](#)]
24. Ryan MB, Fecce de la Cruz F, Phat S, Myers DT, Wong E, Shahzade HA, Hong CB, Corcoran RB, 2020. **Vertical Pathway Inhibition Overcomes Adaptive Feedback Resistance to KRASG12C Inhibition.** *Clin Cancer Res* [[PubMed Abstract](#)]
25. Lou K, Steri V, Ge AY, Hwang YC, Yogodzinski CH, Shkedi AR, Choi ALM, Mitchell DC, Swaney DL, Hann B, Gordan JD, Shokat KM, Gilbert LA, 2019. **KRASG12C inhibition produces a driver-limited state revealing collateral dependencies.** *Sci Signal* [[PubMed Abstract](#)]
26. Anderson GR, Winter PS, Lin KH, Nussbaum DP, Cakir M, Stein EM, Soderquist RS, Crawford L, Leeds JC, Newcomb R, Stepp P, Yip C, Wardell SE, Tingley JP, Ali M, Xu M, Ryan M, McCall SJ, McRee AJ, Counter CM, Der CJ, Wood KC, 2017. **A Landscape of Therapeutic Cooperativity in KRAS Mutant Cancers Reveals Principles for Controlling Tumor Evolution.** *Cell Rep* [[PubMed Abstract](#)]
27. Fedele C, Ran H, Diskin B, Wei W, Jen J, Geer MJ, Araki K, Ozerdem U, Simeone DM, Miller G, Neel BG, Tang KH, 2018. **SHP2 Inhibition Prevents Adaptive Resistance to MEK Inhibitors in Multiple Cancer Models.** *Cancer Discov* [[PubMed Abstract](#)]
28. Ruess DA, Heynen GJ, Ciecieski KJ, Ai J, Berninger A, Kabacaoglu D, Görgülü K, Dantes Z, Wörmann SM, Diakopoulos KN, Karpathaki AF, Kowalska M, Kaya-Aksoy E, Song L, van der Laan EAZ, López-Alberca MP, Nazaré M, Reichert M, Saur D, Erkan MM, Hopt UT, Sainz B Jr, Birchmeier W, Schmid RM, Lesina M, Algül H, 2018. **Mutant KRAS-driven cancers depend on PTPN11/SHP2 phosphatase.** *Nat Med* [[PubMed Abstract](#)]
29. Hillig RC, Sautier B, Schroeder J, Moosmayer D, Hilpmann A, Stegmann CM, Werbeck ND, Briem H, Boemer U, Weiske J, Badock V, Mastouri J, Petersen K, Siemeister G, Kahmann JD, Wegener D, Böhnke N, Eis K, Graham K, Wortmann L, von Nussbaum F, Bader B, 2019. **Discovery of potent SOS1 inhibitors that block RAS activation via disruption of the RAS-SOS1 interaction.** *Proc Natl Acad Sci U S A* [[PubMed Abstract](#)]
30. Gerlach D, Gmachl M, Ramharter J, The J, Fu S-C, Trapani F, Kessler D, Rumpel K, Botesteanu

D-A, Ettmayer P, Arnhof H, Gerstberger T, Kofink C, Wunberg T, Vellano CP, Heffernan TP, Marszalek JR, Pearson M, McConnell DB, Kraut N, Hofmann MH, 2020. **BI-3406 and BI 1701963: Potent and selective SOS1::KRAS inhibitors induce regressions in combination with MEK inhibitors or irinotecan.** AACR Virtual Meeting 1, abstract currently unavailable.

31. Nichols RJ, Haderk F, Stahlhut C, Schulze CJ, Hemmati G, Wildes D, Tzitzilonis C, Mordec K, Marquez A, Romero J, Hsieh T, Zaman A, Olivas V, McCoach C, Blakely CM, Wang Z, Kiss G, Koltun ES, Gill AL, Singh M, Goldsmith MA, Smith JAM, Bivona TG, 2018. **RAS nucleotide cycling underlies the SHP2 phosphatase dependence of mutant BRAF-, NF1- and RAS-driven cancers.** Nat Cell Biol [\[PubMed Abstract\]](#)

[< Older Post](#)

RAS Mutation Tropism

[Newer Post >](#)

Deploying a RAS pipeline against the SARS-CoV-2 pandemic

If you would like to reproduce some or all of this content, see [Reuse of NCI Information](#) for guidance about copyright and permissions. In the case of permitted digital reproduction, please credit the National Cancer Institute as the source and link to the original NCI product using the original product's title; e.g., "SOS signaling in RAS-mutated cancers was originally published by the National Cancer Institute."

We welcome your comments on this post. All comments must follow our [comment policy](#).

0 Comments RAS Central  [Disqus' Privacy Policy](#)

 [Robert Kortum](#) ▾

 [Recommend](#)  [Tweet](#)  [Share](#)

[Sort by Newest](#) ▾



Start the discussion...

Be the first to comment.

 [Subscribe](#)  [Add Disqus to your site](#) [Add Disqus](#)  [Do Not Sell My Data](#)

Archive

[2020 \(7\)](#)

[2019 \(7\)](#)

2018 (7)

2017 (9)

2016 (11)

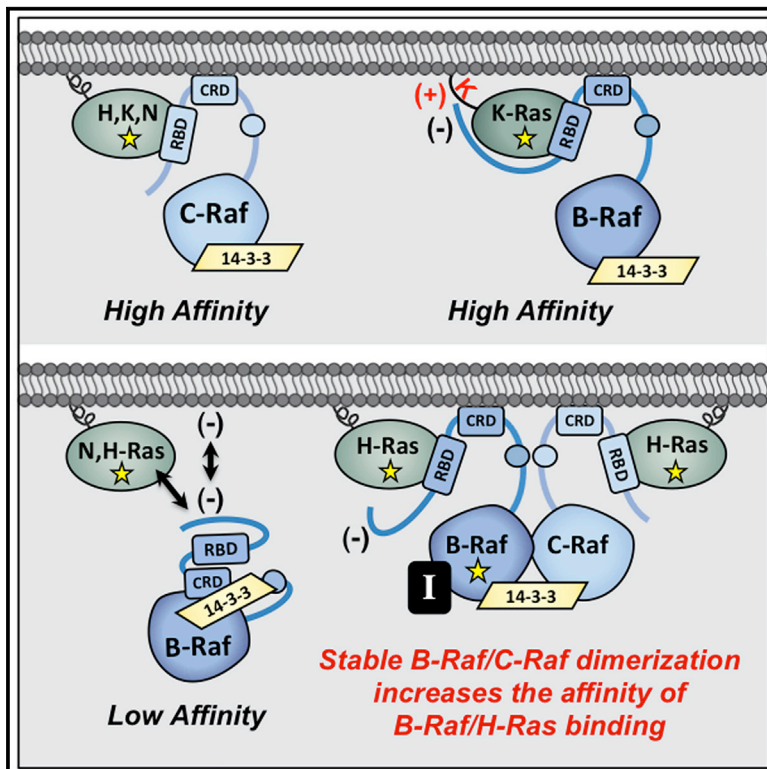
2015 (15)

2014 (5)

Molecular Cell

Distinct Binding Preferences between Ras and Raf Family Members and the Impact on Oncogenic Ras Signaling

Graphical Abstract



Authors

Elizabeth M. Terrell, David E. Durrant, Daniel A. Ritt, ..., John F. Hancock, Robert L. Kortum, Deborah K. Morrison

Correspondence

morrisod@mail.nih.gov

In Brief

The Raf kinases bind to active Ras proteins and function to transmit signals that control cell growth and tumorigenesis. The study by Terrell et al. reveals distinct binding preferences between individual Ras and Raf family members and identifies events that can alter these interactions to upregulate Ras-driven cancer signaling.

Highlights

- C-Raf binds all Ras proteins equivalently, but B-Raf exhibits selectivity for K-Ras
- Raf N-terminal segments and Ras HVR sequences determine binding preferences
- C-Raf is critical for downstream transmission of H-Ras-driven signaling
- Events that increase B-Raf/C-Raf dimerization augment the B-Raf/H-Ras interaction



Distinct Binding Preferences between Ras and Raf Family Members and the Impact on Oncogenic Ras Signaling

Elizabeth M. Terrell,¹ David E. Durrant,¹ Daniel A. Ritt,¹ Nancy E. Sealover,² Erin Sheffels,² Russell Spencer-Smith,¹ Dominic Esposito,³ Yong Zhou,⁴ John F. Hancock,⁴ Robert L. Kortum,² and Deborah K. Morrison^{1,5,*}

¹Laboratory of Cell and Developmental Signaling, NCI-Frederick, Frederick, MD 21702, USA

²Department of Pharmacology and Molecular Therapeutics, Uniformed Services University of the Health Sciences, Bethesda, MD 20814, USA

³NCI-Ras Initiative, Cancer Research Technology Program, Frederick National Laboratory for Cancer Research, Leidos Biomedical Research, Frederick, MD 21702, USA

⁴Department of Integrative Biology and Pharmacology, McGovern Medical School, University of Texas Health Science Center at Houston, Houston, TX 77030, USA

⁵Lead Contact

*Correspondence: morrisod@mail.nih.gov

<https://doi.org/10.1016/j.molcel.2019.09.004>

SUMMARY

The Ras GTPases are frequently mutated in human cancer, and, although the Raf kinases are essential effectors of Ras signaling, the tumorigenic properties of specific Ras-Raf complexes are not well characterized. Here, we examine the ability of individual Ras and Raf proteins to interact in live cells using bioluminescence resonance energy transfer (BRET) technology. We find that C-Raf binds all mutant Ras proteins with high affinity, whereas B-Raf exhibits a striking preference for mutant K-Ras. This selectivity is mediated by the acidic, N-terminal segment of B-Raf and requires the K-Ras polybasic region for high-affinity binding. In addition, we find that C-Raf is critical for mutant H-Ras-driven signaling and that events stabilizing B-Raf/C-Raf dimerization, such as Raf inhibitor treatment or certain B-Raf mutations, can allow mutant H-Ras to engage B-Raf with increased affinity to promote tumorigenesis, thus revealing a previously unappreciated role for C-Raf in potentiating B-Raf function.

INTRODUCTION

Ras proteins are membrane-associated, small GTPases that function to transmit a multitude of cellular signals (Pylayeva-Gupta et al., 2011). All Ras family members, which include H-Ras, K-Ras4A/4B, and N-Ras, can relay signals received by cell surface receptors due to their ability to cycle between a GDP-bound “off” state and a GTP-bound “on” state (Cox and Der, 2010; Simanshu et al., 2017). Typically, receptor engagement results in the recruitment of guanine nucleotide exchange factors (GEFs) to the cell surface where they facilitate the GTP-loading of Ras and, in turn, the interaction of Ras with down-

stream effectors. Following signal transmission, Ras cycles back to its inactive state as a result of GTPase-activating proteins (GAPs) that stimulate the intrinsic GTPase activity of Ras (Bos et al., 2007).

Consistent with its central role in cell signaling, dysregulation of Ras cycling can promote human disease states, with somatic mutations in the *Ras* genes being prominent drivers of tumorigenesis and *Ras* germline mutations contributing to a group of related developmental disorders known as the RASopathies (Fernández-Medarde and Santos, 2011; Schubbert et al., 2007). Importantly, disease-associated mutations tend to render Ras insensitive to GAP stimulation and reduce its intrinsic GTPase activity, leaving Ras in a constitutively active state that promotes pathway activation in an unregulated manner (Prior et al., 2012).

One of the essential effector cascades required for Ras signaling is the ERK cascade, comprised of the Raf, MEK, and ERK protein kinases (Lavoie and Therrien, 2015). All Raf family members, which include A-Raf, B-Raf, and C-Raf, possess a conserved Ras-binding domain (RBD) that resides in the Raf N-terminal regulatory domain. In quiescent cells, the Rafs exist as autoinhibited monomers in the cytosol (Nan et al., 2013). However, when growth signals are received, the Raf kinases are recruited by Ras to the plasma membrane where they become activated through an allosteric mechanism that requires dimerization of the C-terminal Raf kinase domains (Hu et al., 2013). In normal Ras-dependent signaling, B-Raf/C-Raf heterodimers predominate (Freeman et al., 2013) and function to initiate the phosphorylation cascade that results in MEK and ERK activation. Once activated, ERK plays a critical role in the forward transmission of signals but also participates in the attenuation of Ras signaling through the phosphorylation of upstream pathway components, which, in the case of the Rafs, inhibit both Ras/Raf binding and Raf dimerization (Dougherty et al., 2005; Ritt et al., 2010).

Despite being one of the most frequently mutated signaling pathways in human cancer, various aspects of Ras biology are still poorly understood. For example, even though it is well



known that the C-terminal hypervariable region (HVR) of the Ras proteins results in differential lipid processing and membrane localization (Prior and Hancock, 2012), the extent to which these differences influence Ras signaling and/or effector interactions is not clear. Moreover, a puzzling aspect of Ras-induced tumorigenesis is that, although the Ras proteins are highly conserved and rather ubiquitously expressed, their mutational frequency can vary significantly among cancer types, with *K-Ras* mutations being the predominant driver among all Ras-associated tumors but other family members being the primary driver in select tumor types. Therefore, given the central role of the Raf kinases in Ras signaling, studies examining the Ras/Raf interaction in live cells could reveal valuable information needed to tease apart unique tumorigenic properties of individual Ras members and may prove helpful in the pursuit of more effective therapeutic strategies.

Here, we examine the Ras/Raf interaction utilizing bioluminescence resonance energy transfer (BRET), a technique that allows quantitative measurements to be obtained under conditions that preserve crucial features of Ras and Raf regulation, including lipid processing, intracellular trafficking, membrane microdomain targeting, and protein phosphorylation. Strikingly, we find that different Ras and Raf family members exhibit distinct binding preferences and that these differences have important implications for disease-associated Ras signaling.

RESULTS

Live-Cell BRET Analysis of the Ras/Raf Interaction

Bioluminescence resonance energy transfer (BRET) was used to investigate the requirements for Ras/Raf binding in live cells (Pfleger and Eidne, 2006). In this system, a BRET signal is generated when a protein tagged with an energy donor comes in close proximity and can transfer energy to a protein tagged with an energy acceptor. Donor, acceptor, and BRET signals are each monitored individually, providing internal controls for protein expression and producing a sensitive ratiometric readout that is independent of cell number. Quantitative data regarding the interaction can also be obtained by generating a saturation curve in which expression of the energy donor remains constant, while expression of the energy acceptor increases. In this type of analysis, a specific interaction will generate a hyperbolic curve, with $BRET_{max}$ being reflective of the total number of binding pairs that can form and $BRET_{50}$ being a relative measure of binding affinity.

For our analysis, the Raf members functioned as the energy donor, tagged at a conserved C-terminal position with the Rluc8 enzyme, and the Ras proteins served as the energy acceptor, tagged at the N terminus with the Venus fluorophore. It should be noted that our initial studies were performed using proteins that encode the entire Raf regulatory domain (Raf^{rReg}) but lack the kinase domain. This approach was taken in order to mitigate any indirect effects on Ras/Raf binding that might be caused by dimerization of the Raf kinase domains or due to inhibitory feedback loops generated by Raf catalytic activation. As shown in Figure 1A, a strong BRET signal was observed when wild-type (WT) C-Raf^{rReg} was co-expressed with the

Q61R mutant of K-Ras4B (hereon referred to as K-Ras). However, if the RBD of C-Raf^{rReg} contained an arginine to leucine (R > L) mutation known to disrupt the Ras/Raf interaction (Fabian et al., 1994), the BRET signal was dramatically reduced. In addition, when the C-terminal CAAX motif of K-Ras^{Q61R} was mutated to prevent the lipid processing and membrane localization of K-Ras (K-Ras^{Q61R/C>A}), the BRET signal was significantly compromised as was the GTP loading of Ras (Figures 1A and 1B). In co-immunoprecipitation assays, WT-C-Raf^{rReg}, but not the R > L mutant, was strongly detected in K-Ras^{Q61R} complexes, and only faint levels of WT-C-Raf^{rReg} were observed in K-Ras^{Q61R/C>A} complexes (Figure 1B). Moreover, live-cell imaging studies verified the cytosolic localization of K-Ras^{Q61R/C>A} and showed that K-Ras^{Q61R} could recruit WT-C-Raf to the cell surface but not the R > L mutant (Figure 1C). Thus, these findings confirm that the Ras and Raf proteins generated for use in the BRET assay exhibit their expected subcellular localization and protein binding properties.

Next, each Raf family member was evaluated for binding interactions with a panel of K-Ras mutants. As shown in Figure 1D, a BRET signal was detected for all the Raf^{rReg}/K-Ras pairings, with the highest binding affinity (represented by lower $BRET_{50}$ values) and highest $BRET_{max}$ observed with C-Raf, followed by A-Raf, and then B-Raf. For each individual Raf^{rReg} protein, $BRET_{50}$ values were similar for all the K-Ras mutants, indicating a comparable binding affinity (Figure 1E). Interestingly, the highest $BRET_{max}$ signals were observed with K-Ras proteins containing mutations in the Q61 site, likely reflecting the reported increased GTP occupancy of Q61 mutants (Buhrman et al., 2011; Hunter et al., 2015) and an increase in the number of K-Ras proteins available for pairing with the Rafs. Finally, incorporation of the RBD R > L mutation into each Raf member disrupted the Ras/Raf interaction in both the BRET and co-immunoprecipitation assays (Figures 1D–1F).

BRET Analysis Reveals Binding Preferences between Ras and Raf Family Members

To determine whether any of the Raf or Ras family members display preferential binding to one another in live cells, the ability of each Raf^{rReg} protein to interact with G12V or Q61R mutants of H-Ras, N-Ras, or K-Ras was monitored (Figures 2A and S1A). Surprisingly, differences in the $BRET_{max}$ and $BRET_{50}$ values were observed among the different pairings, revealing that the Rafs do not bind the Ras family members equivalently. For A-Raf and B-Raf, the highest $BRET_{max}$ and lowest $BRET_{50}$ values were observed when they were paired with mutant K-Ras. In contrast, when C-Raf was paired with mutant K-Ras, the $BRET_{max}$ signals were lower than those observed with mutant H-Ras or N-Ras; however, all the C-Raf/Ras pairings were of similar high affinity ($BRET_{50}$ values ranging from 0.165–0.172). As expected, the RBD R > L mutation significantly disrupted all Ras/Raf interactions (Figure 2A).

In co-immunoprecipitation assays (Figures 2B and S1B), C-Raf^{rReg} was detected at nearly equivalent levels in all the mutant Ras complexes. A-Raf^{rReg} was also observed in all Ras complexes, but binding to K-Ras was increased. Strikingly, B-Raf^{rReg} was found to co-immunoprecipitate almost exclusively with activated K-Ras. Of note, the observed co-immunoprecipitation

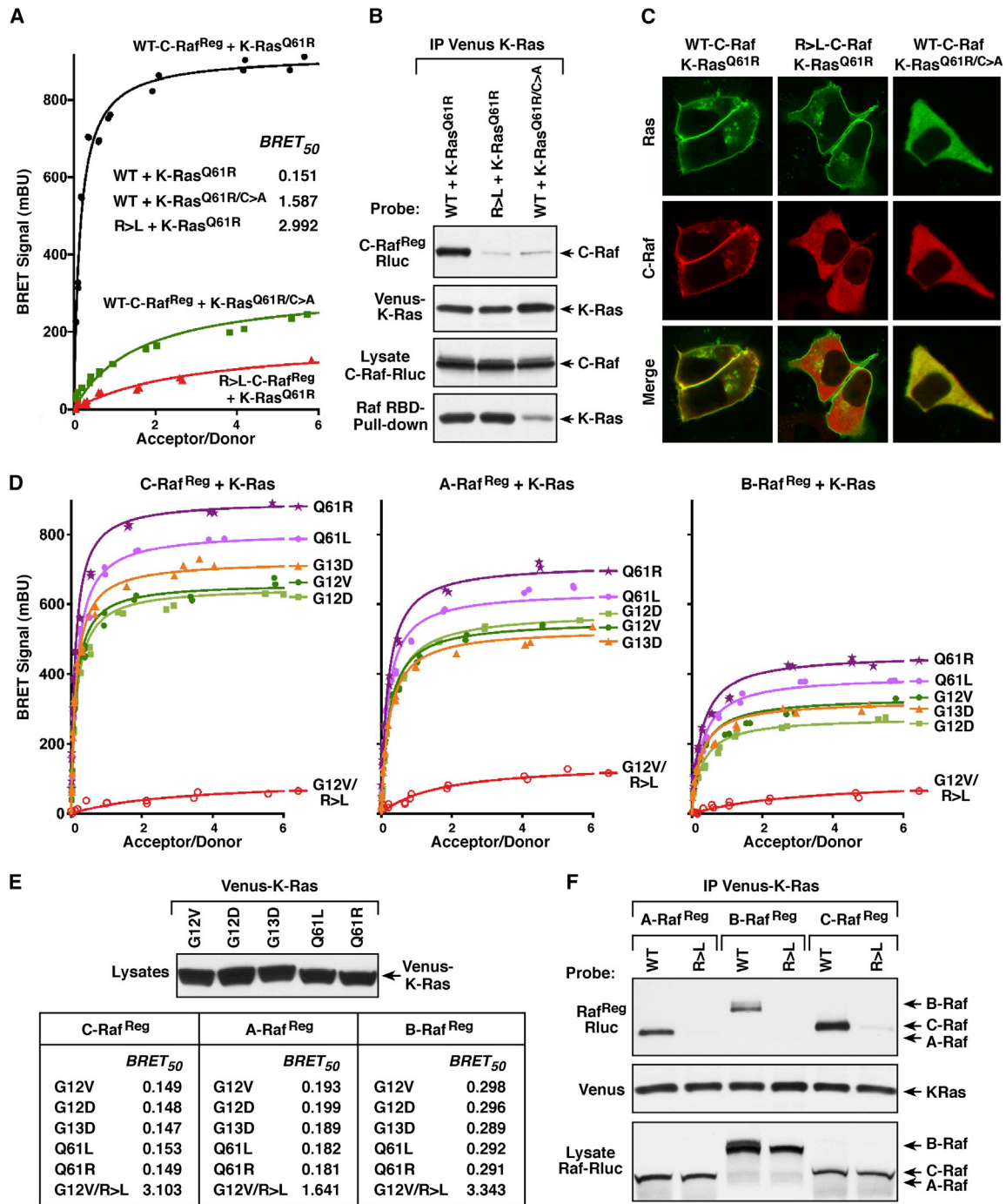


Figure 1. Analysis of Raf-Binding Interactions with Activated K-Ras Mutants

(A) BRET saturation curves are shown examining the interaction of WT or RBD mutant (R > L) C-Raf^{Reg}-Rluc proteins with Venus-K-Ras^{Q61R} and the interaction of WT C-Raf^{Reg}-Rluc with the CAAX mutant (C185A) Venus-K-Ras^{Q61R/C>A}. BRET₅₀ values are listed.

(B) K-Ras and C-Raf proteins analyzed in (A) were examined in co-immunoprecipitation assays. Venus-K-Ras proteins were also evaluated for GTP loading in Raf-RBD pull-down assays.

(C) Live-cell imaging shows the intracellular localization of the indicated K-Ras and C-Raf proteins.

(D) BRET saturation curves are shown examining the interaction of WT or R > L C-Raf^{Reg}-Rluc proteins with the indicated Venus-K-Ras mutants.

(E) BRET₅₀ values from (D) are listed and the expression level of the K-Ras mutants is shown.

(F) WT and R > L C-Raf^{Reg}-Rluc proteins were examined in co-immunoprecipitation assays for binding to Venus-K-Ras^{Q61R}. Lysates were also monitored for C-Raf^{Reg}-Rluc expression, and all experiments were conducted in 293FT cells.

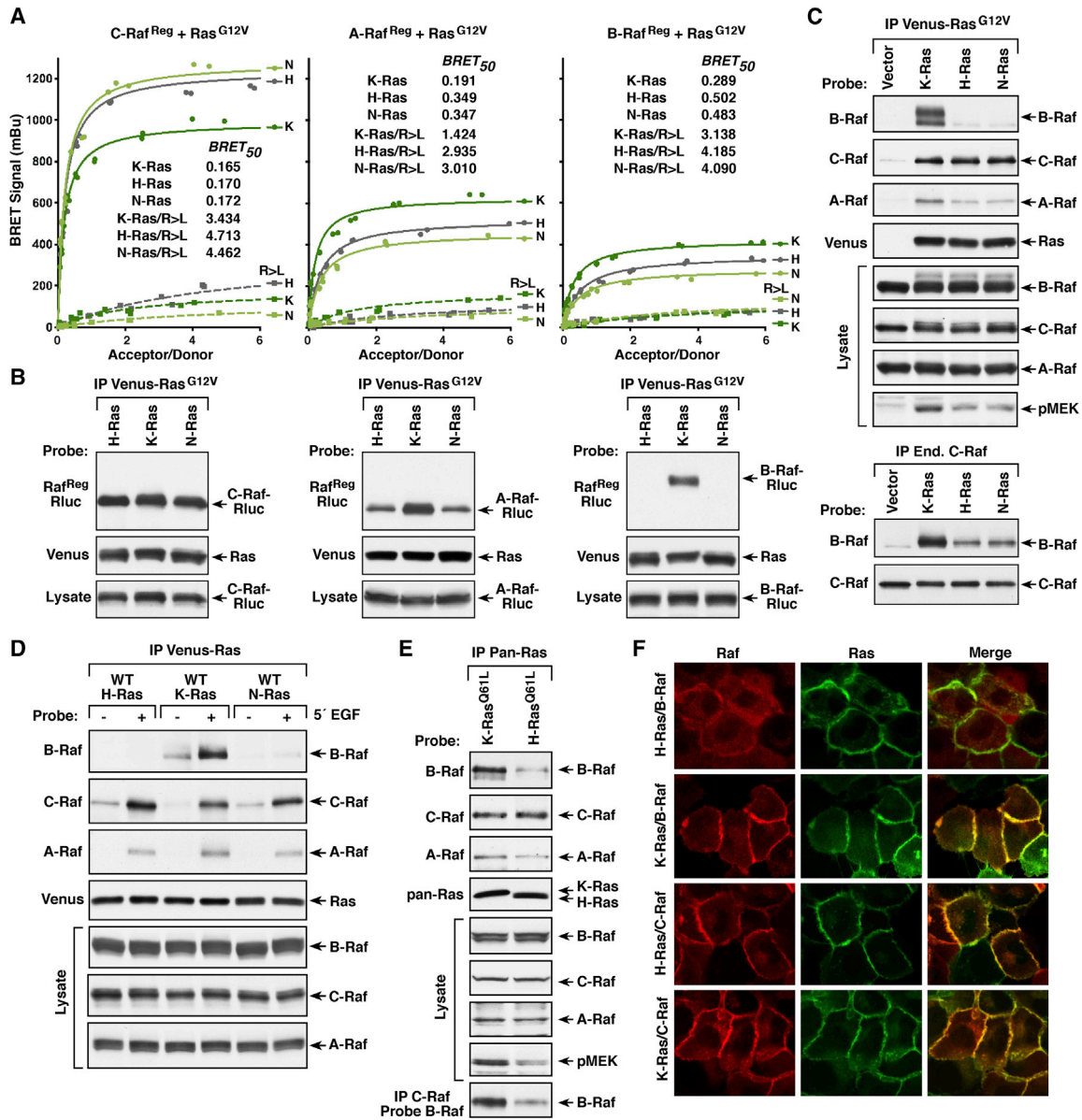


Figure 2. Binding Preferences between Ras and Raf Family Members

(A) BRET saturation curves examining the interaction of WT or R > L Raf^{Reg}-Rluc proteins with the Venus-Ras^{G12V} proteins are shown, and the BRET₅₀ values are listed.

(B) WT Raf^{Reg}-Rluc proteins were examined in co-immunoprecipitation assays for binding to the Venus-Ras^{G12V} proteins.

(C) Immunoprecipitated Venus-Ras^{G12V} complexes were probed for the presence of endogenous B-Raf, C-Raf, or A-Raf and Venus-Ras. Lysates were also examined for B-Raf, C-Raf, A-Raf, and pMEK levels (upper). Endogenous C-Raf complexes were isolated from cells expressing the indicated Venus-Ras^{G12V} proteins and examined for dimerization with B-Raf (lower).

(D) HeLa cells expressing WT Venus-Ras proteins were treated or not with EGF prior to lysis. Immunoprecipitated Venus-Ras complexes were probed for the presence of endogenous B-Raf, C-Raf, or A-Raf and Venus-Ras. Lysates were also examined for Raf levels.

(E) Ras complexes were immunoprecipitated from Ras-deficient MEFs re-expressing either K-Ras^{O61L} or H-Ras^{O61L} and probed for the presence of endogenous B-Raf, C-Raf, or A-Raf and Ras. Endogenous C-Raf was also isolated from the MEF lines and examined for dimerization with B-Raf. Lysates were examined for B-Raf, C-Raf, A-Raf, and pMEK levels.

(F) MCF10A cells stably expressing Halo-tagged K-Ras^{G12V} or H-Ras^{G12V} and B-Raf-Cherry or C-Raf-Cherry were examined by live-cell imaging to visualize recruitment of the Rafs to the plasma membrane. Experiments shown in (A)–(C) were conducted in 293FT cells.

See also Figure S1.

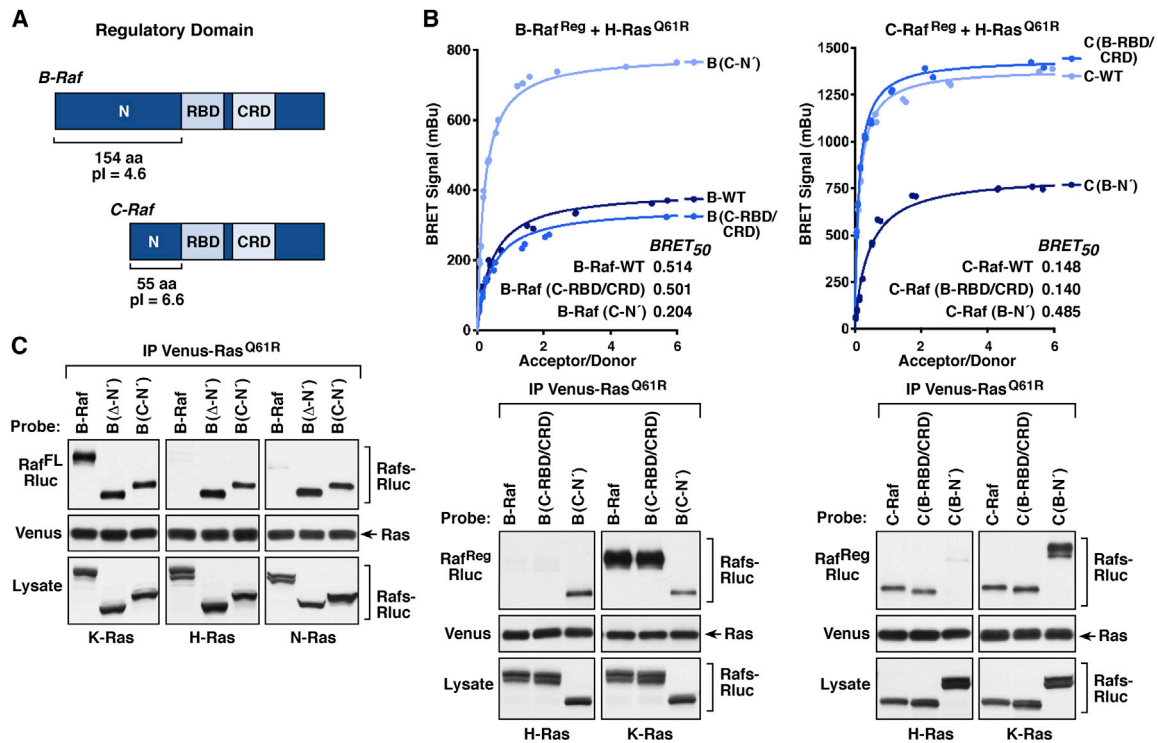


Figure 3. Raf N-Terminal Segment Determines the Ras Binding Selectivity

(A) Schematic depiction of the B-Raf and C-Raf regulatory domains with the RBD, CRD, and N'-segment indicated.

(B) Raf^{Reg}-Rluc proteins were generated in which the RBD/CRD or N'-segment of B-Raf and C-Raf were exchanged. BRET (upper) and co-immunoprecipitation assays (lower) were performed examining the interaction of WT or domain-exchanged Raf^{Reg}-Rluc proteins with Venus-tagged H-Ras^{Q61R} or K-Ras^{Q61R}. BRET₅₀ values are listed.

(C) WT full-length B-Raf^{FL}-Rluc or B-Raf^{FL}-Rluc proteins lacking the N'-segment (Δ-N') or containing the N'-segment of C-Raf (C-N') were examined for their ability to interact with the indicated Venus-Ras^{Q61R} proteins in co-immunoprecipitation assays. Lysates were also monitored for Raf-Rluc expression in (B and C), and all experiments were conducted in 293FT cells.

See also Figure S2.

results appear to align more closely with the BRET₅₀ values, which are reflective of the affinity of the interaction and are consistent with the fact that binding interactions detected in co-immunoprecipitation assays must be of sufficient strength to withstand detergent-based cell lysis and immunoprecipitation.

Similar Ras binding preferences were observed when the endogenous Raf kinases were evaluated for their ability to co-immunoprecipitate with constitutively active Ras mutants or with growth-factor-activated WT Ras proteins (Figures 2C and 2D and S1C). Preferential binding of B-Raf to activated K-Ras was further confirmed in co-immunoprecipitation assays using Ras-deficient mouse embryonic fibroblasts (MEFs) (Drosten et al., 2010) reconstituted to express untagged H-Ras^{Q61L} or K-Ras^{Q61L} at endogenous levels (Figure 2E). Moreover, in live-cell imaging studies using MCF10A cell lines that stably express Halo-tagged H-Ras^{G12V} or K-Ras^{G12V} and Cherry-tagged B-Raf or C-Raf, the plasma membrane recruitment of B-Raf was significantly increased in cells expressing K-Ras^{G12V}, whereas strong membrane localization of C-Raf was observed in both cell lines (Figure 2F). Consistent with the preferred binding of B-Raf to K-Ras, mutant K-Ras was found to be the strongest driver of endogenous B-Raf/C-Raf

dimer formation as well as downstream MEK activation (Figures 2C and 2E). Taken together, these findings indicate that C-Raf and K-Ras can bind with high affinity to all Ras or Raf family members respectively, whereas H-Ras displays preferential binding to C-Raf, and B-Raf exhibits a striking selectivity for K-Ras.

Role of the Raf N-Terminal Segment in Determining Ras Binding Selectivity

Given that B-Raf and C-Raf were found to exhibit the most divergent binding to Ras members, experiments were conducted to determine which regions of the Rafs might account for these differences. The Raf regulatory domain contains two conserved areas: the RBD and the membrane-binding cysteine-rich domain (CRD) (Hekman et al., 2002; Williams et al., 2000). However, preceding the RBD, there lies an N-terminal segment (N'-segment) that varies significantly among the Rafs (Figure 3A). In particular, the N'-segment of B-Raf is comprised of 154 amino acids and has an acidic isoelectric point (pI) of 4.6, whereas the C-Raf N'-segment contains 55 amino acids and has a more neutral pI of 6.6. Of note, the A-Raf N'-segment also has a neutral pI (6.9) and is 18 amino acids in length.

Therefore, B-Raf and C-Raf constructs were generated in which the N'-segments were exchanged, and the resulting proteins were evaluated in BRET and co-immunoprecipitation assays for binding interactions with activated H-Ras or K-Ras. As shown in Figure 3B, when the B-Raf N'-segment was replaced with that of C-Raf (B-Raf^(C-N')), the B-Raf/H-Ras interaction was significantly increased as BRET_{max} signals were higher, BRET₅₀ values were lower, and B-Raf^(C-N') could be detected in H-Ras immunoprecipitates. In contrast, replacing the C-Raf N'-segment with that of B-Raf (C-Raf^(B-N')) greatly reduced the C-Raf/H-Ras interaction. Consistent with the ability of K-Ras to engage all Raf kinases with high affinity, exchange of the Raf N'-segments had no significant effect on the affinity of K-Ras binding in either co-immunoprecipitation or BRET assays (Figures 3B and S2). Exchange of the conserved RBD-CRD domains was also evaluated and found to have little effect on Ras/Raf interactions.

The role of the N'-segment in determining the Ras binding selectivity of B-Raf was further confirmed in co-immunoprecipitation assays using full-length B-Raf proteins in which the N'-segment was either deleted (Δ -N') or replaced with that of C-Raf (C-N'). As shown in Figure 3C, all B-Raf proteins were detected in K-Ras^{Q61R} complexes; however, only proteins lacking the B-Raf N'-segment were present in H-Ras or N-Ras complexes, suggesting that the B-Raf N'-segment may impede or obstruct high-affinity binding to H-Ras and N-Ras.

Contribution of the Ras Hypervariable Region to the Ras/Raf Interaction

Next, we sought to identify the region of the Ras proteins that likewise determines the Raf binding preferences. Members of the Ras family are highly conserved and diverge primarily at the C-terminal hypervariable region (HVR) (Figure 4A), which contains distinct signals for lipid processing and membrane attachment (Parker and Mattos, 2015; Prior and Hancock, 2012). All Ras proteins end with a CAAX motif, which is processed to yield a C-terminal farnesylated cysteine residue that is carboxymethylated. The H-Ras and N-Ras HVRs contain additional cysteine residues that are palmitoylated and function with the farnesyl group to mediate plasma membrane attachment. In contrast, the K-Ras4B HVR uniquely contains a lysine-rich polybasic region (PBR) that aids in membrane binding.

To investigate whether the Ras HVRs might also contribute to the Raf binding preferences, Ras proteins were analyzed in which the HVRs of mutant K-Ras4B (amino acids 165–188) and H-Ras (amino acids 165–189) were exchanged. As shown in Figure 4B, placing the K-Ras4B HVR sequences onto H-Ras^{Q61R} increased the binding of B-Raf^{R^{reg}} such that the BRET_{max} signals and BRET₅₀ values were similar to those observed with K-Ras^{Q61R}. Conversely, exchanging the K-Ras4B HVR with that of H-Ras reduced the K-Ras^{Q61R}/B-Raf^{R^{reg}} interaction to levels observed with H-Ras^{Q61R}. Moreover, B-Raf^{R^{reg}} and endogenous B-Raf were only able to co-immunoprecipitate with Ras proteins that contained the K-Ras4B HVR (Figures 4B and S3A).

Consistent with the high-affinity binding of C-Raf to all Ras members, C-Raf^{R^{reg}} and endogenous C-Raf were detected in all of the mutant Ras complexes, and all C-Raf^{R^{reg}} pairings exhibited high-affinity BRET₅₀ values (Figures 4B and S3A). How-

ever, the highest BRET_{max} signals were observed with proteins that contained the H-Ras HVR, suggesting that the H-Ras HVR sequence itself or the localization of these Ras proteins allows more C-Raf binding pairs to form. In addition, the K-Ras4A splice variant, whose HVR contains a palmitoylated cysteine residue instead of the PBR, interacted with the Rafs in a manner similar to H-Ras and N-Ras, as only C-Raf proteins could bind with sufficient affinity to co-immunoprecipitate with K-Ras4A^{Q61R} (Figures 4C and S3B).

The above findings suggest that the PBR-containing HVR of K-Ras4B also contributes to the B-Raf selectivity, and by utilizing a panel of previously characterized K-Ras^{G12V} PBR mutants (Zhou et al., 2017), we further found that the positive charge of the PBR was critical for high-affinity B-Raf binding. As shown in Figure 4D, substitution of each individual PBR lysine residue to an uncharged glutamine reduced binding of B-Raf^{R^{reg}} but had little effect on C-Raf^{R^{reg}} binding. Moreover, the reduction in B-Raf^{R^{reg}} binding was equivalent for all the PBR mutants, correlating with an equivalent reduction in the net basic charge of the PBR. In addition, replacing all six lysine residues with similarly charged arginine residues (6R) had minimal effect on B-Raf^{R^{reg}} binding; however, mutation of the serine phosphorylation site adjacent to the PBR to a phosphomimetic acidic residue (S181D) reduced the B-Raf^{R^{reg}} interaction, whereas mutation of the site to a neutral alanine residue had little effect (Figure 4D). Similar results were obtained when a subset of these mutants was evaluated for binding to endogenous B-Raf or C-Raf or when they were assessed in BRET assays (Figures S3D and S3E).

Finally, to investigate whether the positively charged K-Ras PBR might interact with the negatively charged B-Raf N'-segment, several cancer-associated mutations that alter acidic residues in the B-Raf N'-segment were analyzed in co-immunoprecipitation assays (Figure 4E). Strikingly, the E46K mutation resulted in reduced binding of B-Raf^{R^{reg}} to mutant K-Ras but increased binding to mutant H-Ras. Collectively, these findings support a model whereby the PBR contributes to the B-Raf/K-Ras interaction by engaging the B-Raf N'-segment, thus disrupting its inhibitory effect to facilitate high-affinity RBD contact.

Dimerization with C-Raf Can Influence the Affinity of the B-Raf/H-Ras^{Q61R} Interaction

B-Raf and C-Raf are known to form heterodimers, and, given that C-Raf exhibits high-affinity binding to all Ras proteins, experiments were initiated to determine whether B-Raf/C-Raf dimerization might alter the ability of B-Raf to interact with Ras members that lack the PBR. For these studies, full-length B-Raf proteins containing well-characterized mutations in the Raf dimer interface were utilized: dimerization-deficient R509H-B-Raf and dimerization-enhanced E586K-B-Raf. These mutants and WT-B-Raf were then evaluated in BRET and co-immunoprecipitation assays for binding to activated H-Ras or K-Ras. As indicated by the BRET₅₀ values, full-length WT-B-Raf (B-Raf^{FL}) exhibited a similar binding affinity to mutant H-Ras, as did the B-Raf^{R^{reg}} protein, and showed little ability to co-immunoprecipitate with H-Ras (Figures 5A and 2A). The R509H mutant also displayed low-affinity binding to H-Ras, whereas E586K-B-Raf exhibited an increased binding affinity and co-immunoprecipitated with mutant H-Ras in a manner that correlated with its increased

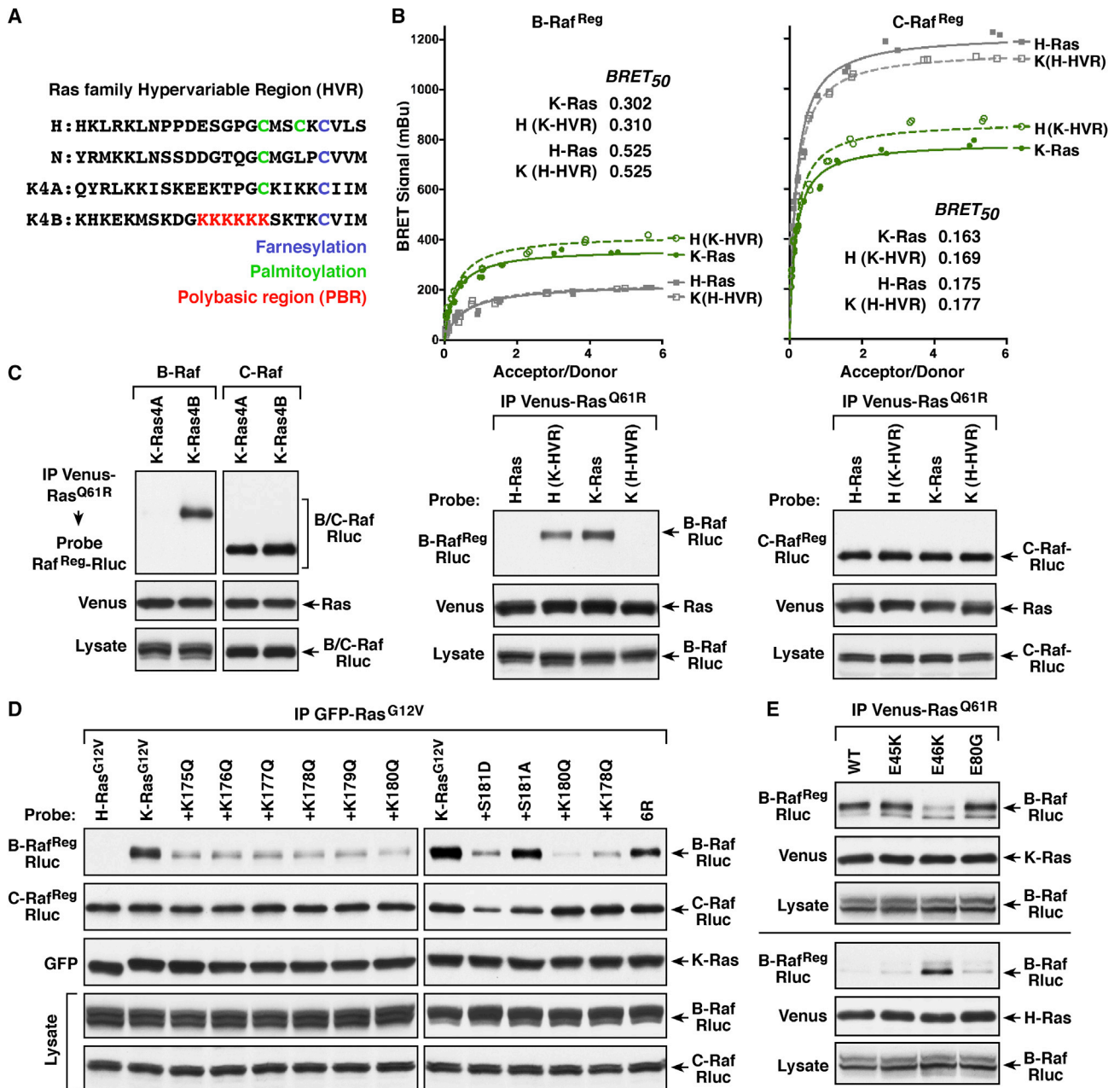


Figure 4. The Ras HVRs Contribute to the Ras/Raf Binding Preferences

(A) Shown are the HVR sequences of the various Ras proteins.

(B) Venus-Ras^{Q61R} proteins were generated in which the HVRs of H-Ras and K-Ras4B were exchanged. BRET (upper) and co-immunoprecipitation assays (lower) were performed examining the interaction of B-Raf^{Reg} or C-Raf^{Reg}-Rluc with WT or HVR-exchanged Venus-Ras^{Q61R} proteins. BRET₅₀ values are listed.

(C) Co-immunoprecipitation assays were performed examining the interaction of B-Raf^{Reg} or C-Raf^{Reg}-Rluc with Venus-tagged K-Ras4A^{Q61R} or K-Ras4B^{Q61R}. (D) Cells co-expressing the indicated GFP-Ras^{G12V} proteins and B-Raf^{Reg} or C-Raf^{Reg}-Rluc were lysed, and GFP-Ras complexes were immunoprecipitated from the cell lysates and examined for Raf^{Reg}-Rluc binding.

(E) WT or N'-segment mutant B-Raf^{Reg}-Rluc proteins were examined in co-immunoprecipitation assays for binding to Venus-tagged K-Ras^{Q61R} or H-Ras^{Q61R}. Lysates were monitored for the indicated proteins in (B–E), and all experiments were conducted in 293FT cells.

See also Figure S3.

ability to dimerize with C-Raf (Figure 5A). As expected, all of the B-Raf^{FL} proteins bound mutant K-Ras with a similar high affinity (Figure S4A).

Further supporting the model that dimerization with C-Raf can facilitate the interaction between B-Raf and H-Ras, stabilizing B-Raf/C-Raf dimers by mutation of the ERK-mediated feedback

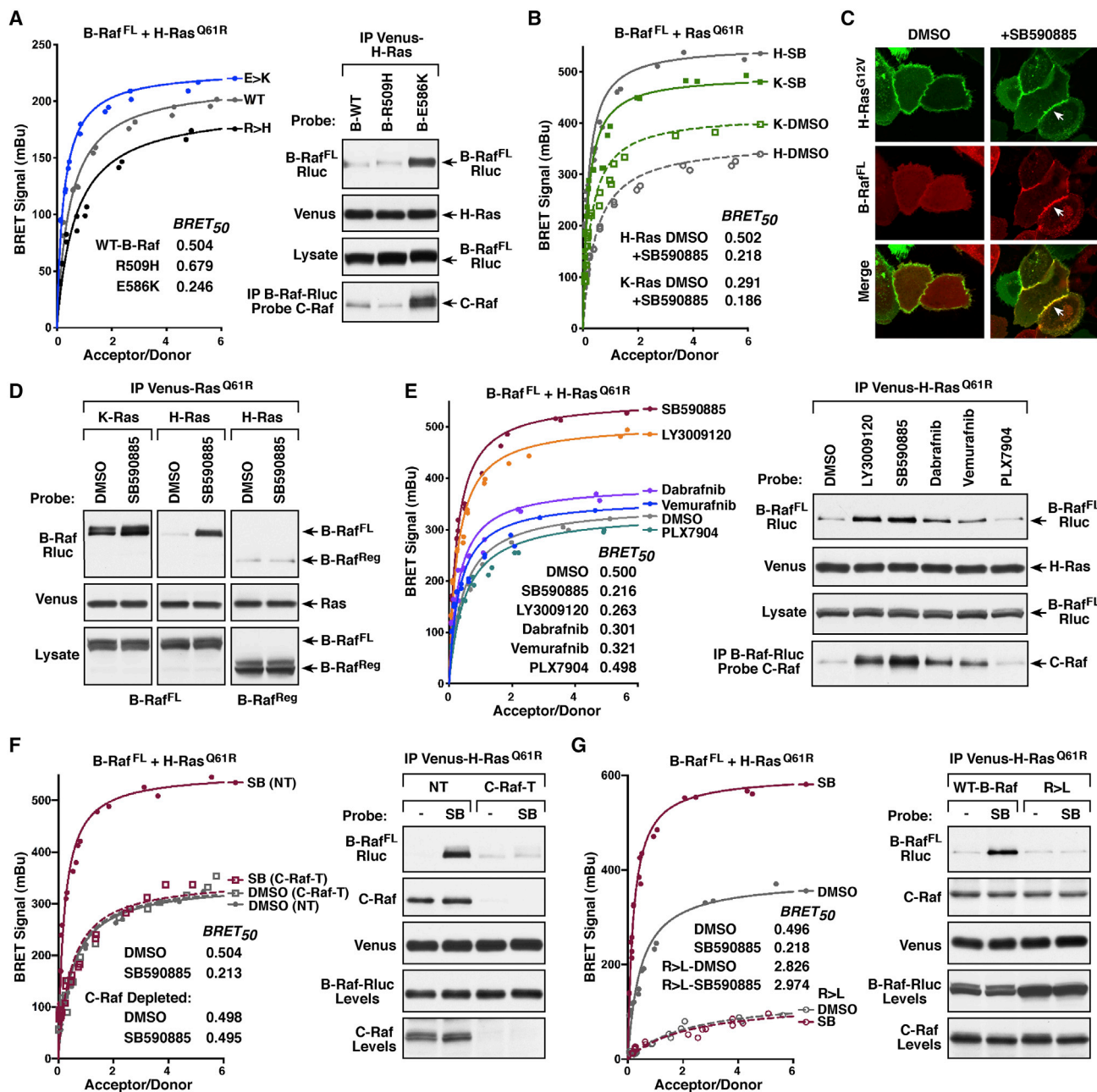


Figure 5. B-Raf/C-Raf Dimerization Can Modulate the B-Raf/H-Ras^{Q61R} Interaction

(A) BRET (left) and co-immunoprecipitation assays (right) are shown examining the interaction of WT, R509H (dimer-defective), or E586K (dimer-enhanced) B-Raf^{FL}-Rluc proteins with Venus-H-Ras^{Q61R}. The B-Raf^{FL}-Rluc proteins were also monitored for dimerization with C-Raf.

(B) BRET saturation curves were performed examining the effect of 1 h DMSO or Raf inhibitor SB590885 (SB) treatment on the interaction of B-Raf^{FL}-Rluc with Venus-tagged H-Ras^{Q61R} or K-Ras^{Q61R}. *BRET*₅₀ values are listed.

(C) MCF10A cells stably expressing Halo-H-Ras^{G12V} and B-Raf^{FL}-Cherry were treated for 1 h with DMSO or SB590885 prior to live-cell imaging. Recruitment of B-Raf to the plasma membrane in SB590885-treated cells is indicated by white arrows.

(D) 293FT cells expressing B-Raf^{FL}-Rluc with Venus-H-Ras^{Q61R} or Venus-K-Ras^{Q61R} or expressing B-Raf^{Reg}-Rluc with Venus-H-Ras^{Q61R} were treated for 1 h with DMSO or SB590885 prior to lysis. Immunoprecipitated Venus-Ras complexes were probed for B-Raf-Rluc and Venus-Ras.

(E) BRET (left) and co-immunoprecipitation (right) assays were performed examining the effect of various Raf inhibitors on the interaction of B-Raf^{FL}-Rluc with Venus-H-Ras^{Q61R}. *BRET*₅₀ values are listed. B-Raf^{FL}-Rluc proteins were also examined for dimerization with C-Raf.

(F) BRET (left) and co-immunoprecipitation (right) assays were performed examining the effect of SB590885 treatment on the interaction of B-Raf^{FL}-Rluc and Venus-H-Ras^{Q61R} in control (NT) or C-Raf-depleted (C-Raf-T) 293FT cells. *BRET*₅₀ values are listed. Co-immunoprecipitation of endogenous C-Raf with Venus-H-Ras^{Q61R} is also shown.

(legend continued on next page)

phosphorylation sites (which function to disrupt Raf dimerization) also resulted in increased B-Raf/H-Ras binding (Figure S4B). Of note, Ras proteins have also been proposed to dimerize; however, a mutation (D154Q) reported to impair Ras dimer formation (Ambrogio et al., 2018) was found to have little effect on Ras/Raf binding in either the BRET or co-immunoprecipitation assays (Figure S4C).

Stable B-Raf/C-Raf dimer formation can also be driven by treatment of cells with ATP-competitive Raf inhibitors (Durrant and Morrison, 2018). Therefore, we next used a B-Raf inhibitor known to strongly promote Raf dimerization, SB590885, to determine whether inhibitor treatment would alter B-Raf interactions (Figures 5B–5D). In the BRET system, SB590885 treatment resulted in a dramatic increase in binding of B-Raf^{FL} to mutant H-Ras, as evidenced by increased BRET_{max} signals and reduced BRET₅₀ values (Figure 5B). SB590885 treatment also allowed B-Raf^{FL} to stably co-immunoprecipitate with mutant H-Ras (Figure 5D) and resulted in a significant increase in the membrane localization of B-Raf-Cherry in MCF10A cells expressing Halo-H-Ras^{G12V} (Figure 5C). Binding between B-Raf^{FL} and mutant K-Ras was also enhanced in SB590885-treated cells; however, the increases were not as pronounced (Figures 5B, 5D, and S5A). Importantly, the enhancing effect of SB590885 treatment required binding of the inhibitor to the B-Raf kinase domain as SB590885 treatment had no effect on the interaction of H-Ras and the B-Raf^{reg} protein, which lacks the kinase domain that mediates Raf dimerization (Figures 5D and S5B).

When a panel of Raf inhibitors was evaluated, we found that all of the inhibitors tested, with the exception of the second-generation “paradox-breaker” inhibitor PLX7904 (Zhang et al., 2015), increased the level and affinity of the B-Raf^{FL}/H-Ras interaction and that the increased affinity correlated with the degree to which the inhibitors promoted B-Raf/C-Raf dimerization (Figure 5E). Further establishing C-Raf as a mediator of the upregulated interaction between B-Raf and H-Ras, depletion of endogenous C-Raf prevented SB590885 from increasing the B-Raf/H-Ras interaction in BRET or co-immunoprecipitation assays (Figure 5F). Finally, our findings suggest that inhibitor-stabilized B-Raf/C-Raf dimerization impacts the ability of B-Raf to directly contact H-Ras, as no increased binding to H-Ras was observed in SB590885-treated cells if the B-Raf^{FL} protein contained the RBD R > L mutation (Figure 5G).

Co-occurrence of B-Raf and H-Ras Mutations

Although H-Ras is not a prevalent driver of human cancer, 85% of Ras mutations in bladder cancer occur in *H-Ras*, and genomic analysis of metadata from cBioPortal and COSMIC databases indicates that mutations in *H-Ras* co-occur with *B-Raf* mutations at a statistically significant level (p value = 0.003). Strikingly, the majority of the co-occurring *B-Raf* mutations cause alterations in the B-Raf kinase domain that are known to promote increased dimerization with C-Raf (Yao et al., 2017). When a panel of these mutants was compared against WT-B-Raf^{FL} in the BRET and

co-immunoprecipitation assays, all of the kinase domain mutants exhibited an increased affinity for H-Ras^{Q61R} that correlated with the extent to which the mutations augmented B-Raf/C-Raf dimerization (Figures 6A and S6A). In these cells, MEK activation was also increased, indicating enhanced H-Ras-driven signaling (Figures 6A and S6A). As was observed for Raf inhibitor treatment, the increased B-Raf/H-Ras interaction was dependent on C-Raf in that co-immunoprecipitation of the G466V- and D594G-B-Raf mutants with H-Ras^{Q61R} was reduced to background levels in C-Raf-depleted cells (Figure 6B). Moreover, the interaction with C-Raf again appeared to promote direct binding of G466V-B-Raf to H-Ras, as no increase in B-Raf/H-Ras co-immunoprecipitation was observed if G466V-B-Raf contained the RBD R > L mutation (Figure S6B).

Importance of C-Raf in H-Ras-Driven Signaling

Given that H-Ras binds C-Raf with the highest affinity and that C-Raf can promote increased B-Raf/H-Ras binding through B-Raf/C-Raf dimer formation, it is possible that C-Raf may be required for efficient transmission of H-Ras-mediated signals. To test this hypothesis, we first monitored the transformation potential of mutant H-Ras in focus-forming assays using NIH 3T3 cells that were depleted or not of endogenous C-Raf. As shown in Figure 6C, the number of foci induced by H-Ras^{G12V} expression was dramatically reduced (~80%) in cells lacking C-Raf, suggesting a dependence on C-Raf. In comparison, K-Ras^{G12V}-induced focus formation was only modestly affected by C-Raf loss (15%–20% reduction), and the effect of C-Raf depletion on H-Ras- and K-Ras-mediated transformation could be reversed by exchanging the C'-terminal HVR sequences (Figure 6C), further demonstrating the role of the Ras HVR in determining Raf engagement.

Next, we examined the effect of C-Raf depletion on the transformation potential and proliferative growth of two human cancer cell lines expressing mutant H-Ras proteins: T24 bladder carcinoma cells and the RL95-2 endometrial carcinoma line. Using the CRISPR/Cas9 system to individually deplete each of the Raf kinases or H-Ras, loss of C-Raf was found to reduce the 2D proliferative and 3D spheroid growth of T24 and RL95-2 cells to a similar extent as did H-Ras depletion, whereas loss of A-Raf or B-Raf had minimal effect (Figure 6D). When a similar analysis was performed on cancer lines expressing mutant K-Ras proteins, H358 lung carcinoma cells and the SW480 colorectal line, individually depleting each Raf member was found to have little effect on 2D proliferation. Spheroid growth could be reduced by depletion of either B-Raf or C-Raf; however, the effect was not as great as that observed for K-Ras depletion (Figure S6C). Taken together, the above depletion experiments demonstrate that C-Raf is critical for H-Ras-mediated transformation.

Finally, the cancer cell lines were utilized to further validate the effects of Raf inhibitor treatment on Ras/Raf binding. For these studies, previously characterized Ras antibodies (Waters et al., 2017) were used to selectively immunoprecipitate the

(G) BRET (left) and co-immunoprecipitation (right) assays were performed examining the effect of SB590885 treatment on the interaction of WT or R > L B-Raf^{FL}-Rluc with Venus-H-Ras^{Q61R}. BRET₅₀ values are listed. Co-immunoprecipitation of endogenous C-Raf with Venus-H-Ras^{Q61R} is also shown. Lysates were monitored for the indicated protein levels in (A, D, and E–G). See also Figures S4 and S5.

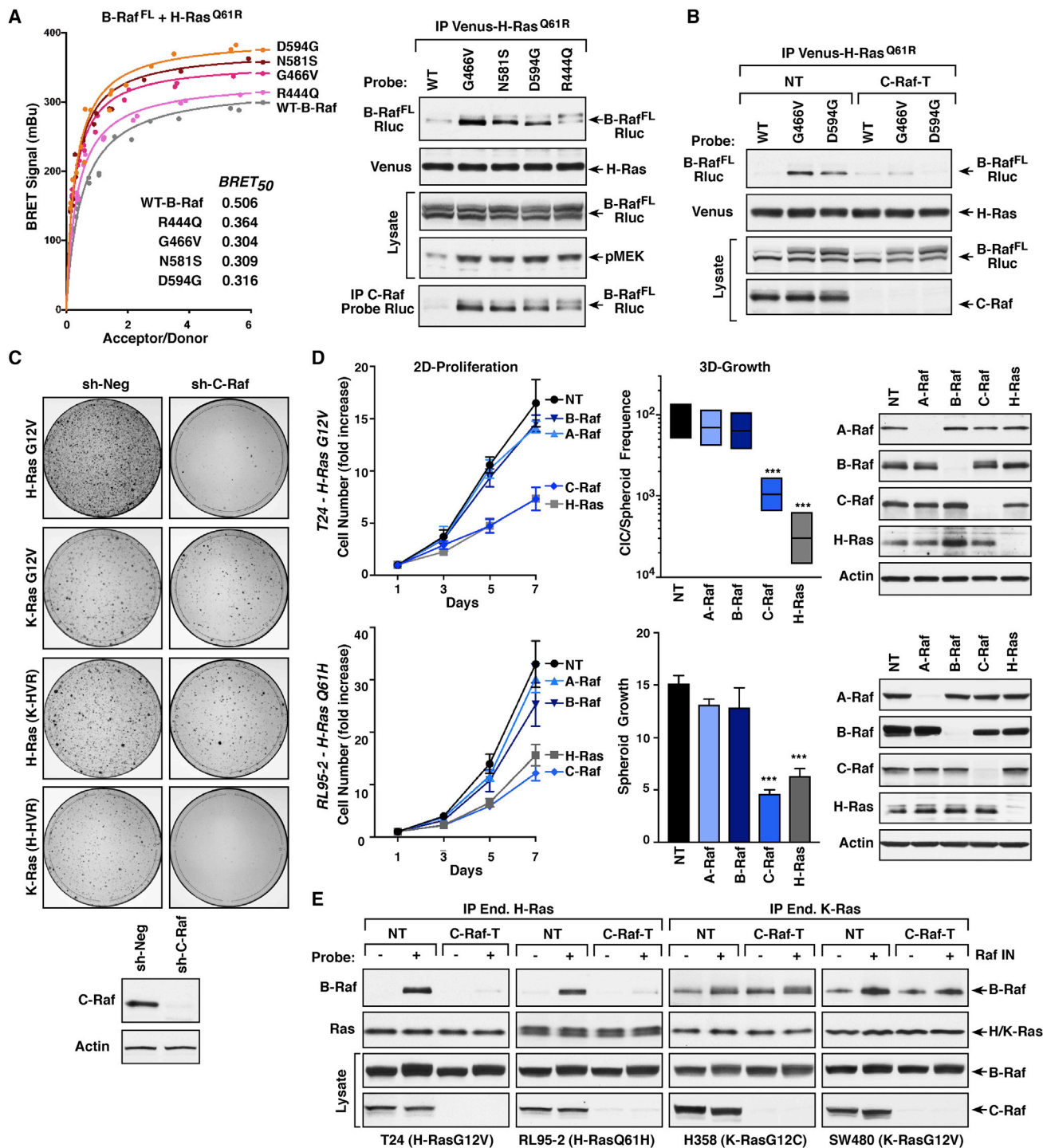


Figure 6. Co-occurring B-Raf and H-Ras Mutations in Cancer

(A) BRET (left) and co-immunoprecipitation assays (right) were performed comparing the interaction of WT and mutant B-Raf^{FL}-Rluc proteins with Venus-H-Ras^{Q61R}. BRET₅₀ values are listed. Endogenous C-Raf was also examined for dimerization with the B-Raf^{FL}-Rluc mutants. Lysates were monitored for pMEK and B-Raf-Rluc levels.

(B) Control (NT) or C-Raf-depleted (C-Raf-T) 293FT cells expressing WT, G466V, or D594G B-Raf^{FL}-Rluc with Venus-H-Ras^{Q61R} were examined in co-immunoprecipitation assays for binding of B-Raf^{FL}-Rluc to Venus-H-Ras^{Q61R}.

(C) Control (sh-Neg) or C-Raf-depleted (sh-C-Raf) NIH 3T3 cells were infected with retroviruses expressing the indicated Ras proteins. After two weeks of culture, focus formation was visualized by methylene blue staining. Shown are focus plates from a representative experiment.

(legend continued on next page)

endogenous mutant Ras proteins from cells that had been depleted or not of C-Raf (Figures 6E and S6D and S6E). In the mutant K-Ras lines, H358 and SW480, co-immunoprecipitation of B-Raf and mutant K-Ras was observed in the presence or absence of Raf inhibitor treatment, and depletion of C-Raf had no significant effect on the B-Raf/K-Ras interaction. However, for the mutant H-Ras lines, T24 and RL95-2, B-Raf was only detected in H-Ras immunoprecipitates from cells that had been treated with Raf inhibitor, and this interaction was reduced to background levels by C-Raf depletion (Figure 6E). These findings further support the model that B-Raf/C-Raf dimerization can allow mutant H-Ras to engage B-Raf with increased affinity and may provide an explanation for why melanoma patients treated with Raf inhibitors often developed secondary cancers driven by activating *H-Ras* mutations.

DISCUSSION

The Raf kinases are essential effectors of Ras signaling, and, although it has been over 20 years since they were first shown to possess a Ras-binding domain, whether these kinases differ in their ability to interact with an individual Ras family member in live cells has been unclear. In this study, we have utilized BRET technologies to further investigate the interactions of the Raf kinases with Ras members. In contrast to *in vitro* Ras/Raf binding studies, the BRET system allows for this important interaction to be monitored in the context of the plasma membrane and under conditions where post-translational modifications and lipid processing still occur, events that can strongly influence protein binding as well as signal progression. Despite the highly conserved nature of the Ras effector domains and the Raf RBDs, our findings reveal pronounced binding preferences between the Ras and Raf family members.

For all Ras proteins, C-Raf was found to exhibit the highest level and affinity of binding, followed by A-Raf, and then B-Raf, which surprisingly demonstrated a strong selectivity for K-Ras. These findings were further supported in co-immunoprecipitation studies, where the ability of the Ras/Raf interaction to withstand detergent cell lysis and immunopurification was found to correlate with lower BRET₅₀ values, which are indicative of higher binding affinities. The preferential binding of B-Raf to activated K-Ras was also observed in live-cell imaging experiments as well as in co-immunoprecipitation assays examining the ability of endogenous B-Raf to bind Ras members in cells overexpressing Venus-tagged Ras proteins, in Ras-deficient MEFs reconstituted to express untagged mutant H-Ras or K-Ras proteins at endogenous levels, and in human cancer cell lines harboring H-Ras or K-Ras mutant alleles.

Through the generation of various chimeric Ras and Raf proteins, we found that the B-Raf N'-segment and polybasic resi-

dues (PBR) in the K-Ras HVR account for the K-Ras binding selectivity of B-Raf. With regard to Ras members that lack the PBR, the B-Raf N'-segment, which carries an acidic charge and is 100–150 amino acids larger than the N'-segment of C-Raf or A-Raf, appears to act in an inhibitory manner as removal of the N'-segment allowed B-Raf to bind all Ras members with high affinity. It should be noted that our findings differ from a previous study where B-Raf was reported to bind with high affinity to farnesylated, GTP-bound H-Ras in surface plasmon resonance (SPR) assays (Fischer et al., 2007). However, in the SPR studies, B-Raf was coupled to the biosensor chip via a GST tag that was fused to the N'-segment, likely causing conformation changes or steric constraints that may have abrogated the inhibitory effect of the B-Raf N'-segment. In addition, the absence of crucial cellular components, including 14-3-3 dimers that stabilize the Raf auto-inhibited state, and the lack of an authentic membrane environment, features which are preserved in the BRET system, may also contribute to the observed differences.

Nevertheless, through BRET, co-immunoprecipitation, and live-cell imaging experiments, all of our results indicate that the B-Raf N'-segment results in reduced binding to Ras proteins that lack the PBR. For these Ras members (H-Ras, N-Ras, and K-Ras4A), it is possible that the B-Raf N'-segment, with its increased size and acidic charge, might occlude the RBD or act to repel B-Raf from the negatively charged plasma membrane such that contact with the RBD cannot be established. However, for K-Ras, our findings suggest that basic residues in the PBR may engage acidic residues in the B-Raf N'-segment to disrupt its inhibitory effect and facilitate high-affinity RBD binding (model depicted in Figure 7). Support for this model comes from the observations that reducing the basic charge of the PBR as well as reversing the charge of an acidic residue in the B-Raf N'-segment could reduce the affinity of the B-Raf/K-Ras interaction. Although further studies are needed to fully define the points of contact between B-Raf and K-Ras, these findings indicate the existence of other interactions, in addition to RBD binding, that uniquely contribute to the B-Raf/K-Ras interaction.

The distinct binding properties of the various Ras and Raf proteins also suggest that certain Raf kinases may play a more important role in cancers driven by a specific Ras family member. For example, our results implicate C-Raf as being required for H-Ras-driven transformation in that depletion of C-Raf, but not B-Raf or A-Raf, could suppress cell proliferation and the spheroid growth of two human cancer cell lines expressing mutant H-Ras alleles, T24 and RL95-2. Moreover, in NIH 3T3 focus-forming assays, C-Raf depletion severely reduced the transformation potential of H-Ras^{G12V}, whereas it had only a modest effect on K-Ras^{G12V}-mediated transformation. Notably, C-Raf was also found to impact the H-Ras/B-Raf interaction as B-Raf mutations or drug treatments stabilizing B-Raf/C-Raf

(D) T24 and RL95-2 cells were infected with lentiviruses expressing Cas9 and either a non-targeting sgRNA (NT) or sgRNAs targeting *A-Raf*, *B-Raf*, *C-Raf*, or *H-Ras*. Cells were assessed for 2D proliferation (left), 3D growth (middle), and expression of A-Raf, B-Raf, C-Raf, or H-Ras proteins (right). Data are represented as mean ± SD. ***p < 0.001.

(E) Control (NT) or C-Raf-depleted (C-Raf-T) lines were serum-starved for 18 h and then treated for 1 h with DMSO or SB590885 prior to lysis. Endogenous mutant H-Ras proteins from T24 and RL95-2 cells and endogenous mutant K-Ras proteins from H358 and SW480 were immunoprecipitated and examined for the presence of endogenous B-Raf. Lysates were monitored for the indicated protein levels in (A–E).

See also Figure S6.

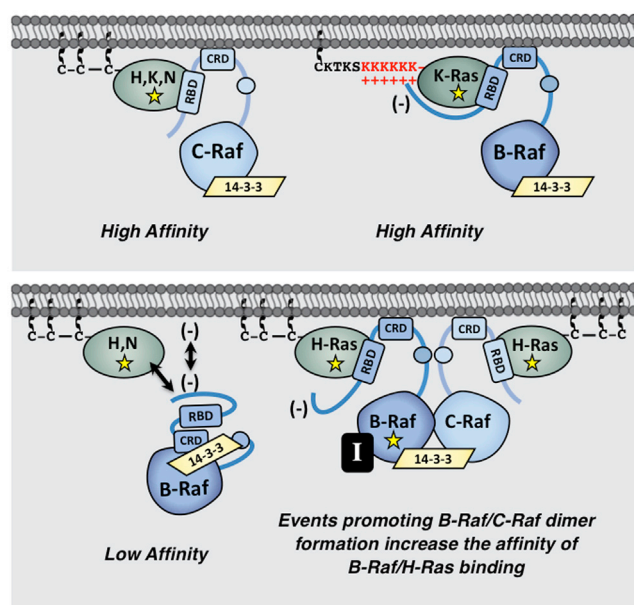


Figure 7. Model for Ras/Raf Binding Preferences

The C-Raf kinase exhibits high-affinity binding to all Ras family members. In contrast, B-Raf, whose N-terminal segment is larger and possesses an overall acidic charge, only binds with high affinity to mutant K-Ras, whose HVR contains a series of polybasic lysine residues (upper). In the context of H-Ras or N-Ras, the B-Raf N'-segment might occlude the RBD or act to repel B-Raf from the negatively charged plasma membrane. However, events that promote stable B-Raf/C-Raf dimer formation, such as B-Raf mutations (depicted as yellow star) or treatment with B-Raf inhibitors (black box containing the letter I), allow mutant H-Ras to engage B-Raf with increased affinity to upregulate ERK cascade signaling (lower).

dimerization significantly increased the affinity of B-Raf/H-Ras binding in a manner that required C-Raf (Figure 7). It is unclear whether dimerization with C-Raf alters the conformation of the B-Raf N-terminal domain or facilitates B-Raf localization at the membrane such that binding of H-Ras to the B-Raf RBD can occur. Nevertheless, augmented dimer formation with C-Raf appears to promote direct contact between B-Raf and mutant H-Ras, as no increase in H-Ras binding was observed if B-Raf contained the RBD R > L mutation.

Finally, our results indicate that the ability of C-Raf to facilitate the binding of B-Raf to non-PBR-containing Ras proteins may have important biological consequences. In particular, these findings likely explain why melanoma patients treated with the B-Raf inhibitors vemurafenib and dabrafenib often developed secondary cancers driven by *H-Ras* mutations (Boussemaert et al., 2016; Oberholzer et al., 2012; Su et al., 2012). In this case, inhibitor-stabilized B-Raf/C-Raf dimerization would allow mutant H-Ras to engage B-Raf with increased affinity, thus upregulating ERK cascade signaling to levels that promote tumorigenesis. Likewise, B-Raf mutations that increase B-Raf/C-Raf dimerization and co-occur with oncogenic mutations in non-PBR-containing Ras members may be functionally relevant, acting to augment the signaling potential of these Ras mutants in human cancer. In conclusion, our study highlights the importance of elucidating the distinct roles of individual Ras and Raf

family members in cell signaling and tumorigenesis and may aid in the design of new therapeutic strategies.

STAR★METHODS

Detailed methods are provided in the online version of this paper and include the following:

- KEY RESOURCES TABLE
- LEAD CONTACT AND MATERIALS AVAILABILITY
- EXPERIMENTAL MODEL AND SUBJECT DETAILS
 - Cell Lines and Culture Conditions
- METHOD DETAILS
 - DNA Constructs
 - BRET Assay
 - Transfection, Lysis, and Co-immunoprecipitation
 - Live-cell Imaging
 - Raf-RBD Pull-down Assays
 - shRNA and CRISPR/Cas9 Vectors
 - Recombinant Lentiviruses and Cell Infection
 - NIH 3T3 Focus Formation Assay
 - Cell Proliferation Assay
 - Transformation and Spheroid Growth Assays
- QUANTIFICATION AND STATISTICAL ANALYSIS
- DATA CODE AND AVAILABILITY

SUPPLEMENTAL INFORMATION

Supplemental Information can be found online at <https://doi.org/10.1016/j.molcel.2019.09.004>.

ACKNOWLEDGMENTS

We thank Linda Miller (LCDS) and Vanessa Wall (FNLCR Protein Expression Laboratory) for technical support. This project has been funded by federal funds from the National Cancer Institute, United States under project number ZIA BC 010329 (D.K.M.) and contract number HHSN261200800001E (D.E.), by federal funds from the National Institutes of Health, United States under grant number R01 GM124233 (J.F.H.), and from the Congressionally Directed Medical Research Program, United States LC160222 (R.L.K.).

AUTHOR CONTRIBUTIONS

E.M.T., R.L.K., and D.K.M. conceived the project, designed the experiments, and interpreted the data. E.M.T. performed the majority of the experiments (BRET and co-immunoprecipitation assays) with crucial help from D.E.D., D.A.R., and R.S.-S. (live-cell imaging, co-immunoprecipitation, and transformation assays); N.E.S. and E.S. (2D and 3D growth assays); and D.E., Y.Z., and J.F.H. (generation and analysis of critical reagents). E.M.T. and D.K.M. wrote the manuscript.

DECLARATION OF INTERESTS

The authors declare no competing interests.

Received: October 8, 2018

Revised: July 22, 2019

Accepted: September 5, 2019

Published: October 9, 2019

REFERENCES

Ambrogio, C., Köhler, J., Zhou, Z.W., Wang, H., Paranal, R., Li, J., Capelletti, M., Caffarra, C., Li, S., Lv, Q., et al. (2018). KRAS Dimerization Impacts MEK

- Inhibitor Sensitivity and Oncogenic Activity of Mutant KRAS. *Cell* 172, 857–868.e15.
- Bos, J.L., Rehmann, H., and Wittinghofer, A. (2007). GEFs and GAPs: critical elements in the control of small G proteins. *Cell* 129, 865–877.
- Boussemart, L., Girault, I., Malka-Mahieu, H., Mateus, C., Routier, E., Rubington, M., Kamsu-Kom, N., Thomas, M., Tomasic, G., Agoussi, S., et al. (2016). Secondary Tumors Arising in Patients Undergoing BRAF Inhibitor Therapy Exhibit Increased BRAF-CRAF Heterodimerization. *Cancer Res.* 76, 1476–1484.
- Buhrman, G., Kumar, V.S., Cirit, M., Haugh, J.M., and Mattos, C. (2011). Allosteric modulation of Ras-GTP is linked to signal transduction through RAF kinase. *J. Biol. Chem.* 286, 3323–3331.
- Cox, A.D., and Der, C.J. (2010). Ras history: The saga continues. *Small GTPases* 1, 2–27.
- Dougherty, M.K., Müller, J., Ritt, D.A., Zhou, M., Zhou, X.Z., Copeland, T.D., Conrads, T.P., Veenstra, T.D., Lu, K.P., and Morrison, D.K. (2005). Regulation of Raf-1 by direct feedback phosphorylation. *Mol. Cell* 17, 215–224.
- Drosten, M., Dhawahir, A., Sum, E.Y., Urosevic, J., Lechuga, C.G., Esteban, L.M., Castellano, E., Guerra, C., Santos, E., and Barbacid, M. (2010). Genetic analysis of Ras signalling pathways in cell proliferation, migration and survival. *EMBO J.* 29, 1091–1104.
- Durrant, D.E., and Morrison, D.K. (2018). Targeting the Raf kinases in human cancer: the Raf dimer dilemma. *Br. J. Cancer* 118, 3–8.
- Fabian, J.R., Vojtek, A.B., Cooper, J.A., and Morrison, D.K. (1994). A single amino acid change in Raf-1 inhibits Ras binding and alters Raf-1 function. *Proc. Natl. Acad. Sci. USA* 91, 5982–5986.
- Fernández-Medarde, A., and Santos, E. (2011). Ras in cancer and developmental diseases. *Genes Cancer* 2, 344–358.
- Fischer, A., Hekman, M., Kuhlmann, J., Rubio, I., Wiese, S., and Rapp, U.R. (2007). B- and C-RAF display essential differences in their binding to Ras: the isotype-specific N terminus of B-RAF facilitates Ras binding. *J. Biol. Chem.* 282, 26503–26516.
- Freeman, A.K., Ritt, D.A., and Morrison, D.K. (2013). Effects of Raf dimerization and its inhibition on normal and disease-associated Raf signaling. *Mol. Cell* 49, 751–758.
- Hekman, M., Hamm, H., Villar, A.V., Bader, B., Kuhlmann, J., Nickel, J., and Rapp, U.R. (2002). Associations of B- and C-Raf with cholesterol, phosphatidylserine, and lipid second messengers: preferential binding of Raf to artificial lipid rafts. *J. Biol. Chem.* 277, 24090–24102.
- Hu, Y., and Smyth, G.K. (2009). ELDA: extreme limiting dilution analysis for comparing depleted and enriched populations in stem cell and other assays. *J. Immunol. Methods* 347, 70–78.
- Hu, J., Stites, E.C., Yu, H., Germino, E.A., Meharena, H.S., Stork, P.J.S., Kornev, A.P., Taylor, S.S., and Shaw, A.S. (2013). Allosteric activation of functionally asymmetric RAF kinase dimers. *Cell* 154, 1036–1046.
- Hunter, J.C., Manandhar, A., Carrasco, M.A., Gurbani, D., Gondi, S., and Westover, K.D. (2015). Biochemical and Structural Analysis of Common Cancer-Associated KRAS Mutations. *Mol. Cancer Res.* 13, 1325–1335.
- Inouye, K., Mizutani, S., Koide, H., and Kaziro, Y. (2000). Formation of the Ras dimer is essential for Raf-1 activation. *J. Biol. Chem.* 275, 3737–3740.
- Lavoie, H., and Therrien, M. (2015). Regulation of RAF protein kinases in ERK signalling. *Nat. Rev. Mol. Cell Biol.* 16, 281–298.
- Nan, X., Collisson, E.A., Lewis, S., Huang, J., Tamgüney, T.M., Liphardt, J.T., McCormick, F., Gray, J.W., and Chu, S. (2013). Single-molecule superresolution imaging allows quantitative analysis of RAF multimer formation and signaling. *Proc. Natl. Acad. Sci. USA* 110, 18519–18524.
- Oberholzer, P.A., Kee, D., Dziunycz, P., Sucker, A., Kamsukom, N., Jones, R., Roden, C., Chalk, C.J., Ardlie, K., Palescandolo, E., et al. (2012). RAS mutations are associated with the development of cutaneous squamous cell tumors in patients treated with RAF inhibitors. *J. Clin. Oncol.* 30, 316–321.
- Parker, J.A., and Mattos, C. (2015). The Ras-Membrane Interface: Isoform-specific Differences in The Catalytic Domain. *Mol. Cancer Res.* 13, 595–603.
- Pfleger, K.D., and Eidne, K.A. (2006). Illuminating insights into protein-protein interactions using bioluminescence resonance energy transfer (BRET). *Nat. Methods* 3, 165–174.
- Prior, I.A., and Hancock, J.F. (2012). Ras trafficking, localization and compartmentalized signalling. *Semin. Cell Dev. Biol.* 23, 145–153.
- Prior, I.A., Lewis, P.D., and Mattos, C. (2012). A comprehensive survey of Ras mutations in cancer. *Cancer Res.* 72, 2457–2467.
- Pylayeva-Gupta, Y., Grabocka, E., and Bar-Sagi, D. (2011). RAS oncogenes: weaving a tumorigenic web. *Nat. Rev. Cancer* 11, 761–774.
- Ritt, D.A., Monson, D.M., Specht, S.I., and Morrison, D.K. (2010). Impact of feedback phosphorylation and Raf heterodimerization on normal and mutant B-Raf signaling. *Mol. Cell. Biol.* 30, 806–819.
- Sanjana, N.E., Shalem, O., and Zhang, F. (2014). Improved vectors and genome-wide libraries for CRISPR screening. *Nat. Methods* 11, 783–784.
- Schubbert, S., Shannon, K., and Bollag, G. (2007). Hyperactive Ras in developmental disorders and cancer. *Nat. Rev. Cancer* 7, 295–308.
- Sheffels, E., Sealover, N.E., Theard, P.L., and Kortum, R.L. (2019). Anchorage-independent growth conditions reveal a differential SOS2 dependence for transformation and survival in RAS-mutant cancer cells. *Small GTPases*, 1–12.
- Simanshu, D.K., Nissley, D.V., and McCormick, F. (2017). RAS Proteins and Their Regulators in Human Disease. *Cell* 170, 17–33.
- Su, F., Viros, A., Milagre, C., Trunzer, K., Bollag, G., Spleiss, O., Reis-Filho, J.S., Kong, X., Koya, R.C., Flaherty, K.T., et al. (2012). RAS mutations in cutaneous squamous-cell carcinomas in patients treated with BRAF inhibitors. *N. Engl. J. Med.* 366, 207–215.
- Waters, A.M., Ozkan-Dagliyan, I., Vaseva, A.V., Fer, N., Strathern, L.A., Hobbs, G.A., Tessier-Cloutier, B., Gillette, W.K., Bagni, R., Whiteley, G.R., et al. (2017). Evaluation of the selectivity and sensitivity of isoform- and mutation-specific RAS antibodies. *Sci. Signal.* 10, eaao3332.
- Williams, J.G., Drugan, J.K., Yi, G.S., Clark, G.J., Der, C.J., and Campbell, S.L. (2000). Elucidation of binding determinants and functional consequences of Ras/Raf-cysteine-rich domain interactions. *J. Biol. Chem.* 275, 22172–22179.
- Yao, Z., Yaeger, R., Rodrik-Outmezguine, V.S., Tao, A., Torres, N.M., Chang, M.T., Drosten, M., Zhao, H., Cecchi, F., Hembrough, T., et al. (2017). Tumours with class 3 BRAF mutants are sensitive to the inhibition of activated RAS. *Nature* 548, 234–238.
- Zhang, C., Spevak, W., Zhang, Y., Burton, E.A., Ma, Y., Habets, G., Zhang, J., Lin, J., Ewing, T., Matusow, B., et al. (2015). RAF inhibitors that evade paradoxical MAPK pathway activation. *Nature* 526, 583–586.
- Zhou, Y., Prakash, P., Liang, H., Cho, K.J., Gorfe, A.A., and Hancock, J.F. (2017). Lipid-Sorting Specificity Encoded in K-Ras Membrane Anchor Regulates Signal Output. *Cell* 168, 239–251.e16.

STAR★METHODS

KEY RESOURCES TABLE

REAGENT or RESOURCE	SOURCE	IDENTIFIER
Antibodies		
B-Raf (H-145) rabbit polyclonal	Santa Cruz Biotechnology	cat# sc-9002; RRID:AB_2067494
B-Raf (F-7) mouse monoclonal	Santa Cruz Biotechnology	cat# sc-5284; RRID:AB_2721130
C-Raf (C-12) rabbit polyclonal	Santa Cruz Biotechnology	cat# sc-133; RRID:AB_632305
C-Raf mouse monoclonal	BD Pharmagen	cat# 610152; RRID:AB_397553
A-Raf (C-20) rabbit polyclonal	Santa Cruz Biotechnology	cat# sc-408; RRID:AB_630882
H-Ras (C-20) rabbit polyclonal	Santa Cruz Biotechnology	cat# sc-520; RRID:AB_631670
N-Ras (F155) mouse monoclonal	Santa Cruz Biotechnology	cat# sc-31; RRID:AB_628041
K-Ras mouse monoclonal	Sigma	cat# WH0003845M1; RRID:AB_1842235
pS217/221-MEK rabbit polyclonal	Cell Signaling Technology	cat# 9121; RRID:AB_331648
Rluc rabbit polyclonal	MBL International	cat# PM047; RRID:AB_1520866
GFP mouse monoclonal	Roche	cat# 11814460001; RRID:AB_390913
GFP rat monoclonal	MBL International	cat# D153-3; RRID:AB_591817
Pan-Ras [EPR3255] rabbit monoclonal	Abcam	cat# 108602; RRID:AB_10891004
Pan-Ras [Ras10] mouse monoclonal	EMD Millipore	cat# 05-516; RRID:AB_11211664
Actin (I-19) goat polyclonal	Santa Cruz Biotechnology	cat# sc-1616; RRID:AB_630836
Donkey anti-goat IgG-HRP	Santa Cruz Biotechnology	cat# sc-2020; RRID:AB_631728
Donkey anti-rabbit IgG-HRP	GE Healthcare	cat# NA934; RRID:AB_772206
Sheep anti-mouse IgG-HRP	GE Healthcare	cat# NA931; RRID:AB_772210
Goat anti-rat IgG-HRP	Cell Signaling Technology	cat# 7077; RRID:AB_10694715
Chemicals, Peptides, and Recombinant Proteins		
Vemurafenib (PLX4032)	SelleckChem	Cat# S1267
Dabrafenib (GSK2118436)	SelleckChem	Cat# S2807
LY3009120	SelleckChem	Cat# S7842
PLX7904	SelleckChem	Cat# S7964
SB-590885	SelleckChem	Cat# S2220
Coelenterazine-h	Promega	Cat# S2011
Halo Oregon Green ligand	Promega	Cat# G2802
Epidermal Growth Factor (EGF)	ThermoFisher	cat# PHG0311
GST-RBD	Millipore	cat# 14-863
X-tremeGENE 9	Roche/Sigma	cat# 06365809001
Collagen, Human Placenta Type IV	Millipore/Sigma	cat# C7521
Critical Commercial Assays		
CellTiter-Glo 2.0	Promega	cat# G9241
TransIT®-Lenti Transfection Reagent	Mirus	cat# MIR 6603
Mission Lentiviral Packaging Mix	Sigma	cat# SHP001
GeneArt Seamless Cloning and Assembly Kit	Life Technologies	cat# A13288
QuickChange II Kit	Agilent	cat# 200523
Deposited Data		
Raw data of immunoblots and live cell imaging	Mendeley Data	https://doi.org/10.17632/r6vvxjpskf.1
Experimental Models: Cell Lines		
293FT (human)	Invitrogen	cat# R70007
Phoenix-Eco (human)	ATCC	cat# CRL-3214; RRID:CVCL_H717

(Continued on next page)

Continued

REAGENT or RESOURCE	SOURCE	IDENTIFIER
NIH 3T3 (mouse)	ATCC	cat# CRL-1658; RRID:CVCL_0594
HeLa (human, female)	ATCC	cat# CCL-2; RRID:CVCL_0030
SW480 (human, male)	ATCC	cat# CCL-228; RRID:CVCL_0546
RL95-2 (human, female)	ATCC	cat# CRL-1671; RRID:CVCL_0505
H358 (human, male)	ATCC	cat# CRL-5807; RRID:CVCL_1559
T24 (human, female)	ATCC	cat# HTB-4; RRID:CVCL_0554
MCF10A (human, female)	ATCC	cat# CRL-10317; RRID:CVCL_0598
Ras ^{-/-} MEF + KRas Q61L (mouse)	NCI-Ras Initiative	N/A
Ras ^{-/-} MEF + HRas Q61L (mouse)	NCI-Ras Initiative	N/A
Oligonucleotides		
CRISPR A-Raf sgRNA (TGGTCTACCGACTCATCAAG)	This paper	N/A
CRISPR B-Raf sgRNA (GGGCCAGGCTCTGTTCAACG)	This paper	N/A
CRISPR C-Raf sgRNA (GCCGAACAAGCAAAGAACAG)	This paper	N/A
CRISPR H-Ras sgRNA (ACGGAATATAAGCTGGTGG)	Sheffels et al., 2019	N/A
CRISPR K-Ras sgRNA (TCATTGCACTGTACTCCTCT)	Sheffels et al., 2019	N/A
CRISPR NT sgRNA (CCATATCGGGGCGAGACATG)	Sheffels et al., 2019	N/A
shCRaf (CGGAGATGTTGCAGTAAAGAT)	Open Biosystems	TRCN0000001066
Recombinant DNA		
pLHCX-WT-Raf ^{Reg} -Rluc8 (A-, B-, C-Raf)	This paper	N/A
pLHCX-R > L-Raf ^{Reg} -Rluc8 (A-, B-, C-Raf)	This paper	N/A
pLHCX-Raf ^{FL} -Rluc8 (A-, B-, C-Raf)	This paper	N/A
pLHCX-C-Raf ^{Reg} /B-Raf N'-segment-Rluc8	This paper	N/A
pLHCX-C-Raf ^{Reg} /B-Raf RBD/CRD-Rluc8	This paper	N/A
pLHCX-B-Raf ^{Reg} /C-Raf N'-segment-Rluc8	This paper	N/A
pLHCX-B-Raf ^{Reg} /C-Raf RBD/CRD-Rluc8	This paper	N/A
pLHCX-B-Raf ^{Reg} N'-segment mutants-Rluc8	This paper	N/A
pLHCX-B-Raf ^{FL} kinase domain mutants-Rluc8	This paper	N/A
pLHCX-R188L-B-Raf ^{FL} -Rluc8	This paper	N/A
pUBC-Raf-mCherry (B-, C-Raf)	NCI-Ras Initiative	N/A
pCMV5-Venus-Ras ^{Q61R} (H-, N-, K-Ras4A, 4B)	NCI-Ras Initiative	N/A
pCMV5-Venus-Ras ^{G12V} (H-, N-, K-Ras4B)	NCI-Ras Initiative	N/A
pCMV5-Venus-Ras ^{G12D} (H-, N-, K-Ras4B)	NCI-Ras Initiative	N/A
pCMV5-Venus-Ras ^{G13D} (H-, N-, K-Ras4B)	NCI-Ras Initiative	N/A
pCMV5-Venus-Ras ^{Q61L} (H-, N-, K-Ras4B)	NCI-Ras Initiative	N/A
pCMV5-Venus-WT Ras (H-, N-, K-Ras4B)	NCI-Ras Initiative	N/A
pCMV5-Halo-Ras ^{G12V} (H-, K-Ras4B)	NCI-Ras Initiative	N/A
EGFP-K-Ras4B ^{G12V} PBR mutants	Zhou et al., 2017	N/A
pCMV-Venus-H-Ras ^{Q61R} /K-Ras4B HVR	NCI-Ras Initiative	N/A
pCMV-Venus-K-Ras ^{Q61R} /H-Ras HVR	NCI-Ras Initiative	N/A
pLKO.1 lentiviral vector	Open Biosystems/Dharmacon	cat# RHS4080
pLKO.1 shCRaf lentiviral construct	Open Biosystems/Dharmacon	cat# RHS3979-201733340; TRCN0000001066
pLentiCRISPRv2	Addgene	cat# 52961
Software and Algorithms		
GraphPad Prism	GraphPad	https://www.graphpad.com
ImageJ	ImageJ	https://imagej.nih.gov/ij/

LEAD CONTACT AND MATERIALS AVAILABILITY

Further information and requests for resources and reagents should be directed to and will be fulfilled by the Lead Contact, Deborah Morrison (morrisod@mail.nih.gov). Plasmids and cell lines are available for use upon request to the Lead Contact.

EXPERIMENTAL MODEL AND SUBJECT DETAILS

Cell Lines and Culture Conditions

293FT, NIH 3T3, Phoenix-Eco, RL95-2, and RAS-deficient MEFs were cultured in DMEM. H358 cells were cultured in RPMI, T24 cells in McCoy's 5a, and SW480 in L-15. All media was supplemented with 10% fetal bovine serum (FBS), 2 mM L-glutamine, and 1% penicillin/streptomycin. MCF10A cells were cultured in DMEM/F12 supplemented with 5% horse serum, 0.5 μ g/mL hydrocortisone, 20 ng/mL EGF, 100 ng/mL cholera toxin, 10 μ g/mL insulin, and 1% penicillin/streptomycin. All cell lines were cultured at 37°C under 5% CO₂ except for SW480 cells, which were cultured at 37°C under atmospheric conditions. Ras-deficient MEFs were sequenced by the provider (NCI-Ras Initiative) to confirm loss of endogenous Ras and integration of the transgene.

METHOD DETAILS

DNA Constructs

The full-length Raf kinases and the Raf regulatory domain proteins were tagged at the C terminus with the Rluc8 enzyme and cloned into the pLHCX-CMV vector. The Raf regulatory domain constructs encode amino acids 1-288 of A-Raf, amino acids 1-435 of B-Raf, and amino acids 1-327 of C-Raf. Chimeric Raf proteins with various regions in the Raf regulatory domain exchanged were constructed using the GeneArt Seamless Cloning and Assembly Kit from Life Technologies. The Raf regions exchanged are based on the following amino acid designations: B-Raf N'-segment: amino acids 1-154, B-Raf RBD/CRD: amino acids 155-280, C-Raf N'-segment: amino acids 1-55, C-Raf RBD/CRD: amino acids 56-184. The Ras family members were tagged at the N terminus with the Venus fluorophore and cloned into the pCMV5 vector. For Ras HVR-exchanged constructs, the HVR of K-Ras4B was defined as amino acids 165-188, and the HVR of H-Ras as amino acids 165-189. Point mutations were generated by site-directed mutagenesis using the QuickChange II Kit from Agilent.

BRET Assay

293FT cells were seeded into 12-well dishes at a concentration of 1×10^5 cells/well. 16 h after plating, Venus-tagged and Rluc8-tagged constructs were transfected into cells using a calcium phosphate protocol. A 12-point saturation curve was generated in which the concentration of the energy donor construct (Rluc8) was held constant (62.5 ng) as the concentration of the energy acceptor plasmid (Venus) increased (0-1.0 μ g). Live cells were collected 48 h after transfection, washed, and plated in PBS. The Rluc8 cofactor coelenterazine-h was added to a final concentration of 3.375 μ M, and the BRET signal read 2 min after addition. The BRET signal was measured at 535 nm (bandwidth 30 nm) on the PHERAstar *Plus* plate reader (BMG Labtech) and the Rluc8 signal was simultaneously measured at 475 nm (bandwidth 30 nm). Venus fluorescence was measured independently using an excitation wavelength of 485 nm (5 nm bandwidth), and the emission spectra measured at 530 nm (5 nm bandwidth) on the Tecan Infinite M1000 plate reader. The BRET value for each data point was calculated by dividing the BRET ratio (BRET/Rluc8) by the background signal. The acceptor/donor ratio was equalized against a control where equal quantities of Venus and Rluc8 constructs were transfected. Data was analyzed using GraphPad Prism. Non-linear regression was used to plot the best fit hyperbolic curve and values for BRET_{max} and BRET₅₀ were obtained from the calculated best fit curves.

Transfection, Lysis, and Co-immunoprecipitation

The indicated cell lines were plated at ~70% confluency 18-24 h prior to transfection. Cells were then transfected using the XtremeGENE9 transfection reagent per the manufacturer's instructions, using a 2:1 ratio of XtremeGENE9 to DNA. For cell lysis, cells were washed twice with ice cold PBS and lysed for 15 min at 4°C in 1% NP-40 buffer (20mM Tris [pH 8.0], 137 mM NaCl, 10% glycerol, 1% NP-40 alternative, 0.15 U/mL aprotinin, 1 mM phenylmethylsulfonyl fluoride, 0.5 mM sodium vanadate, 20 μ M leupeptin). Lysates were clarified by centrifugation at 14,000 rpm for 10 min at 4°C, following which the protein content was determined by Bradford assays. Lysates containing equivalent amounts of protein were incubated with the appropriate antibody and protein G Sepharose beads for 2 h at 4°C on a rocking platform. Complexes were washed extensively with 1% NP-40 buffer and then examined by immunoblot analysis along with aliquots of equalized lysate.

Live-cell Imaging

293FT or MCF10A cells expressing the indicated Halo- and mCherry-tagged proteins were plated onto collagen-coated glass surfaces (10 μ g/mL human placenta type IV collagen). On the day of live cell imaging experiments, cells were washed with media lacking phenol red and incubated with the Halo Oregon green ligand for 15-30 min at 37°C. Cells were then washed in phenol red-free media and maintained in growth media lacking phenol red for the duration of image acquisition using either Zeiss Axiovert Z1 and LSM710.

Raf-RBD Pull-down Assays

To monitor the GTP-bound state of Ras, equalized cell lysates containing 5 μM MgCl_2 were incubated with GST-tagged Raf-RBD bound to glutathione-Sepharose beads (Millipore) for 1 h at 4°C on a rocking platform. Complexes were washed extensively with 1% NP-40 buffer and then examined by immunoblot analysis.

shRNA and CRISPR/Cas9 Vectors

For depletion of C-Raf protein levels in NIH 3T3 cells, pLKO.1 lentiviral vectors expressing shC-Raf (TRCN0000001066) sequences were obtained from Open Biosystems. For CRISPR/Cas9 studies, a non-targeting (NT), single guide RNA (sgRNA) or sgRNAs targeting the *A-Raf*, *B-Raf*, *C-Raf*, *H-Ras*, or *K-Ras* gene were each cloned into pLentiCRISPRv2 (Sanjana et al., 2014).

Recombinant Lentiviruses and Cell Infection

For protein depletion experiments, lentiviral particles expressing the desired targeting constructs were generated by co-transfecting the pLKO.1 or pLentiCRISPRv2 constructs with the MISSION lentiviral packaging mix (Sigma) into 293T cells using the Mirus Trans-IT lenti transfection kit. 48 h post-transfection, viral supernatants were collected, centrifuged twice at 1500 rpm for 7 min, and either stored at -80°C or used directly. Cells were infected with viral supernatants containing 8 $\mu\text{g}/\text{mL}$ polybrene. 48 h post-infection, cells were placed into selection media containing 6 $\mu\text{g}/\text{mL}$ puromycin for 4 days and then shifted into media containing 3 $\mu\text{g}/\text{mL}$ puromycin for an additional 6 days, prior to analysis. For protein expression studies, lentiviral particles were generated by co-transfecting the pUBC-Raf-mCherry or pCMV-Halo-Ras^{G12V} constructs with packaging plasmids pMD2.G and psPAX2 (3:1:2 ratio) into 293T cells using XtremeGENE9. 48 h post-transfection, viral supernatants were collected, centrifuged twice at 1500 rpm for 7 min, and either stored at -80°C or used directly. MCF10A cells were infected with lentivirus supernatants containing 8 $\mu\text{g}/\text{mL}$ polybrene for 24 h, following which growth media supplemented with the appropriate antibiotic selection was added (Puromycin: 1 $\mu\text{g}/\text{mL}$, Hygromycin: 40 $\mu\text{g}/\text{mL}$).

NIH 3T3 Focus Formation Assay

Recombinant retroviruses expressing Halo-H-Ras^{G12V} or Halo-K-Ras^{G12V} constructs were generated by transfecting the pBabe-Halo-Ras constructs into Phoenix-Eco cells using the X-tremeGENE9 protocol described above. Viral supernatants were collected 3 days post-transfection, centrifuged twice at 1500 rpm for 7 min, and either stored at -80°C or used directly. Control (shNeg) or C-Raf-depleted (shC-Raf) NIH 3T3 cells were plated into 60 mm dishes at a concentration of $2 \times 10^5/\text{dish}$. After 18 h, cells were infected with the indicated recombinant retrovirus in media containing 4% FBS and 8 $\mu\text{g}/\text{mL}$ polybrene for 24 h. Cells were trypsinized and plated into two 100 mm dishes, one of which contained 5 $\mu\text{g}/\text{mL}$ puromycin. After two weeks of culture, cells were fixed with 3.7% formaldehyde and stained with 1% methylene blue.

Cell Proliferation Assay

Cell proliferation was assessed using the CellTiter-Glo 2.0 Reagent (Promega) with luminescence determined using a GloMax Discover Plate Reader (Promega). 1×10^3 cells were seeded into white-walled cell culture-coated 96-well plates (Promega). Cell number was assessed 24 h after plating (day 1) and then every 48 h for 7 days. Data were analyzed as an increase in luminescence over day 1.

Transformation and Spheroid Growth Assays

Transformation of T24 cells was assessed by CSC/spheroid frequency as previously described (Inouye et al., 2000). Briefly, serially diluted T24 cells were seeded into ultra-low attachment 96-well, flat-bottomed plates (1 cell/well – 1000 cells/well, Corning Corstar #3474), with 24 wells per condition. Cells were cultured for 7-10 days, and wells with spheroids > 100 μm were scored as spheroid positive. CSC/CIC frequency was calculated by ELDA website (<http://bioinf.wehi.edu.au/software/elda/>) (Hu and Smyth, 2009). Spheroid growth of R95-2, H358 and SW480 cells were conducted as described in (Sheffels et al., 2019). RL95-2, H358 or SW480 cells were seeded at 500-1000 cells/well in ultra-low attachment 96-well round bottomed plates (Corning Costar #7007). Cell number was assessed 18 h after plating to allow spheroids to form (day 0), and then at day 7 using CellTiter-Glo 2.0 reagent (Promega), which measures ATP content as a surrogate of overall cell number. Spheroid growth for each cell line was normalized to the CellTiter Glo signal at day 0, and the results are expressed as a fold-increase over day 0.

QUANTIFICATION AND STATISTICAL ANALYSIS

BRET data were transferred to GraphPad Prism for statistical analysis and curve fitting. Data was plotted as the acceptor to donor ratios versus mBRET values. Non-linear regression was used to fit a hyperbolic curve to the dataset and determine R-squared values. The BRET_{max} and BRET₅₀ values as well as the corresponding 95% confidence intervals were calculated using GraphPad Prism8 software. For cell proliferation and spheroid growth assays, replicate wells (n = 6 per experiment) were seeded into 96-well plates and cell number was quantified at the indicated times. Data represent 3 independent experiments and are presented as mean \pm

SD. Significance was determined by ANOVA using the Tukey's multiple comparisons test and calculated using GraphPad Prism8 software. The co-immunoprecipitation, live cell imaging, and BRET experiments shown are representative and reflect at least 3 independent experiments.

DATA CODE AND AVAILABILITY

The datasets analyzed during this study are available at cBioPortal [<http://www.cbioportal.org>] and COSMIC [<https://cancer.sanger.ac.uk/cosmic>]. Raw data of immunoblots and live cell imaging are available through Mendeley Data (<https://doi.org/10.17632/r6v vxjpskf.1>). This study did not generate any code.